

AD-A067 090

AIR WEATHER SERVICE SCOTT AFB ILL
SATELLITE METEOROLOGY.(U)
AUG 76 H W BRANDLI
AWS-TR-76-264

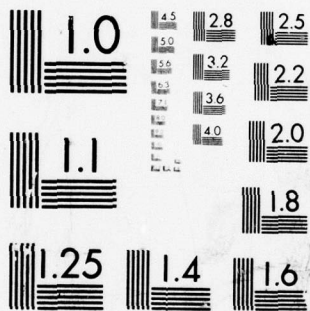
F/G 4/2

UNCLASSIFIED

NL

1 OF 3
AD
A067090





MICROCOPY RESOLUTION TEST CHART
NATIONAL BUREAU OF STANDARDS-1963-A

ADA067090

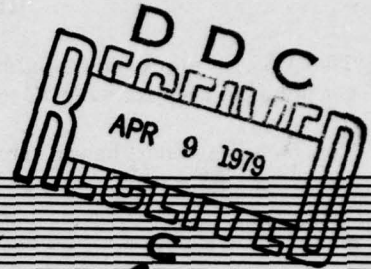
DDC FILE COPY



52
B.S.

AWS-TR-76-264

LEVEL



SATELLITE METEOROLOGY

By

Henry W. Brandli, Lt Col, USAF
Detachment 11, 2 Weather Squadron
Patrick AFB, Florida

August 1976

Approved for Public Release; distribution unlimited

HQ AIR WEATHER SERVICE (MAC)
UNITED STATES AIR FORCE
SCOTT AFB, ILLINOIS 62225

49 07 09 155

August 1976

REVIEW AND APPROVAL STATEMENT

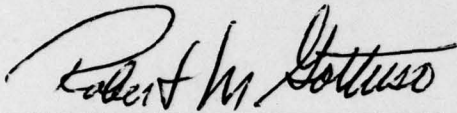
This report is approved for public release. There is no objection to unlimited distribution of this report to the public at large, or by DDC to the National Technical Information Service (NTIS).

This technical report has been reviewed and is approved for publication.



WILLIAM F. JOHNSON, Lt Col, USAF
Chief, Atmospheric Dynamics
Reviewing Officer

FOR THE COMMANDER



ROBERT M. GOTTUSO, Col, USAF
DCS/Aerospace Sciences
Air Weather Service

UNCLASSIFIED

SECURITY CLASSIFICATION OF THIS PAGE (When Data Entered)

REPORT DOCUMENTATION PAGE		READ INSTRUCTIONS BEFORE COMPLETING FORM
1. REPORT NUMBER 14 AWS-TR-76-264	2. GOVT ACCESSION NO.	3. RECIPIENT'S CATALOG NUMBER
4. TITLE (and Subtitle) 6 Satellite Meteorology.	5. TYPE OF REPORT & PERIOD COVERED 9 Technical report	
7. AUTHOR(s) 10 Henry W. Brandli Lt Col, USAF Detachment 11, 2 Weather Squadron Patrick AFB, Florida 32925	8. CONTRACT OR GRANT NUMBER(s)	
9. PERFORMING ORGANIZATION NAME AND ADDRESS Headquarters Air Weather Service (MAC) Scott AFB, Illinois 62225	10. PROGRAM ELEMENT, PROJECT, TASK AREA & WORK UNIT NUMBERS	
11. CONTROLLING OFFICE NAME AND ADDRESS Headquarters Air Weather Service (MAC) Scott AFB, Illinois 62225	12. REPORT DATE 11 August 1976	13. NUMBER OF PAGES
14. MONITORING AGENCY NAME & ADDRESS (if different from Controlling Office) 12 203p.	15. SECURITY CLASS. (of this report) Unclassified	
15a. DECLASSIFICATION/DOWNGRADING SCHEDULE		
16. DISTRIBUTION STATEMENT (of this Report) Approved for public release; distribution unlimited.		
17. DISTRIBUTION STATEMENT (of the abstract entered in Block 20, if different from Report)		
18. SUPPLEMENTARY NOTES		
19. KEY WORDS (Continue on reverse side if necessary and identify by block number) Meteorological Satellites Sun Synchronous Satellites Automatic Picture Transmission (APT) Satellites Applications Technology Satellites (ATS) (over)		
20. ABSTRACT (Continue on reverse side if necessary and identify by block number) This report describes the different types of meteorological satellites that are in operational use in the United States. Using examples of satellite imagery, both in the visible and infrared spectrums, the report shows how to identify various meteorological phenomena and various cloud types.		

DDC
RECEIVED
APR 9 1979
RECEIVED

DD FORM 1473 EDITION OF 1 NOV 65 IS OBSOLETE

UNCLASSIFIED

SECURITY CLASSIFICATION OF THIS PAGE (When Data Entered)

014 670

111

Gue

UNCLASSIFIED

SECURITY CLASSIFICATION OF THIS PAGE(When Data Entered)

19. Continued:

Defense Meteorological Satellite Program (DMSP)

Geostationary Satellites

SMS/GOES

ESSA

TIROS

Nimbus

Infrared Imagery

Visual Imagery

PREFACE

The author, who has worked almost exclusively with satellite meteorology since 1966, wrote this report while assigned as a Staff Meteorologist to the Air Force Eastern Test Range (AFETR), Patrick Air Force Base, Cocoa Beach, Florida. Meteorologists will naturally find this book useful. However, environmentalists, aerospace engineers, oceanographers, and hydrologists should find this treatise on satellite meteorology useful in their work. Forestry and public health people should find it beneficial also. Science students as well as everyday weather enthusiasts will find this book interesting.

Many people are responsible for the publishing of this report. Naming them all would take too much space and someone's name would probably be left out. To all those people, "Thank you." Special appreciation is also given to Technicolor, Inc., and its fine operating personnel at the AFETR; their excellent work is evident in the satellite photographs. The photographs in this report were mostly reproduced from original satellite images from the National Oceanic and Atmospheric Administration (NOAA), National Aeronautics and Space Administration (NASA), and Department of Defense (DOD) meteorological satellites.

The author wishes to especially thank Staff Sergeant Shirley Janes for her editing and indexing of the manuscript and Mrs. Alberta Terry for her typing of the manuscript.

ACCESSION for	
NTIS	White Section <input checked="" type="checkbox"/>
SDC	Buff Section <input type="checkbox"/>
UNANNOUNCED	<input type="checkbox"/>
JUSTIFICATION	
BY	
DISTRIBUTION/AVAILABILITY CODES	
Dist. and/or SPECIAL	
A	

79.04 09 155

TABLE OF CONTENTS

<i>Chapter</i>	<i>Title</i>	<i>Page</i>
	LIST OF FIGURES.....	ix
	LIST OF TABLES.....	xvi
1	METEOROLOGICAL SATELLITES	1
	Sun Synchronous.....	1
	ESSA	3
	NOAA.....	3
	Nimbus.....	3
	DMSP.....	3
	Geostationary.....	4
	ATS.....	4
	SMS/GOES.....	5
2	TYPES OF IMAGERY.....	12
	Visual.....	12
	Day Visual.....	12
	Night Visual	12
	Infrared	14
	Calibration.....	17
	Rectification and Normalization	19
	Stereographic Viewing and Movie Loops.....	19
	Vertical Temperature Profiles	22
	Other Meteorological Satellite Imagery and Data.....	22
3	CLOUDS.....	32
	Low-Level Clouds	32
	Stratocumulus	32
	Stratocumulus Lines.....	33
	Cumulus.....	33
	Cumulus Cloud Lines or Streets	33
	Stratus Fog	38
	Actiniform Clouds	38
	Lee Waves	41
	Billow and Invisible Low-Level Clouds.....	41
	Miscellaneous Cloud Lines.....	41
	Mid-Level Clouds.....	43
	High-Level Clouds.....	43
	Thunderstorms or Cumulonimbus Clouds	43
	Cirrus Clouds.....	48
	High-Level Billow Clouds.....	50
	High-Level Anomalous Cloud Lines	51
	Miscellaneous Phenomena.....	51
	Smog-Haze.....	51
	Dust.....	56
	Smoke.....	57

	Anomalous Gray Areas	59
	Aurora Borealis and Aurora Australis	59
4	WEATHER SYSTEMS	68
	Fronts	68
	Cold Fronts	68
	Warm Fronts and Occluded Fronts	68
	Sea-Breeze Fronts	74
	Squall Lines	75
	Severe Weather (Tornadoes)	75
	Lightning	77
	Vorticies	79
	Hurricanes, Typhoons, and Cyclones	80
	Troughs	89
	Positive Vorticity Advection Areas	91
	Cut-Off Lows	95
	Ridge Lines	95
	Screaming Eagles	101
	Easterly Waves	101
	Intertropical Convergence Zone (ITCZ)	103
5	WIND	105
	Low-Level Flow	105
	Stratocumulus/Cumulus Cloud Patterns	105
	Stratocumulus/Cumulus Streets or Lines	105
	Sea/Land Breeze	106
	Lee Waves	106
	Other Low-Level Phenomena	106
	High-Pressure Center	107
	Mid-Level Flow	109
	High-Level Flow	109
	Plume Blowoff	109
	Transverse Cloud Bands	110
	Wind Shear	110
	Jet-Stream Cirrus Shadow	110
	Billow and High-Level Lee-Wave Clouds	114
	Cirrus Streaks and Filaments	114
	Cloud Movement	117
6	EARTH SURFACE AND OTHER MISCELLANEOUS FEATURES	122
	Geology (Geologic Resources)	122
	Land Features	122
	Volcanoes	122
	Meteors	122
	Hydrology, Oceanology	132
	Rainfall	132
	Flooding	132
	Snow	132
	Ice	140
	Ocean Surface Temperatures & Features	140
	Wave Heights	147
	Fire Detection	147
	Other Phenomena	147

7	DATA PREPARATION AND PRESENTATION	162
	Preparation	162
	Mission and Data Type	162
	Ephemeris	162
	Synoptic Situation	162
	Contingency	162
	Gridding Devices	162
	Gridding	163
	Presentation	166
	Press Type	166
	Data Display	166
	REFERENCES AND BIBLIOGRAPHY	179
	LIST OF ABBREVIATIONS, ACRONYMS AND SYMBOLS	184
	INDEX	185

LIST OF FIGURES

<i>Figure</i>		<i>Page</i>
1.	Sun Synchronous Meteorological Satellites of the United States	1
2.	ESSA-8 Imagery Received on the 7th Anniversary of Its Launch (18 Dec 75)	2
3.	Diagram of ITOS/NOAA Satellite	3
4.	NOAA-3 Infrared Imagery (1 May 74)	4
5.	The DMSP Meteorological Satellite	5
6.	DMSP Infrared View of United States (9 Jan 76)	6
7.	Geostationary Meteorological Satellites in Orbital Schematic	7
8.	ATS-3 Visual Image of the Earth's Disk	7
9.	Schematic of SMS/GOES Satellite System	8
10.	Visual Photograph Received from SMS-1 (28 May 74)	8
11.	Infrared Photograph Received from SMS-2 (14 Feb 75)	9
12.	SMS/GOES-1 Visual Photograph (14 Feb 76)	10
13.	Synchronous Meteorological Satellite Sector over the Southeast United States (29 May 74)	13
14.	NOAA-4 Visual Image of Southeastern United States (1 Apr 76)	13
15.	Defense Meteorological Satellite Program (DMSP) Visual Image (11 Feb 74)	14
16.	An Expanded DMSP View of the Mississippi River and Delta (11 Feb 74)	15
17.	Nighttime Visible No-Moonlight DMSP Mosaic Over Russia	16

18.	Nighttime Visible Moonlight Scene over Most of the United States.....	17
19.	NOAA-4 VHRR Infrared Image (4 Feb 76).....	18
20.	Simultaneous Visual/Infrared Imagery from NOAA-2 (7 Oct 74).....	19
21.	DMSP VHR Image of the Eastern United States (23 Feb 76).....	20
22.	Schematic Showing Different Amounts of Infrared Radiation Emitted by Different Surfaces.....	21
23.	Simultaneous NOAA-2 Visual and Infrared Data With Temperature Conversion for Cloud Tops (21 Nov 73).....	21
24.	NOAA-3 VTPR Versus a Cape Canaveral Upper-Air Sounding.....	23
25.	Nimbus IV IDCS of Snow Melt on the Kamchatka Peninsula, USSR, during April and May 1970.....	27
26.	Nimbus IV IDCS and THIR of a Sahara Dust Storm Recorded on 21 Apr 70.....	28
27.	Nimbus IV DRIR and THIR Comparison for 25 May 71.....	28
28.	Nimbus V Daytime THIR Image Recorded over the Central U.S. on 3 Apr 74.....	29
29.	Nimbus V SCMR Nighttime Infrared Image Recorded over Florida and Cuba on 24 Dec 72.....	30
30.	A Comparison of Nimbus V THIR and ESMR Pictorial Data.....	31
31.	Nimbus V ESMR Taken 11 Jan 73.....	31
32.	A SMS Visual View Showing Stratocumulus in the Eastern Atlantic.....	32
33.	A SMS Infrared View of Low Stratocumulus Clouds with the Higher ITCZ Near the Equator.....	33
34.	A DMSP Visual View of Clouds Forming over the Atlantic as the Cold Air Moves Across the Warmer Water (18 Jan 74).....	34
35.	DMSP Infrared View of Stratocumulus Lines (12 Mar 76).....	35
36.	A DMSP VHR View of Florida with Cumulus Clouds (15 Jul 75).....	36
37.	DMSP Visual Image Showing Cumulus Clouds Behind a Cold Front in the North Pacific (10 Mar 70).....	37
38.	DMSP Visual View of Cumulus Cloud Lines North of South America (24 Jan 75).....	37
39.	ESSA-8 Visual Imagery showing fog and stratus in the Gulf of Mexico (2 Jan 74).....	38
40.	DMSP Infrared Photograph of Warm Clouds over Florida (3 Feb 76).....	39
41.	DMSP Visual Image Showing Fog in the San Joaquin Valley of Central California (27 Nov 72).....	39
42.	A SMS-1 Visual Image Showing Sea Fog in the Eastern Gulf of Mexico Off the Coast of Florida (31 Dec 74).....	40
43.	DMSP Visual Imagery of Actiniform Clouds.....	40
44.	DMSP Infrared Imagery of Actiniform Clouds.....	41
45.	DMSP Visual Image Depicting Low-Level Lee Waves in the Hawaiian Islands (22 Oct 70).....	42
46.	DMSP Visual Image Showing Lee Waves in the Appalachian Mountains (16 Apr 74).....	43

47.	DMSP VHR Imagery Showing Billow Clouds off the Coast of Texas (3 Apr 74)	44
48.	DMSP Visual Image of Anomalous Cloud Lines off the West Coast of the U.S.	45
49.	DMSP VHR Image Illustrating Cloud Lines around the Island of Hainan (6 Nov 72)	45
50.	DMSP Visual Image Illustrating "Bow Shock"	46
51.	DMSP VHR Image of the Cloud Lines left as a Thunderstorm Dissipates (5 Mar 73)	46
52.	DMSP Visual Photograph off the West Coast of the U.S. Showong an Anomalous Line in the Cloud Deck (11 May 73)	47
53.	DMSP Photograph of Altostratus in the Great Lakes Area (Nov 73)	47
54.	DMSP Visual over Europe Showing Middle Clouds (16 Aug 74)	48
55.	A DMSP Visual Image off the Mexican Coast showing the Plumes of Thunderstorm Cells (14 Jan 74)	49
56.	NOAA Simultaneous Visual and Infrared Photograph showing Thunderstorm Activity in a Cold Front and Squall Line (3 Apr 74)	50
57.	DMSP Visual Imagery of Hurricane Carmen (1 Sep 74)	51
58.	DMSP Infrared Display of Typhoon Rita (Jul 72)	52
59.	DMSP Visual and Infrared Photographs Illustrating the Importance of Corresponding Infrared Photographs (5 May 72)	52
60.	DMSP Nighttime Visual and Infrared Imagery of Thin Cirrus over Georgia (5 Dec 74)	53
61.	A SMS-1 Visual and Infrared Illustration of High Cirrus Clouds over Lower Stratocumulus (22 Nov 74)	54
62.	DMSP Visual Image of Several Cirrus-Cloud Patterns (23 Jan 74)	54
63.	DMSP and SMS-1 Visual and Infrared Photographs Showing Transverse Banding East of Florida (27 Jun 74)	55
64.	DMSP Visual Data of Low- and High-Level Billow Clouds (3 Apr 74)	56
65.	DMSP Visual Photograph of Unusual Cloud Lines Extending from the San Francisco Bay Area (11 May 73)	57
66.	High-Altitude Jet Airways Chart for the San Francisco Bay Area	57
67.	Smog along the East Coast of the U.S. on a Daytime DMSP Visual Presentation (30 Aug 73)	58
68.	SMS Visual Photograph of Haze off the Coast of the Eastern U.S. (25 Aug 75)	58
69.	SMS Visual Photograph of Haze and Haze Glint (26 Aug 75)	59
70.	ATS-3 Photographs Tracking a Dust Cloud from Africa to Barbados (29 Jun - 4 Jul 69)	60
71.	SMS Visual Photograph of Dust Layer in the Atlantic (8 Jul 74)	61

72.	DMSP Visual Photograph of Volcanic Smoke Plume on the Japanese Island of Kyushu (14 Dec 73)	61
73.	NOAA-3 VHRP Photograph of Smoke Emanating from a Fire in the Everglades (1 May 74)	62
74.	DMSP Visual Illustration of Both Reefs and Anomalous Gray Areas	63
75.	A DMSP Visual Image of Anomalous Gray Areas in the Hawaiian Islands (12 Sep 74)	63
76.	DMSP Visual Photograph of Anomalous Gray Areas (13 Nov 75)	64
77.	A Nighttime DMSP H Image of the Aurora Australis over the Southern Hemisphere (8 Sep 70)	64
78.	DMSP Nighttime HR Image of Aurora Borealis over Western Europe	65
79.	DMSP Nighttime Imagery over North America (18 Apr 74) with Solar Disk (14 Apr 74) Superimposed	67
80.	DMSP Imagery of a Cold Front Moving into Florida (28 Nov 73)	69
81.	DMSP Imagery of Cold Front Moving through Florida (29 Nov 73)	70
82.	DMSP Visual Photograph of a Rope Cloud (3 Apr 75)	71
83.	Surface Charts for 1700 GMT and 1800 GMT	71
84.	Charts from Cape Canaveral AFS WIND System	72
85.	NOAA-2 Infrared Image of a Shallow Cold Front South of Florida (27 Nov 72)	73
86.	SMS-1 Nighttime Infrared Photographs Illustrating the Development of a Vortex in the Atlantic (21 Jun 74)	73
87.	SMS-1 Visual Image of a Small-Scale Frontal System (15 Aug 74)	74
88.	NOAA-2 Infrared Image Depicting a Large-Scale Vortex	75
89.	Diagram of a Sea-Breeze Circulation	76
90.	SMS-2 Visual View of Sea-Breeze Front (3 Sep 75)	76
91.	DMSP Daytime Visual Photograph of a Squall Line through Northern Florida (8 Apr 74)	77
92.	DMSP Photograph of Tornado Area in Gulf of Mexico through Florida (31 Dec 75)	78
93.	Tornado Forecast Scheme	78
94.	NOAA-4 Infrared Imagery of a Frontal Area in the Midwest (27 Mar 75)	79
95.	DMSP Nighttime Visual Photograph of Lightning Flashes (14 Nov 72)	80
96.	DMSP Nighttime Visual Photograph Depicting Lightning Flashes in an Intense Cold Front (3 Apr 74)	81
97.	DMSP Simultaneous Visual and Infrared Photographs of a Vortex and Associated Frontal Systems (5 Dec 73)	82
98.	DMSP 0.62-km Resolution Visual Image of a Vortex in a Stratiform Low-Level Cloud Formation (11 May 73)	83
99.	DMSP Image of an Induced Small-Scale Vortex	84
100.	DMSP Day and Night Visual Data of a Developing Vortex over a 3-Day Period (24-26 Sep 74)	85
101.	Cyclone Patterns and Wind Speed	86

102.	ESSA-8 Visual Data of Tropical Storm Alice (1 Jul 73)	87
103.	ESSA-8 View of Hurricane Alice (3 Jul 73)	87
104.	DMSP Day and Night Visual Sequence of Hurricane Eloise (17-23 Sep 75)	88
105.	A DMSP VHR Photograph of Typhoon Betty in the Western Pacific (12 Aug 72)	89
106.	DMSP Visual Image of Typhoon Patsy (9 Oct 73)	90
107.	DMSP VHR Image of Typhoon Pamela (7 Nov 72)	90
108.	DMSP Night Visual and Infrared Imagery of a Typhoon in the Arabian Sea (29 Oct 71)	91
109.	DMSP View of a Southern Hemisphere Cyclone	92
110.	Diagram of Upper-Level Trough in Northern Hemisphere	92
111.	NOAA-3 Simultaneous Visual and Infrared Imagery of a Trough in conjunction with a Cold Front (14 Nov 74)	93
112.	SMS-1 View of a Trough off the Southern Coast of Florida (29 May 74)	94
113.	DMSP Nighttime Visual and Infrared Data Illustrating a Sharp Trough Line	94
114.	ATS-1 View of a PVA Maturing into a Frontal System (9-10 Mar 70)	95
115.	PVA East of Trough Line Near Florida (19 Jun 74)	96
116.	DMSP Visual Image of a Cut-Off Low (15 Aug 75)	97
117.	Diagram of Low-Level Ridge Lines	97
118.	Diagram of an Upper-Level Ridge Line	98
119.	DMSP Image of a Ridge Line Determined from Cumulus Cloud Lines (24 Mar 74)	98
120.	DMSP Visual Photograph of Sun Glint and Ridge Line (15 Aug 75)	99
121.	DMSP Night Visual of Moon Glint and Ridge Line (8 Nov 73)	99
122.	ATS Visual Photograph of High-Level Ridge Lines (11 Mar 70)	100
123.	DMSP Visual Image of a High-Level Ridge Line	100
124.	ATS-1 Photograph Depicting the "Screaming Eagles" Near the Hawaiian Islands (8 Mar 70)	101
125.	Expanded View of "Screaming Eagles" (8 Mar 70)	102
126.	DMSP Visual and Infrared Imagery of "Screaming Eagles" (9 Mar 70)	102
127.	DMSP Visual and Infrared Imagery of an Easterly Wave	103
128.	SMS Visual Image of ITCZ (27 Jun 74)	104
129.	SMS Infrared Imagery of ITCZ between South America and Africa (27 Jun 74)	104
130.	DMSP Visual Image of Low-Level Wind Flow in a "Closed Cell" Pattern (29 Oct 71)	106
131.	"Open Cell" Cumulus (19 Feb 73)	107
132.	DMSP View of Stratocumulus Lines off the Coast of New England (3 Oct 75)	108

133.	DMSP Night Visual View of Stratocumulus Lines off the Coast of Texas (23 Sep 75).....	108
134.	Cumulus Streets and Lines in the Atlantic (4 Dec 75).....	109
135.	Lee Waves over Southeast Asia (Mar 73).....	110
136.	DMSP Visual Photograph with High-Pressure Center (12 Dec 75).....	111
137.	Surface Chart for 12 December 1975.....	112
138.	Diagram of Plume Length Versus Wind Speed	112
139.	Plume Blowoff in Caribbean (24 Sep 75).....	113
140.	Cirrus Plumes Blowing Off CBs in Atlantic and Gulf of Mexico	113
141.	Plumes in an Intense Cold Front (27 May 73).....	114
142.	Transverse Banding Around Hurricane Gladys (2 Oct 75).....	115
143.	DMSP View of Transverse Banding South of Florida	115
144.	DMSP Infrared Photograph of a Wind-Shear Pattern (25 Jan 76).....	116
145.	DMSP Visual Photograph of Cirrus Shadow	116
146.	Jet Stream and Cirrus Shadow over Europe (10 Sep 74).....	117
147.	Lee Waves in the Rocky Mountains (6 Apr 74).....	118
148.	SMS-1 Visual Photograph of Cirrus Filaments (27 Dec 74).....	119
149.	Many Upper-Level Wind-Flow Indicators (24 Sep 74)	119
150.	DMSP Visual and Infrared Photographs of a Frontal System (28 Nov 73)	120
151.	Current and Forecast Positions of The Front	121
152.	Surface Position of Front (29 Nov 73).....	121
153.	Terrain Features of Montana and Wyoming (22 Aug 74)	124
154.	Mountains of Luzon (10 May 73)	125
155.	Mountainous Areas of Italy and Islands (13 Aug 74)	126
156.	Forests of Cyprus (Jan 72).....	127
157.	Fertile Nile River and Delta (6 Oct 73)	127
158.	Sand and Sand Dunes in Saudi Arabia	128
159.	No-Moonlight DMSP View of Volcano (28 Dec 70)	129
160.	Geometry of Volcanic-Produced Halo	130
161.	DMSP View of Meteor (20 Nov 74)	131
162.	DMSP Inverted Visual of Swollen Rivers (4 Feb 72).....	133
163.	Dendritic Snow in Turkey	134
164.	Snow and Cloud Cover Along West Coast of North America	135
165.	Snow in Hawaiian Islands.....	136
166.	Snow Depth and Coverage over Midwest (9 Feb 71)	137
167.	Snow Cover Extent and Depiction of Rivers, Highways and Cities (15 Jan 74)	138
168.	Snow Cover and Observed Snow Depth (22 Nov 75)	139
169.	NOAA-3 Visual and Infrared Imagery of Ice (15 Apr 75).....	141
170.	DMSP Infrared and Visual Imagery of Ice in Antartica	142

171.	DMSP Visual Image of Ice and Icebergs in Weddell Sea (24 Jan 74)	143
172.	DMSP Visual and Infrared Composite of Warm Eddies (20 Nov 75)	144
173.	DMSP Infrared Image of a Developing Shelf Water Vortex (24 Feb 76)	145
174.	DMSP Infrared Image of the Vortex (25 Feb 76)	146
175.	DMSP Infrared Images of a Warm Eddy (11 Apr 76)	148
176.	DMSP Infrared Image of a Cold Eddy (25 Feb 76)	149
177.	Composite Photograph of Japan and Fishing Fleet	150
178.	ATS View of Record Wave Heights in Hawaii (30 Nov - 1 Dec 69)	151
179.	Sun Glint off the Coast of New England (29 Apr 74)	151
180.	DMSP Nighttime Visual Photograph of Forest Fire (30 Apr 74)	152
181.	Simultaneous Visual and Infrared of Fire (30 Apr 74)	152
182.	DMSP Nighttime Visual of North American Lights	154
183.	Oil Fields of South America (26 Jan 74)	155
184.	Oil Fields of the Middle East (2 Apr 75)	156
185.	Oil Fields of Africa (19 Mar 75)	157
186.	Oil Fields of Australia (Oct 74)	158
187.	DMSP View of the Eclipse of the Sun (30 Jun 73)	159
188.	DMSP Infrared before Earthquake (23 Jan 76)	160
189.	DMSP Infrared after Earthquake (10 Feb 76)	161
190.	NOAA-3 Ephemeris and Plotted Satellite Ground Track	163
191.	Recommended Gridding Tools	164
192.	DMSP Visual Illustrating Daily Operational Use of Satellite Imagery (10 Sep 75)	166
193.	DMSP Nighttime Infrared Photograph Showing Similar Land and Water Temperatures (5 Jan 76)	167
194.	ESSA-8 Photographs Illustrating Every Degree of Gridding (27 Sep - 1 Oct 71)	168
195.	ESSA-8 Computer Gridding Error (9 Apr 74)	169
196.	SMS Computer Gridding Error (24 Dec 75)	169
197.	Gridding Error of 600 Nautical Miles	170
198.	Overlay Error of Southeast Asia Visual Imagery (21 Nov 70)	171
199.	Gridding Check Points Along Vietnam Coast (8 Apr 73)	172
200.	Example of Customized Lettersheet	173
201.	Transparent Data Display Using a Vertical Light Table	174
202.	ESSA-8 Imagery Display for a SKYLAB Mission	175
203.	Data Display for the Apollo-Soyuz Test Project (14-15 Jul 75)	176
204.	Unlettered DMSP Image (Nov 73)	177
205.	Lettered DMSP Nighttime Visual Image of Japan (Nov 73)	178

LIST OF TABLES

<i>Table</i>		<i>Page</i>
1.	U.S. Applications Satellites Weather Observation	11
2.	Nimbus III Meteorological Experiments	24
3.	Nimbus IV Meteorological Experiments	25
4.	Nimbus V Experiments	26
5.	Important Emissions in Auroral Display	66
6.	DMSP Nonmeteorological Applications	123

Chapter 1

METEOROLOGICAL SATELLITES

There are basically two types of meteorological satellites: sun synchronous and geostationary. Both systems provide a wide variety of data that can be used by meteorologists in their day to day operations.

Sun Synchronous Satellites

The low-level sun synchronous satellite is one type of meteorological satellite whose photographs can be used by meteorologists. A sun synchronous satellite always passes over the earth's equator at the same sun time on each of its orbits. All sun synchronous satellites are polar orbiting (satellite passes over both of the poles) and see every location of the earth twice a day at the same approximate time. For example, a 9 a.m. National Oceanic and Atmospheric Administration (NOAA) meteorological satellite will view New York (i.e., have New York somewhere on the photo) at approximately 9 a.m. and 9 p.m. The paths of the NOAA meteorological sun synchronous satellites (ESSA, ITOS/NOAA), the National Aeronautics and Space Administration (NASA) meteorological sun synchronous satellites (Nimbus), as well as those of the Department of Defense (DMSP) are shown in Figure 1.

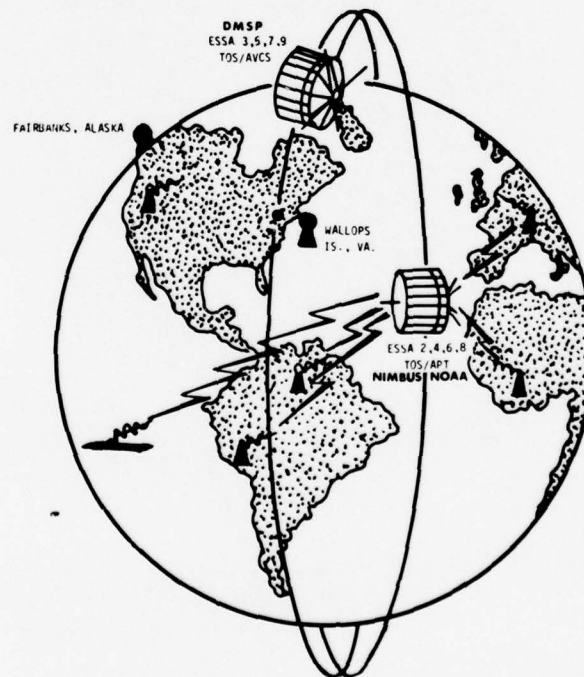


Figure 1. Sun synchronous meteorological satellites of the United States (NSSDC, [84].

ESSA-8

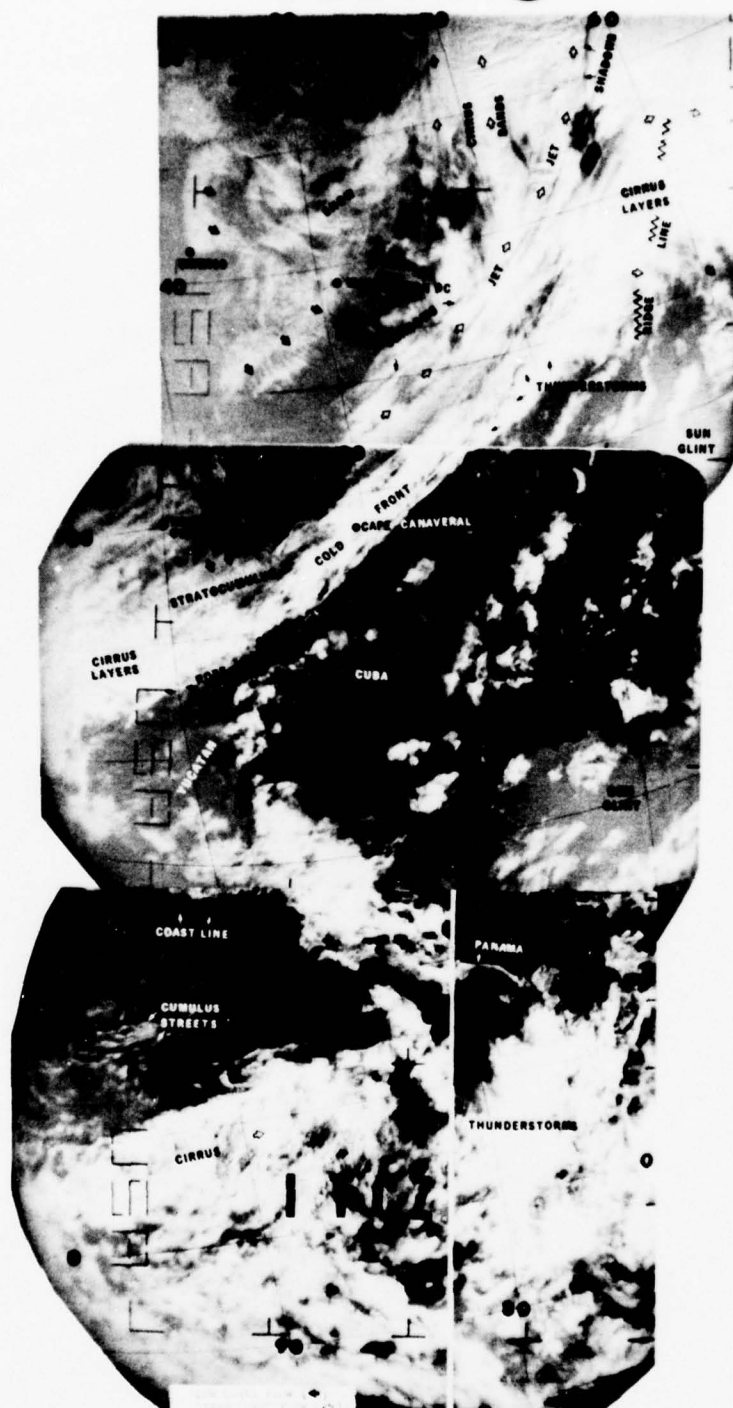


Figure 2. ESSA-8 imagery received on the 7th anniversary of its launch (18 Dec 75).

a. **ESSA.** The ESSA series was the last of the Automatic Picture Transmission (APT) satellites. The APT subsystem consisted of a camera and FM transmitter designed to broadcast television pictures of the cloud cover below. Transmission was automatic and could be read out worldwide by anyone who had the proper equipment.

Each satellite in the series was launched with a planned usable life of 6 months. However, the average life span of the satellites was 2 years. ESSA-8 surpassed even that average with over 7 years of usable data (see Figure 2).

b. **NOAA.** The Improved Tiros Operational Satellites (ITOS) are designated NOAA satellites after successful launch. Each NOAA satellite contains a scanning radiometer with daytime and nighttime capability from a viewing platform of approximately 1400 km. This image taking is done one line at a time and all the lines together form the image. A diagram of the NOAA satellite containing these radiometers is shown in Figure 3. An example of NOAA imagery is seen in Figure 4.

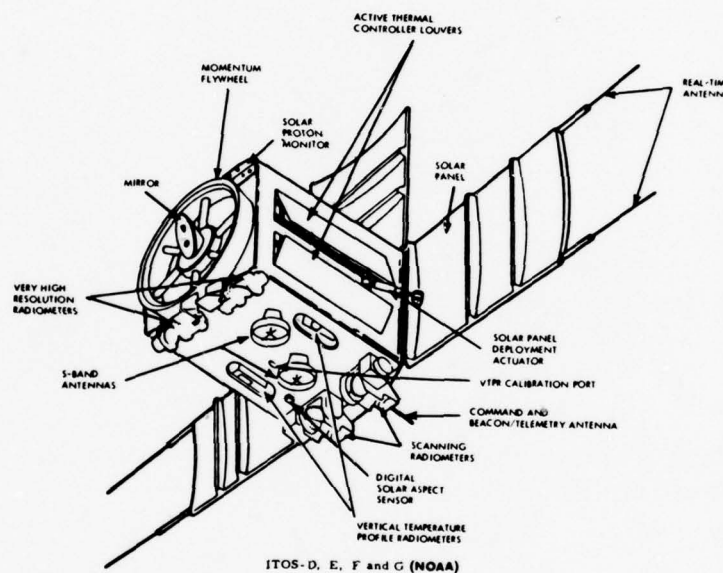


Figure 3. Diagram of ITOS/NOAA satellite (NSSDC, [84]).

c. **Nimbus.** The Nimbus satellite series are research and development spacecraft designed for the testing of advanced systems for the sensing and collecting of meteorological data. Nimbus was the first meteorological satellite series capable of providing both daytime and nighttime coverage of the earth on a daily basis. A multitude of sensors provided measurements of many parameters including vertical soundings of temperature and moisture from around the globe (NSSDC, [84]).

d. **DMSP.** The Department of Defense also operates a sun synchronous meteorological satellite under the Defense Meteorological Satellite Program (DMSP). Each DMSP satellite orbits at approximately 800 km and contains sensors for both day and night visual, near infrared, and infrared viewing. The satellites collect data continuously, scanning an area approximately 3000 km wide. The final product is either in computer program format or film product directly usable for imagery analysis. Operationally, there are usually two satellites available; an early morning ascending mode (0700-0800 local), and a noontime ascend-

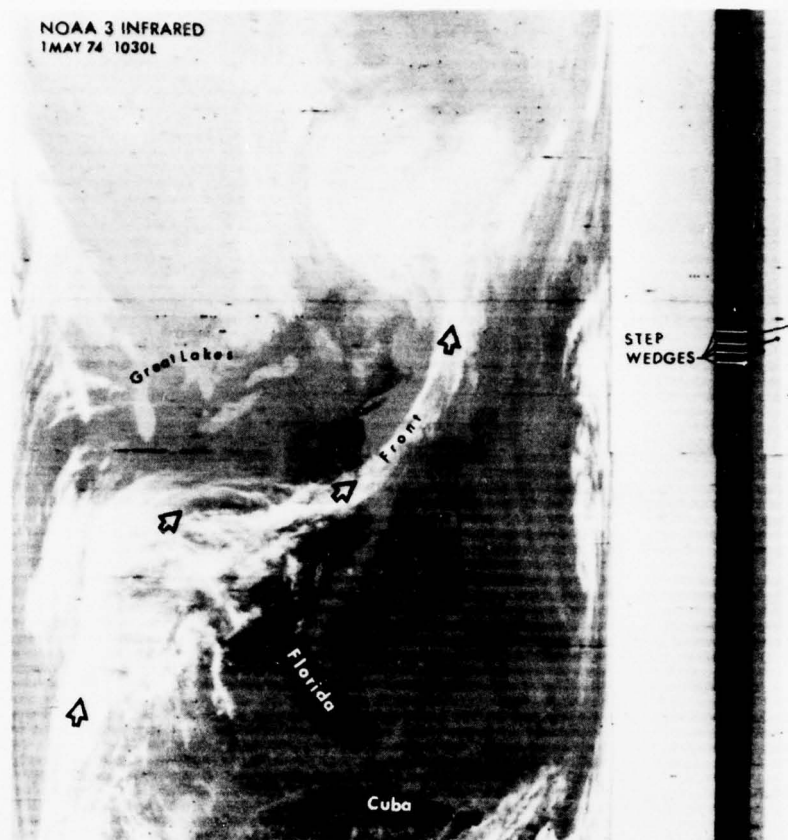


Figure 4. NOAA-3 infrared imagery (1 May 74).

ing node (1130-1230 local). An actual DMSP satellite is depicted in Figure 5. Figure 6 is an example of the imagery received from the DMSP satellite.

Geostationary Satellites

Another type of meteorological satellite is the geostationary satellite. A geostationary satellite is in equatorial orbit synchronized in period with the rotation of the earth. At an altitude of approximately 35,600 km, its orbital period is 24 hours so it appears to hover above one spot on the earth. Present and future plans for the location of geostationary meteorological satellites are shown in Figure 7.

Some day a satisfactory global coverage of the earth might be achieved by using a combination of geostationary and sun synchronous satellites. The geostationary satellites could relay data received from the sun synchronous satellites to those points of the earth not in direct view of the polar satellites (Fishlock, [48]).

a. **ATS.** The Application Technology Satellites (ATS) with meteorological sensors scanned the earth's disks from orbits over the equator at 151°W longitude (ATS-1) and 48°W longitude (ATS-3). After the ATS-3 reached its initial position, the satellite position was varied between 45° and 95°W longitude in support of meteorological operations. Both of the sensors on the ATS satellites covered nearly one-sixth the earth's surface area using sensors operating in the visible spectrum only. Routine operation of the ATS spin-scan cameras has been completely terminated. However, both the ATS-1 and ATS-3 satellites continue to make weather facsimile (WEFAX) transmissions. An example of ATS-3 data is shown in Figure 8.

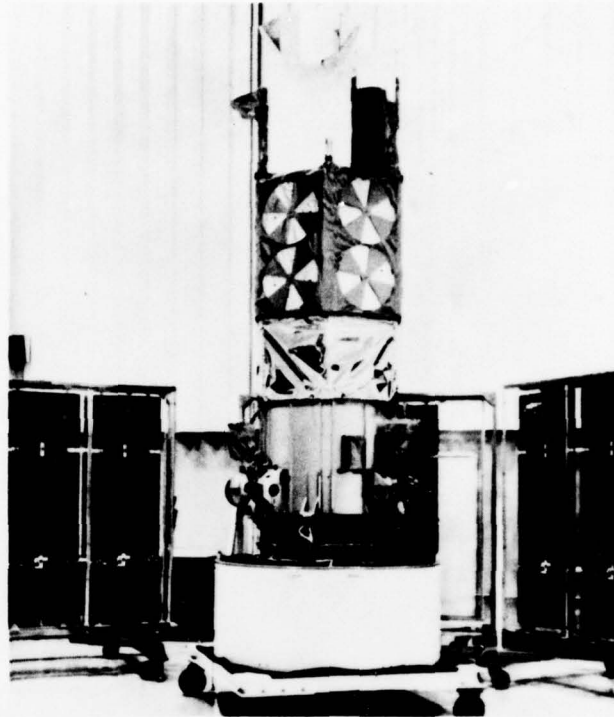


Figure 5. The DMSP meteorological satellite (USAF photo).

b. **SMS/GOES.** The geostationary satellite system, currently in use, is the Synchronous Meteorological Satellite (SMS). There are three satellites in geosynchronous equatorial orbit; SMS-1, SMS-2, and GOES-1. The first two vehicles served as prototypes for the Geosynchronous Operational Environmental Satellite (GOES). SMS-1 and SMS-2 were initially positioned at 85°W longitude and 95°W longitude, respectively. GOES-1 is currently positioned at 75°W longitude, replacing SMS-1. After the final positioning of GOES-1, SMS-1 was moved to 105°W and placed on operational standby to serve as an in-orbit backup. SMS-2 was moved to 135°W to serve as the western operational satellite. All three satellites are equipped with a visible and infrared radiometer capable of taking both day and night pictures. However, the visible spectrum is limited to day only. These sensors can take both full and partial pictures of the earth's disk. Data from the SMS/GOES is transmitted every 30 minutes. A schematic of the SMS/GOES is shown in Figure 9.

Photographs from SMS-1, SMS-2, and GOES-1 are shown in Figures 10, 11, and 12, respectively. A list of United States meteorological satellites, excluding Department of Defense vehicles, is shown in Table 1.

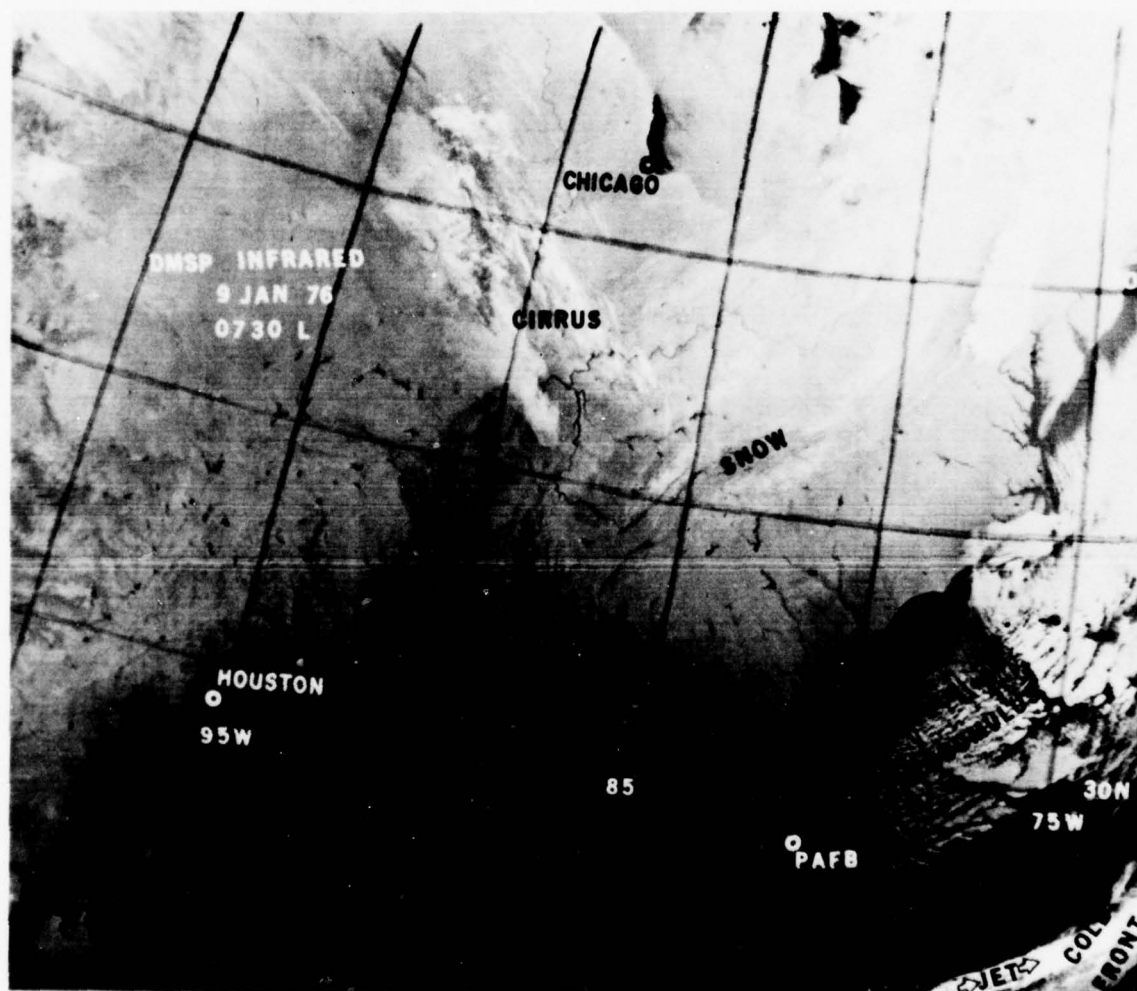


Figure 6. DMSP infrared view of United States (9 Jan 76).

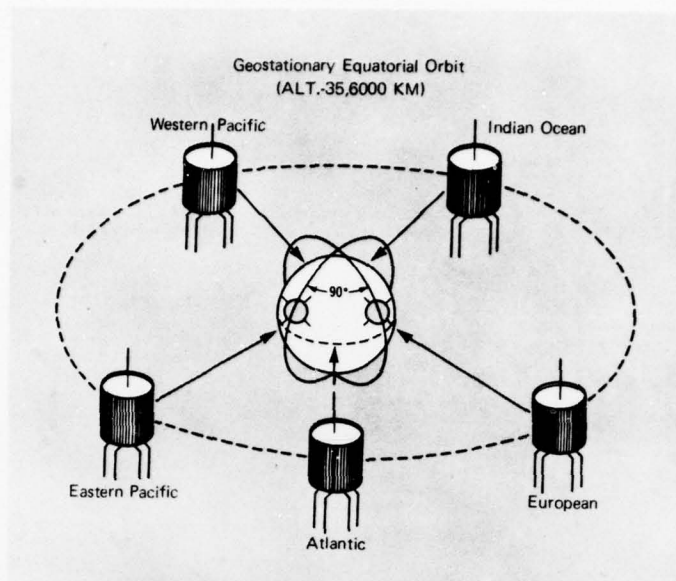


Figure 7. Geostationary meteorological satellites in orbital schematic (NSSDC, [84]).

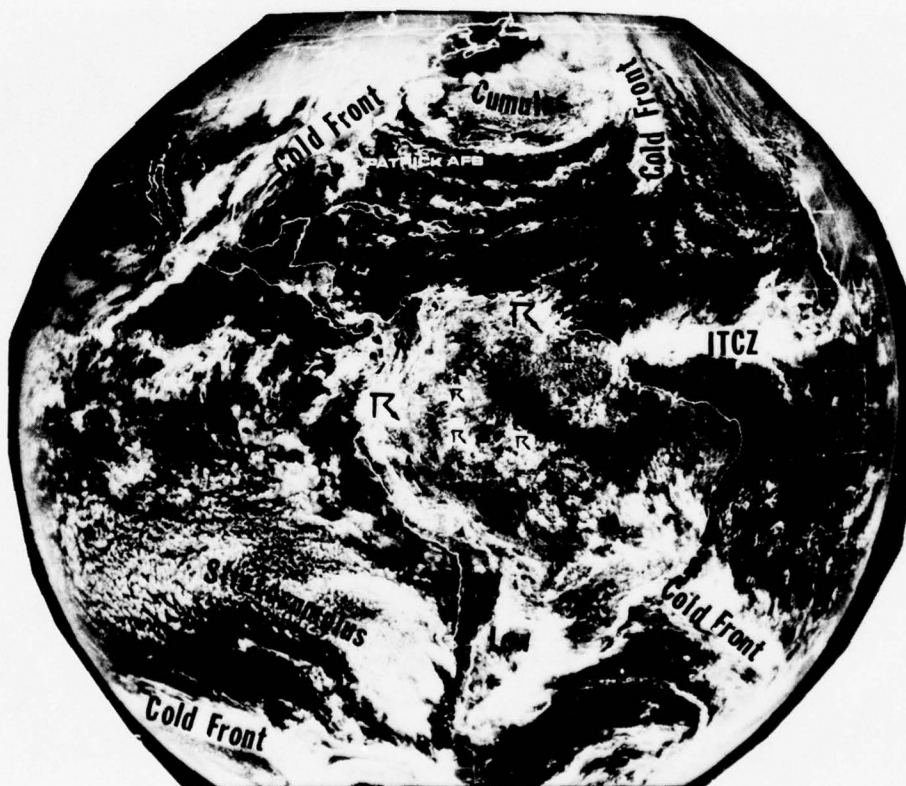


Figure 8. ATS-3 visual image of the earth's disk (date unknown).

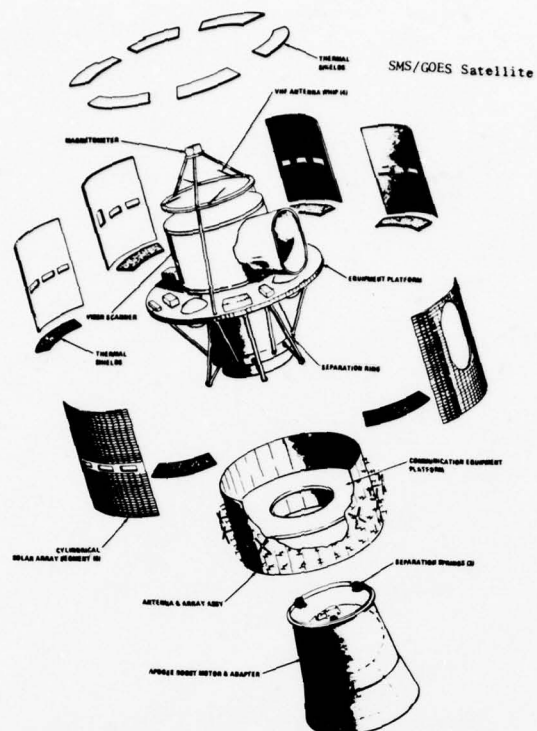


Figure 9. Schematic of SMS/GOES satellite system (NSSDC, [84]).

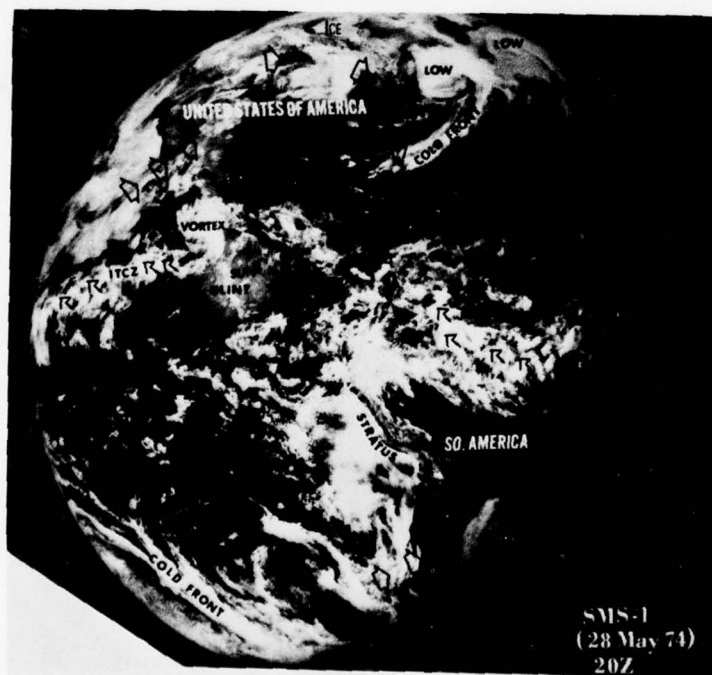


Figure 10. Visual photograph received from SMS-1 (28 May 74).

13:00 045:75 22-A 0006-1640 4X4 IR IMAGE

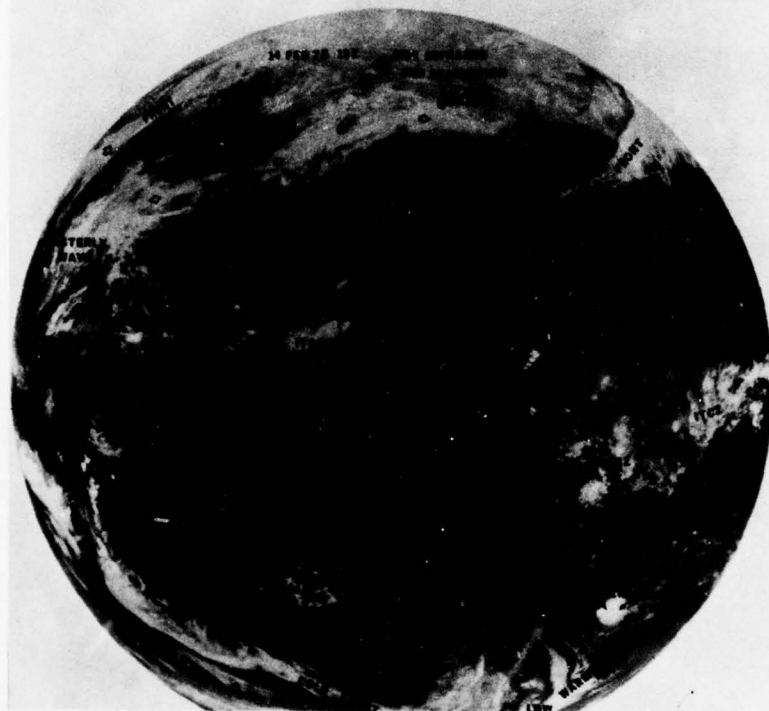


Figure 11. Infrared photograph received from SMS-2 (14 Feb 75).

↑ 16:00 14FE76 13A-2 00191 19141 WC1

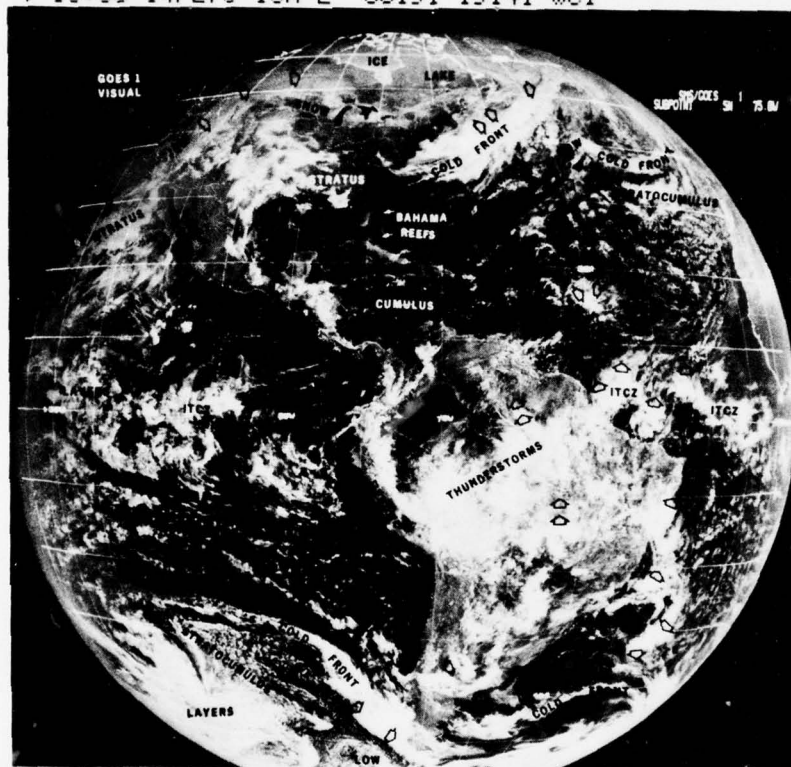


Figure 12. SMS/GOES-1 visual photograph (14 Feb 76).

Table 1. US.S Applications Satellites—Weather Observation (NSSDC, [84]).

<i>Date</i>	<i>Name</i>	<i>Launch Vehicle</i>
01 Apr 60	Tiros I	Thor-Able
23 Nov 60	Tiros II	Thor-Delta
12 Jul 61	Tiros III	Thor-Delta
08 Feb 62	Tiros IV	Thor-Delta
19 Jun 62	Tiros V	Thor-Delta
18 Sep 62	Tiros VI	Thor-Delta
19 Jun 63	Tiros VII	Thor-Delta
21 Dec 63	Tiros VIII	Thor-Delta
28 Aug 64	Nimbus I	Thor-Agena B
22 Jan 65	Tiros IX	Thor-Delta
02 Jul 65	Tiros X	Thor-Delta
03 Feb 66	ESSA-1	Thor-Delta
28 Feb 66	ESSA-2	Thor-Delta
15 May 66	Nimbus II	Thor-Agena B
02 Oct 66	ESSA-3	Thor-Delta
06 Dec 66	ATS-1	Atlas-Agena D
26 Jan 67	ESSA-4	Thor-Delta
20 Apr 67	ESSA-5	Thor-Delta
05 Nov 67	ATS-3	Atlas-Agena
10 Nov 67	ESSA-6	Thor-Delta
16 Aug 68	ESSA-7	Thor-Delta
15 Dec 68	ESSA-8	Thor-Delta
26 Feb 69	ESSA-9	Thor-Delta
14 Apr 69	Nimbus III	Thor-Agena
23 Jan 70	ITOS-1 (Tiros M)	Thor-Delta
08 Apr 70	Nimbus IV	Thor-Agena
11 Dec 70	NOAA-1 (ITOS-A)	Thor-Delta
15 Oct 72	ITOS-D (NOAA-2)	Delta
10 Dec 72	Nimbus-V	Delta
07 Nov 73	ITOS-F (NOAA-3)	Delta
17 May 74	SMS-1	Delta
15 Nov 74	ITOS-G (NOAA-4)	Delta
06 Feb 75	SMS-2	Delta
12 Jun 75	Nimbus VI	Delta
10 Oct 75	GOES-1	Delta
Jul 76	ITOS-E2 (NOAA-5)	Delta

Chapter 2

TYPES OF IMAGERY

There are basically two types of meteorological satellite imagery, visual and infrared. The visual photographs from satellites depict what we would see if we were on a satellite looking down and took a black and white photograph. Infrared sensors "see" temperatures and temperature differences (i.e., warm or cold land, water, and clouds at different height levels).

Visual

The visual sensors on board the operational meteorological satellites provide a wide range of spectral intervals. The human eye sees light in the wave lengths of 0.4 to 0.7 microns. NOAA currently uses an interval of 0.5 to 0.7 microns in the visual range. An expanded spectral interval is carried on board the DMSP satellites. This satellite "sees" in the visible and near infrared with a range of 0.4 to 1.1 microns. This increased sensitivity allows for better land and water contrast, cloud detail, and sensing of the aurora. The National Oceanic and Atmospheric Administration (NOAA) plans to use this expanded viewing interval on future meteorological satellites (NSSDC, [85]). Throughout the remainder of the report, the term "visual" will imply that the satellite image was taken at least in part in the visible spectrum.

a. Day Visual. The most commonly used camera/sensor on board meteorological satellites is one which provides black/gray/white visible photographs. Different gray shades correspond to scene information. White can be clouds, snow, ice, and even sand, similar to what the human eye sees. Clouds of varying heights or thickness, and/or vegetation can appear as shades of gray to black to white.

The newest SMS/GOES satellite takes day visual photographs of the earth's disk every 25 minutes. These visual disks have a resolution of 1, 2, and 8 km at the subpoint (a point on the earth directly below the satellite at photo time). The resolution (i.e., 1 or 2 km) of a satellite image simply means that any clouds or ground elements as small as 1 or 2 km across can be detected. In addition to the full disks, the SMS/GOES can take sectors of the earth disk with resolutions of 1, 2, 4, and 8 km. An example of an SMS sector taken over the southeastern United States shortly after the SMS was placed in geosynchronous orbit is shown in Figure 13.

This 1-km sector contains a wealth of meteorological information. Thunderstorms (⚡), low-level cumulus clouds, low-level wind flow (➡), and high-level wind flow (↗), are just some of the data labeled on the photographs. Sectors such as this every half-hour aid the meteorologist in forecasting cloud movement, development, and dissipation (Brandli, et. al., [11]).

The sensors on board NOAA-3 and NOAA-4 provide pictures with a resolution of 1 and 4 km in the visible channel. Figure 14 is a NOAA-4 4-km resolution visual photograph of the southeastern United States and surrounding waters.

The DMSP satellite system operates with two visual data channels. The very high resolution (VHR) visual channel has a resolution of 0.62 km. The high resolution (HR) visual channel has a resolution of 4 km. However, the very high resolution visual channel operates only during or near daylight. Figure 15 is a DMSP 0.62-km resolution photograph of the southeast United States. An expanded photograph of the marked area is seen in Figure 16. This detailed photograph contrasts the Mississippi River and surrounding surface variations.

b. Night Visual. In addition to daytime visual imagery, which shows white and gray clouds, the Department of Defense's meteorological satellite (DMSP) also takes nighttime visual imagery (HR). This low light sensor sees by the light of the moon. If there is moonlight, the clouds will be illuminated. If there is no moonlight, only city lights and other phenomena, such as the aurora will be depicted. Examples of

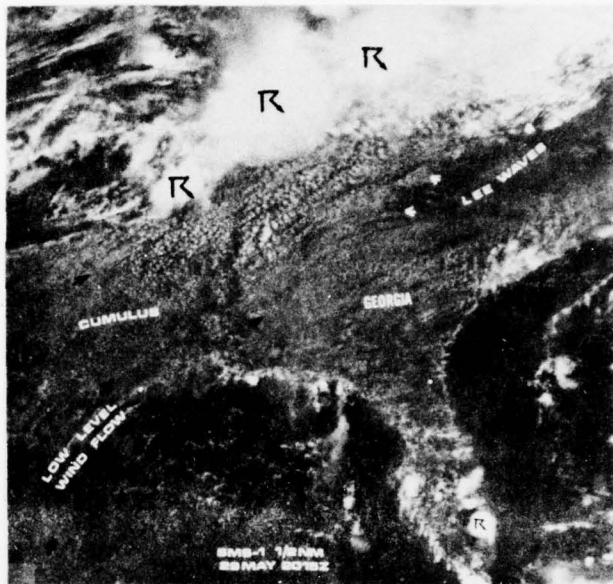


Figure 13. Synchronous meteorological satellite sector (1 km resolution) over the southeast United States (29 May 74).

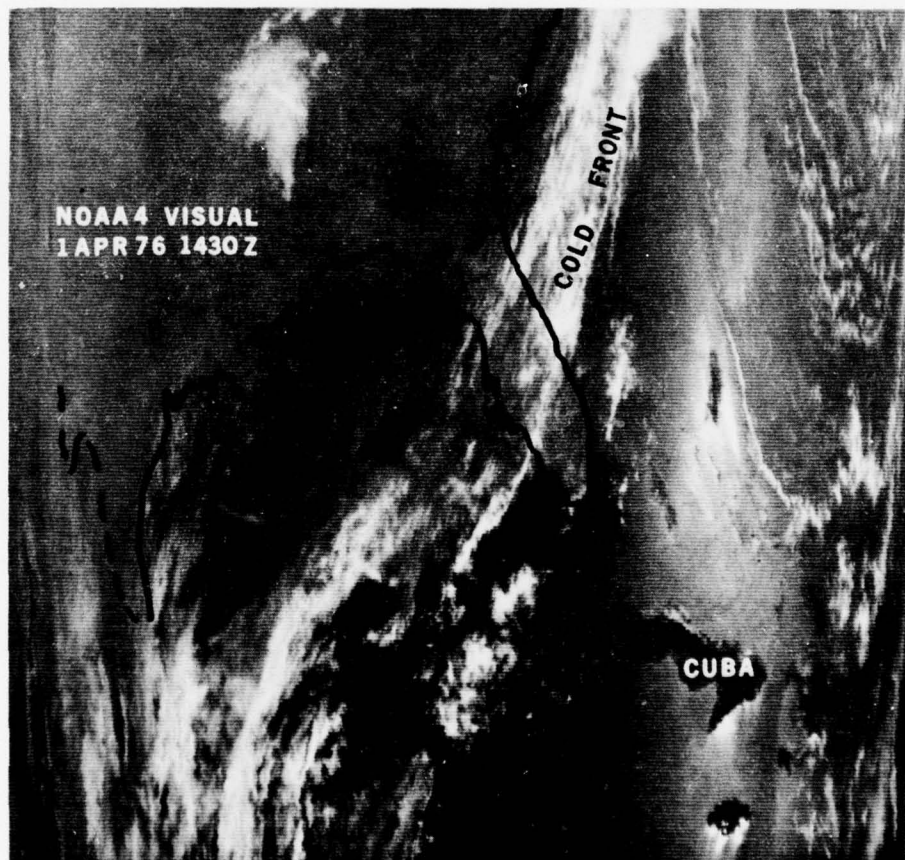


Figure 14. NOAA-4 visual image of southeastern United States (1 Apr 76).

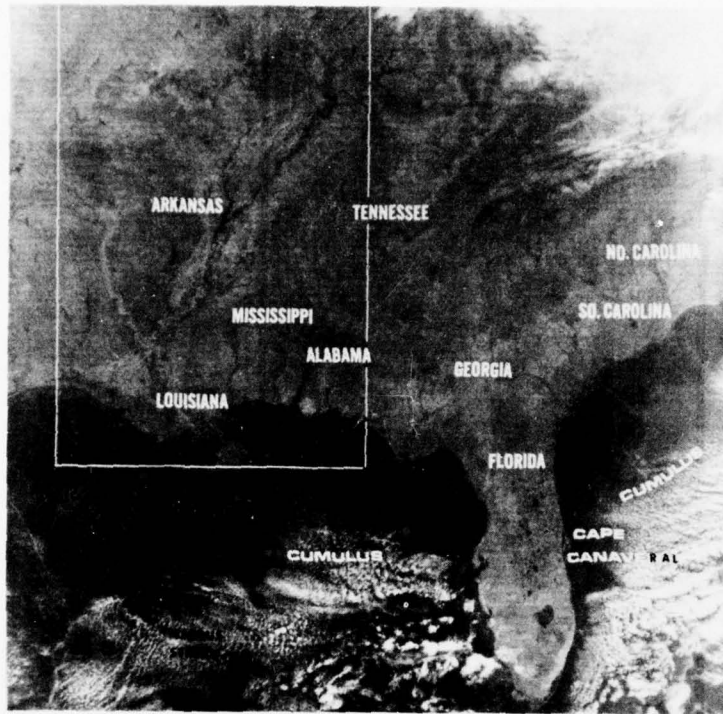


Figure 15 Defense Meteorological Satellite Program (DMSP) visual image (11 Feb 74).

this product are shown in Figure 17 and Figure 18. These illustrations provide graphic examples of nighttime images taken near local midnight. City lights, auroral displays, volcanoes, oil and gas field fires, and forest fires are some of the phenomena that can be detected by this radiometric sensor of the DMSP (Brandt, [10]). This high-resolution radiometer of the DMSP system also "sees" in the spectral interval of 0.4 to 1.1 microns. Therefore, the information displayed in these nighttime images provides important sub-visual and supervisual events (see Chapter 6). The DMSP satellites record imagery at a map scale of 1:7,500,000 or 1:15,000,000.

Infrared

Currently, all operational meteorological satellite systems take infrared pictures. In meteorological infrared photographs, the pictures are usually processed to show high cold clouds as white, low-level clouds as gray, and hot land or water as black. This scheme can be reversed or color film can be used to illustrate various features, including ocean currents. This latter technique, however, is expensive. In this report, black, gray, and white infrared photographs will be used with black as hot or warm, and white as cool or cold, relatively speaking.

Thermal infrared viewing is usually done in an interval of 8 to 13 microns. NOAA and SMS/GOES use 10.5 to 12.5 microns. The DMSP utilizes the full 8 to 13 microns. The difference depends on temperature range. With the increased range, certain atmospheric contaminants, such as aerosols and particulate matter, are introduced.

The infrared instruments carried on NOAA satellites are the scanning radiometer (SR), which provides pictures with a resolution of 8 km, and the very high resolution radiometer (VHRR), which provides pictures with a 1-km resolution. Figure 19 is an infrared VHRR image from NOAA-4.

One of the main advantages of infrared satellite data is the ability to make subjective comparisons between infrared and visual information to produce estimations of cloud heights. The infrared and visual data from Figure 20 provide several excellent examples of cloud heights by subjective comparison.

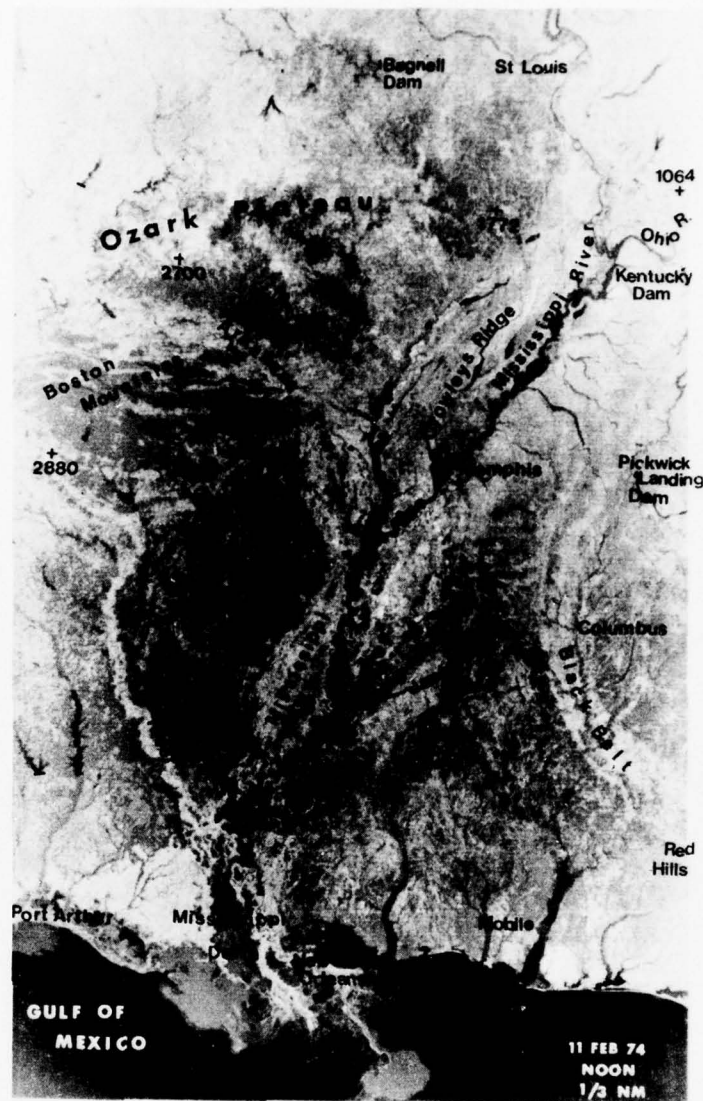


Figure 16. An expanded DMSP view of the Mississippi River and Delta (11 Feb 74).

In Figure 20 the visual data shows extensive cloud cover over Florida which could be interpreted as being convective activity related to the low-pressure center located east of the North Carolina coast. A comparison with the infrared data shows that the clouds over Florida are quite warm and extremely difficult to detect, implying that the cloud tops are low and the cloud type is stratiform. These stratus clouds were verified by pilot reports which gave overall cloud tops over Florida at 1000 to 1400 meters. A second area of interest is the low-cloud pattern ahead of the active cold front that extends from Arkansas to New England. On the visual picture, a bright area of clouds associated with the front extends from Arkansas to West Virginia. An examination of the infrared picture shows that the clouds are dark gray, thus implying low cloud tops. A third area of interest is the cloud pattern related to the jet stream located over the Midwestern States. In the visual picture, the clouds appear as gray and could be related to low clouds, either cumulus or altocumulus. The infrared data shows the cloud pattern to be bright white implying high cold clouds with tops at the cirrus level.

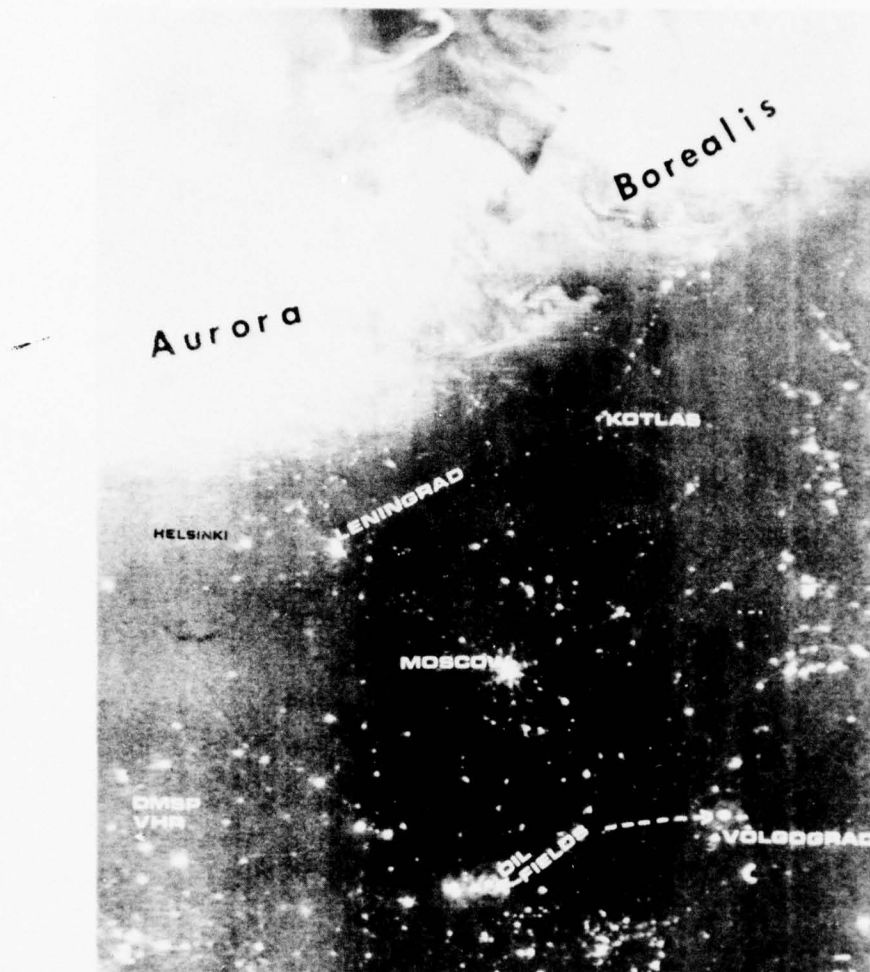


Figure 17. Nighttime visible no moonlight DMSP mosaic over Russia (date unknown).

SMS/GOES satellites also contain infrared sensors. The infrared instrument system on these satellites is the spin-scan radiometer (VISSR) which provides 8-km resolution. This system does not process infrared sectors as does the visible channel.

The DMSP system has two infrared channels. Very high resolution infrared (VHR) photos have a resolution of 0.62 km and the high resolution infrared (I) photographs have a resolution of 4 km. The system is configured in such a way that there are two options in requesting imagery: a combination of VHR, HR, and I; or a combination of VHR, HR, and I. VHR data are not available when VHR data are being sensed. These infrared products depict emitted thermal energy from 310°K to 210°K. Flexibility allows the display of from 2 to 64 gray shade steps with each step representing 1°K to 100°K intervals. The most common settings for determining emission temperatures are four temperature values set to give four distinct gray shades. For example, settings at 280°K, 270°K, and 260°K result in four shades. Temperatures greater than 280°K appear black on the photograph, those between 270°K and 280°K appear dark gray, those between 260°K and 270°K appear light gray, and those less than 260°K appear white (Dickinson, et. al., [39]).



Figure 18. Nighttime visible moonlight scene over most of the United States (date unknown).

Figure 21 is a WHR photograph of the eastern United States. The temperature range of this picture is 290°K (black) to 240°K (white). Cloud detail and land and water contrasts stand out very clearly.

a. Calibration. Since the temperature of the atmosphere usually decreases with increasing altitude, the height of cloud tops can be determined from their temperatures. The temperatures obtained relate to the temperatures one would get with a thermometer. The difference is dependent upon the sensor and its viewing path. Systematic corrections are not difficult to calculate if one does not try to be overly precise. Just knowing cloud tops are high or low is an achievement in itself. Different surfaces or clouds will emit different amounts of infrared radiation. A schematic showing the amount of radiation is shown in Figure 22.

Infrared calibration varies with each satellite. Near the subpoint, most sensors record 4° to 9°C colder temperatures than the land, water, or low-cloud tops in the mid-latitudes. The 9°C correction is for the DMSP radiometer (Dickinson, et. al., [39]), and the 4°C correction is for the NOAA radiometer (Brandli, et. al., [25]). Once computed, the corrections are good for any data from their respective satellite and/or sensor. Of course, these corrections to actual temperatures are for the subpoint of the satellite and ap-



Figure 19. NOAA-4 VHIRR infrared image (4 Feb 76).

proximately 800 km either side of the subpoint. As the radiometer path length increases, or as you approach the edge of the imagery, these corrections will double. Low cloud tops will be overestimated by 900 to 1500 meters. The reverse is usually true for high clouds, i.e., infrared temperatures will indicate tops are 1500 meters lower than they really are. High clouds are underestimated because the thermal emissions detected by radiometers usually are from land or thicker cloud emissions below the thin high cloud. These warmer radiating land and/or clouds tend to cause a false cloud top below the actual high cloud tops.

Figure 23 is a simultaneous visual and infrared picture from NOAA-2. The infrared temperatures are shown on a step wedge below the infrared imagery. By using this wedge and/or a densitometer, cloud/land temperatures can be determined. In the example, cloud-top temperatures of -64°C were measured in the Florida Panhandle and Gulf of Mexico. These tops were computed and verified to be near 16,000 meters.

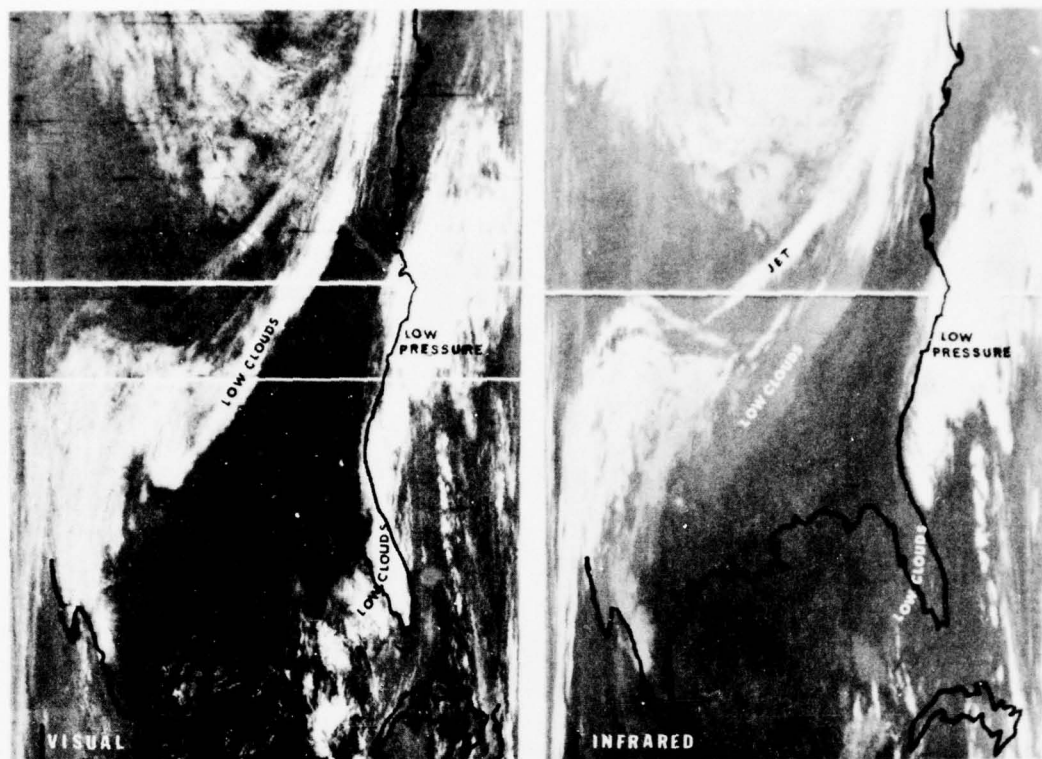


Figure 20. Simultaneous visual/infrared imagery from NOAA-2 (7 Oct 74).

Rectification and Normalization

In gridding and viewing some of the newer scanning radiometer imagery, difficulty can be encountered because the data is not rectified. For example, the horizon is presented on the edges of the photograph. This causes significant distortion which makes large gridding errors possible. Also, the altitude variability of polar-orbiting satellites as well as wobbly geostationary vehicles moving in a figure "8" pattern cause some difficulty in geographical positioning. The DMSP satellite images are already rectified and normalized. In addition, altitude compensation can be incorporated into the data for easy gridding with one grid normalized for 800 km (Dickinson, et. al., [39]).

Stereographic Viewing and Movie Loops

With the original Automatic Picture Transmission (APT) photographs which overlapped at the top and bottom, some meteorologists used stereo viewing to examine cloud structure. The newer satellites, such as NOAA, have two cameras on board (the second camera is a backup). Some investigators have turned on both visual cameras to achieve a 3-D effect (Bristor and Pichel, [31]).

Movie loops originally evolved from ATS-1 and ATS-3 views of the Eastern and Western Hemispheres every half-hour. Movie frames were made from the visual imagery of the earth (there were no infrared sensors aboard these early satellites). These remarkable movies followed the sun's terminator across the earth. The progression of cloud systems on these movie loops have been used by forecasters as well as instructors to show large-scale meteorological phenomena. Of course, continuity was broken as the sun set. Sometimes, inaccurate gridding of the photographs created false movements and development (see Chapter 7).

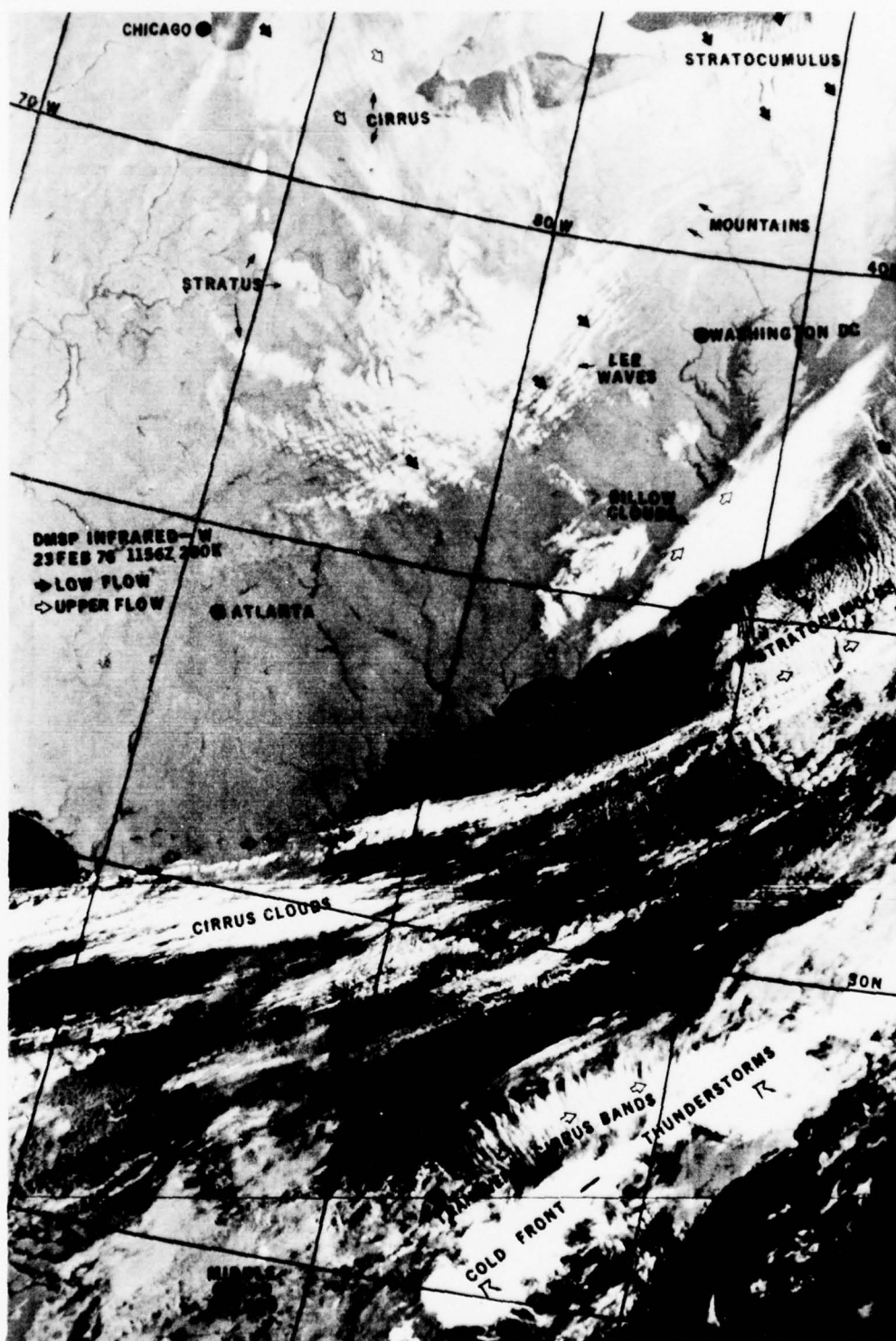


Figure 21. DMSF WHR image of the eastern United States (23 Feb 76).

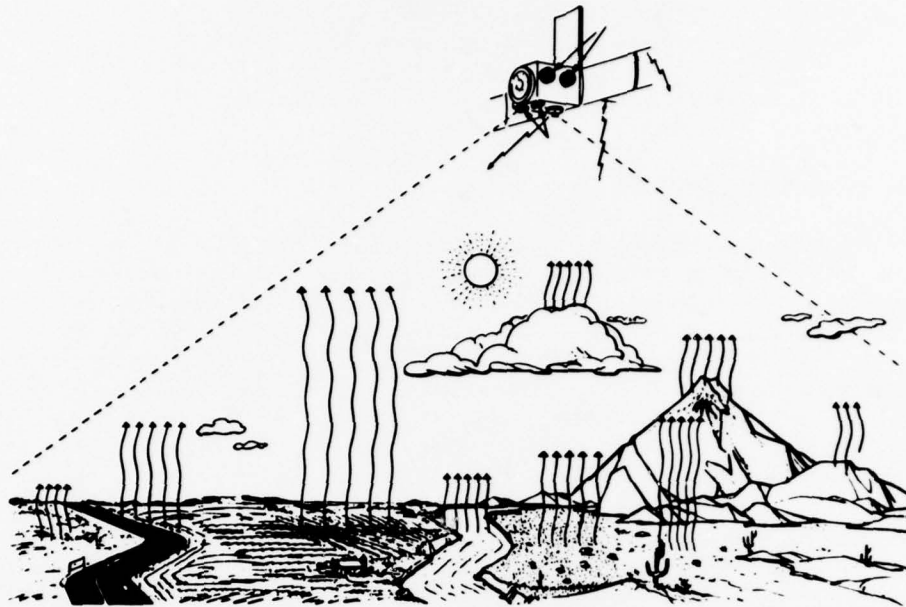


Figure 22. Schematic showing different amounts of infrared radiation emitted by different surfaces (Corliss, [36]).

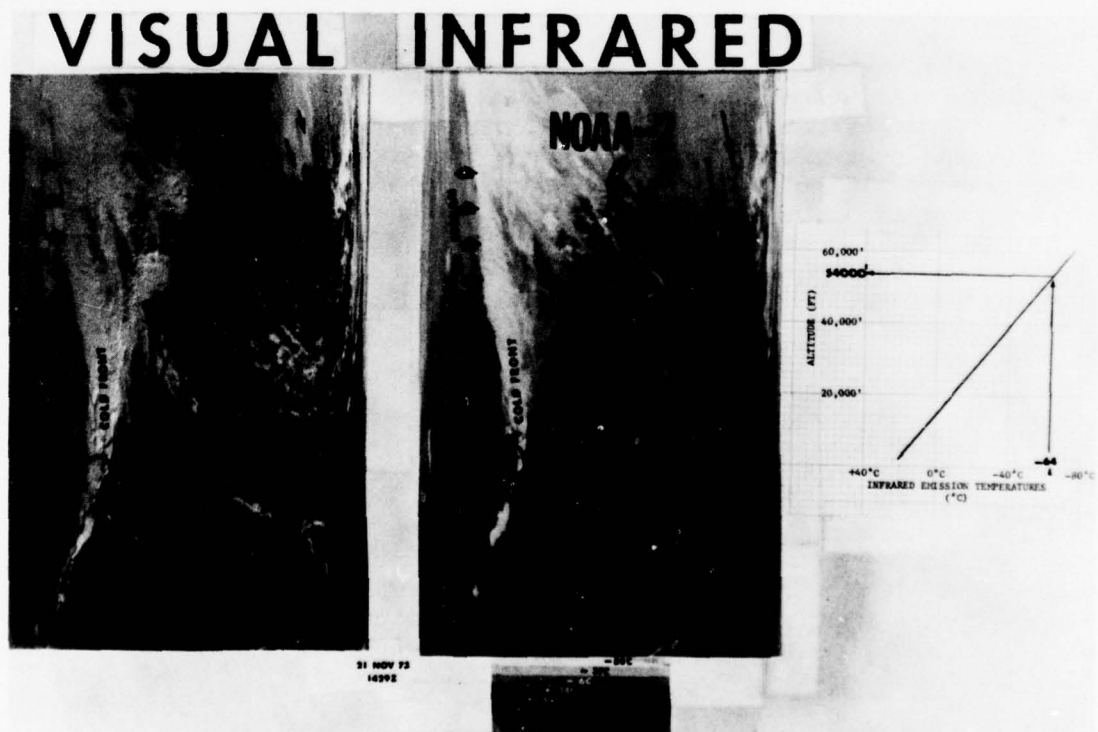


Figure 23. Simultaneous NOAA-2 visual and infrared data with temperature conversion for cloud tops (21 Nov 73).

The launch of SMS-1, SMS-2, and GOES-1 improved the movie-loop product with the addition of infrared disk pictures. As discussed earlier, the infrared product depicts the vertical development of clouds. This latter product is ideal for continuous movie products, day and night. The current locations of SMS-2 and GOES-1 allow simultaneous views of the United States and parts of the Eastern and Western Hemispheres.

Vertical Temperature Profiles (VTPR)

Another important meteorological data source available from NOAA, DMSP, and Nimbus vehicles are vertical temperature profiles. At the time of this report, all vertical temperature profile radiometer data are received in a playback-stored mode by the Air Force Global Weather Central (AFGWC), NOAA National Environmental Satellite Service (NESS), and NASA Goddard Space Flight Center (GSFC). In the future, these temperature soundings, or a reasonable facsimile, may replace nearly all data presently acquired by balloons and rockets. At present, these data require considerable correction and, at times, show excellent agreement with conventional measurements. An example of a VTPR from NOAA-3 versus a nearby sounding from Cape Canaveral (Figure 24) shows how good the vertical temperature profile can be. Daytime heating in the lower levels would make the curves almost identical. A visual and an infrared (NOAA-3) photograph are also on the figure showing the sounding location and cloud condition (weather). In the retrieval of these temperature-profile data the gridding and examining of the data stream for clouds which would give faulty sounding data are performed by computer. In these two phases of the computer VTPR program, human examination and quality control are a must in the evaluation of data from this system. The remainder of the program which involves lengthy data processing is a computer function.

Other Meteorological Satellite Imagery and Data

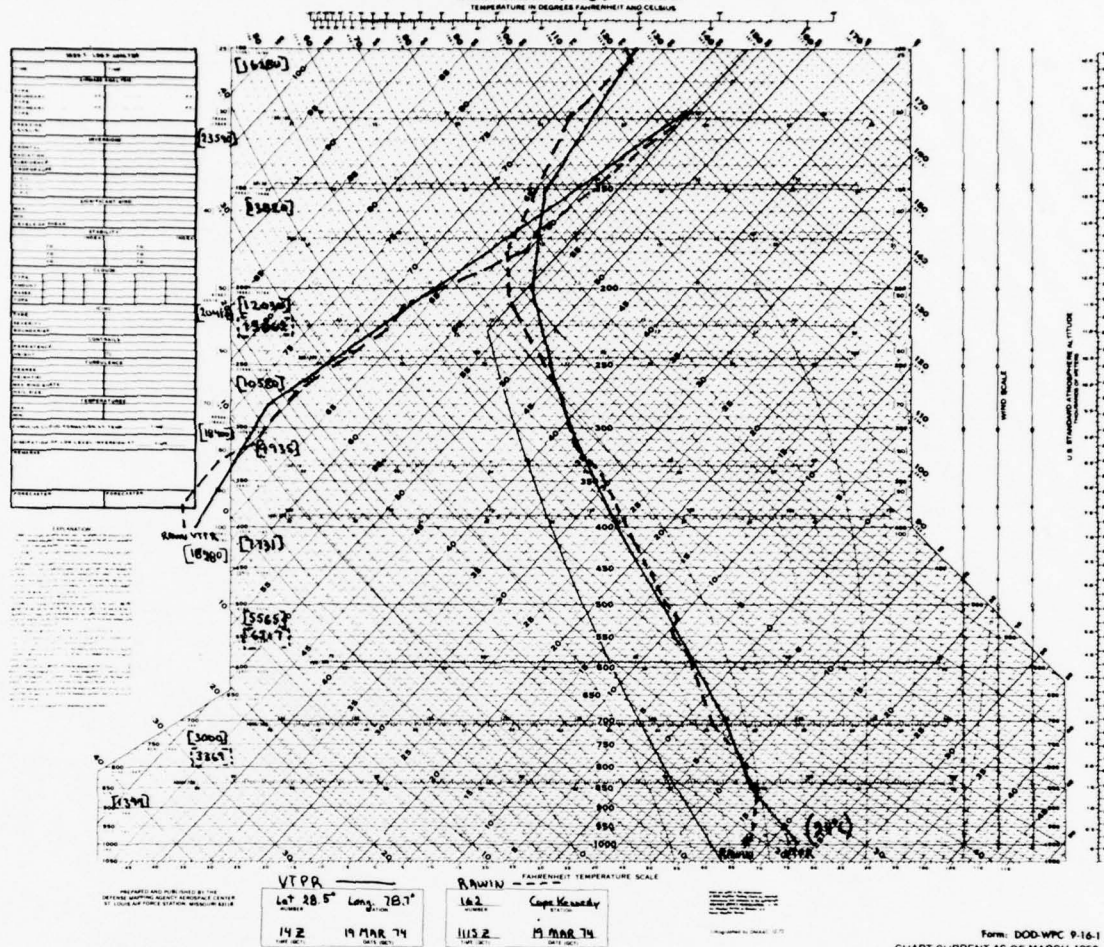
The meteorological satellite imagery presented in this report is available in a near real-time mode directly or indirectly to a variety of customers worldwide. Some of the imagery is more difficult to obtain than others. NASA has launched several Nimbus satellites since the early sixties. The first two had APT and AVCS transmitters that enabled most satellite receiving stations to acquire the imagery. Since Nimbus III and up to Nimbus V, most of the experiments on board the vehicles have been available to only Goddard Space Flight Center. Tables 2, 3 and 4 show some of the experiments on board these space vehicles. Examples of the imagery from some of the experiments are presented in Figures 25 through 31.

Nimbus VI was launched to sound the atmosphere with advanced techniques, extending and refining the sounding and atmospheric structure measurement capabilities demonstrated by previous Nimbus satellites. Instruments on board this satellite include a high-resolution infrared radiation sounder, an electronically scanning microwave radiometer, digital solar aspect sensor, temperature/humidity infrared radiometer, tropical wind energy reference level experiment antenna, pressure modulator radiometer, limb radiance infrared radiometer, scanning microwave spectrometer, and an instrument to measure the synoptic and planetary earth radiation budget [82].

DMSP spacecraft also carry special sensors for research. The atmospheric density sensor provides a measure of major atmospheric constituents (nitrogen, oxygen, and ozone) in the earth's thermosphere (100 to 250 km) by making earth-limb observations of the ultraviolet radiation from this atmospheric region. The precipitating electron spectrometer counts ambient electrons with energies ranging from 500 eV to 20 KeV. Providing global data, the temperature water-vapor ozone radiometer yields vertical temperature profiles, vertical water-vapor profiles, and total ozone concentration. The passive microwave temperature sounder is a scanning radiometer that measures radiation in the 5- to 6-mm wavelength region to provide data for profiling, on a global basis, atmospheric temperatures from the earth's surface to altitudes above 30 km. The lightning detector operates only at night to detect lightning flashes in the 1.1-micron range. Its primary use will be to aid in the forecasting of severe storms (*Block 5D-A Compendium*, [2]).

Form: DOD-WPC 9-16-1

DEPARTMENT OF DEFENSE
USAF SKEW T, log p DIAGRAM



Form: DOD-WPC 9-16-1
CHART CURRENT AS OF MARCH 1969



VTPR
NOAA-3

1919 9 2008 19140
 1919 0902
 1919 9999 1913 00000
 00000 0000 0000 0000 1911 1912 1913 1914 20045
 0000 0000 0000 0000 0000 0000 0000 0000
 1919
 1919 00
 1919 00 1913 00000
 0000 0000 0000 0000 0000 0000 0000 0000
 0000 0000 0000 0000 0000 0000 0000 0000
 1919



Figure 24. NOAA-3 VTPR versus a Cape Canaveral upper-air sounding.

Table 2. Nimbus III Meteorological Experiments [77].

Nimbus III Meteorological Experiments		
Experiment	Spectral Bands Microns	Main Purpose
High Resolution Infrared Radiometer (HRIR)*	3.4-4.2 0.7-1.3*	Nighttime surface and cloud top temperatures, and cloud mapping Daytime cloud mapping
Medium Resolution Infrared Radiometer (MRIR)	6.5-7.0 } 20-23* } 10-11 14.5-15.5 0.2-4.0	Atmospheric water vapor and cirrus cloud mapping Surface and cloud top temperatures Stratospheric temperatures Daytime cloud mapping, albedo
Infrared Interferometer Spectrometer (IRIS)*	5-20	Atmospheric temperature profile, O_3 , water vapor, surface temperature and minor atmospheric gases
Satellite Infrared Spectrometer (SIRS)*	11-15	Multilevel atmospheric temperature
Monitor of Ultraviolet Solar Energy (MUSE)*	0.12 } 0.16 } 0.18 } 0.20 } 0.26 }	Monitors changes in solar radiation
Image Dissector Camera System (IDCS)**	0.45-0.65	Daytime cloud mapping
Interrogation, Recording and Location System (IRLS)*	—	Data collection from platforms

*Experiment or spectral band was not flown on previous Nimbus satellites.

**IDCS and HRIR data, besides being recorded for transmission to the DAF, are also broadcast to Automatic Picture Transmission (APT) ground stations throughout the world.

Table 3. Nimbus IV Meteorological Experiments [78].

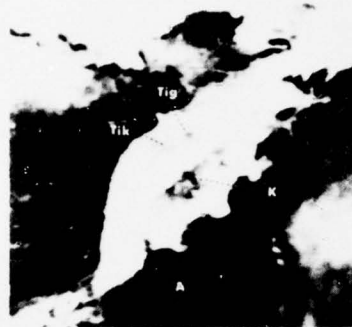
Nimbus IV Meteorological Experiments

Experiment	Spectral Bands Microns	Main Purpose
Temperature Humidity Infrared Radiometer (THIR)	10.5-12.5	Daytime and Nighttime Surface and Cloud Top Temperatures and Cloud Mapping
	6.5-7.0	Atmospheric Water Vapor Mapping
Infrared Interferometer Spectrometer (IRIS)	8-20	Atmospheric Temperature Profile, O ₃ , Water Vapor Surface Temperature and Minor Atmospheric Gases
Satellite Infrared Spectrometer (SIRS)	11	Surface and Cloud Top Temperatures
	13-15	Atmospheric Temperature Profile
	19-36	Atmospheric Humidity Profile
Monitor of Ultraviolet Solar Energy (MUSE)	0.12	Monitors Changes in Solar Radiation
	0.16	
	0.18	
	0.21	
	0.26	
Selective Chopper Radiometer (SCR)	13-15	Atmospheric Temperature Profile
Filter Wedge Spectrometer (FWS)	1.2-2.4	Atmospheric Water Vapor
	3.2-6.4	
Backscatter Ultraviolet Spectrometer (BUV)	0.25-0.34	Atmospheric Ozone Distribution
Image Dissector Camera System (IDCS)	0.45-0.65	Daytime Cloud Mapping
Interrogation, Recording, Location System (IRLS)	—	Data Collection from Platforms

Table 4. Nimbus V Meteorological Experiment [79].

Nimbus 5 Experiments

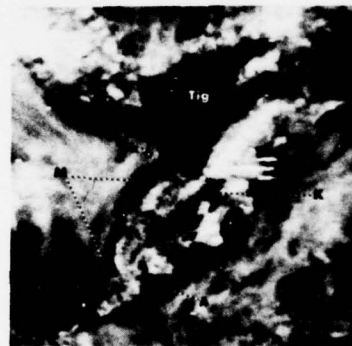
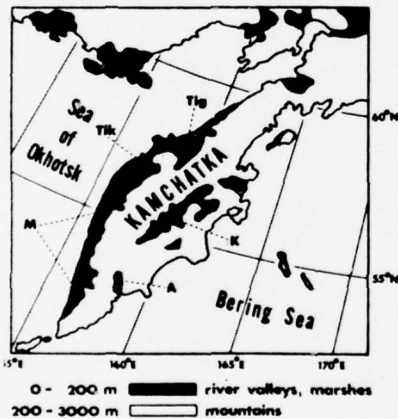
Experiment	Spectral Bands	Main Purpose	Experimenter
Temperature Humidity Infrared Radiometer (THIR)	10.5-12.5 μm 6.5-7.0 μm	Daytime and nighttime surface and cloud top temperatures Cloud mapping Atmospheric water vapor mapping	A. Mc Culloch, NASA/GSFC Greenbelt, Maryland 20771
Surface Composition Mapping Radiometer (SCMR)	8.3-9.3 μm 10.2-11.2 μm 0.8-1.1 μm	Distinguish acidic from basic rocks Map surface temperatures Map surface features	W. Hovis, NASA/GSFC Greenbelt, Maryland 20771
Electrically scanning Microwave Radiometer (ESMR)	19.225-19.475 GHz	Map surface features even in the presence of clouds Map distribution of polar ice Map precipitating clouds over ocean areas	T. Wilheit, NASA/GSFC Greenbelt, Maryland 20771
Infrared Temperature Profile Radiometer (ITPR)	3.8 μm 11 μm 15 μm (4 bands) 20 μm	Vertical temperature profile of the atmosphere	W. L. Smith, NESS/NOAA Suite 300, 3737 Branch Avenue Hillcrest Heights, Maryland 20031
Selective Chopper Radiometer (SCR)	2.08 μm 2.59 μm 2.65 μm 3.5 μm 11.1 μm 13.8-14.8 μm (4 bands) 15 μm (4 bands) 18.6 μm 46.5 μm 100 μm	Vertical temperature profile of the atmosphere Water vapor distribution in the atmosphere Density of ice particles in cirrus clouds	J. T. Houghton, Oxford University Oxford, England S. D. Smith, Heriot-Watt University Edinburg, Scotland
Nimbus E Microwave Spectrometer (NEMS)	27.23 GHz 31.4 GHz 53.65 GHz 54.90 GHz 58.80 GHz	Vertical temperature profile of the atmosphere even in presence of clouds Atmospheric water vapor	D. H. Staelin, MIT Cambridge, Massachusetts 02139



22 April 1970 - Snow melt has begun in the Kamchatka (K), Avacha (A), Tikhaya (Tik), and Tigil (Tig) river valleys.



27 April 1970 - Further snow melt in these river valleys is evident. Note also, overall peninsular reflectances have decreased.



27 May 1970 - All river valleys (K, A, Tik, Tig) and marshland (M) snow cover has melted.

Figure 25. Nimbus IV IDCs of snow melt on the Kamchatka Peninsula, USSR, during April and May 1970 (Nimbus IV Data Catalog, [81]).

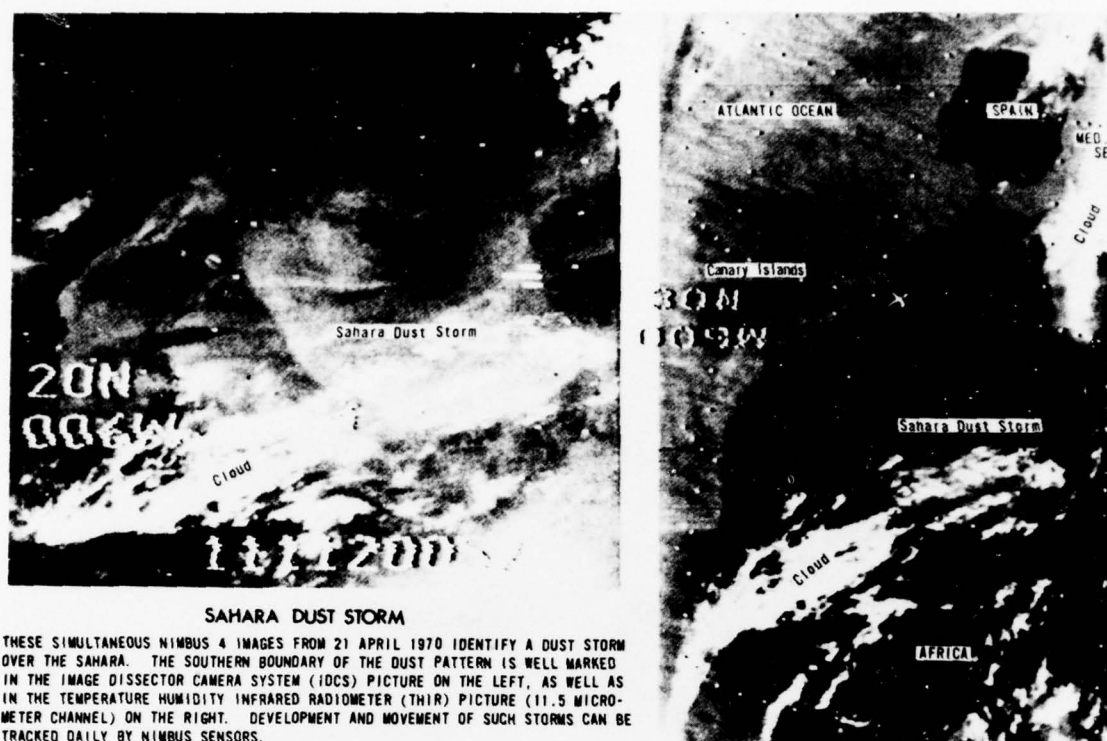


Figure 26. Nimbus IV IDCS and THIR of a Sahara dust storm recorded on 21 Apr 70 (Nimbus IV Data Catalog. [81])

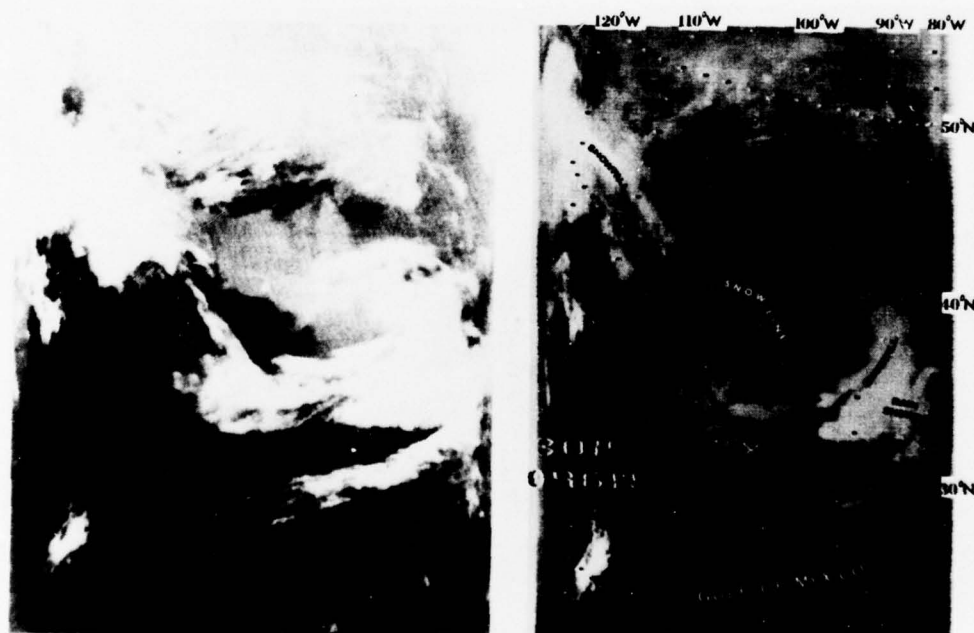


Figure 27. Nimbus IV DRIR and THIR comparison for 25 Mar 71 (Nimbus IV Data Catalog. [81]).



Nimbus 5 Daytime THIR ($11.5\mu\text{m}$ channel) Image Recorded over the Central United States on 3 April 1974. This image was recorded at approximately 1:20 p.m. EDT. A few hours after this image was recorded, tornadoes devastated many areas from Alabama to Ohio. Over 300 people were killed. The tornado activity was associated with the large globular clouds to the right center of the image.

Figure 28. Nimbus V daytime THIR image recorded over the central U.S. on 3 Apr 74 (Nimbus V Data Catalog, [82]).



Figure 29 Nimbus V SCMR nighttime infrared image recorded over Florida and Cuba on 24 Dec 72 (Nimbus V Data Catalog, [82])

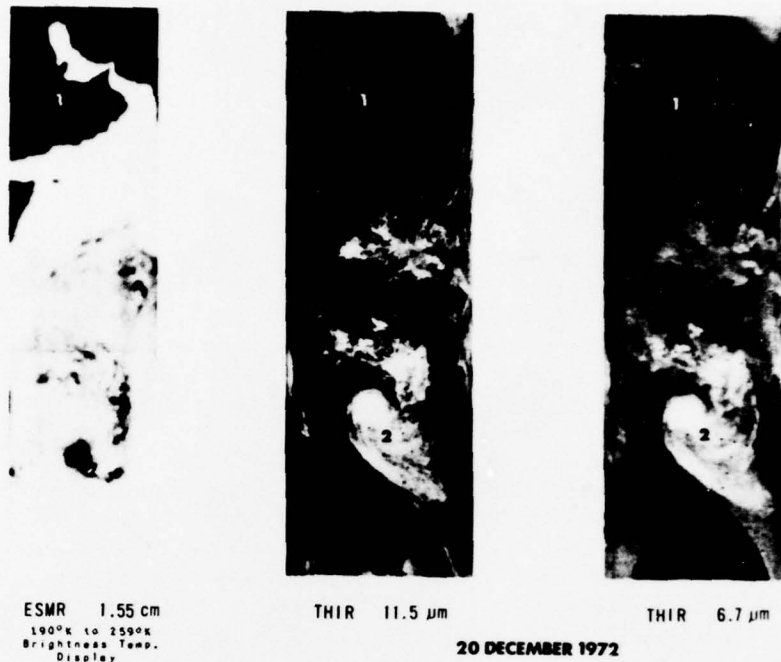


Figure 30. A comparison of Nimbus V THIR and ESMR pictorial data (Nimbus V Data Catalog, [82]).

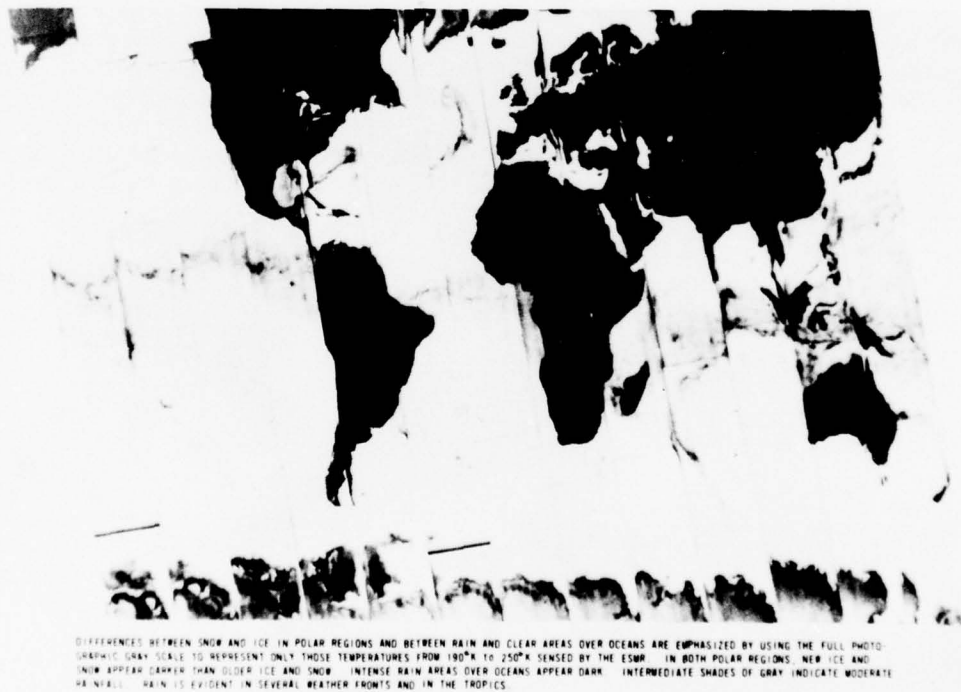


Figure 31. Nimbus V ESMR (electrically scanning microwave radiometer) taken 11 Jan 73 (orbits 413 to 425) (Nimbus V Data Catalog, [82]).

Chapter 3

CLOUDS

The most common meteorological features seen on satellite photos are clouds and cloud systems. The accurate location of clouds and recognition of cloud types can be accomplished by a satellite meteorologist. This knowledge can be conveyed quickly and easily to the military or civilian customer by identification on the photographs. Clouds, cloud extent, cloud tops, and cloud movement can be explained pictorially with high-quality satellite images. Cloud types, such as low-level stratocumulus, stratus, and cumulus and high-level cumulonimbus (thunderstorm) and cirrus with their weather-related phenomena (wind, rain, hail, icing, etc.), are depicted on the photographs.

In this chapter cloud types are classified as low level, mid level, and high level. The low level covers the altitudes of less than 3000 meters. These clouds are stratocumulus, cumulus, stratus, fog, anomalous lines, and lee waves when the terrain is less than 3000 meters. Mid-level clouds include those clouds in the 3000- to 6000-meter levels. Most of the clouds that occur in this level are not "seen" by the satellite. These clouds occur in layers in frontal systems, hurricanes, typhoons, intertropical convergence zone (ITCZ) etc., where cirrus clouds are above the mid-level clouds. High-level clouds usually include those at all levels above 6000 meters. These clouds include thunderstorms and cirrus (cirrus streaks, plumes, billows, transverse bands).

Low-Level Clouds

a. **Stratocumulus (Strato Cu).** The stratocumulus cloud pattern is easily recognized on meteorological satellite imagery. This lumpy "closed cell" pattern is caused by low-level convection under higher level subsidence or sinking motion in the atmosphere. These clouds are usually seen in satellite pictures off the west coast of major continents in the middle and lower latitudes. The bases of these clouds are from 500 to 800 meters with cloud tops between 1400 and 1800 meters. The smallest stratocumulus elements are 2-4 km in diameter while the largest elements are 20-40 km in diameter. Figures 32 and 33 are Synchronous

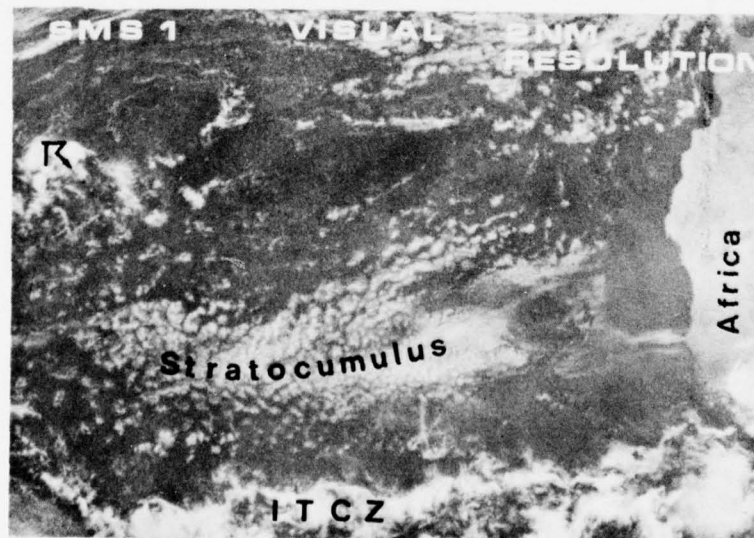


Figure 32. A SMS visual view showing stratocumulus in the eastern Atlantic (date unknown).

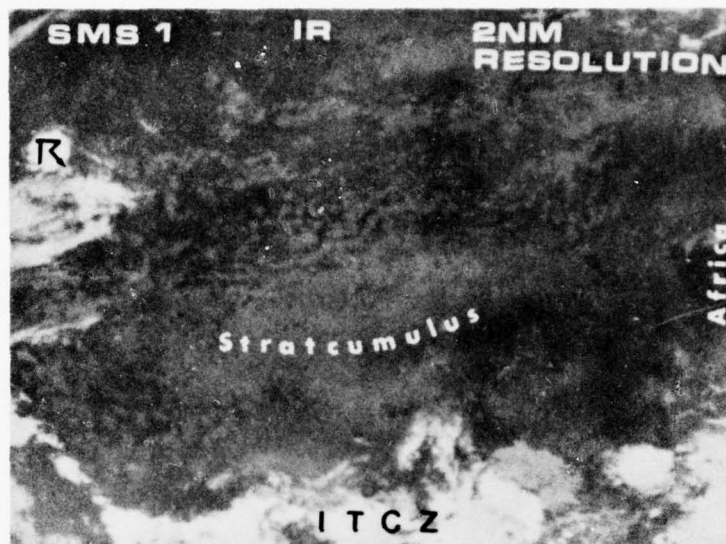


Figure 33. A SMS infrared view of low stratocumulus clouds (gray) with the higher (white) ITCZ near the equator (date unknown).

Meteorological Satellite (SMS-1) simultaneous visual and infrared photographs, respectively, off the west coast of Africa.

b. Stratocumulus Lines. Stratocumulus clouds can form in lines. This formation occurs as cold air moves off continents onto warmer water where the clouds form and align themselves to the wind flow. A DMSP visual example is shown in Figure 34. Figure 35 is an infrared view of these stratocumulus lines. Stratocumulus lines are seen in both figures forming off the coast of New England. The stratocumulus clouds become larger as the water gets warmer and the wind speed slows down. In these figures the smaller stratocumulus have bases of 500 to 800 meters, whereas the larger stratocumulus are between 800 and 1400 meters.

c. Cumulus (Cu). Cumulus clouds are a very common cloud type seen on satellite imagery. These small, puffy, fair-weather clouds are detected by the new very high-resolution meteorological satellites. The earlier meteorological satellites could not resolve each and every cumulus cloud. Figure 36 is an example of the individual cumulus clouds seen over the state of Florida and surrounding areas.

Cumulus clouds usually have bases of 600 to 900 meters with cloud tops anywhere from 1500 to 3000 meters. Those with tops above 3000 meters are called towering cumulus and are easily identified on the high-resolution visual data. Infrared imagery can also be used in the determination of these cloud tops above 3000 meters.

Cumulus clouds can form "open cell" patterns in contrast to stratocumulus "closed cell" patterns. These chaotic patterns resemble geometric shapes such as polygons or ellipses (Figure 37). The chaotic patterns behind cold fronts in the higher latitudes are marked as cumulus. In some cases, this cumulus extends above 3000 meters and should have properly been called towering cumulus. Considerable low-level turbulence could be expected in some "open cell" cumulus patterns with a wind shear involved.

d. Cumulus Cloud Lines or Streets. Cumulus clouds usually align themselves more or less parallel to the low-level wind flow (see Chapter 5). These low-level cloud patterns can be continuous or joined in lines, or can be individual cloud elements spaced in such an array as to be called streets.

Some lines can be towering cumulus. Usually, towering cumulus lines do not align themselves with the low-level wind flow, but with wind shear in the cloud layer. Figure 38 is an example of cumulus cloud streets north of Columbia, South America. The bases and tops of these cloud streets or lines usually range from 600 to 1500 meters.



Figure 34. A DMSP visual view of clouds forming over the Atlantic as the cold air moves across the warmer water (18 Jan 74).

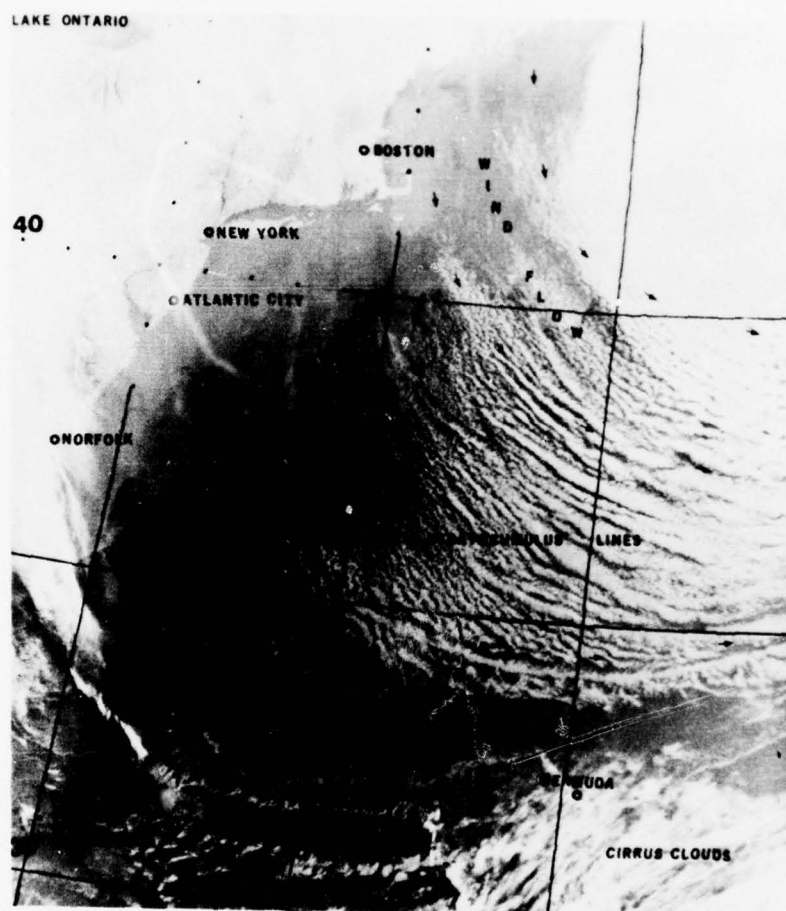


Figure 35. DMSP infrared view of stratocumulus lines (12 Mar 76).



Figure 36. A DMSP VHR view of Florida with cumulus (Cu) clouds (15 Jul 75).

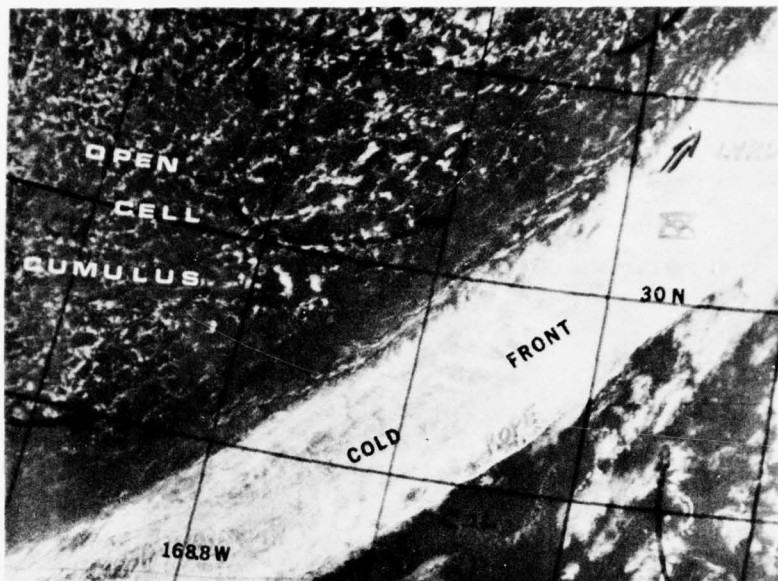


Figure 37. DMSP visual image showing cumulus clouds behind a cold front in the North Pacific (10 Mar 70).



Figure 38. DMSP visual view of cumulus cloud lines north of South America (24 Jan 75).

e. **Stratus/Fog.** Stratus and fog are also low-level formations and are usually uniform and textured, white or gray, depending on density and sun angle. Boundaries are sharply defined and the stratus/fog often outline the topography, such as coast lines, mountains, and valleys. Figure 39 is an example of fog and stratus in the Gulf of Mexico along the Texas and Mexican coasts. Poor visibilities and light winds prevail in this cloud pattern. A vertical temperature sounding by a balloon would be the best way to determine the depth of the fog in this figure.

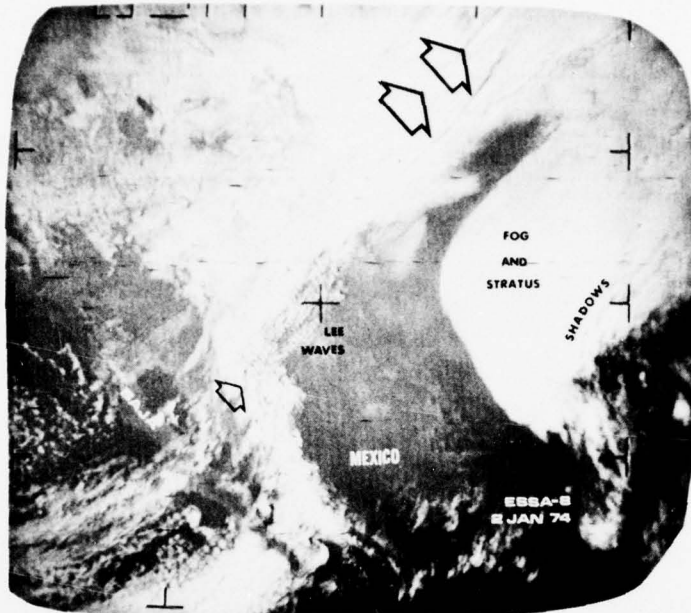


Figure 39. ESSA-8 visual imagery showing fog and stratus in the Gulf of Mexico (2 Jan 74).

Infrared imagery as well as topography can also be used to determine thickness although infrared pictures can be misleading when subsidence inversions occur. A subsidence inversion occurs when warm air from aloft descends, warms, and overlays cooler air below. The infrared imagery would show the clouds warmer than the surrounding land. In Figure 40, the temperatures in northern Florida appeared much warmer than those in the southern part of the state. Upon closer examination, the warm region was shown to be a stratus layer at the top of a strong nocturnal inversion (Reinke and Brandli, [90]).

Figure 41 was taken over the west coast of the United States. This visual imagery shows the snow-covered Sierra Nevada mountains east of the fog-filled San Joaquin Valley. In this example, careful location of the stratus against the mountains could assist in the determination of the thickness of the stratus and fog.

The existence and extent of fog at sea (especially in waters not frequently "fogged in") is of great importance to seamen. Satellite photographs can pinpoint sea fog and, with a series of pictures, show its movement and changes. Figure 42 is an example of sea fog in the eastern Gulf of Mexico.

f. **Actiniform Clouds.** Actiniform cloud patterns are usually seen in conjunction with stratocumulus and cumulus patterns. These clouds look like cumulus in a "spider web" array. In stratocumulus layers, actiniform clouds will occur in patches where the stratocumulus appear to be dissipating. Another area of actiniform cloud formation is on the edge of cumulus and stratocumulus or in cumulus patterns near the equator. A common location for these actiniform clouds to form is in the subtropics off the west and east coasts of continents. A visual and infrared example is shown in Figures 43 and 44, respectively.



Figure 40. DMS infrared (WHR) photograph of warm clouds over Florida (3 Feb 76).



Figure 41. DMS visual image showing fog in the San Joaquin Valley of central California (27 Nov 72).

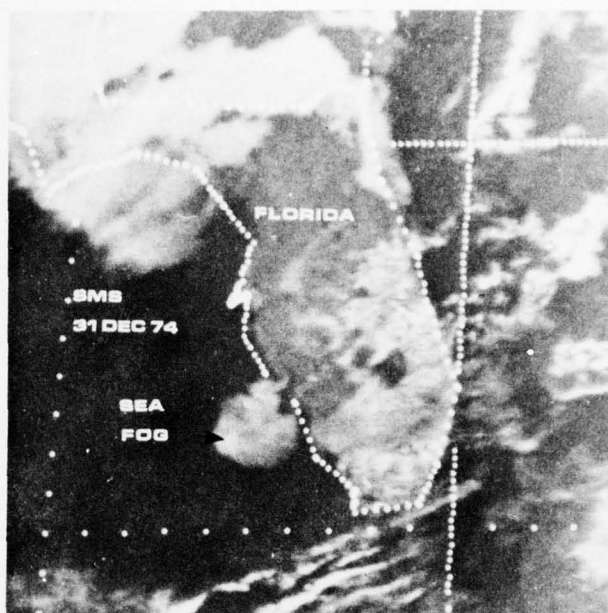


Figure 42. An SMS-1 visual image showing sea fog in the eastern Gulf of Mexico off the coast of Florida (31 Dec 74).



Figure 43. DMSP visual imagery of actiniform clouds (date unknown).

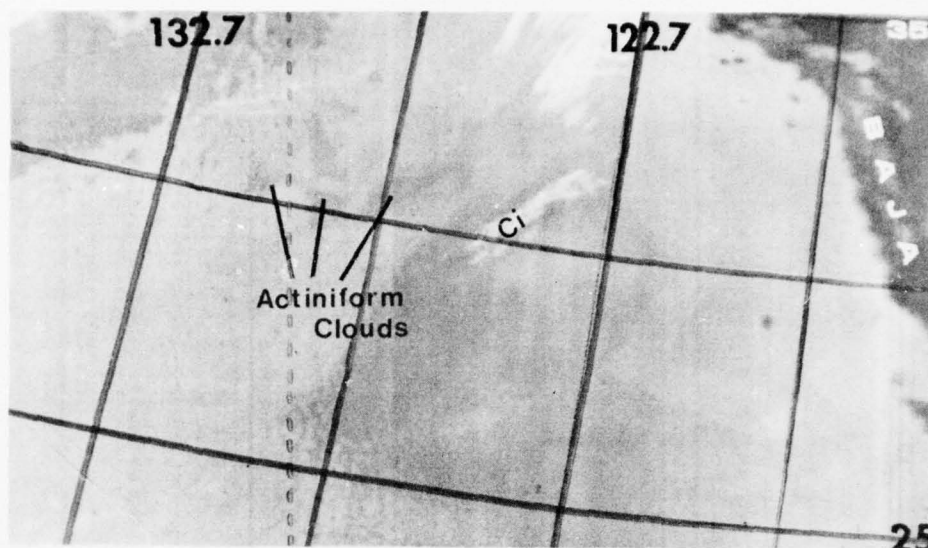


Figure 44. DMSP infrared imagery of actiniform clouds (date unknown).

g. Lee Waves. Lee-wave clouds appear downwind from mountain ranges or hills when the wind flow is nearly perpendicular to the high terrain. They have a "washboard" appearance and can be differentiated from cumulus streets by their location and the fact that they are perpendicular to the wind, not parallel to it. Turbulent flow is to be expected in the area around the lee waves. The height of the clouds can be determined from the height of the terrain inducing the clouds or from the infrared imagery, provided the resolution is right for viewing the narrow wave clouds. An example of low-level lee waves is shown in Figure 45. In this photograph, the lee-wave clouds are overhead and west of Oahu. These clouds were induced by the Koolau mountain range. These "mountains" are less than 1200 meters high. Other low-level, small lee-wave clouds are shown west of the island of Maui. They were induced by the small hills on that island which are perpendicular to the trade winds. In Figure 46 low-level lee waves are shown in the Appalachian Mountains.

h. Billow and Invisible Low-Level Clouds. Billow clouds are formed and maintained by wave motion just as lee waves are. They also have a "washboard" appearance. However, they are not associated with terrain influences. Figure 47 shows a DMSP very high-resolution (VHR) image from two satellite passes over the coast of Texas. In this figure, billow clouds are shown which are perpendicular to each other. The low-level billow clouds, which were confirmed on infrared imagery, lie parallel to the Galveston coast. A close examination of the 1412 GMT VHR image shows the white billows becoming gray before reappearing again southwest of Galveston. Because of the expanded viewing interval of the DMSP sensor, water droplets, ice crystals, or other aerosol particles invisible to the human eye can be detected and processed. The marked area on the 1412 GMT photograph outlines "invisible clouds" that show up 3 hours later as visible clouds (Brandli and Taylor, [30]).

i. Miscellaneous Cloud Lines. Anomalous cloud lines appear as bright lines in ocean areas, usually under the influence of high-pressure areas. These lines are aligned in ways which are unrelated to the synoptic circulation (Brandli and Orndorff, [28]). Figure 48 is a DMSP visual image of anomalous lines.

Many cloud lines are caused by land barriers to the air flow. Figure 49 is an example of cloud lines emanating from the eastern tip of Hainan Island in the South China Sea. In this example, these lines are "eddy" clouds caused by the low-level wind flow from the east. Island "eddy" clouds are a common occurrence on meteorological satellite imagery. However, in this figure, the unique alignment of the eddies look like a "cone" shock wave.

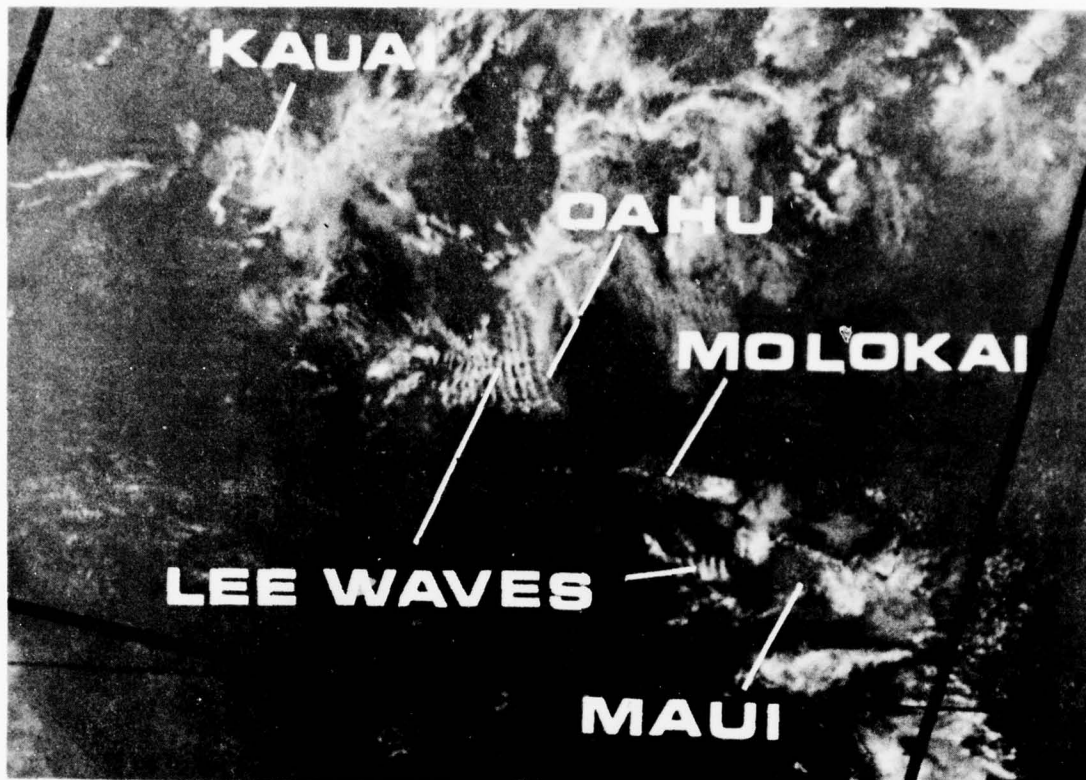


Figure 45 DMSP visual image depicting low-level lee waves in the Hawaiian Islands (22 Oct 70).

Another island effect is shown in Figure 50. In this example, a "bow shock" appearing cloud is seen east of the island of Hawaii. This early morning phenomenon is caused by a westerly land breeze meeting the easterly trade winds. The land breeze is caused by cool night air sinking down the island's mountain slopes and moving out in a radial direction over the adjacent Pacific waters. Large "eddy" clouds, caused by the trade winds blowing around the mountains, are also visible downwind from Hawaii.

Another cloud formation like the "bow shock" is a nearly circular cloud on the edge of a dissipating thunderstorm. A downdraft of cold air occurs in a thunderstorm as it dissipates. This cold air mass moves out over the water, similar to the island land breeze, forming a narrow or roughly circular line of cumulus clouds. Such cloud arcs or circles are shown in Figure 51. A large area of lines labeled "fingerprint" appears on this figure. Different film types enable fingerprints to be clearly depicted and these prints have been mistaken for lee waves, billow clouds, cloud lines, etc.

Low-level perturbations or lines can appear in cloud decks where clouds are dissipated by aircraft. Such phenomena have been seen from the ground and air but are usually not large enough to be captured by a meteorological satellite. In Figure 52, a cloud deck of low-level stratocumulus off the west coast of the United States is seen perturbed by a vortical cloud line caused, perhaps, by aircraft. However, the author checked the area for low-level aircraft maneuvers, and found none. Other cloud lines will be discussed in the section on high-level clouds.

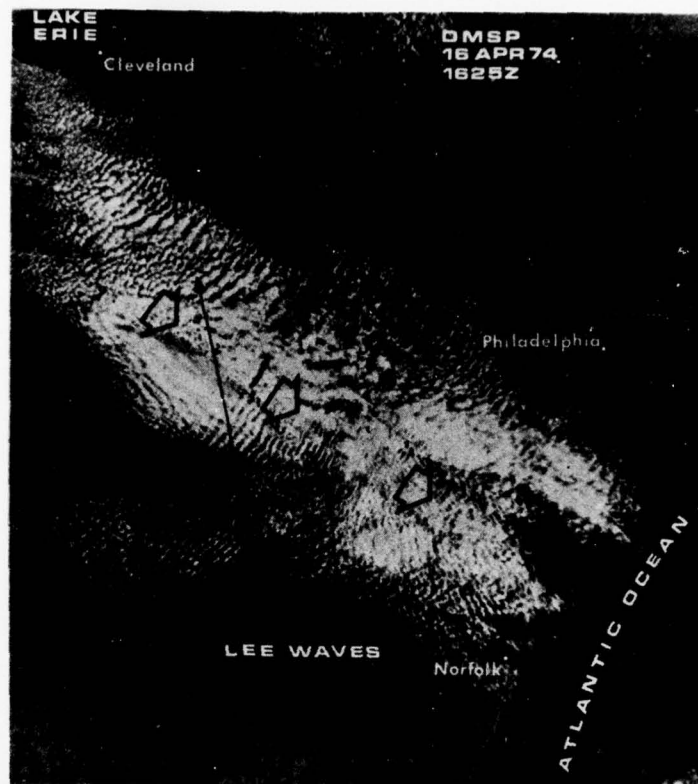


Figure 46. DMSP visual image showing lee waves in the Appalachian Mountains (16 Apr 74).

Mid-Level Clouds

Middle clouds occur in the levels from 2000 to 6000 meters. This author, for convenience, uses 3000 to 6000 meters as the limits for middle clouds. Middle clouds consist of altostratus and altocumulus, although other clouds, such as towering cumulus, extend into this height range. Some lee waves form downstream from high mountain ranges with bases and tops in the mid level. Most areas of middle-cloud occurrence are not seen by satellites because higher clouds, such as cirrus and cirrus layers, obscure the middle clouds. Infrared imagery is the most advantageous way to determine the presence of middle clouds. Figure 53 is an example of altostratus near the Great Lakes. On this photograph, the clouds are simply labeled middle clouds.

Another example of mid-level clouds is shown in Figure 54. This DMSP image shows lee waves downstream from the Alps. Also on the figure are many areas of layered and frontal cloud cover where middle clouds can be inferred.

High-Level Clouds:

a. **Thunderstorms or Cumulonimbus Clouds.** Thunderstorms are vividly presented on satellite imagery. These cloud systems routinely extend above 15,000 meters in the tropics. Anvil clouds or plumes, indicating wind flow, can be seen on top of these thunderstorms. Thunderstorms usually form in clusters and are very white in day visual imagery. Sometimes, visual protuberances can be seen on top of the cumulonimbus poking through the cirrus. An example of some thunderstorm cells is shown in Figure 55. The visual imagery shows the cell protuberances and cirrus blowoffs. Throughout this report, the thunderstorm symbol (\mathcal{R}) is seen on many of the photos where cumulonimbus clouds are present.

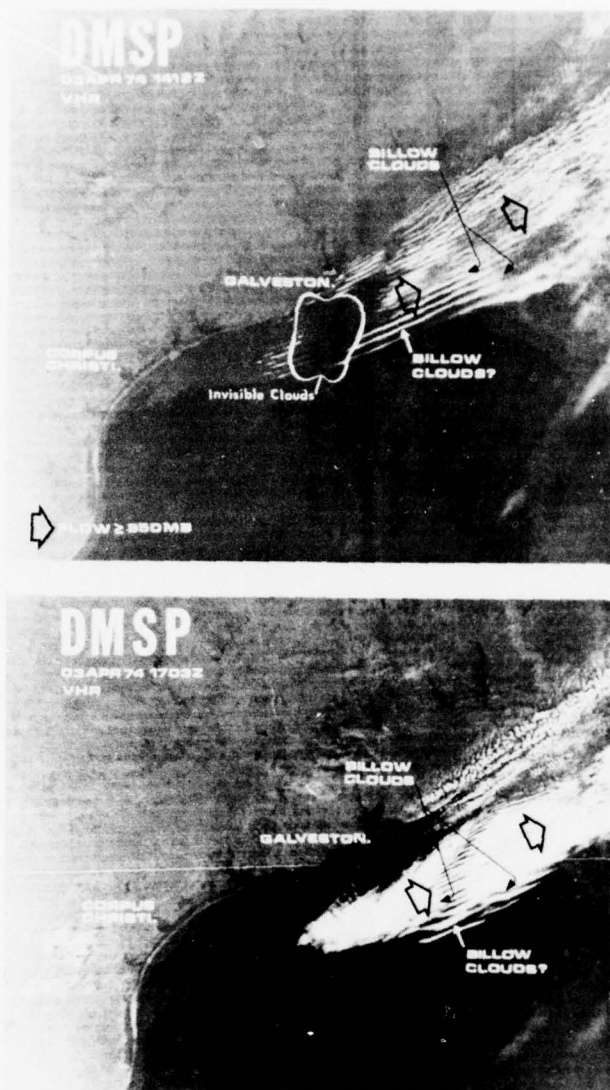


Figure 47. DMSP VHR imagery showing billow clouds off the coast of Texas (3 Apr 74).

Lines of thunderstorms are imbedded in fronts and along squall lines. Tornadoes also form in these areas. Visual photographs tend to mask some of the thunderstorms seen on infrared imagery. Such a case is shown in Figure 56. If there is a sharp line of small thunderstorms surrounded by low clouds, the infrared photograph delineates the thunderstorm activity better than the visual photograph, as seen in the Alabama and Tennessee areas on this simultaneous visual and infrared image.

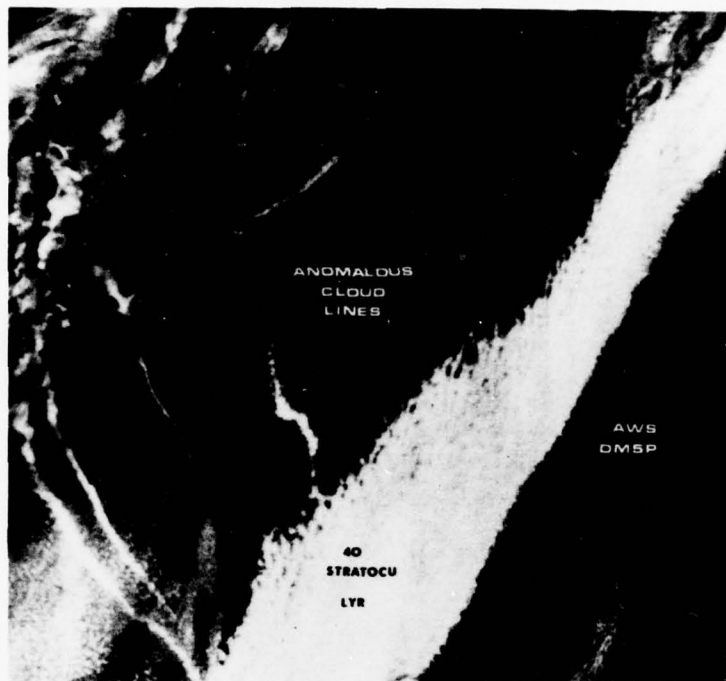


Figure 48. DMSP visual image of anomalous cloud lines off the west coast of the U.S. (date unknown).

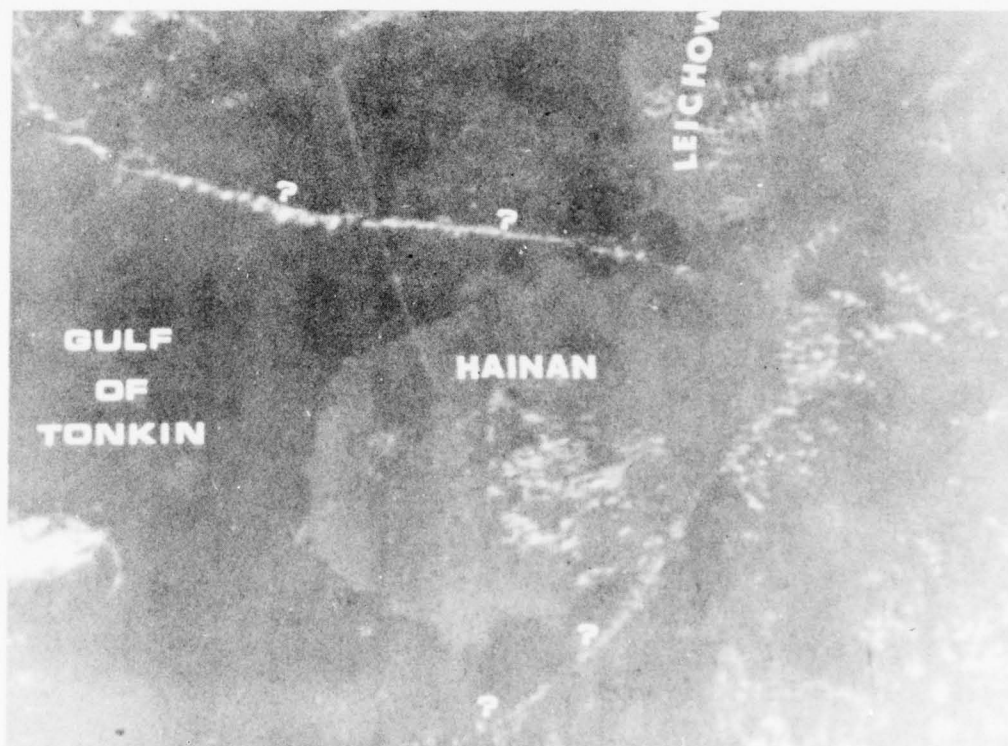


Figure 49. DMSP VHR image illustrating cloud lines around the island of Hainan (6 Nov 72).

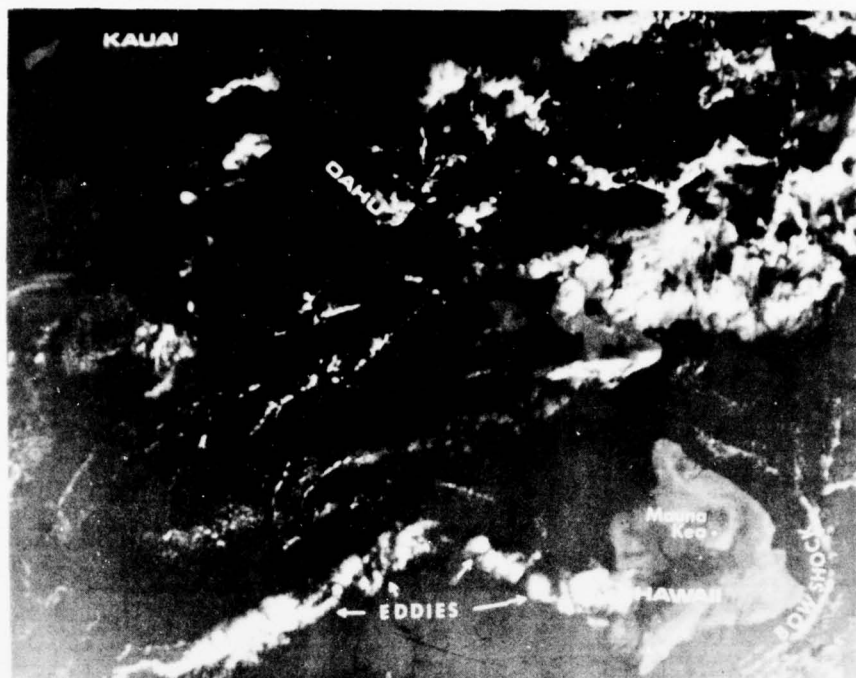


Figure 50. DMSP visual image illustrating "bow shock." Also shown are "eddies" (date unknown).

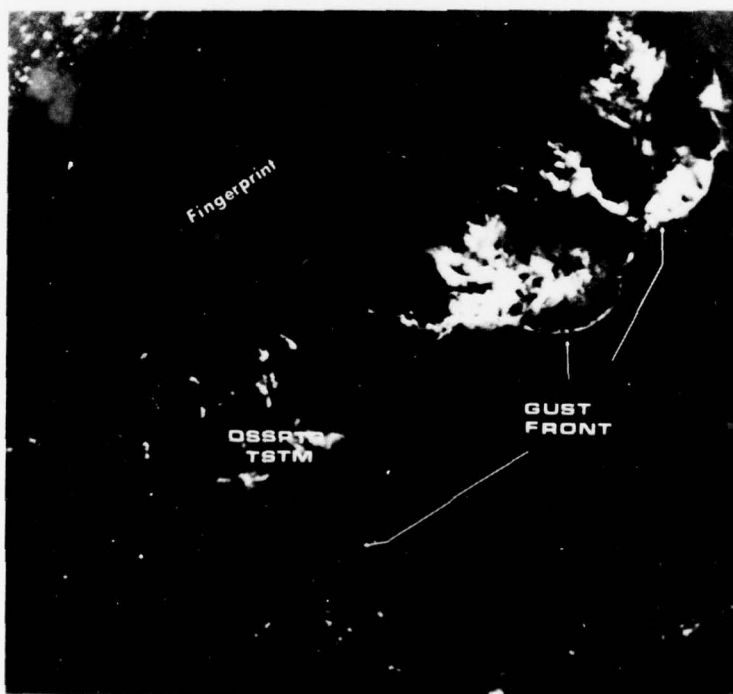


Figure 51. DMSP VHR image of the cloud lines left as a thunderstorm dissipates (5 Mar 73).

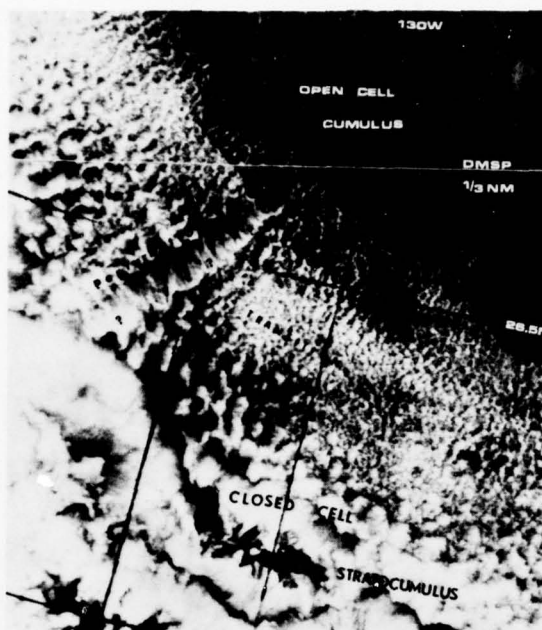


Figure 52. DMSP visual photograph off the west coast of the U.S. showing an anomalous (perturbation) line in the cloud deck (11 May 73).

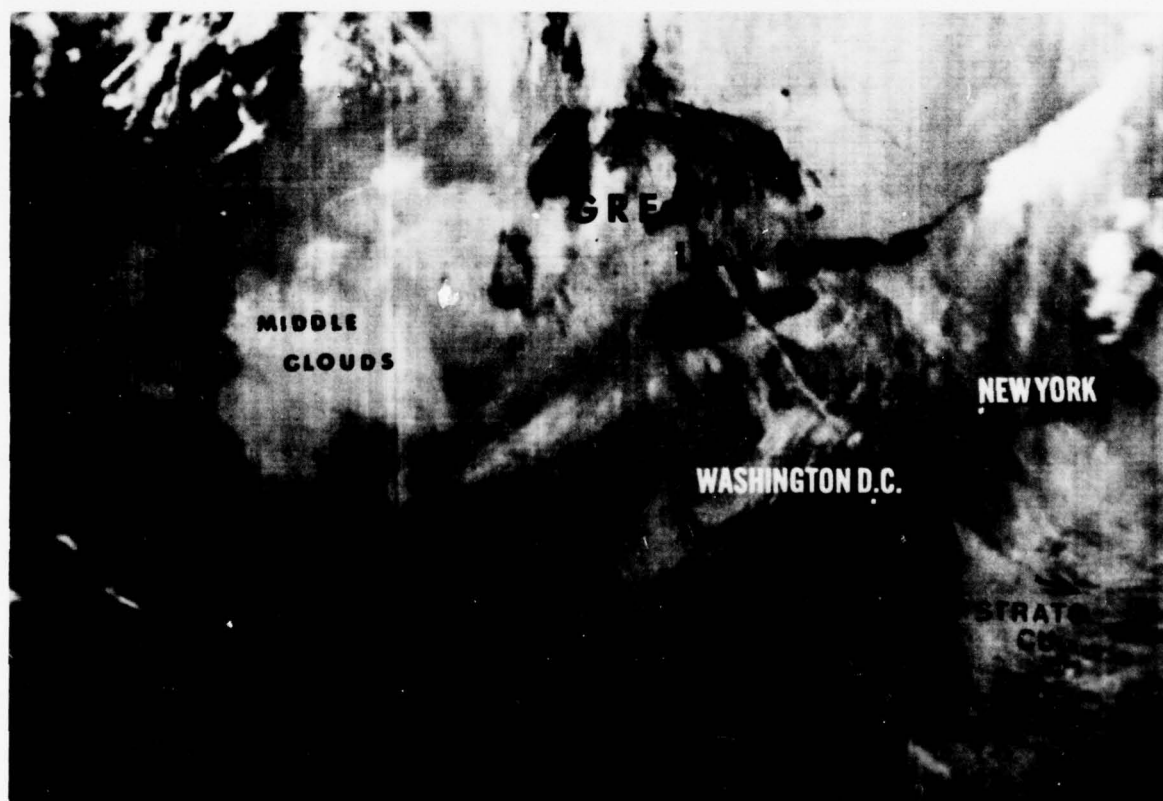


Figure 53. DMSP photograph of altostratus in the Great Lakes area (Nov 73).



Figure 54. DMSP visual over Europe showing middle clouds (16 Aug 74).

b. Cirrus Clouds. High-level cirrus clouds are found alone or in conjunction with numerous weather situations. Used together, the visual and infrared imagery can usually help the meteorologist detect thin cirrus. On the infrared, the high cold clouds appear as white patches whereas the visual picture of the same area is gray (almost transparent). Cirrus plumes are also seen blowing off thunderstorm activity and are an indicator of the upper-level wind flow. Cirrus cloud also occurs in jet-stream cirrus shadows, transverse bands, billow or gravity waves, and cirrus streaks or filaments. Considerable cirrus cloud occurs in layers in the intertropical convergence zone (ITCZ). Cirrus also occurs over storm areas such as hurricanes, typhoons, easterly waves, and fronts (warm, cold, and occluded).

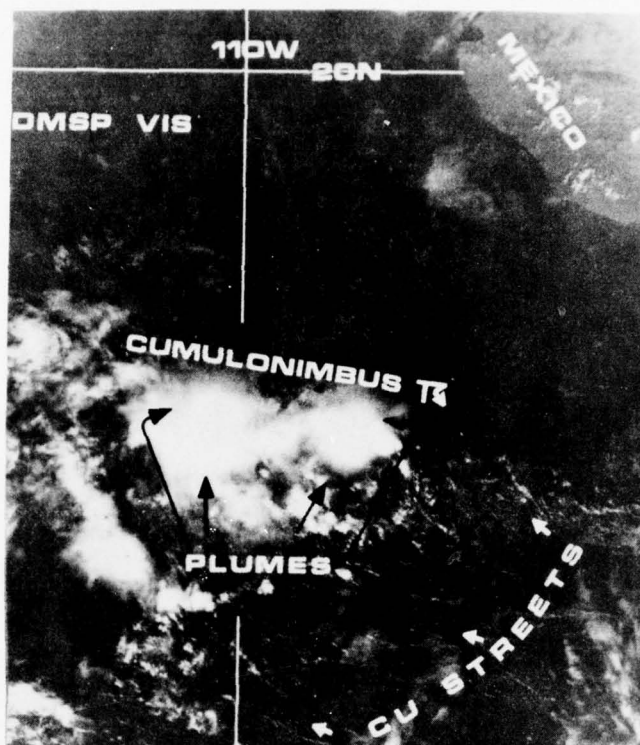


Figure 55. A DMSP visual image off the Mexican coast showing the plumes of thunderstorm cells (14 Jan 74).

Figure 57 was taken during the day before Hurricane Carmen hit the Yucatan Peninsula. A large cirrus cloud mass, seen emanating from the hurricane, is shown from east of the Yucatan Peninsula to southeast of Miami. This thin cirrus overflow is very common from the tops of hurricanes, typhoons, and in the Southern Hemisphere—cyclones. A cirrus overflow can be used to determine the upper level wind flow (see Chapter 5).

Infrared contouring can be used to isolate different heights of cirrus clouds in and above weather systems. The infrared thresholding capability of the DMSP is ideal for this type of presentation. Figure 58 is such an infrared display of Typhoon Rita. The high-level cirrus clouds on top of this storm are mapped as different gray shades. Near the eye of the storm, high-level white clouds of temperatures less than 210°K are depicted. These clouds around the eye can extend above 18,000 meters.

In some cases, simultaneous visual and infrared data is important in the examination of thin cirrus. Figure 59 is an example of ice-crystal cirrus shown in both the visual and infrared. The visual image (DMSP VHR) indicates a pattern of thin, almost transparent, clouds. Identification of thin cirrus on visual data is aided by the expanded spectral interval in the DMSP to include the near infrared. However, accurate cloud-height and wind-flow determination cannot be done without the infrared imagery. The combination of the two pieces of data indicates the thin ice-crystal cirrus to be between 10,000 and 12,000 meters with a northwest flow.

When viewing thin cirrus, the infrared imagery can sometimes give false cloud height information. In the absence of any cloud layers below the thin cirrus layer, radiation from the ground penetrates the thin layer and is also sensed by the infrared sensor on the satellite. Thus, the combined cloud and ground radiation indicates a false cloud height. For example, clouds that are at 12,000 meters could be shown on the infrared imagery as clouds at 6000 meters. Figure 60 contains simultaneous DMSP visual and infrared photographs and a synoptic weather map that illustrate this fact. The visual photograph indicates the presence of a thin cloud layer by the hazy appearance of the city lights. The gray shade of the cloud layer

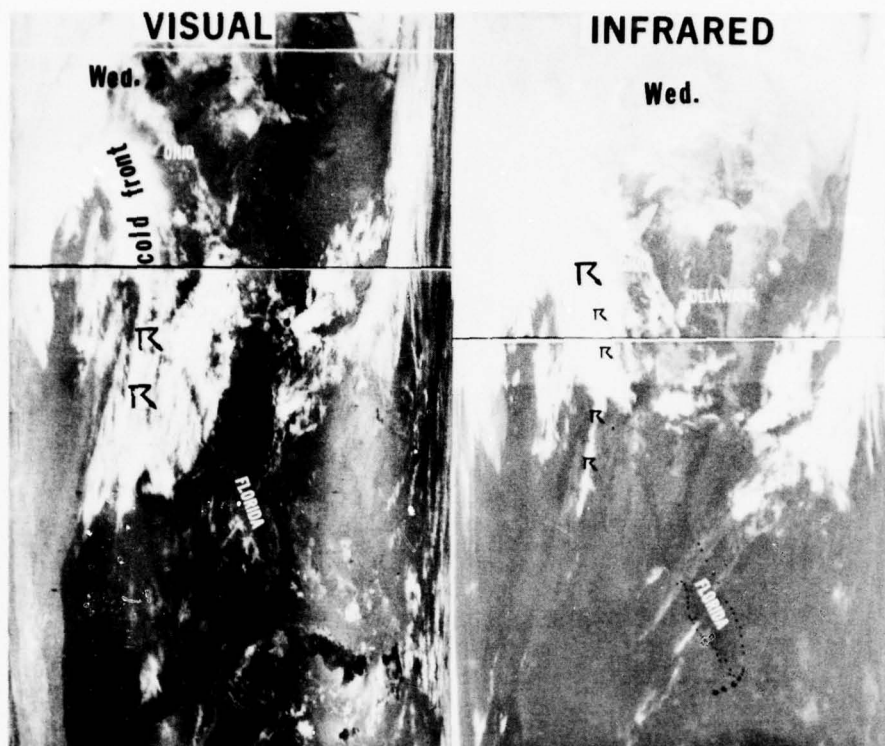


Figure 56. NOAA simultaneous visual and infrared photograph showing thunderstorm activity in a cold front and squall line (3 Apr 74).

on the infrared image indicates temperatures that would be associated with middle-level clouds. However, the observations of cirrus clouds on the synoptic chart and the texture of the cloud in the infrared photograph verify that the cloud is thin cirrus.

Cirrus is often difficult to detect when there is extensive low-cloud formations. Figure 61 is an SMS-1 visual and infrared pair taken off the west coast of South America. Stratus, stratocumulus, and cumulus are easily identifiable on the visual imagery. In examining the infrared, these low, gray clouds can also be seen. However, a white cirrus (Ci) band is clearly depicted, extending from the northwest to the southeast. This high-level cirrus band could not be recognized or detailed without a combination of the visual and the infrared.

Various cirrus clouds are shown in Figure 62. Due to the angle of the sun, the cirrus cloud casts shadows on the lower clouds. The thin cirrus streaks on the lower left side of the photograph align themselves to the wind flow, thus causing the thin strung-out effect. Cirrus filaments in the upper left of the photograph are similar to transverse bands but occur in a more chaotic pattern.

Transverse bands are seen in Figure 63. This composite of DMSP and SMS data clearly shows the transverse bands of cirrus. These bands are caused by the air spreading out to give a divergent pattern.

c. **High-Level Billow Clouds.** In a previous section on low clouds, low-level billow clouds were discussed. High-level billow clouds are a much more common phenomena and are shown in Figure 64. These high-level billow clouds are very easy to recognize on the newer high-resolution satellites of the National Oceanic and Atmospheric Administration (NOAA) as well as on the DOD's DMSP satellite imagery. High-level wave clouds are equally spaced and look like "washboards."

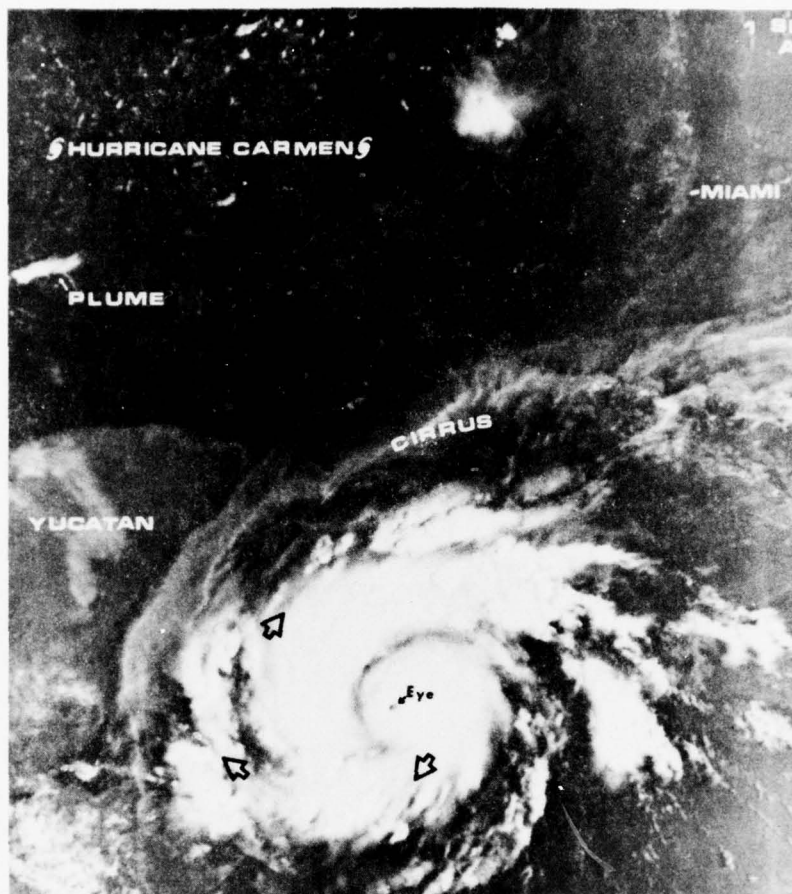


Figure 57. DMSP visual imagery of Hurricane Carmen (1 Sep 74).

d. **High-Level Anomalous Cloud Lines.** Anomalous lines are another high-level phenomena. In Figure 65 two unusual cloud lines converge near Sacramento, just east of San Francisco Bay. These two cloud lines correspond to the inbound and outbound high-level jet traffic of the San Francisco Bay area (Figure 66). Cloud shadows appear on the northern part of these lines. Although the cause has not been confirmed or publicized yet, many analysts believe that these are contrails along the much-traveled routes from the Bay area eastward.

Cloud lines on satellite imagery are very important phenomena and may be used in meteorological determination of contrails as well as air-pollution indicators and, in some cases, wind indicators.

Miscellaneous Phenomena:

a. **Smog-Haze.** Heavy smog or industrial pollution can be seen on satellite imagery. The expanded visual and near-infrared spectral interval of the Defense Meteorological Satellite Program (DMSP) or the Earth Resources Technology Satellite (ERTS) captures smog. The gray, nearly transparent feature is persistent on the satellite imagery in a small or large area. Meteorological conditions have to be right for the smog to persist. A stagnant high-pressure area or inversion where warm air is trapped aloft to prevent the pollution from escaping upward are the common meteorological conditions for smog. In Figure 67, a stagnant air mass, extending from the Great Lakes south and east to the Carolinas and over the

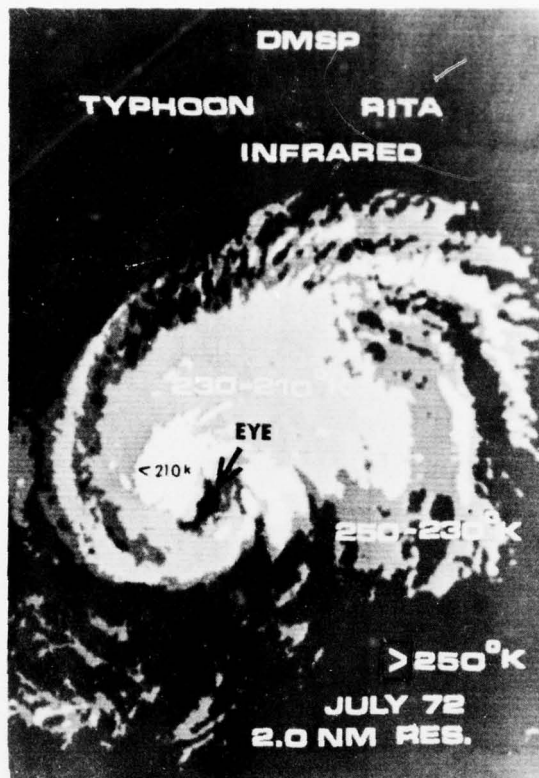


Figure 58. DMSP infrared display of Typhoon Rita (Jul 72).



Figure 59. DMSP visual and infrared photographs illustrating the importance of corresponding infrared photographs (5 May 72).

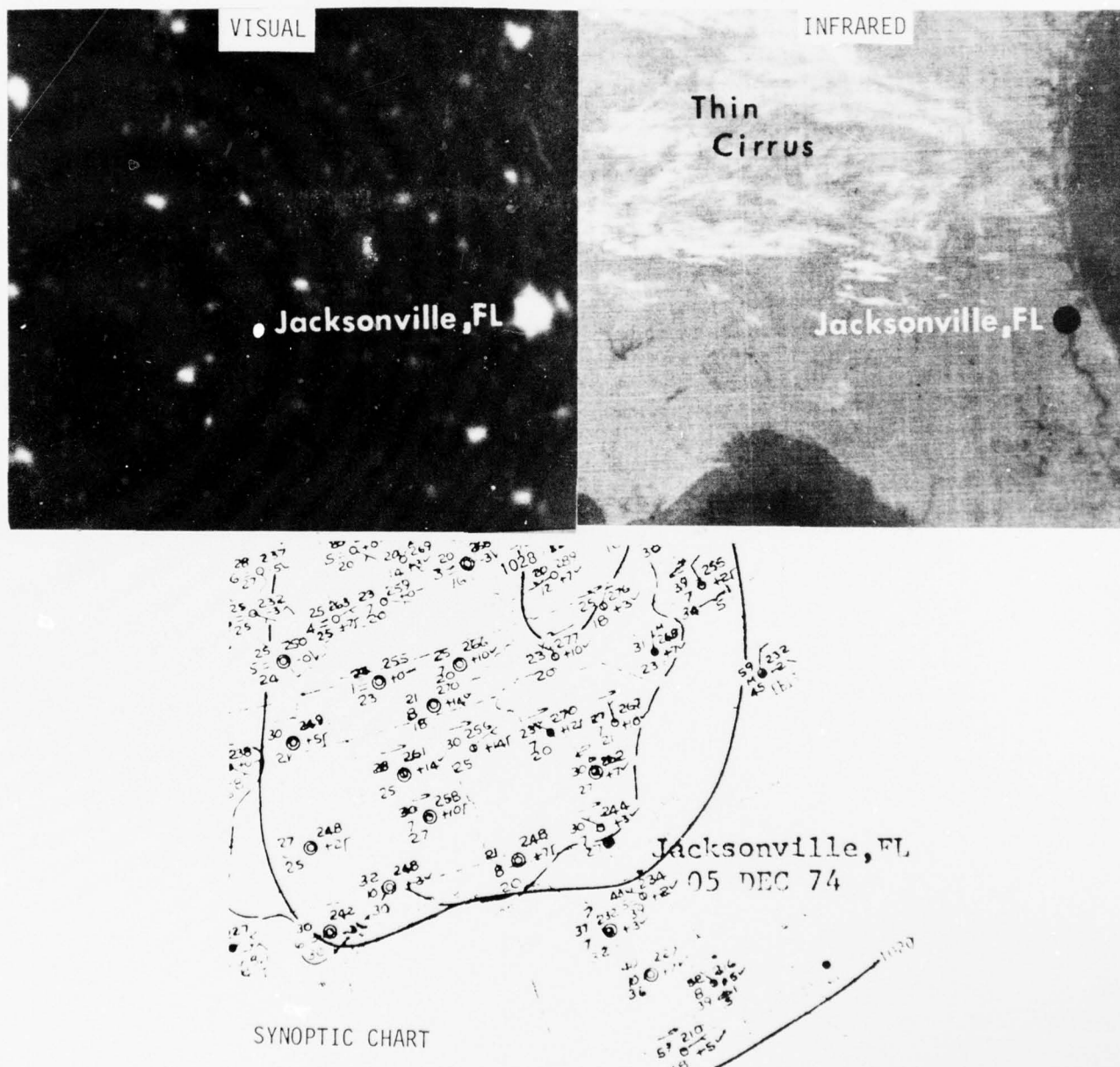


Figure 60. DMSP nighttime visual and infrared imagery of thin cirrus over Georgia (5 Dec 74).

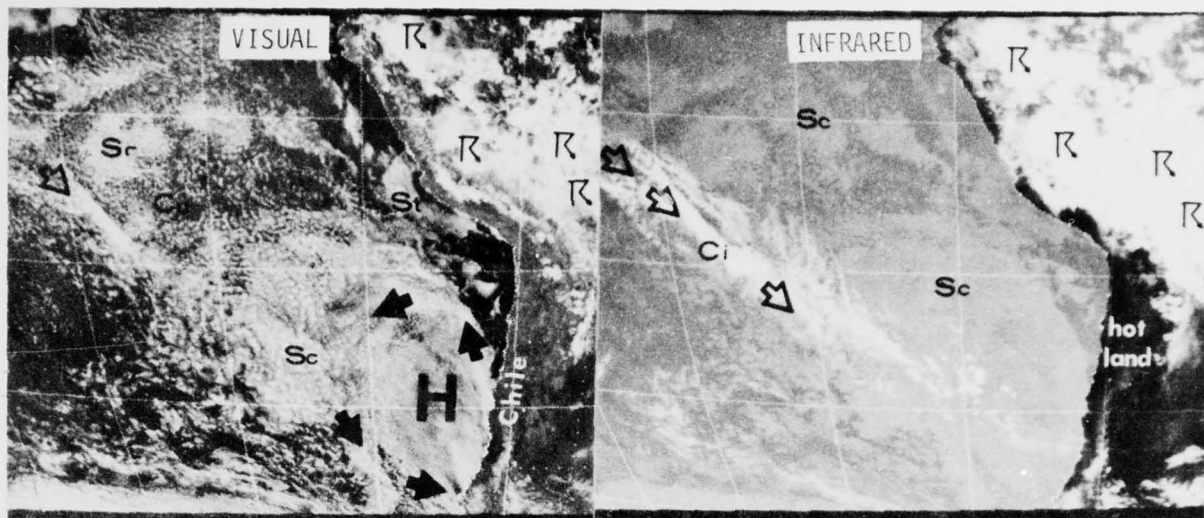


Figure 61. An SMS-1 visual and infrared illustration of high cirrus clouds over lower stratocumulus (22 Nov 74).

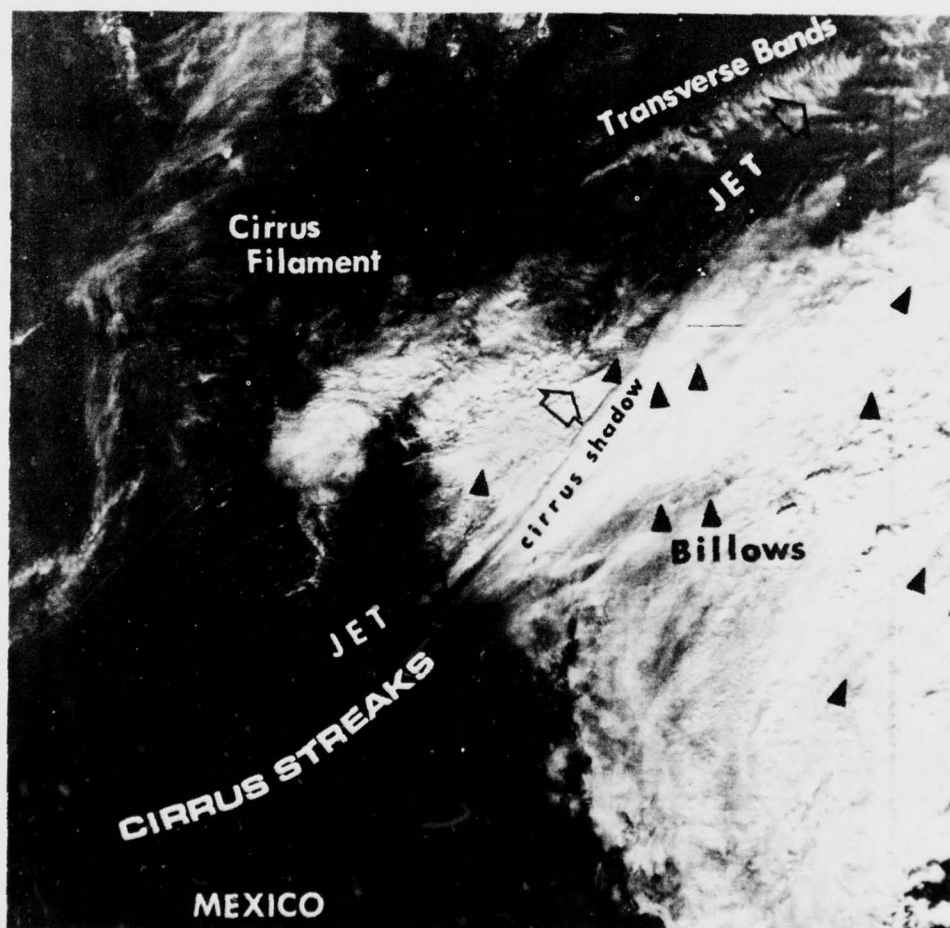


Figure 62. DMSP visual image of several cirrus-cloud patterns (23 Jan 74).

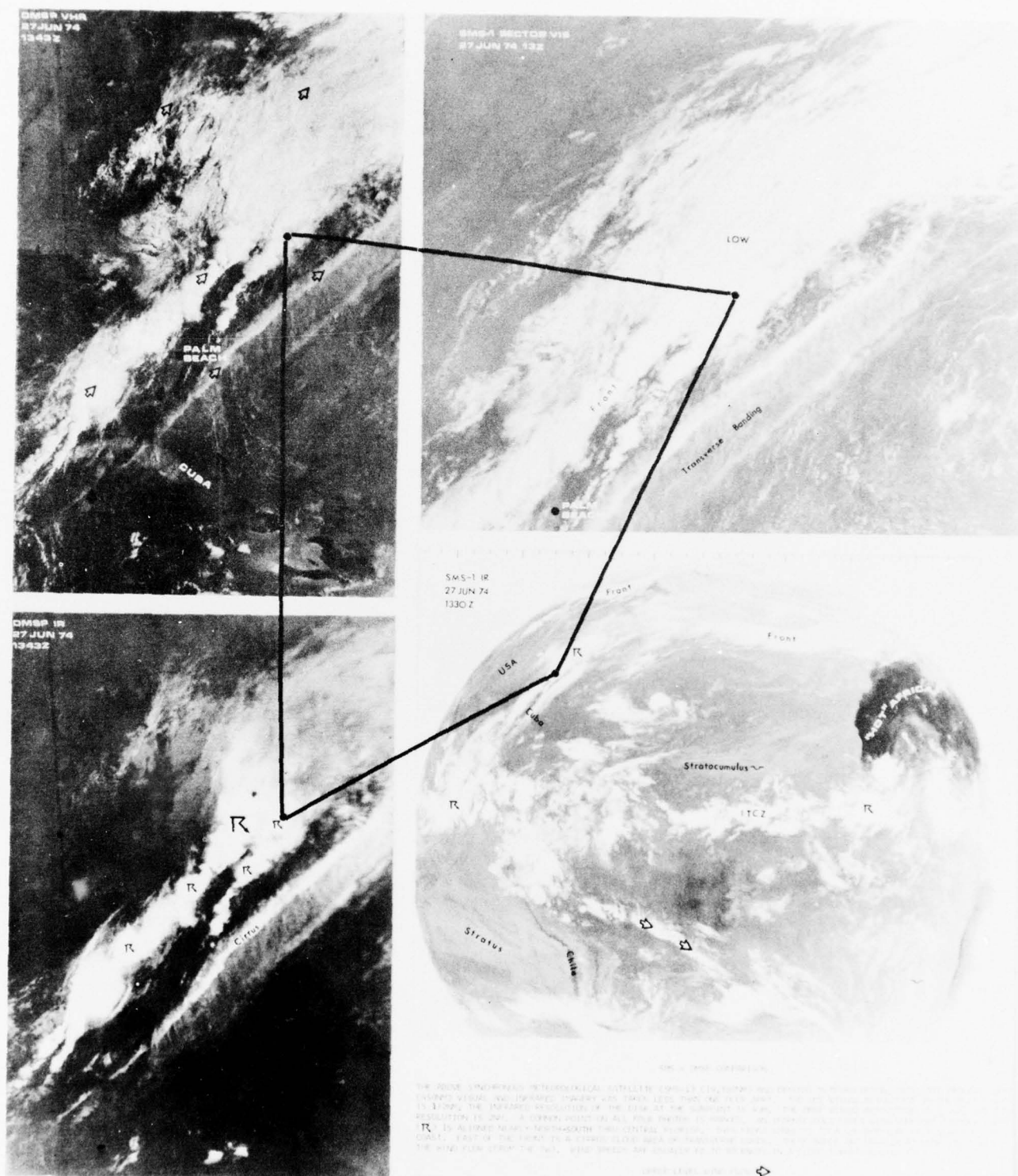


Figure 63. DMSP and SMS-1 visual and infrared photographs showing transverse banding east of Florida (27 Jun 74).

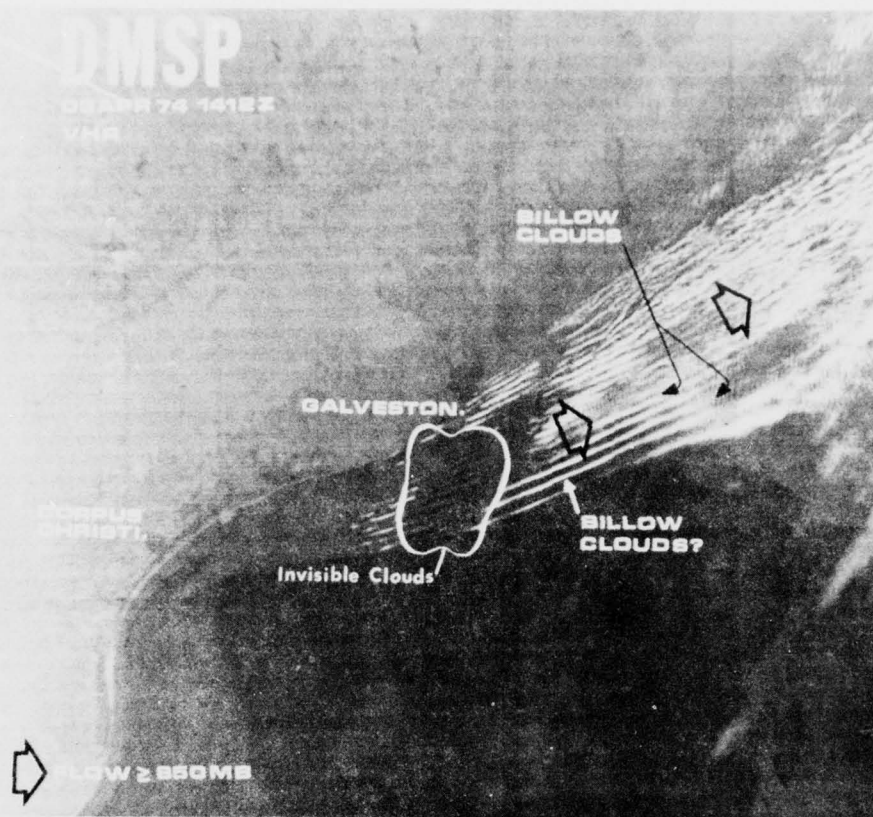


Figure 64. DMSP visual data of low- and high-level billow clouds (3 Apr 74).

Atlantic, is filled with smog and industrial pollution. The smog-alert index for Washington, DC on that date was 150, the second highest in history.

Haze, caused by salt particles, is another form of reduced visibility that can be seen on the expanded visual/near infrared imagery. Because vegetation or city areas can have a gray appearance, one has to be careful in making sure the gray is not a permanent topographical feature. To distinguish between real smog (haze) and vegetation, one would need corroborating information.

Haze occurred during August 1975 on two successive days in Florida. This haze was advected south off the coast of the United States and then west into Florida. The source of the haze was the industrial pollution in the northeast and salt particles over the western Atlantic. Figure 68 is an SMS visual photograph taken on the first day the haze was sensed by the SMS satellite. Figure 69 is an SMS visual photograph from 26 August. The sun angle was such as to give a haze "glint." A weak low, which shows on Figure 69, caused the unusual haze pattern to be pushed south.

b. Dust. Dust has been observed on satellite imagery blowing off continents and traveling for great distances. Figure 70 is an ATS-3 track of a dust cloud that originated in Africa and traveled across the Atlantic to Barbados. Dust clouds can significantly increase the normal amount of incoming solar radiation absorbed in the atmosphere; consequently, less solar energy reaches the surface. All dust-cloud effects on weather are not known; however, the increased sensitivity of current and future satellites should help clarify dust cloud/weather interrelationships. Another dust layer moved across the Atlantic in July of 1974 and is shown in Figure 71.

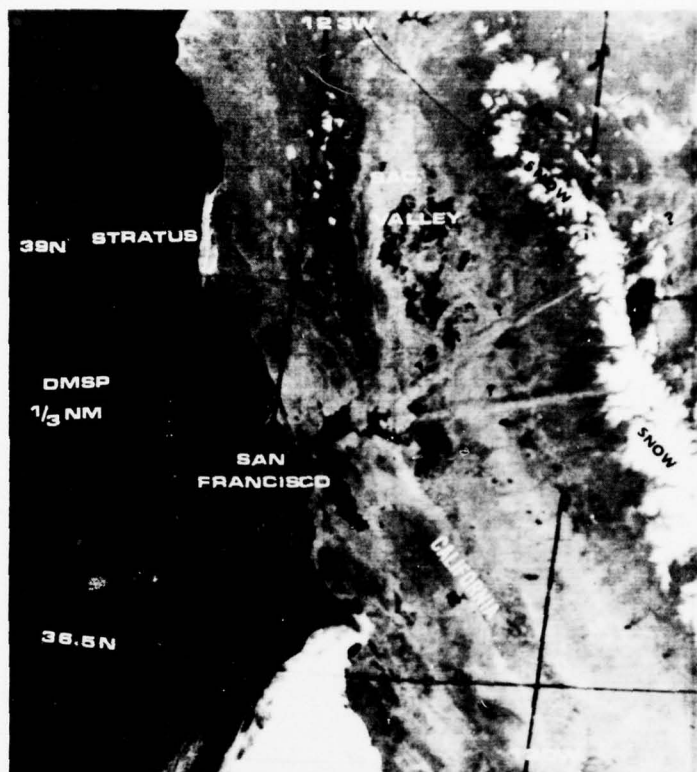


Figure 65. DMSP visual photograph of unusual cloud lines (high-level anomalous lines) extending from the San Francisco Bay area (11 May 73).

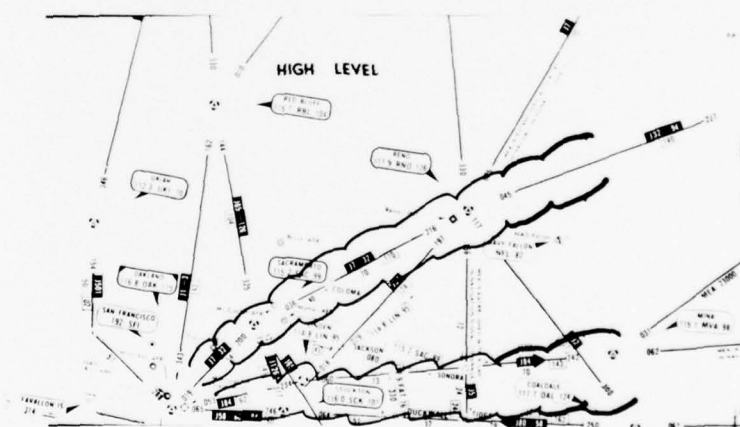


Figure 66. High-altitude jet airways chart for the San Francisco Bay area (High-Level Navigation Chart).

c. **Smoke.** Smoke is another phenomena that is visible on meteorological satellite photographs. It is also a wind flow indicator. In Figure 72 a smoke plume from an active volcano on the Japanese Island of Kyushu is seen. The extent of the smoke and the low-level wind flow is apparent from this figure. Figure 73 is a photograph of a fire in the Everglades which caused a great deal of smoke and reduced visibility as far away as Cape Canaveral Air Force Station, Florida.

August 1976

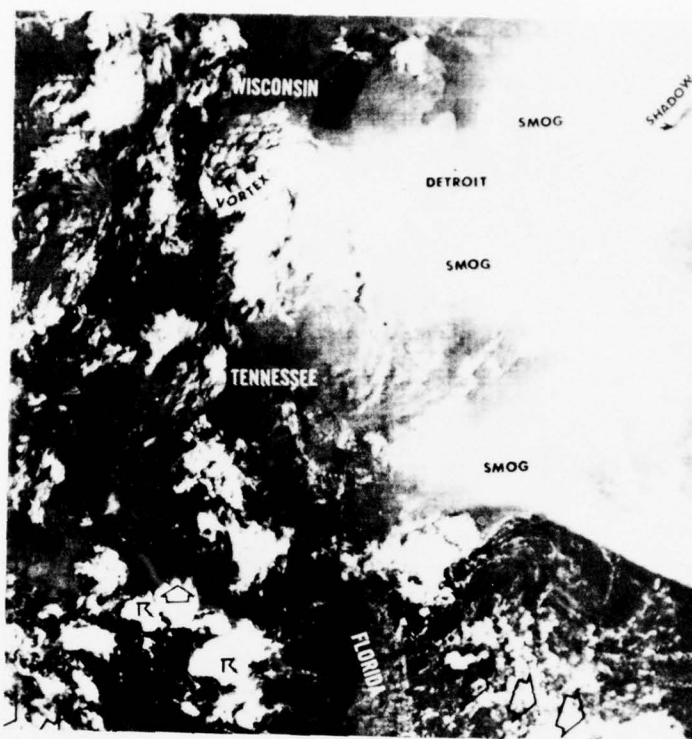


Figure 67. Smog along the east coast of the U.S. on a daytime DMSP visual presentation (30 Aug 73).

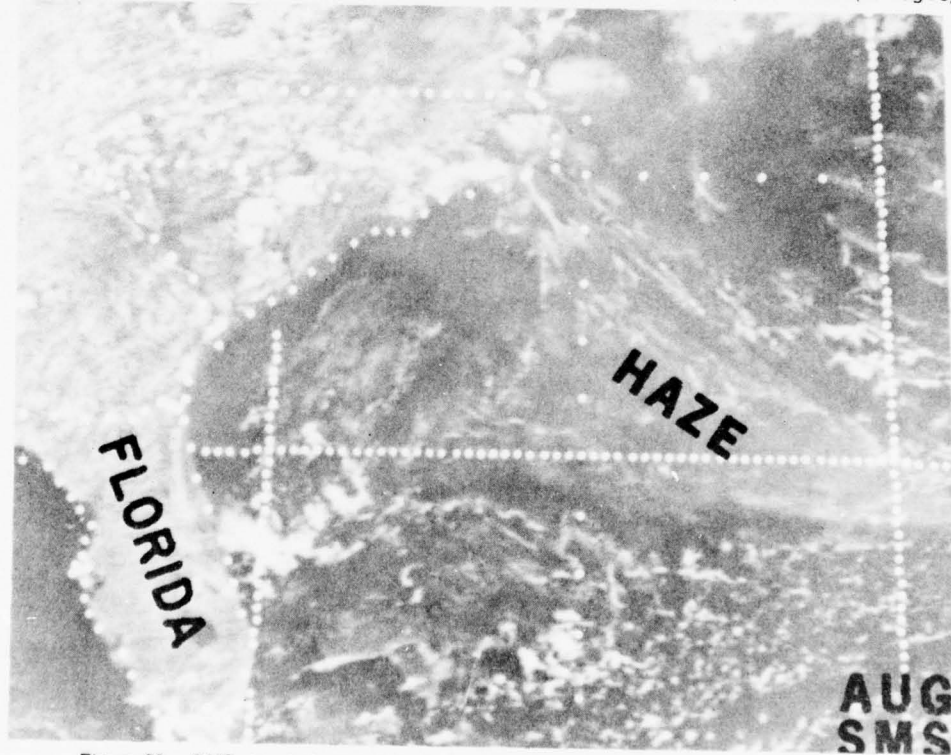


Figure 68. SMS visual photograph of haze off the coast of the eastern U.S. (25 Aug 75).

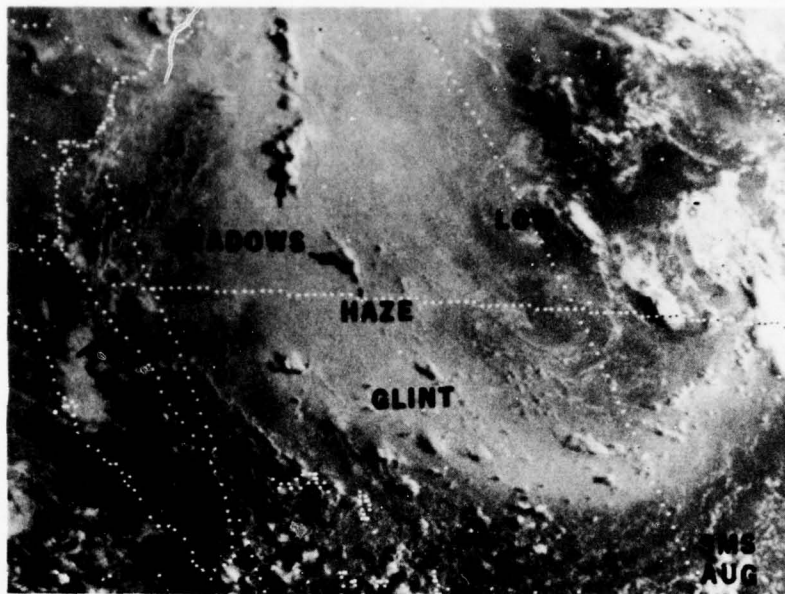


Figure 69. SMS visual photograph of haze and haze glint (26 Aug 75).

d. **Anomalous Gray Areas.** Gray patches appear on many of the DMSP very high-resolution day-time imageries. These gray patches are called anomalous gray areas (Fett and Rabe, [48]). The gray areas have been attributed to many things, including faulty film processing. Gray areas coincide with reefs, lagoons, shoals, and other shallow water phenomenon. Figure 74 is a DMSP photograph of Florida and the Bahamas. Both anomalous gray areas and reefs are presented. A relief map would aid in identifying the reefs from an anomalous area.

Figure 75 shows anomalous gray patches in the Hawaiian Islands. The dark areas could be clear areas with respect to aerosol or water-droplet content in the air. These anomalous gray areas could be extremely important for weather modification, cloud or storm development, atmospheric seeding, and transmission effects. Figure 76 is a DMSP visual photograph showing both clear areas and areas of water droplets.

e. **Aurora Borealis and Aurora Australis.** The aurora borealis and aurora australis, sometimes called the northern and southern lights, respectively, are regularly observed on the nighttime visual data of the DMSP. With the sun-synchronous satellite sensors, the aurora activity of the Northern and Southern Hemispheres can be observed once or twice each night.

The aurora australis and aurora borealis are shown in Figures 77 and 78. The mapping and study of this important phenomenon have been a challenge since the first auroral observations from the ground. In December of 1970, the Air Force Geophysics Laboratory (AFGL), with support from Air Weather Service, initiated a research program to correlate DMSP auroral photographs with the structure of the polar ionosphere. AFGL's NKC-135 flying laboratory probed the bottomside of the ionosphere as the International Satellite for Ionospheric Studies (ISIS) acquired topside soundings and measured particle fluxes. By analyzing such data and correlating them with the DMSP satellite photographs, they found that the location of the auroral-affected D, E, and F layers could be determined, and the occurrence of polar magnetic substorms could be observed. This technique permits real-time observations of the extremely complex and variable polar atmosphere (AFCRL Newsletter, [1]). This new technology resulted from the coupling of two Air Force Systems Command (AFSC) activities: first, systems engineering by which the Air Force Space and Missile Systems Organization (SAMSO) developed the DMSP satellites which had the unexpected ability to photograph the aurora; second, the auroral ionospheric research conducted at

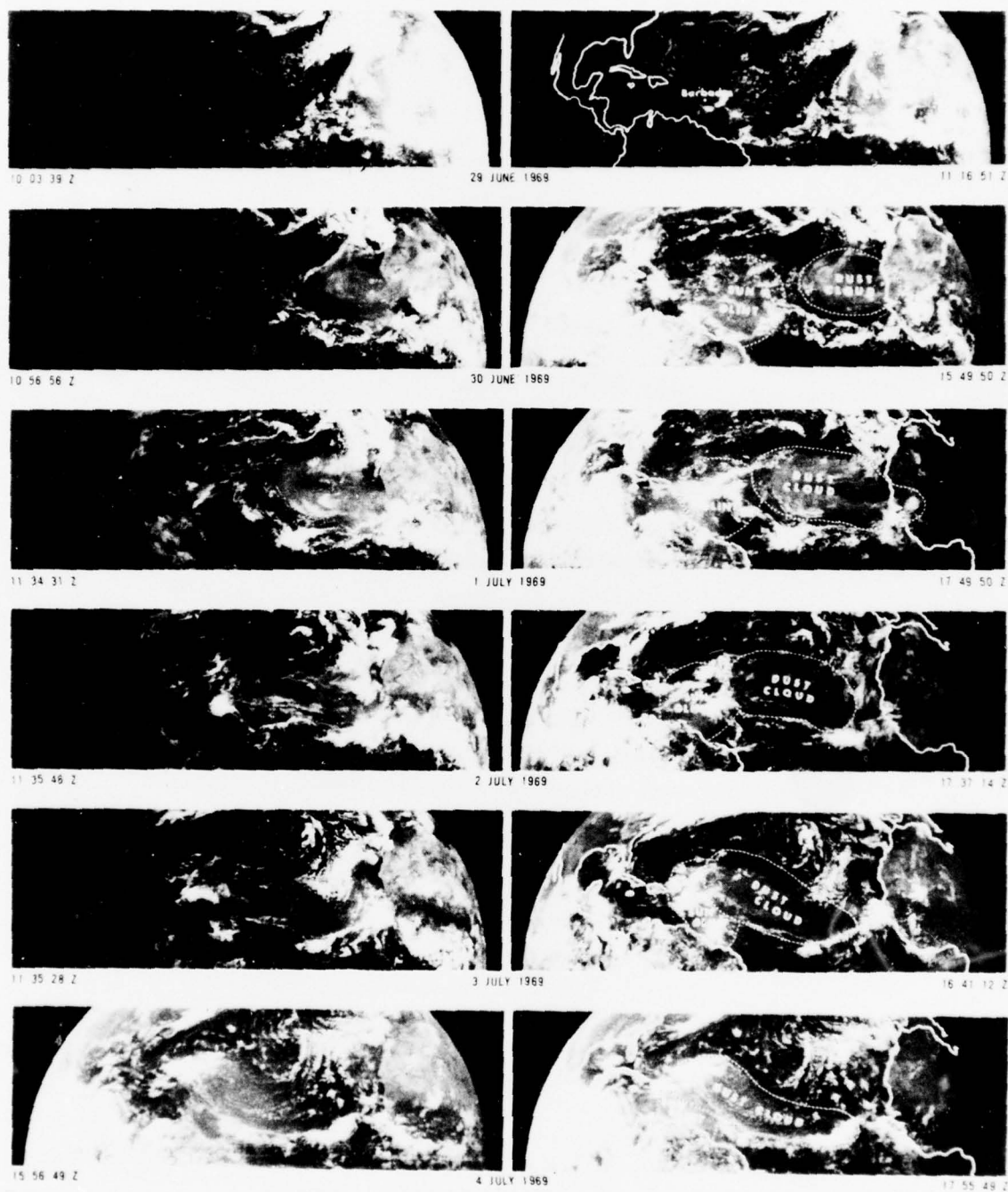


Figure 70. ATS-3 photographs tracking a dust cloud from Africa to Barbados (29 Jun - 4 Jul 69).

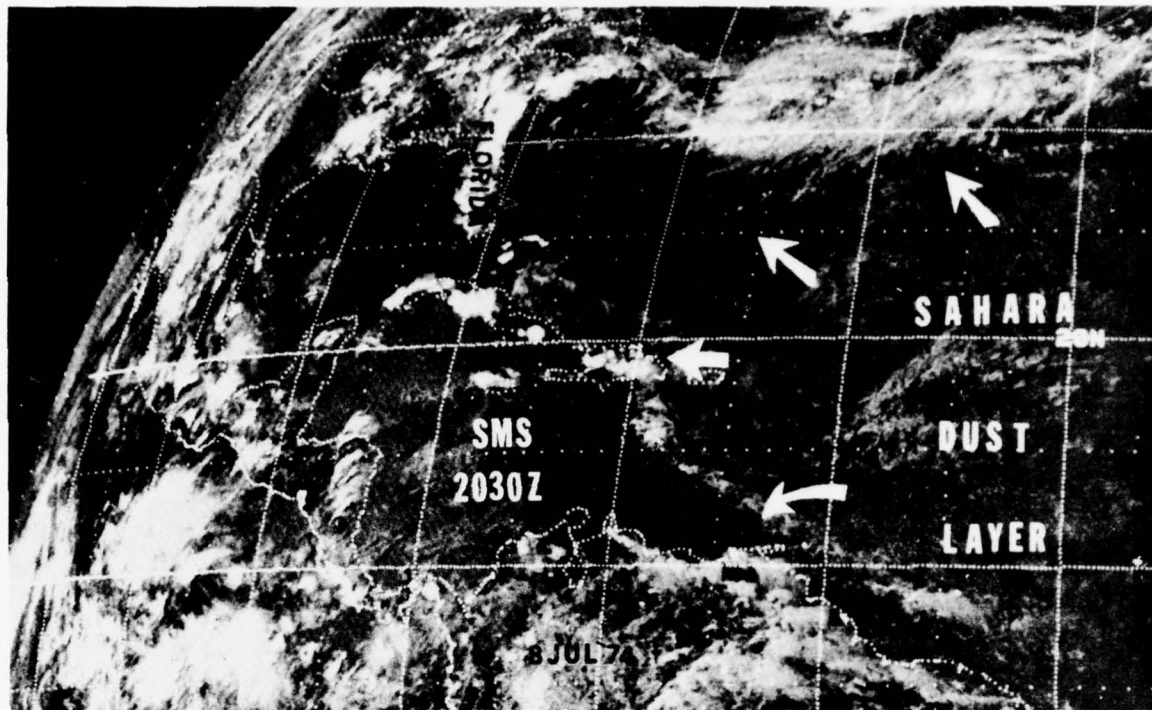


Figure 71. SMS visual photograph of dust layer in the Atlantic (8 Jul 74).

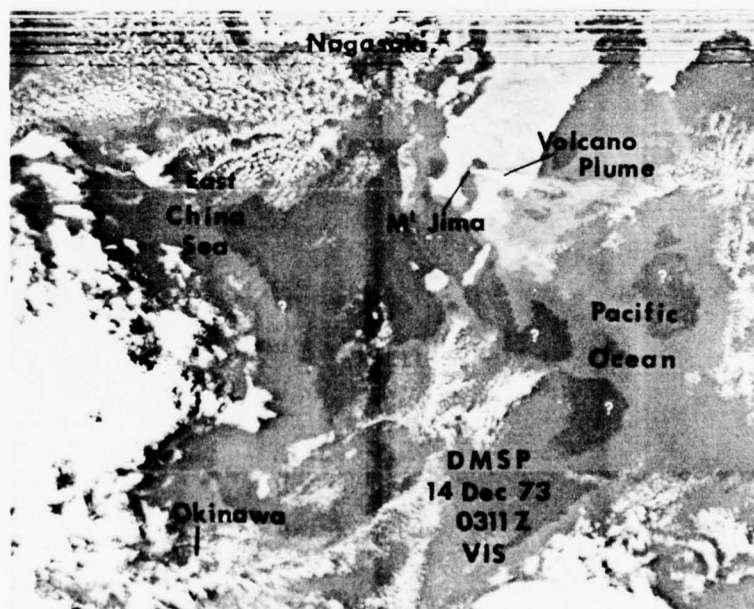


Figure 72. DMSP visual photograph of volcanic smoke plume on the Japanese Island of Kyushu (14 Dec 73).

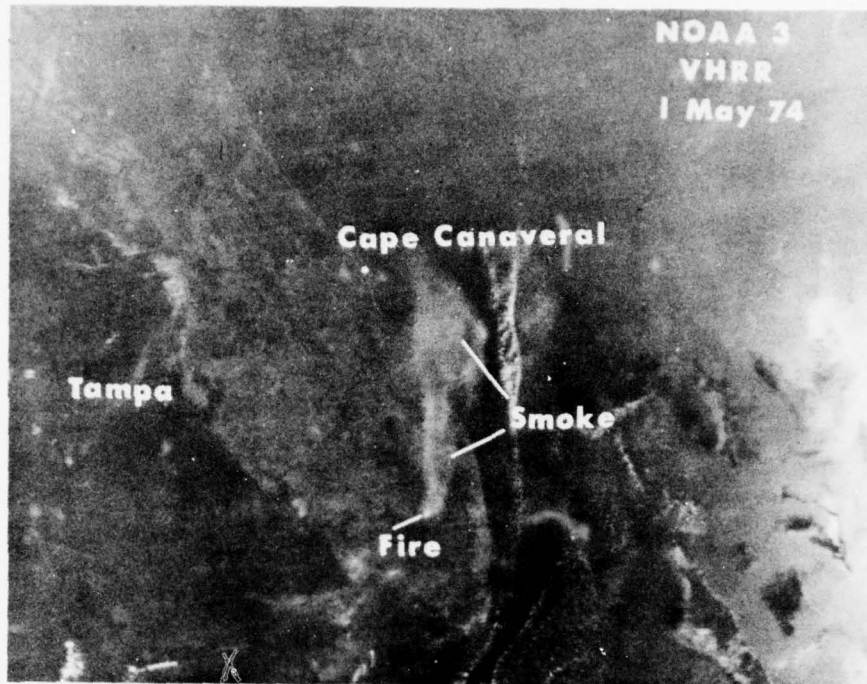


Figure 73. NOAA-3 VHRR photograph of smoke emanating from a fire in the Everglades (1 May 74).

AFGL which enabled initial interpretation of the DMSP auroral photographs in terms of ionospheric and magnetospheric phenomenon (Pike, [88]). The important emissions in the auroral display are shown in Table 5.

Figure 79 is a nighttime visual photograph of North America. Above the 4-km resolution imagery is a photograph of the sun taken by the Air Force Solar Observatory in Puerto Rico on 14 April 1974. This storm intensified the auroral activity. High-frequency (HF) radio transmissions at high latitudes were degraded and some short-wave communication losses were reported during the storm.

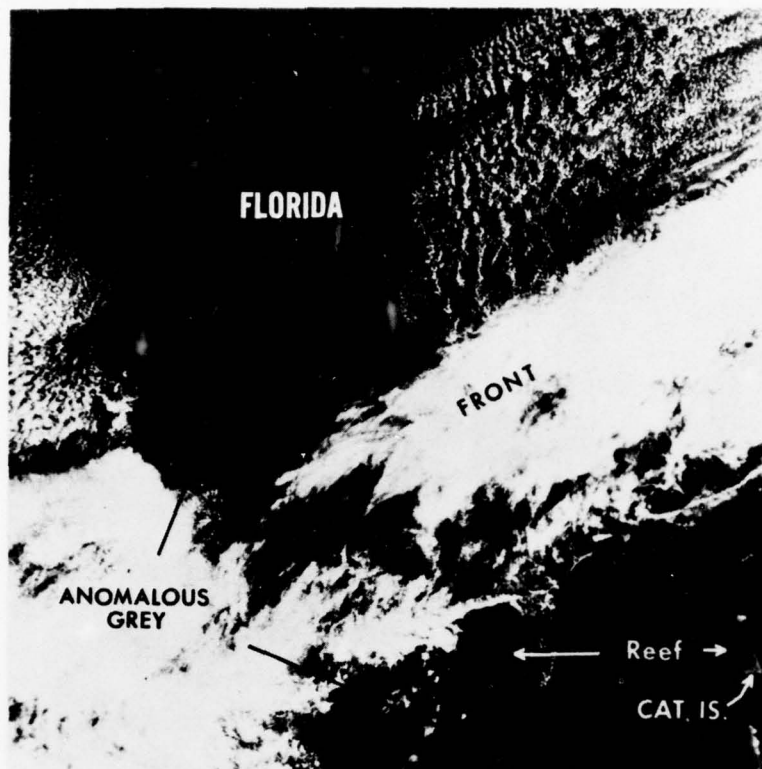


Figure 74. DMSP visual illustration of both reefs and anomalous gray areas (date unknown).

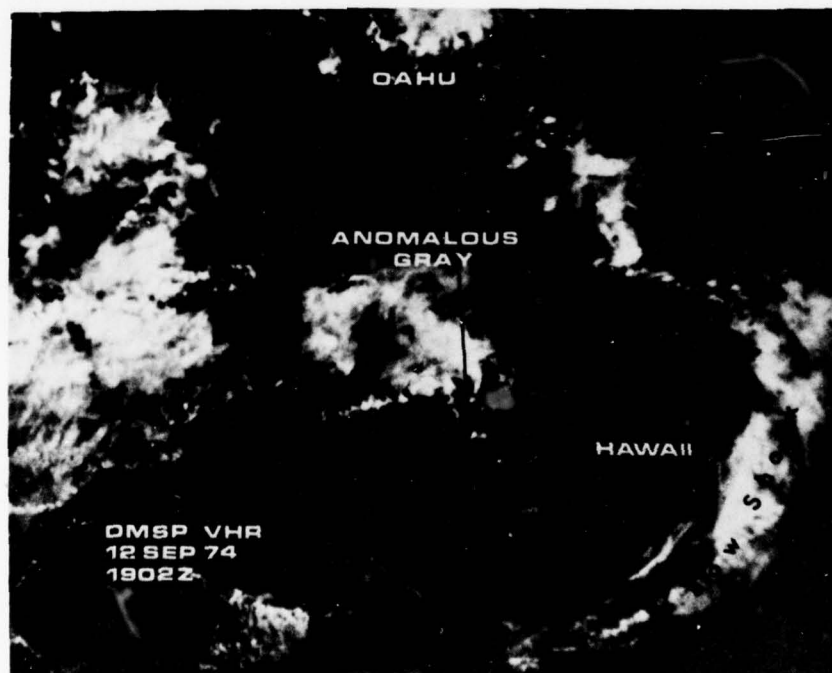


Figure 75. A DMSP visual image of anomalous gray areas in the Hawaiian Islands (12 Sep 74).

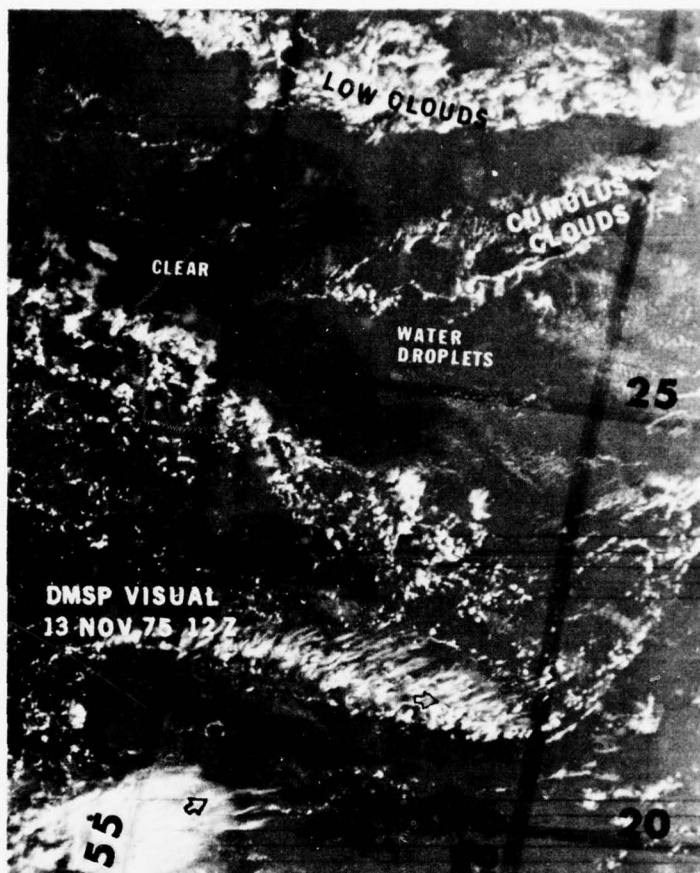


Figure 76. DMSP visual photograph of anomalous gray areas (13 Nov 75).



Figure 77. A nighttime DMSP H image of the aurora australis over the Southern Hemisphere (8 Sep 70).



Figure 78. DMSP nighttime HR image of aurora borealis over Western Europe (date unknown).

Table 5. Important Emissions in Auroral Display (Dandekar [37]).

<i>Emission Gases (lines)</i>	<i>Wavelength (μm)</i>
N_2^+	0.4278
HB	0.4861
*OI	0.5577
HeI	.5876
*OI	0.6300
OH	0.6861
HeI	1.0830

*I indicates spectra of a neutral atom as opposed to single and double ionized atoms, which would be denoted by II or III, respectively.

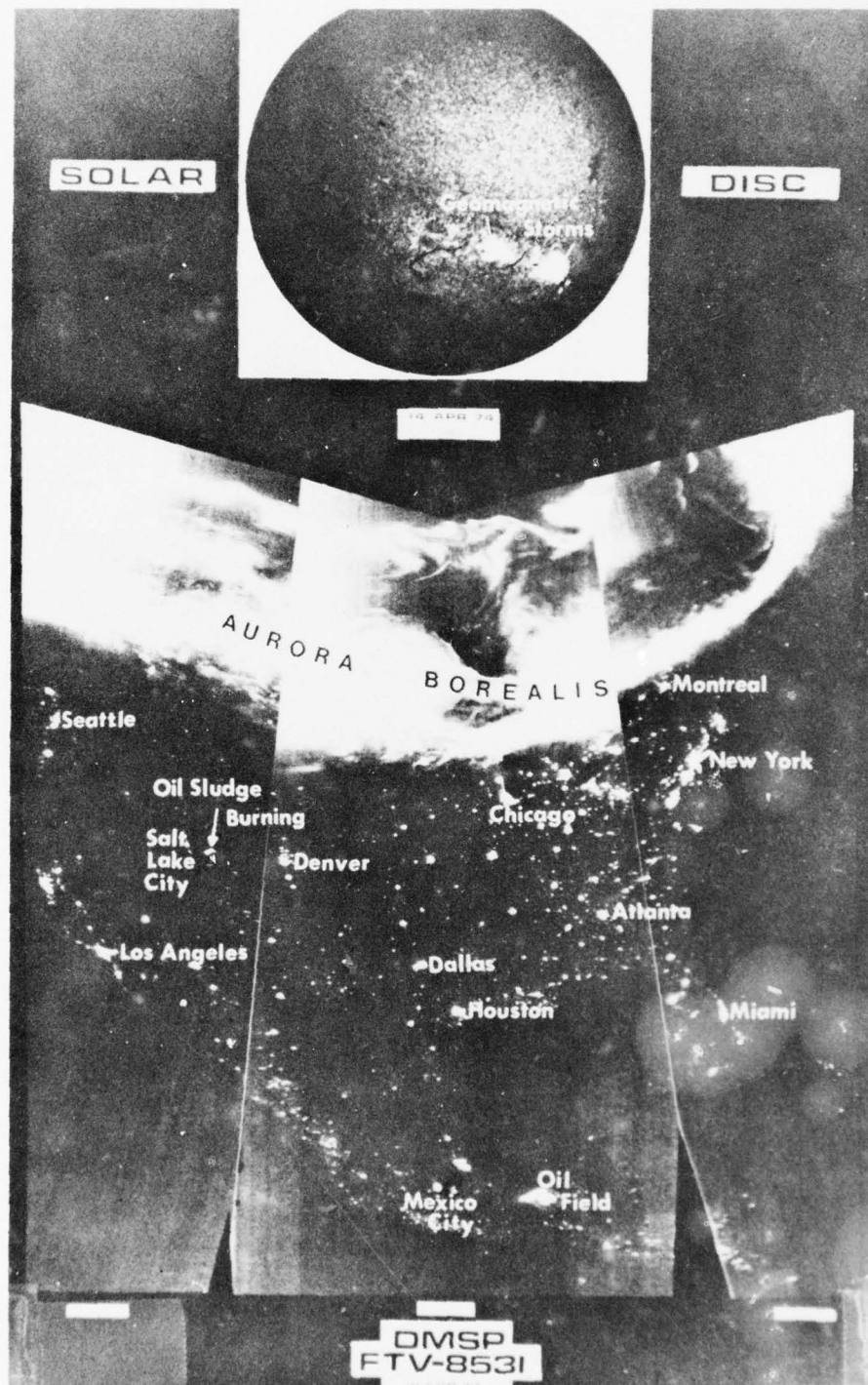



Figure 79. DMSP nighttime imagery over North America (18 Apr 74) with solar disk (14 Apr 74) superimposed.

Chapter 4

WEATHER SYSTEMS

Fronts

Weather systems, such as fronts, are vividly shown on meteorological satellite photographs. However, not all cloud bands are fronts. Shear zones, upper-level systems (such as troughs and vorticity maximums), areas of orographic lifting over wide areas, and tropical convergence zones can look like fronts.

A front is a transition zone separating air masses of differing character, especially of markedly different temperatures. The natural tendency is for the warm air to lie above the colder air in a horizontal layer, but continuous forces of pressure and the earth's rotation never permit this state of equilibrium to be reached. If a cold-air mass is replacing a warm-air mass at the surface, the zone of transition is known as a cold front. If warm air is replacing cold air, the zone of transition is called a warm front. Sometimes, one front overtakes another front bringing into close proximity three different air masses. As the fronts meet, the warmest air mass is completely occluded from the ground and the frontal structure becomes known as an occluded front. Fronts are characterized on satellite imagery by wide bands of multi-layered clouds. A satellite meteorologist should never place frontal symbolism (i.e., ) on any imagery unless other conventional meteorological data is extensive and coincides with the satellite imagery. Placing the symbols without sufficient data spoils the photographic intelligence.

a. Cold Fronts. Figures 80 and 81 are examples of a fast-moving cold front moving through the southeast United States into Florida. On the visual and infrared imagery, the cold front is labeled frontal band. Its movement indicates a cold front. Without other data, this is the way the photograph should be labeled. The infrared sequence over the two days shows the high-level clouds as white and other clouds as different shades of gray. The nighttime visual imagery shows some of the lightning associated with the frontal band.

The photographs also contain a feature labeled the frontal rope cloud. During the past few years the rope cloud has been observed quite frequently. Unfortunately, most of these data were over the ocean or over areas of sparse synoptic data. Because of the sparsity of conventional data, no confirmation of the rope cloud's coincidence with the surface position of the cold front could be proven.

On 3 April 1975, a narrow fast-moving cold front passed over central Florida. The rope cloud could clearly be seen on DMSP visual photographs (Figure 82). The rope cloud retained its identity as it intersected the west coast of Florida, where it slowed down due to surface friction. Fortunately, a multitude of meteorological observations were available for this time period. Figure 83 contains sectional surface charts for 1700 GMT and 1800 GMT. Further creditability is added to the rope cloud by data obtained from the WIND (Weather Information Network and Display) system at Cape Canaveral AFS (Figure 84). A close comparison of the satellite imagery and the plotted charts reveals that, in this case, the rope cloud is coincident with the "blue line" (Janes, et. al., [60]).

Frontal bands are not always easy to identify. Figure 85 is a NOAA-2 infrared image of two cloud bands that resemble a front. On this infrared photograph, a wide band of white (high-level) clouds appears in the southern part of Florida. South and east of this wide band of clouds is another cloud band with a gray shade indicating a lower cloud. In this case, a very shallow cold front has moved through Florida. The white band of clouds in southern Florida is the high-level cirrus associated with the jet stream behind the cold front. This photograph demonstrates the care that must be taken when trying to identify fronts on infrared imagery.

b. Warm Fronts and Occluded Fronts. Figure 86 is an infrared frontal sequence taken from SMS-1. In the first photograph of the sequence (upper left corner), the cold front is moving out in the Atlantic. A

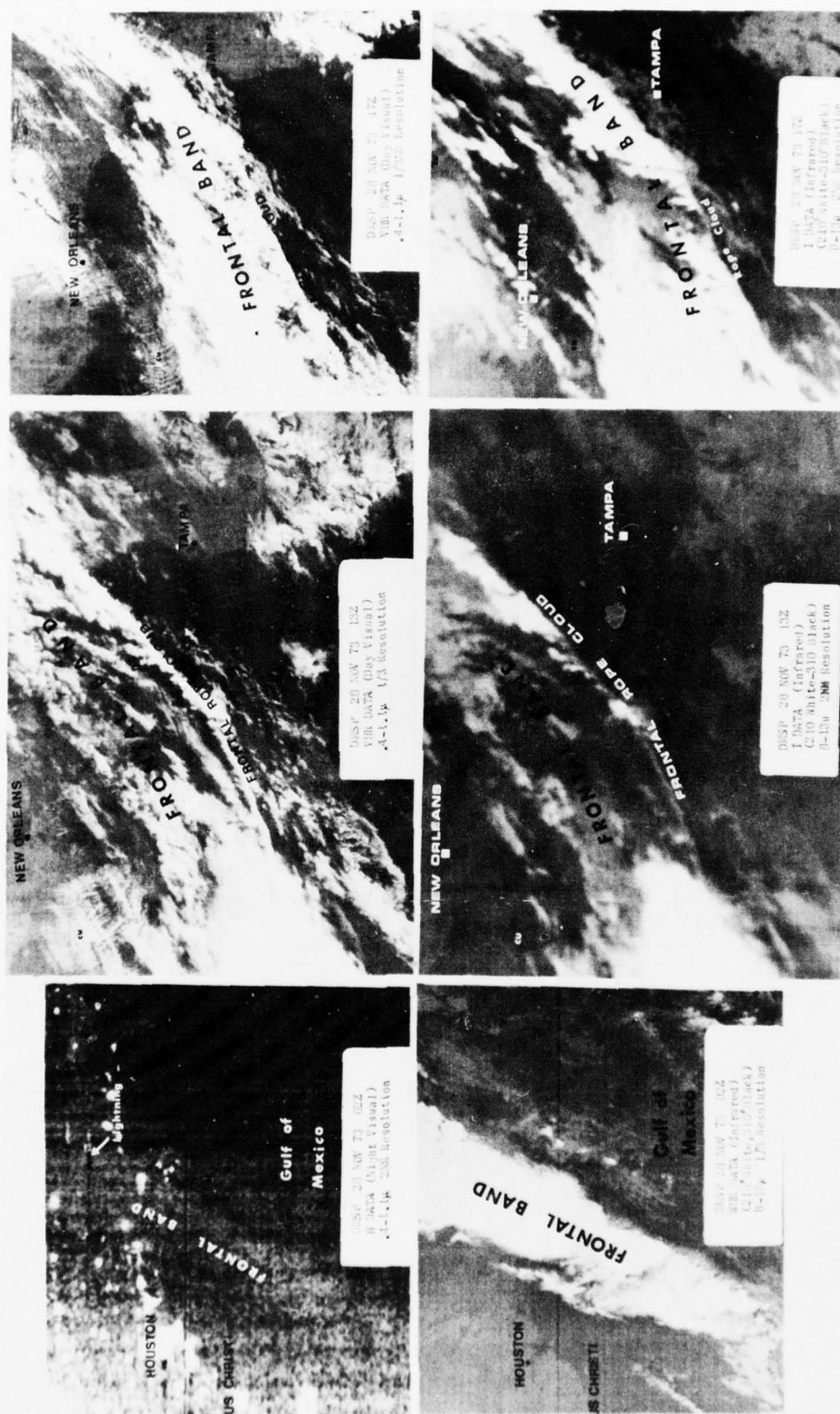


Figure 80. DMSP imagery of a cold front moving into Florida (28 Nov 73).

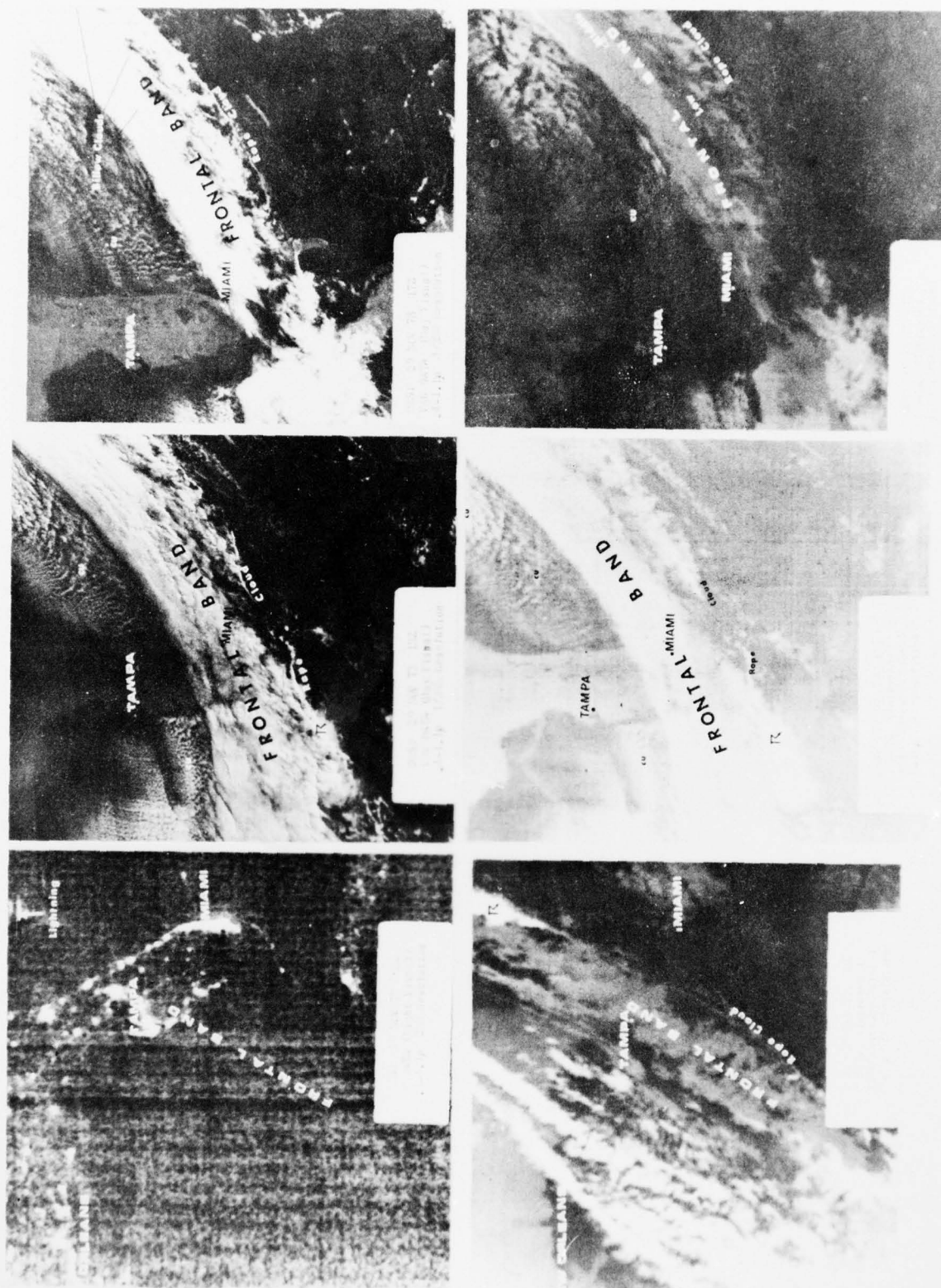


Figure 81. DMSP imagery of cold front moving through Florida (29 Nov 73).

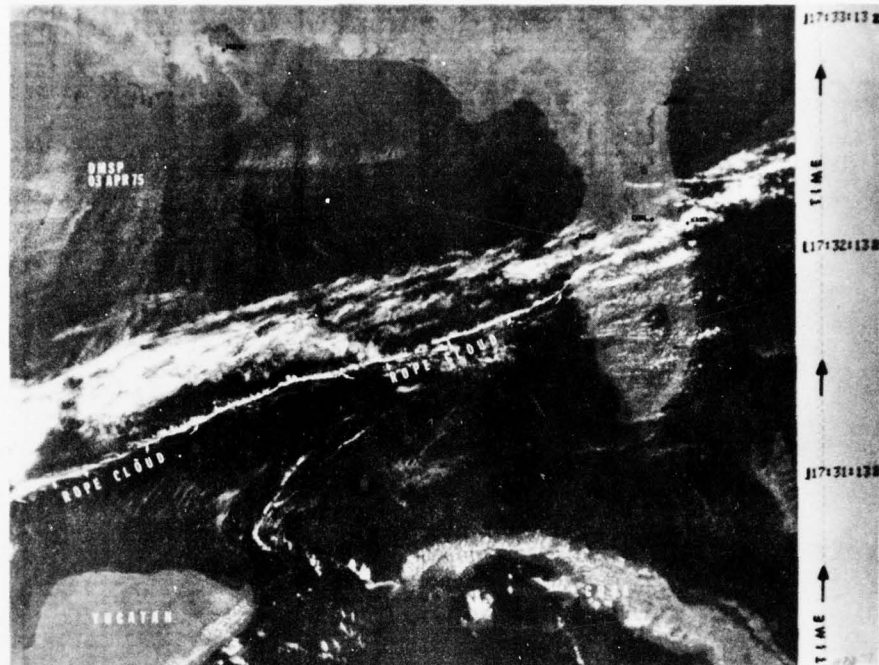


Figure 82. DMSP visual photograph of a rope cloud (3 Apr 75).

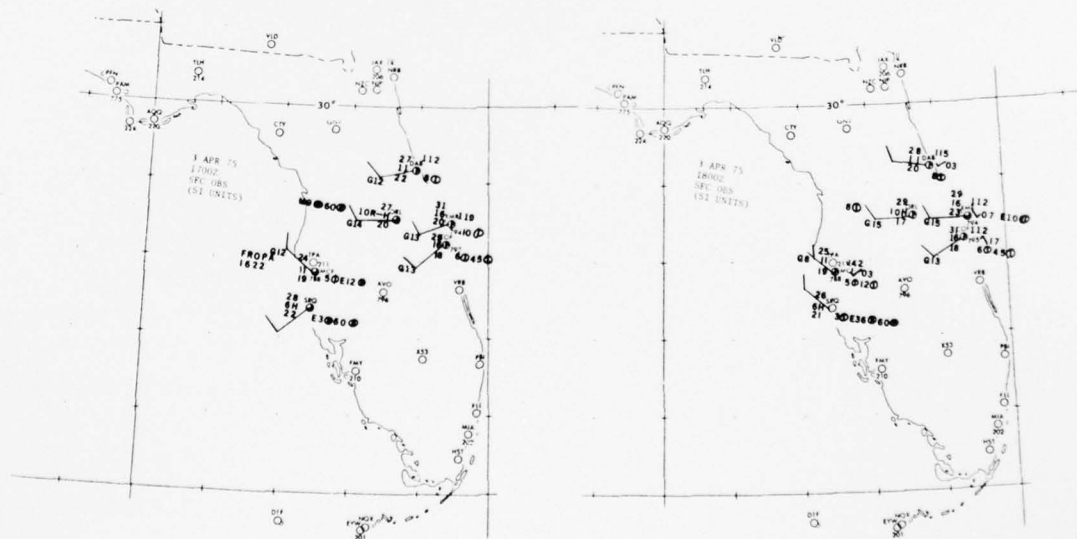


Figure 83. Surface charts for 1700 GMT and 1800 GMT (synoptic units)

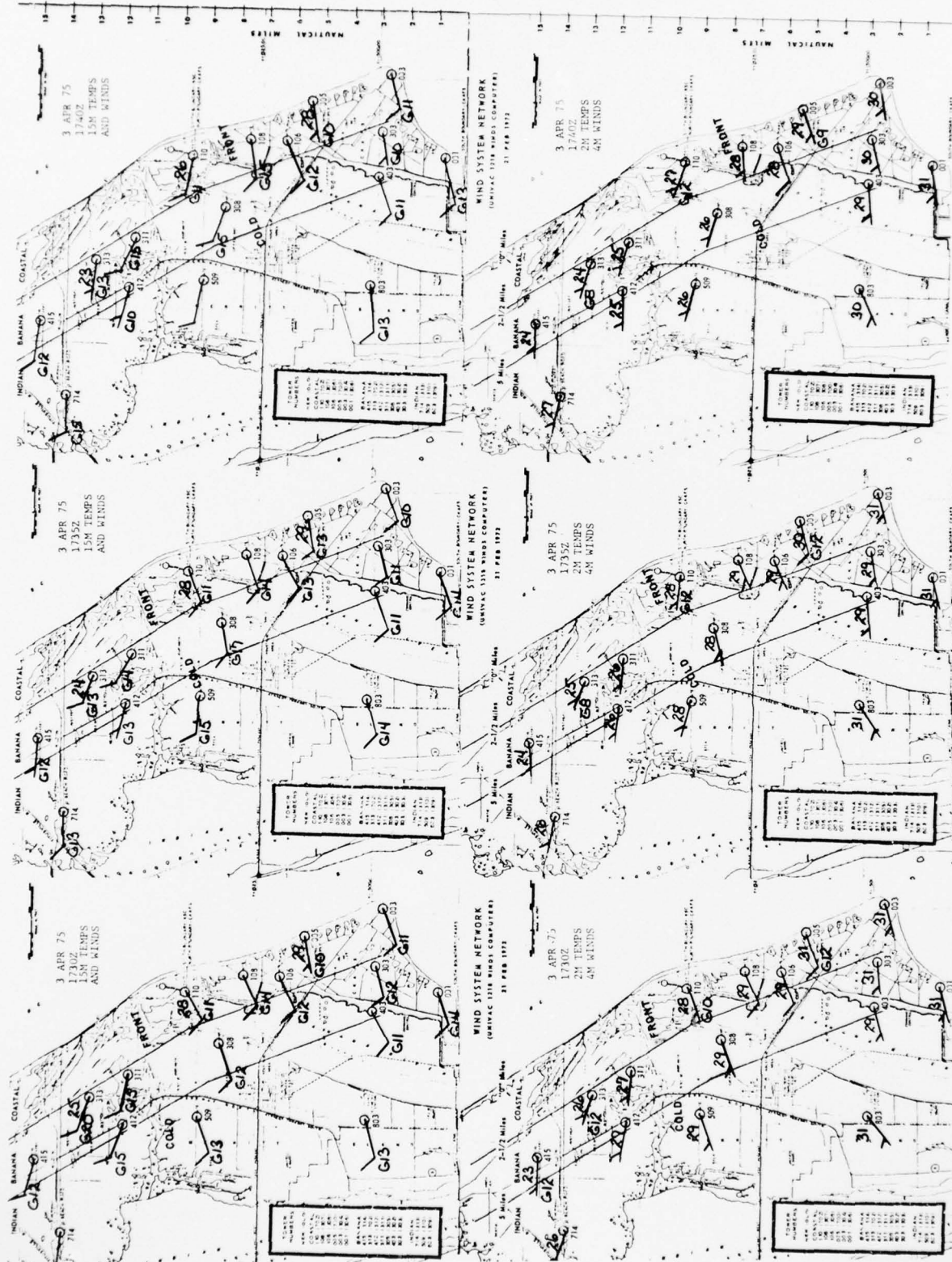


Figure 84. Charts from Cape Canaveral AFS WIND System (temps, °C; wind speed, meters/second).

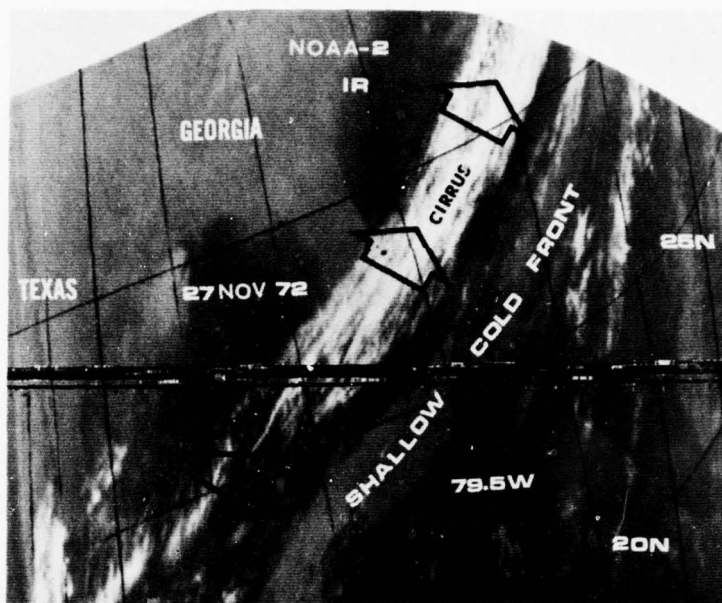


Figure 85. NOAA-2 infrared image of a shallow cold front south of Florida (27 Nov 72).

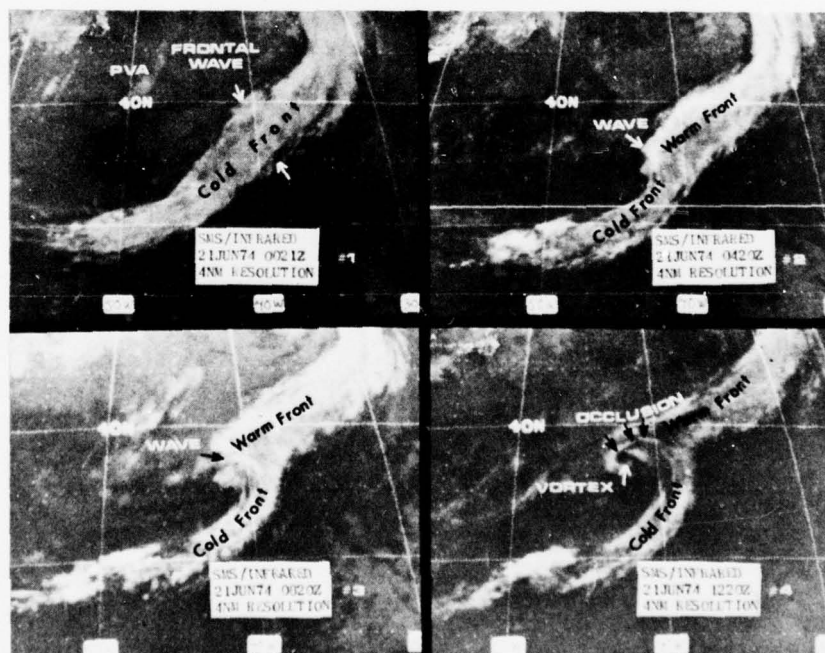


Figure 86. SMS-1 nighttime infrared photographs illustrating the development of a vortex in the Atlantic (21 Jun 74).

bulge on the cold front, known as a frontal wave, is developing. This wave continues to intensify with the creation of a warm front north and east of the wave. This wave front is the boundary between warm air to the south and cold air to the north. As the wave continues to develop, a vortex begins to form. The cold front starts to overtake the warm front near this vortex, and an occlusion forms. This occlusion process occurs many times in the mid and high latitudes of the Northern and Southern Hemispheres. This particular system has a scale of hundreds of miles.

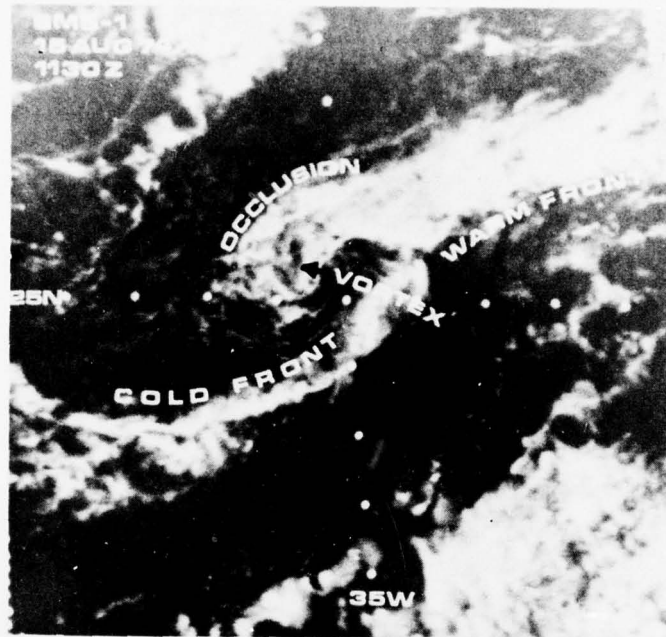


Figure 87. SMS-1 visual image of a small-scale frontal system (15 Aug 74).

Figure 87 shows a small-scale frontal system about a hundred miles in scale. This system, in the Atlantic north of the equator, consists of a cold front, warm front, occlusion, and vortex. These formations have been seen by the author in many areas of the Northern and Southern Hemispheres and have escaped satellite meteorologists because of the poor resolution of past satellite systems (Brandli, [17]). With the new 0.62, 1- and 2-km resolution satellite imagery available, small-scale systems can be seen, monitored, and forecast for possible intensification into more severe large-scale storms.

Figure 88 is an infrared photograph that shows a large-scale frontal system in the central United States with an occlusion extending into the Ohio Valley meeting with a warm front and a cold front. This system is typical of those found over the United States. It is a large-scale system and the fronts are fairly hard to pinpoint, especially the occlusion and the warm front. Thunderstorm symbols (R) are seen where the intense cold front triggered tornadoes.

c. **Sea Breeze Fronts.** Another type of front is the sea breeze front. A sea breeze occurs when the land heats up during the day to such a degree that off-shore air flows on shore, creating a circulation (Figure 89). Sometimes the clouds over the land resemble a front as in Figure 90 over Baja and Mexico. This figure clearly shows the low-level wind flow moving in over the land causing a sea-breeze front to form. At night, this circulation can reverse itself causing a land-breeze effect with resulting cloud line over the water.

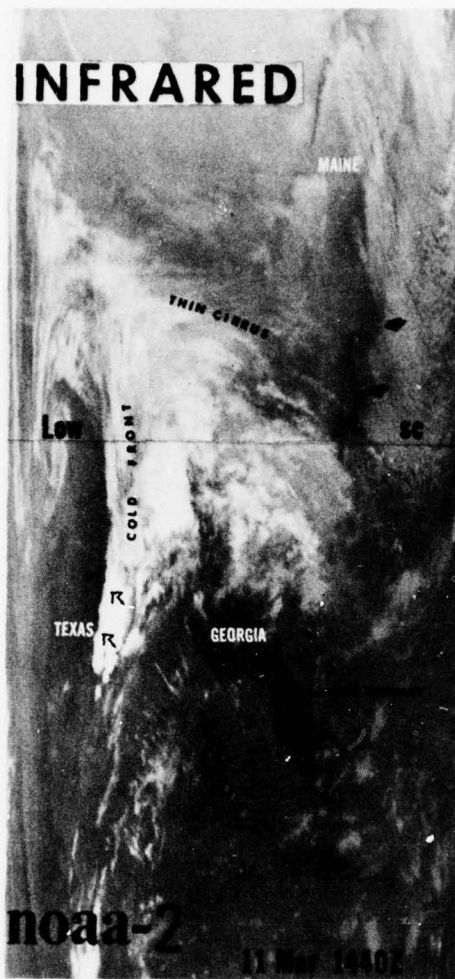


Figure 88. NOAA-2 infrared image depicting a large-scale vortex (date unknown).

Squall Lines

Squall lines are intense lines of thunderstorms and tornadic activity that form ahead of cold fronts. Sometimes, the squall line can be more intense than the front itself. Rapidly converging air ahead of a cold front leads to the immense thunderstorms and tornadic activity which are characteristic of a squall line. Of course, the time of year and location are factors in repeated squall-line development. Warm moist air can also be a precursor of these intense lines of weather. Figure 91 is a DMSP visual photograph of a squall line moving into Florida.

Severe Weather (Tornadoes)

Tornadoes are often found in squall lines and in intense cold fronts, but they are difficult to locate by using satellite data alone. Hook echoes on weather radars are precursors of tornadic activity. There is one cloud pattern, however, where tornado formation is favored. In Figure 92 a cloud pattern is shown where tornado activity is likely to occur. This activity will generally be found at or near the apex of the cloud (Figure 93).

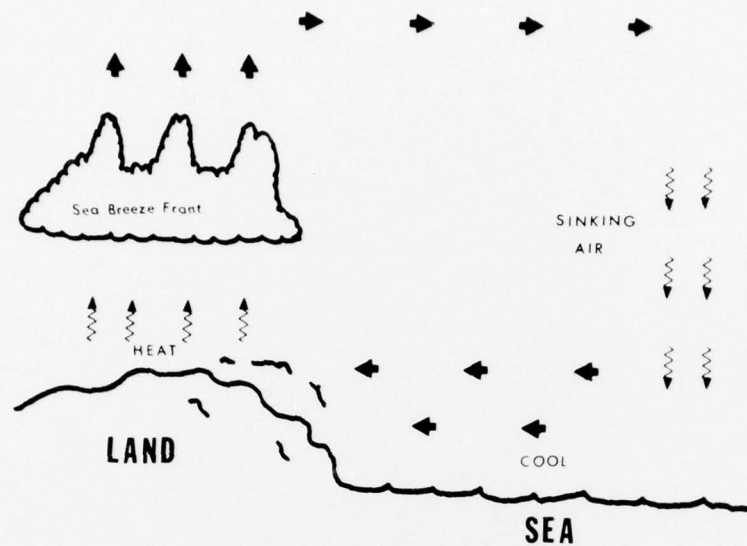


Figure 89. Diagram of a sea-breeze circulation.

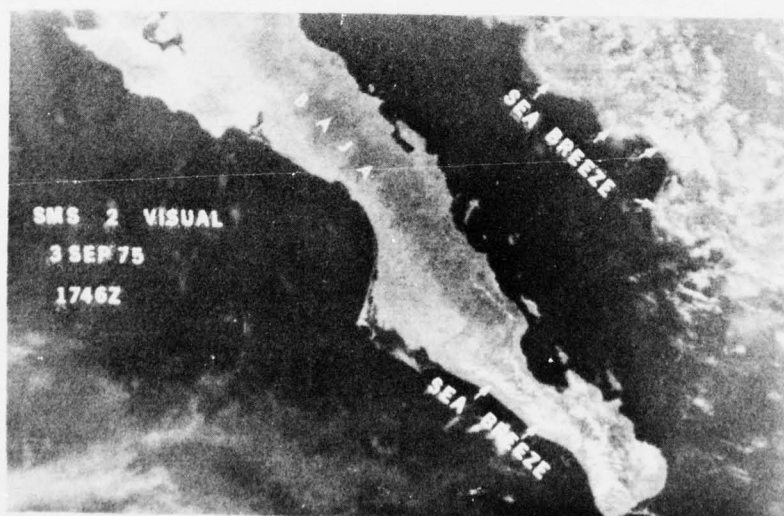


Figure 90. SMS-2 visual view of sea-breeze front (3 Sep 75).



Figure 91. DMSP daytime visual photograph of a squall line through northern Florida (8 Apr 74).

The infrared imagery, in most cases, will show upper-level (white on the infrared) divergence (spreading out of the wind flow). This spreading out of the flow at high levels is accompanied by low-level convergence and strong updrafts. The severe weather, including tornadoes, occurs near the apex and downstream to where the clouds become cirrus only. This break from solid clouds to thin cirrus is observed better on the visual imagery. Consequently, simultaneous visual and infrared data would be desirable for the detection of tornadoes.

In the next figure (Figure 94), a NOAA-4 daytime infrared image is labeled to show the severe weather recorded. The infrared presentation resembles a real tornado (white tornado). The severe weather, as observed from the surface, is numbered on the photograph as follows:

1. Tornado 14NNE, Dallas, Texas, 1625 GMT
2. Funnel Cloud, Alvord, Texas, 1330 GMT
3. Hail, 1-3/4", 12WSW, Ft. Smith, Arkansas, 1530 GMT
4. Hail, 1", 23WNW, Ft. Smith, Arkansas, 1510 GMT

a. Lightning. In Figure 95, a DMSP night visual photograph with no moonlight, lightning flashes are shown in a squall line as it moves into central Florida. The lightning flashes are presented in short bursts of white lines. The DMSP sensor detected the lightning, but the radiometer on board the satellite could not pinpoint the lightning and, as a result, a line appeared. Figure 96 is a night visual photograph of lightning associated with an intense cold front. In this case, a full moon illuminated the clouds. The lightning flashes are shown all along the front extending into the Ohio Valley. Coincidentally, this imagery was recorded shortly after the time of the Xenia, Ohio, tornado. All nighttime DMSP visual photographs are taken in the descending node. The sensor scans from left to right. Consequently, the lightning causing the white lines is at the left end of the line in the photograph.

August 1976

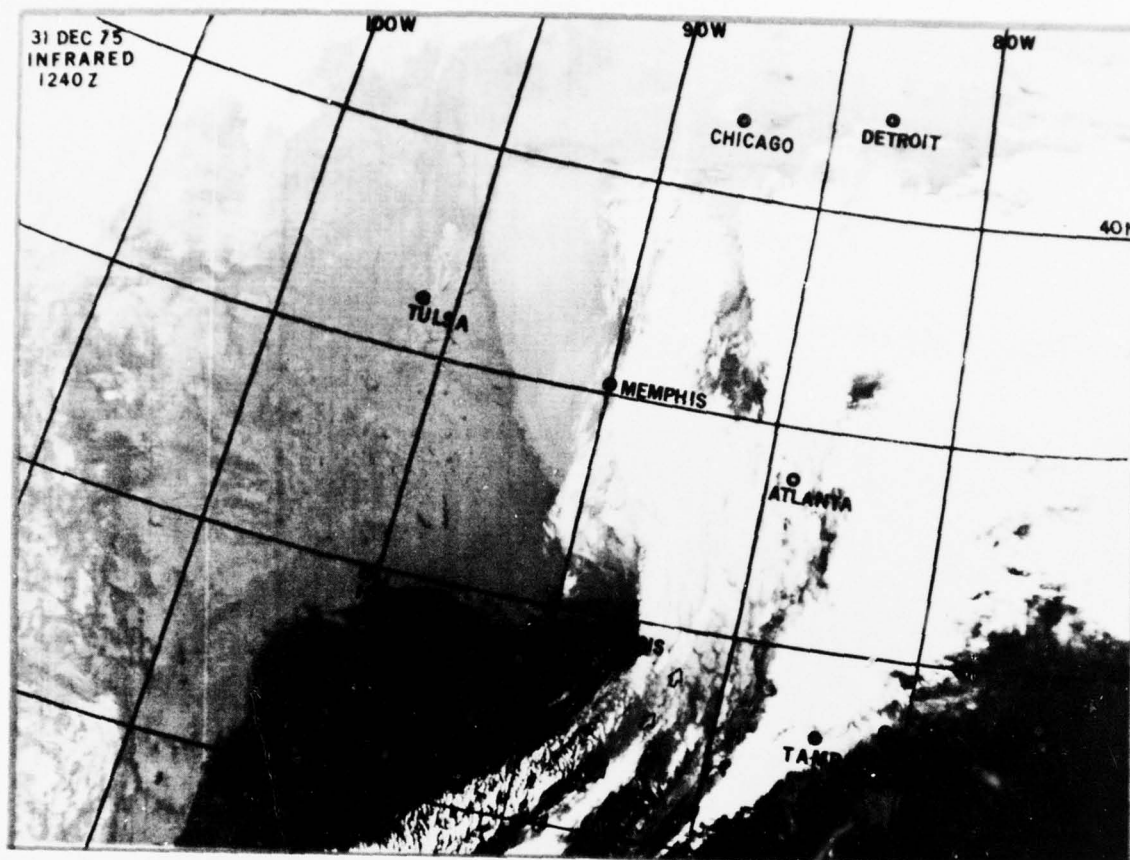


Figure 92. DMSP photograph of tornado area in Gulf of Mexico through Florida (31 Dec 75).

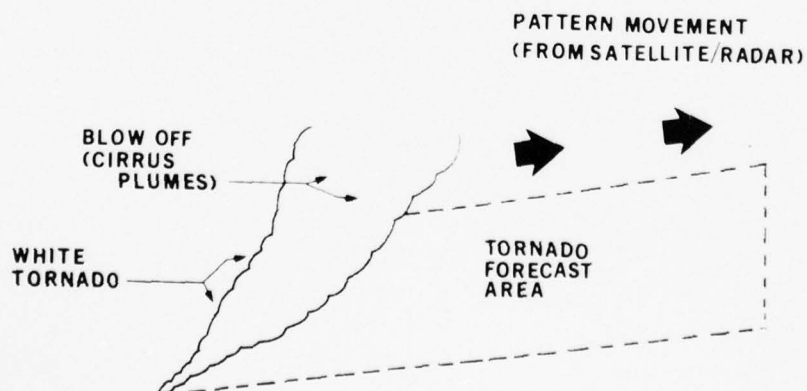


Figure 93. Tornado forecast scheme.

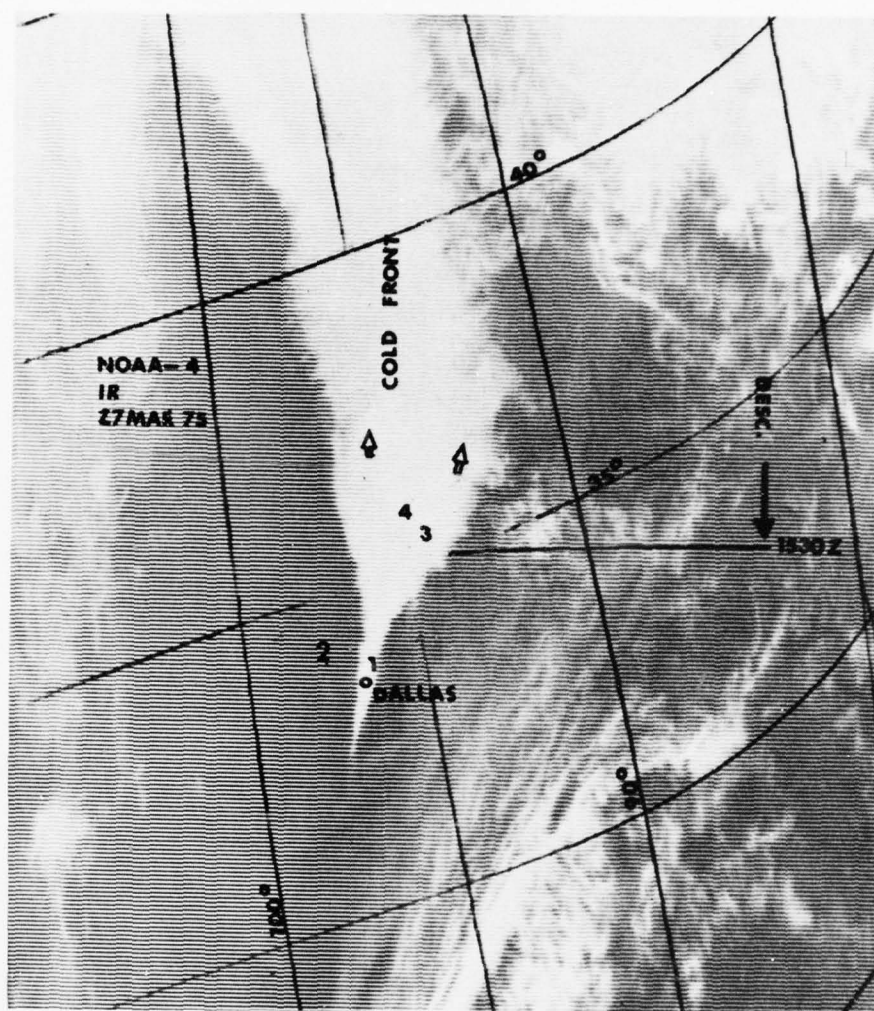


Figure 94. NOAA-4 infrared imagery of a frontal area in the Midwest (27 Mar 75).

Vorticies

Vorticies of all sizes are a common cloud pattern seen on both visual and infrared meteorological satellite imagery. Large-scale vorticies occur in occluded weather frontal systems where a cold front has overtaken the warm front ahead of it. Figure 97 is DMSP visual and infrared photographs of a large-scale vortex over the Great Lakes and its associated frontal systems. The low-level clouds streaming into the vortex from the south complement the outward upper level flow to the north. As the frontogenesis continues, the large vortex goes through its stages to maturity and then dissipation.

Figure 98 shows a vortex in a stratiform low-level cloud formation south of San Francisco off the west coast of the United States. The formation of fog and stratus off the coast of California is caused by the upwelling of cold water which, in turn, cools the overlying air. The vortex in the stratus is a low-level phenomenon. However, in this case, one can almost indicate an anticyclonic flow. This flow occurs because of the inducement of wind flow in the terrain upwind of the stratus formation.

An example of a small-scale terrain-induced vortex is shown in Figure 99. This low-level vortex is seen between Corsica and Italy. Although no infrared imagery is available to help estimate the cloud tops, the tops of this vortex are probably no more than 900 meters. This cloud pattern could cause severe

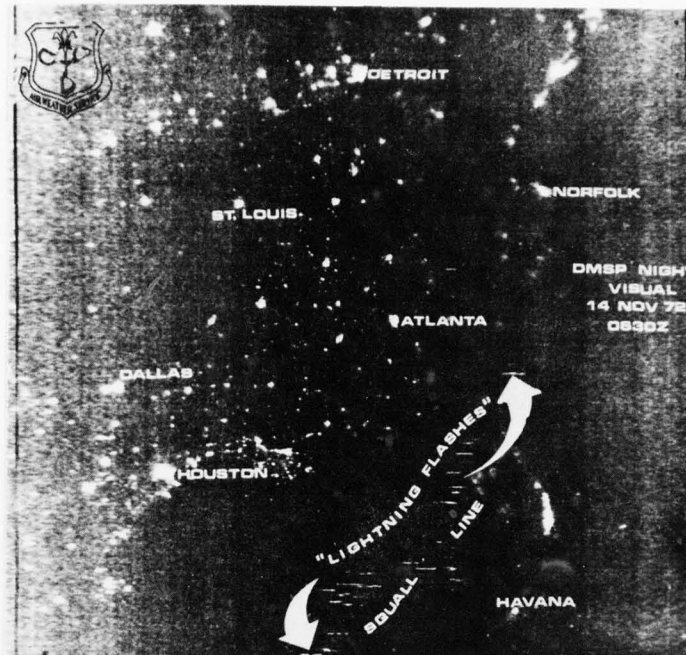


Figure 95. DMSP nighttime visual photograph of lightning flashes (14 Nov 72).

low-level turbulence for aircraft or rough local high-sea conditions that would affect boating.

Small-scale vortices appear on meteorological satellite photographs more often in the lower latitudes. The persistent trade winds cause vortex cloud patterns to form near coast lines and down stream from islands. The trade-wind pattern is favorable for inducing the vortices which eventually become tropical depressions or tropical storms (Brandli, [11]). Figure 100 depicts a small-scale vortex in the Yucatan Straits moving northeastward through the Gulf of Mexico and becoming a tropical depression.

Hurricanes, Typhoons, and Cyclones

Hurricane, typhoon, and cyclone monitoring by meteorological satellite imagery has been a huge success over the last few years, especially with the DMSP support at the Joint Typhoon Warning Center in Guam. Selective aircraft reconnaissance has been possible with the use of this high-resolution day and night visual and infrared imagery. Because of this real-time data every 6 hours or less, the use of weather reconnaissance aircraft for the exploring and probing of storms can be reevaluated and probably redirected. Using these reconnaissance aircraft to help calibrate satellite instrumentation would help reach the ultimate goal of using satellite imagery exclusively for storm detection and forecasting. The intensity of hurricanes and typhoons can be roughly determined now with already recorded satellite data.

The origin of a hurricane can be traced to a diffuse and fairly large area of low pressure over warm water. The winds around the low-pressure area are modest and cumulus clouds and showers are numerous, but there is no organized system of clouds and weather. Such low-pressure areas may be present for several days before the development commences, and often none takes place. As the storm begins to organize itself into a coherent pattern, it goes through various stages of increasing intensity. The first recognizable pattern of a hurricane on satellite imagery is that of the tropical depression. In this stage the storm has wind speeds of less than 34 kt. As the storm develops into a tropical storm, wind speeds increase from 34 kt to less than 64 kt. The storm is now well organized and has a very distinct rotary circulation. As the wind speeds increase to greater than 64 kt, the storm becomes known as a hurricane.

Tropical storms are classified by the cloud features they exhibit. The classifications have been em-

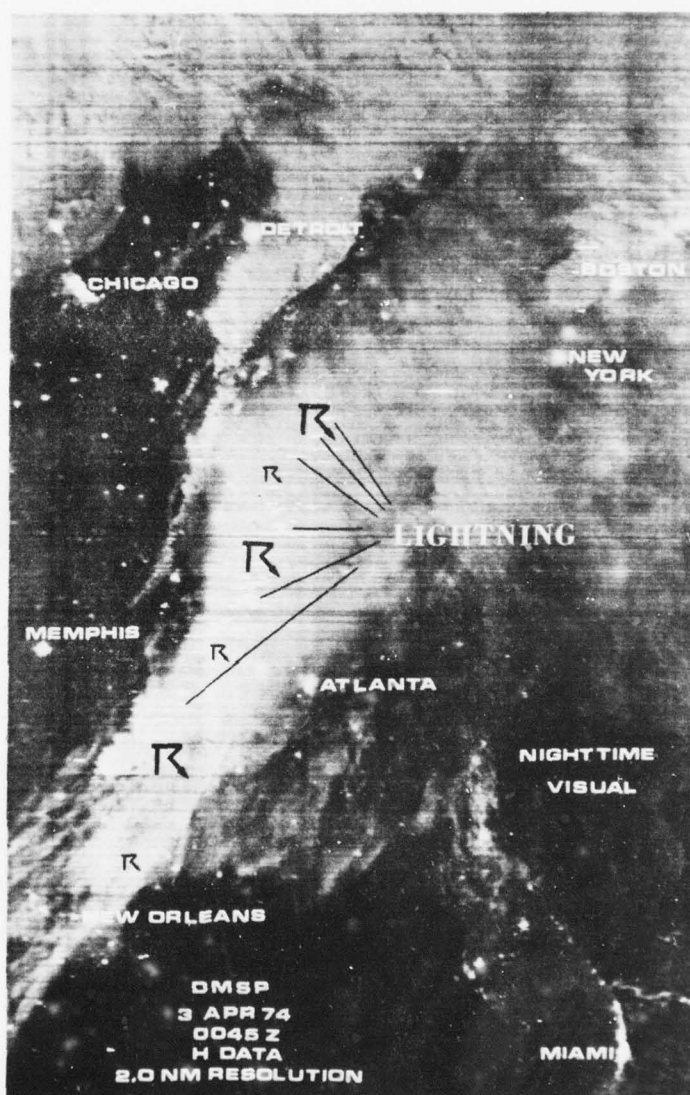


Figure 96. DMSP nighttime visual photograph depicting lightning flashes in an intense cold front (3 Apr 74).

AD-A067 090

AIR WEATHER SERVICE SCOTT AFB ILL
SATELLITE METEOROLOGY.(U)

F/G 4/2

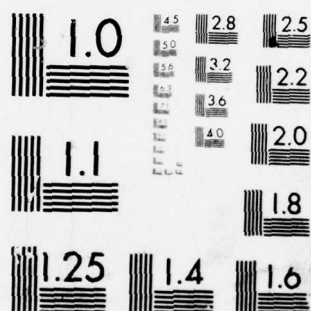
UNCLASSIFIED

AUG 76 H W BRANDLI
AWS-TR-76-264

NL

2 of 3
AD
A067090





MICROCOPY RESOLUTION TEST CHART
NATIONAL BUREAU OF STANDARDS-1963-A

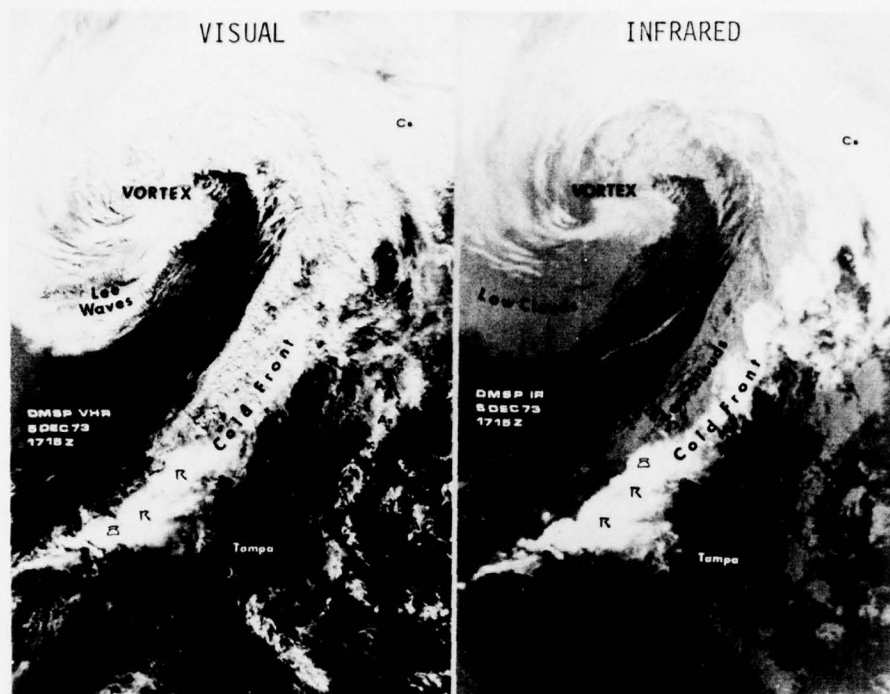


Figure 97. DMSF simultaneous visual and infrared photographs of a vortex and associated frontal systems (5 Dec 73).

pirically determined by comparing the cloud patterns with measured storm data for a 5-year period. A model of tropical-cyclone development and weakening (Dvorak, [41]) serves as guidance for the subsequent life expectation of the storm. Considerable work on hurricane monitoring using satellite photographs has been done by Fett [47], and others.

The daily analysis of a cyclone is threefold. First, the satellite data over the storm area is analyzed for the changes in cloud features between yesterday and today. Then, the storm is given a T-number that describes the current intensity of the system in terms of its cloud features. Finally, the age and current intensity of the storm are applied to a model which predicts the developmental trend over the next 24 hours.

Hurricanes and typhoons exhibit a great variety of cloud patterns, but most can be described as having a comma configuration (Johnson, et. al., [61])—The comma tail is composed of convective clouds that appear to curve cyclonically into a center. As the storm develops, the clouds form bands that wrap around into a center, producing a circular cloud system that often has a cloud-free, dark eye. Figure 101 shows some of the typical cloud patterns that these tropical systems exhibit.

The T-number assigned storms range from T1 and T2 for developing pre-storm patterns to T6 and T8 for fully developed hurricanes or typhoons. This figure shows three of the cloud configurations typical to a developing and mature storm. Below the schematics are actual satellite-observed cloud patterns. Note that in the pre-storm state (T1), the clouds form into a somewhat hooked-shaped area. As the storm starts to develop, the cloud becomes more comma-shaped and, as in type T4, the cloud band completes one revolution into the center. The number and width of the bands, the solidness of the central dense overcast, and the presence of an eye all enter into the daily assessment of the storm. The average maximum wind speed for each T-number is listed under the schematics.

A tropical storm (Alice) is shown in Figure 102. Tropical storm Alice is seen with its low-level developing eye south and west of Bermuda. As the storm approached Bermuda, Alice developed into a hurricane (Figure 103). The eye is faintly visible on this satellite photograph. With accurate geographical gridding (placing latitude-longitude lines on the photograph using known geographical landmarks),

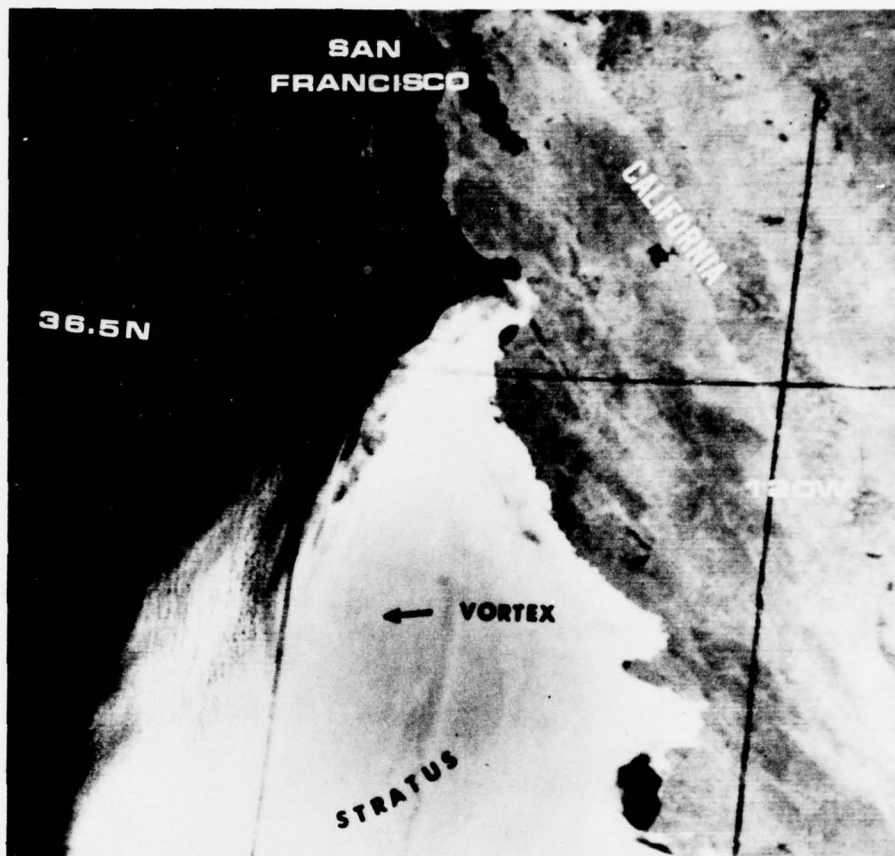


Figure 98. DMSP 0.62-km resolution visual image of a vortex in a stratiform low-level cloud formation (11 May 73).

tracking the hurricane becomes a simple operation. Predicting the movement for periods up to 48 hours is possible, but for longer periods, curvatures become too complex for accurate predictability.

Two main feeder bands are seen spiraling into Alice from the south and east. These feeder bands can contain intense thunderstorms and tornadoes in addition to this same severe weather that is present in the main circulation. Upper level outflow of cirrus spiraling in a counterclockwise (anticyclonic) manner is seen by examining the thin cirrus on the outer rim of the storm to the west and north. Better cloud detail of storms is possible with the newer higher resolution meteorological satellites of the last few years.

Figure 104 is a DMSP visual sequence of a recent hurricane in the northern Caribbean that moved into the Gulf of Mexico and struck the Florida panhandle. Tropical Storm Eloise formed in the northern boundary of the Caribbean on 16 September 1975. Later that day, the storm became a hurricane (lower right). As the storm moved west over Cuba, it decreased in intensity to a tropical storm on 18 September (lower left photos). The storm again picked up intensity in the Gulf of Mexico and on 22 September posed a serious threat to the Gulf coast (upper left photos). Landfall occurred at approximately 1200GMT/23 September, 2 hours before the DMSP satellite passed over the stricken area (upper left).

The huge eye of Typhoon Betty is shown in Figure 105. The eye of this storm had a diameter of 100 km. The use of eye location as a point becomes meaningless when examining this figure (eye positions are given by aircraft at a specific latitude/longitude). Along the bottom of the eye edge are huge embedded thunderstorms whose tops can extend over 20,000 meters. A close examination of this bottom part of the eye reveals what appears to be a smaller cloud circulation which could be the eye as sometimes detected by weather reconnaissance. This small-scale phenomenon is in the low levels and rotates with the storm (in this case, counterclockwise). If this "wheel within a wheel" were used as a point of storm location, the



Figure 99. DMSP image of an induced small-scale vortex (date unknown).

"erraticity" of these unpredictable storms would have some credence.

The next figure (Figure 106) shows the sloping eye of Typhoon Patsy in October 1973 in the Western Pacific. This large eye is tilting toward the west.

In the case where a vivid eye is not visible, the expanded spectral view of the DMSP can be an asset in finding the cloud-covered storm center. In Figure 107, Typhoon Pamela is shown. The covered eye is seen on this heavy cloud-layered storm. This large eye appears to have a lower smooth stratus cloud deck in the storm center.

Figure 108 is an example of a typhoon in the Indian Ocean. The night visual photograph was taken during a full moonlit night as the land and clouds stand out. The city lights of India and Pakistan are bright as are the oil field fires of Oman in the left center of the photograph. The eye of this typhoon is more obvious on the infrared photograph than on the visual photograph. A typhoon, such as this one, could go undetected without the aid of satellite photographs since conventional meteorological observations are sparse in this area. Ship observations could help locate a storm, but plotting the location and movement accurately is possible only with this type of satellite imagery.

In the Southern Hemisphere, storms similar to hurricanes and typhoons affect Australia and Africa as well as many islands such as Madagascar. These storms are called cyclones. A nickname of "Willy-Willy" has also been used in Australia. Figure 109 shows a cyclone east of Madagascar. The huge eye of the storm is marked on the figure. Upper level cirrus outflow in a counterclockwise direction is indicated by open arrows. In the Southern Hemisphere, the storms rotate in the opposite direction of their counterparts in the Northern Hemisphere. They rotate clockwise in the low levels and their outflow at the top spirals out in a counterclockwise fashion.

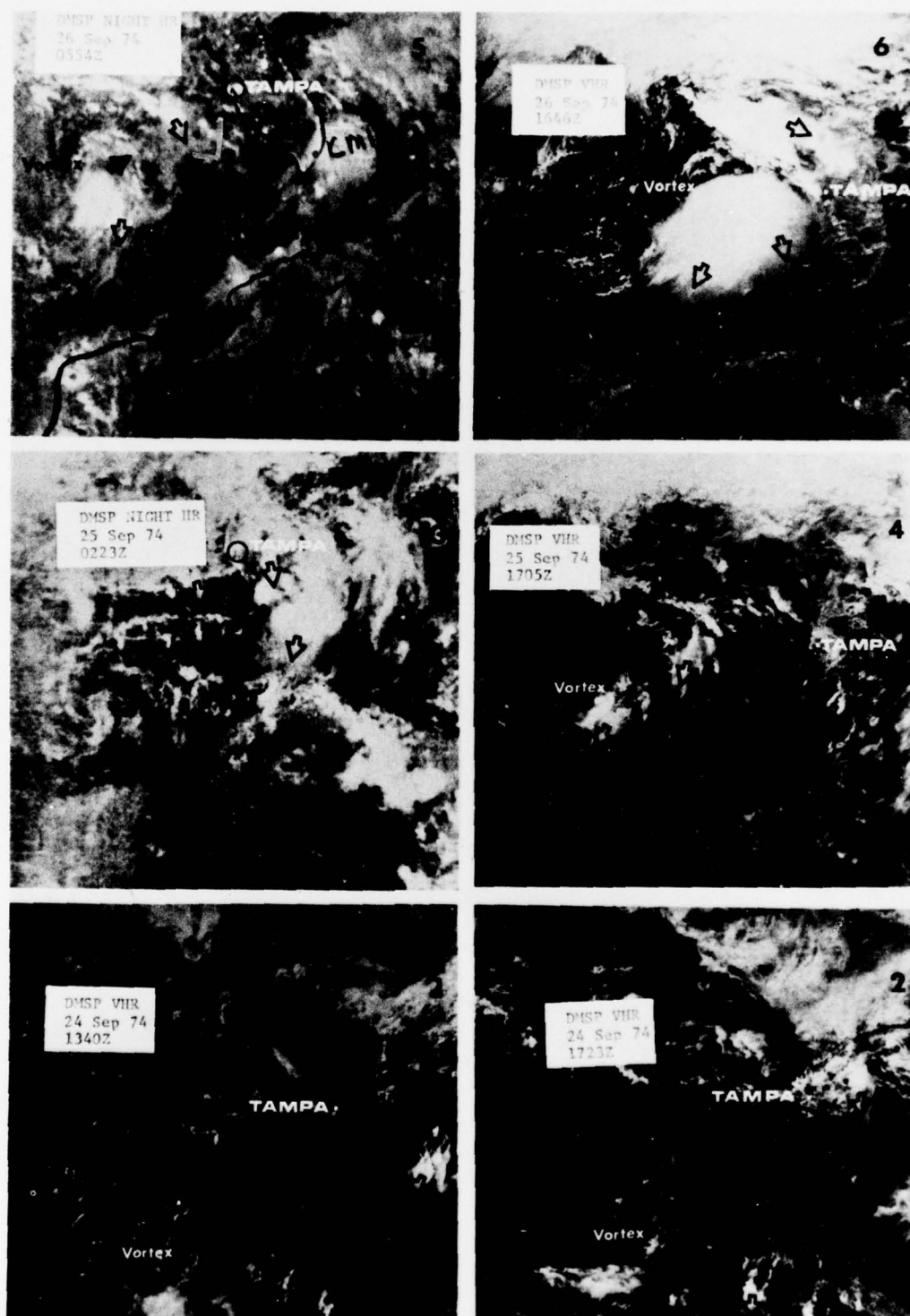


Figure 100. DMSP day and night visual data of a developing vortex over a 3-day period (24-26 Sep 74).

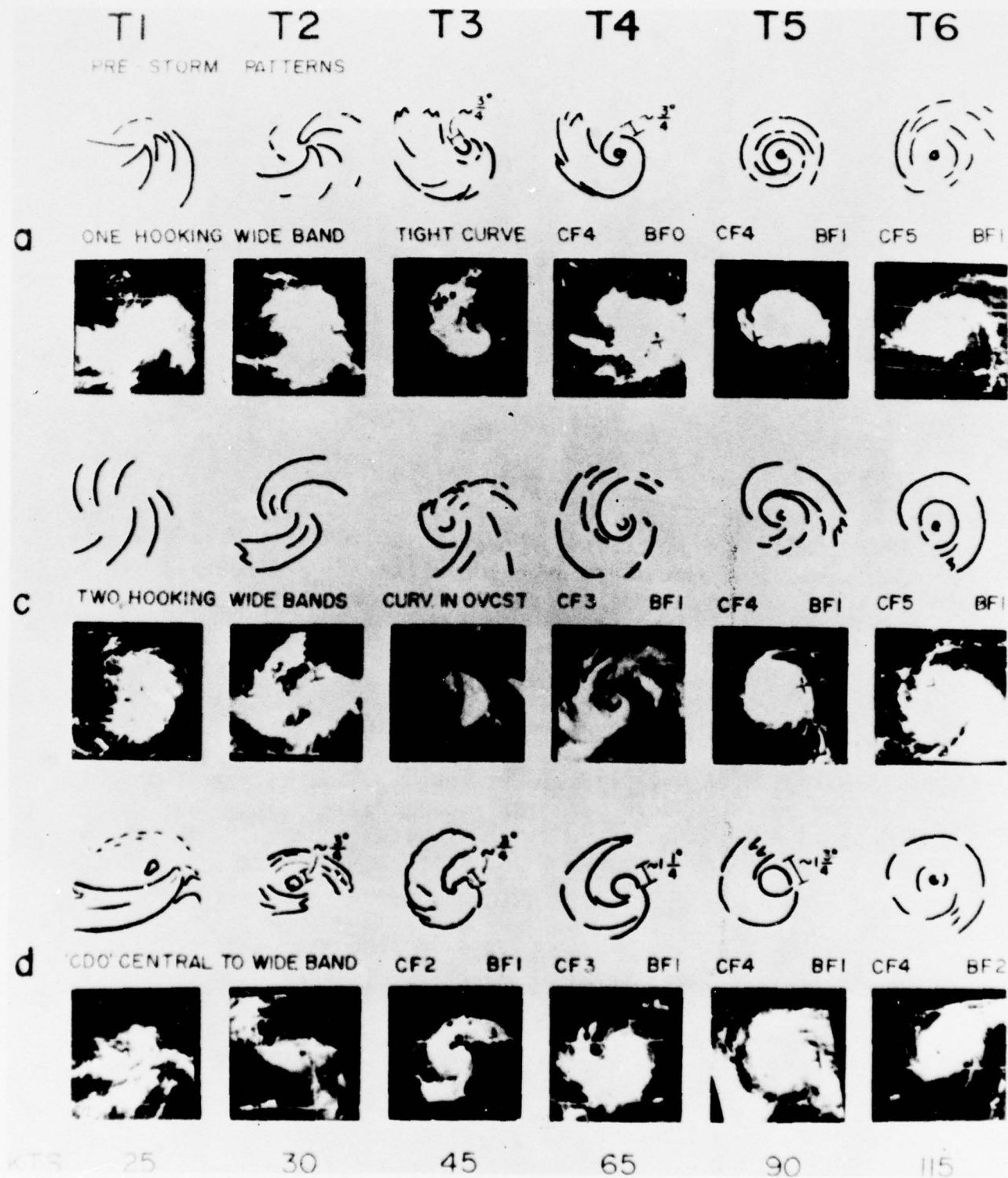


Figure 101. Cyclone patterns and wind speed (Johnson, et al., [61]).

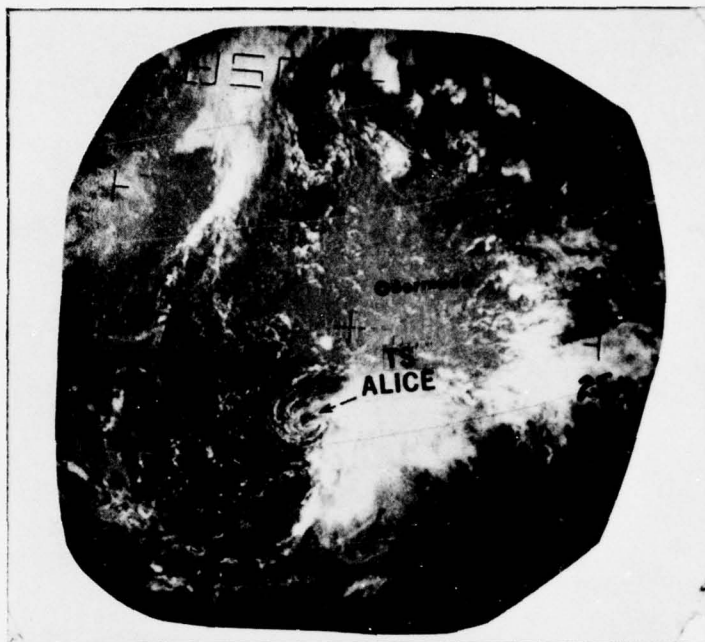


Figure 102. ESSA-8 visual data of Tropical Storm Alice (1 Jul 73).

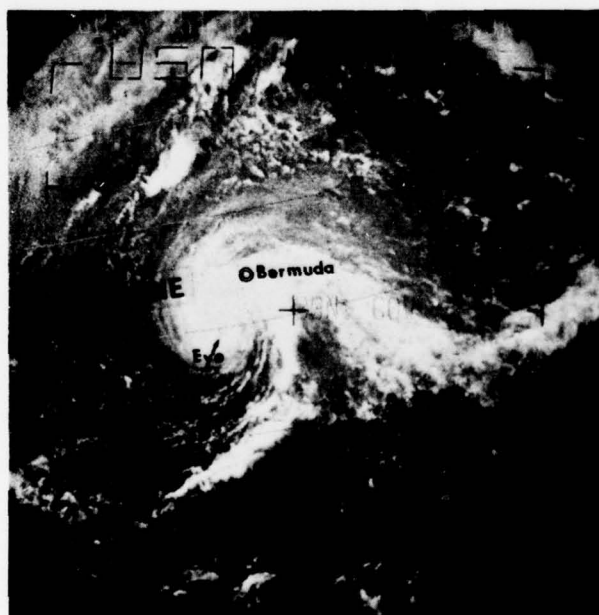


Figure 103. ESSA-8 view of Alice after it was upgraded to a hurricane (3 Jul 73).



Figure 104. DMSP day and night visual sequence of Hurricane Eloise (17-23 Sep 75).



Figure 105. A DMSP VHR photograph of Typhoon Betty in the Western Pacific (12 Aug 72).

Troughs

Just as fronts are an important meteorological system affecting surface winds, air mass changes, clouds, and severe weather, upper level troughs also affect weather features. Troughs are defined as upper level areas where the wind shifts from one direction to another across a zone or line. The line where the shift takes place is called the trough. In Figure 110, upper level flow is seen undergoing a wind-direction change from the northwest behind the trough to the southwest ahead of it. In the Southern Hemisphere the wind shifts from the southwest upstream of the trough to the northwest downstream. This wind shift can occur at any level above the ground, e.g., 3000, 6000 meters, etc. The shift can occur at each level so that the trough line itself has a slope or tilt to the east or west.

Wind shifts across the trough lines cause dynamic changes to surface fronts and induce upward vertical motion. This vertical motion can trigger thunderstorms. Usually, the trough's induced vertical motion occurs east of the trough line in both hemispheres.

On satellite imagery the position of the trough can be determined from the upper level wind flow. As the trough moves, it can be tracked using the wind-flow techniques, as well as the relationship between fronts and troughs. Where a trough line intersects a front, significant interactions can occur between the two (Anderson, et. al., [5]). This change could occur at the end of the front or where the cloud tops in the front drop from high level to low level. Figure 111 is an example of a trough intersecting a front. The trough is placed in a north-south line northward from where the front abruptly ends in Texas. The upper level open arrows on the infrared photograph show the wind direction change in this area. The slope of a low-

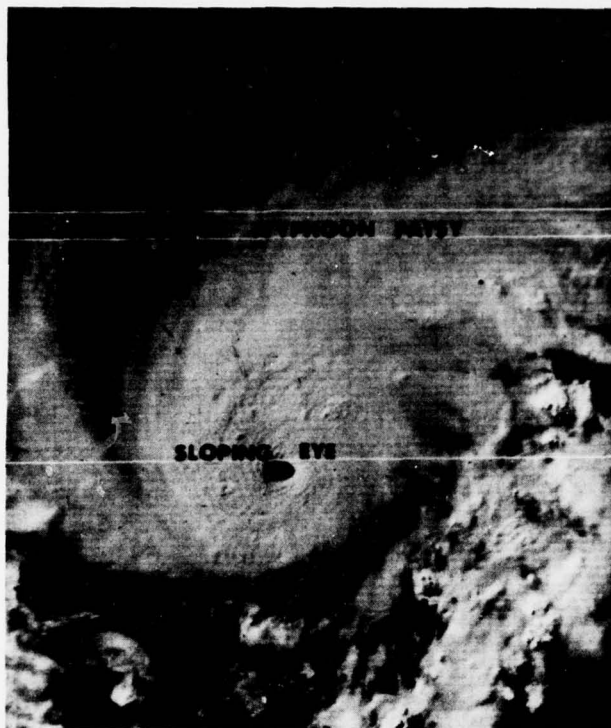


Figure 106. DMSP (0.6 km) visual image of Typhoon Patsy (9 Oct 73).

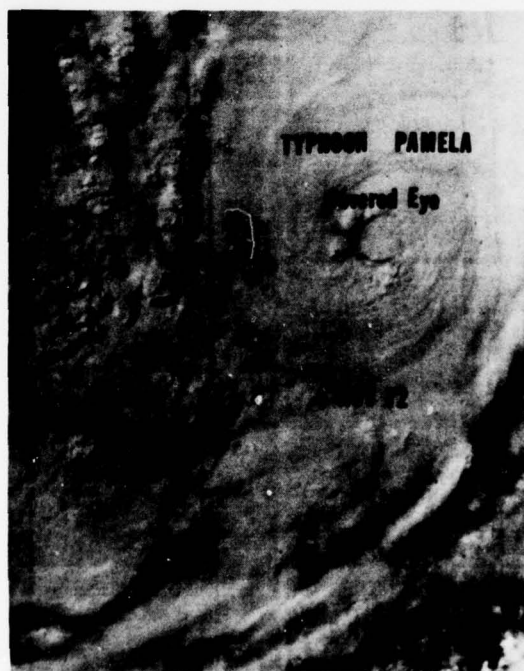


Figure 107. DMSP VHR image of Typhoon Pamela (7 Nov 72).

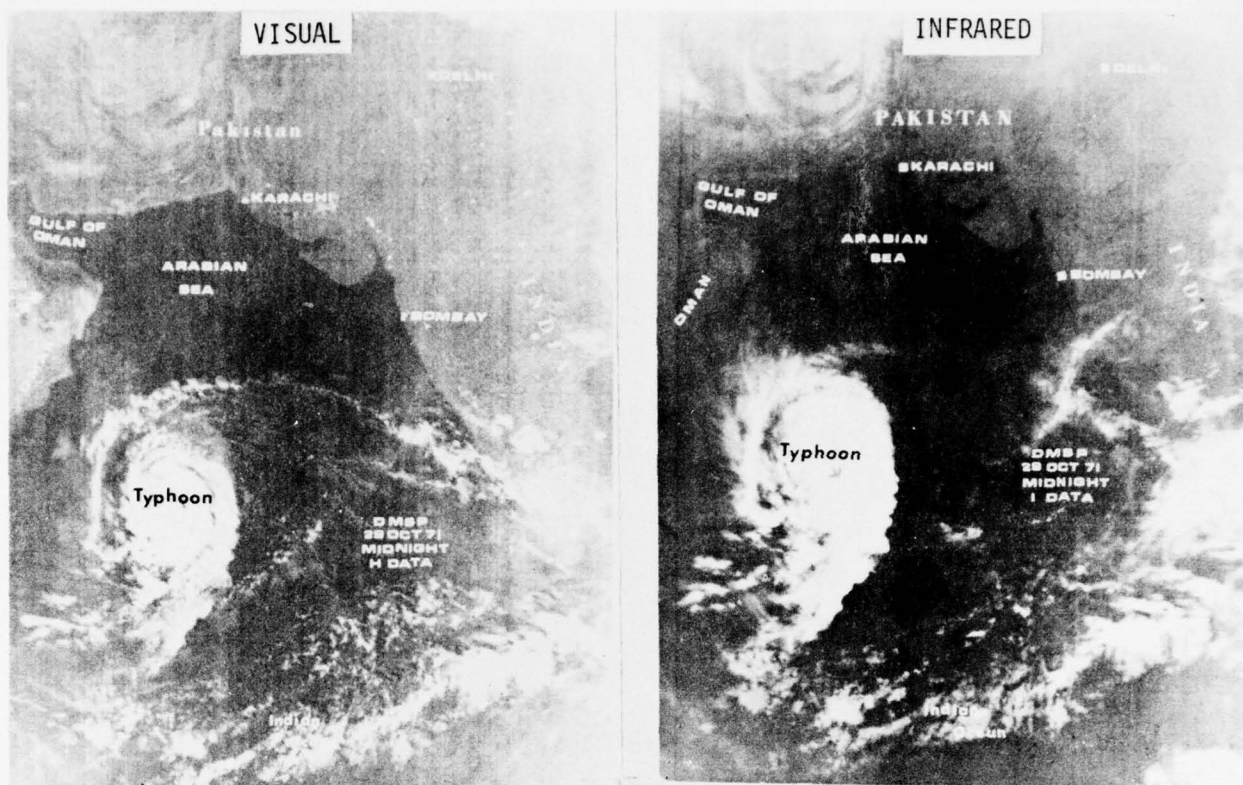


Figure 108. DMSP night visual and infrared imagery of a typhoon in the Arabian Sea (29 Oct. 71).

pressure area is also shown on the photograph. A surface low appears in Canada on the visual, but this low-pressure area is seen further south on the infrared image coinciding with the high-cloud pattern.

In a frontal case, conventional upper level wind measurements would have identified the trough. However, over open water where little or no upper level wind is available, the satellite imagery is an important tool for locating the trough line. The importance of accurate trough-line location is such that this persistent feature can then be tracked and forecast with confidence. Consequently, the trough's influence on the weather patterns can be predicted. In the next figure (Figure 112), the upper level wind plumes from thunderstorms (∇) indicate a trough. Actually, the trough occurred first and caused the thunderstorms.

Sometimes, the upper level trough is very sharp; i.e., the clouds caused by the vertical motion to the east of the trough line began abruptly. In Figure 113, an upper level trough is shown east of the Lesser Antilles on a night visual and infrared image from the DMSP.

Positive Vorticity Advection Areas

Positive vorticity advection (PVA) is a very common phenomenon on satellite imagery. An area of PVA resembles a large "comma" on the satellite photos (Anderson, et. al., [5]). PVAs (or the troughs associated with them) can induce frontal waves which develop into mature vortices. A weak PVA appeared in Figure 86. PVAs sometimes attach themselves to fronts and generate occlusions. PVAs can also generate complete frontal systems while dissipating the fronts they are approaching. An example of the latter is shown in Figure 114.

A more prominent PVA east of a trough line is shown in Figure 115. This PVA caused multi-layered clouds with a few imbedded thunderstorms. Note the trough behind this PVA. Because of the vertical air motion accompanying this "comma cloud pattern," considerable turbulence at all levels can be expected.

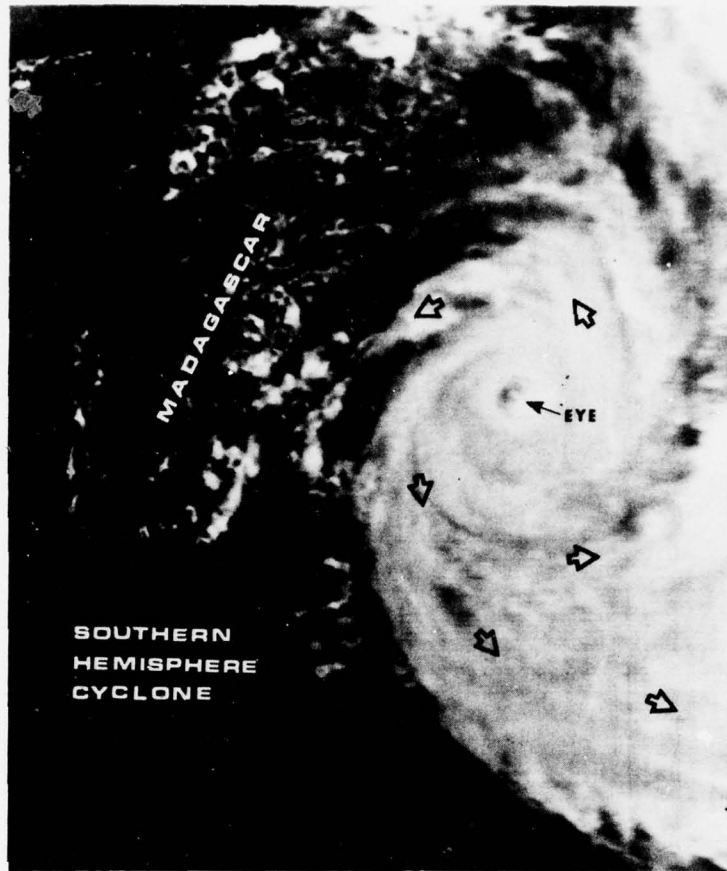


Figure 109. DMSP view of a Southern Hemisphere cyclone (date unknown).



Figure 110. Diagram of upper level trough in Northern Hemisphere.

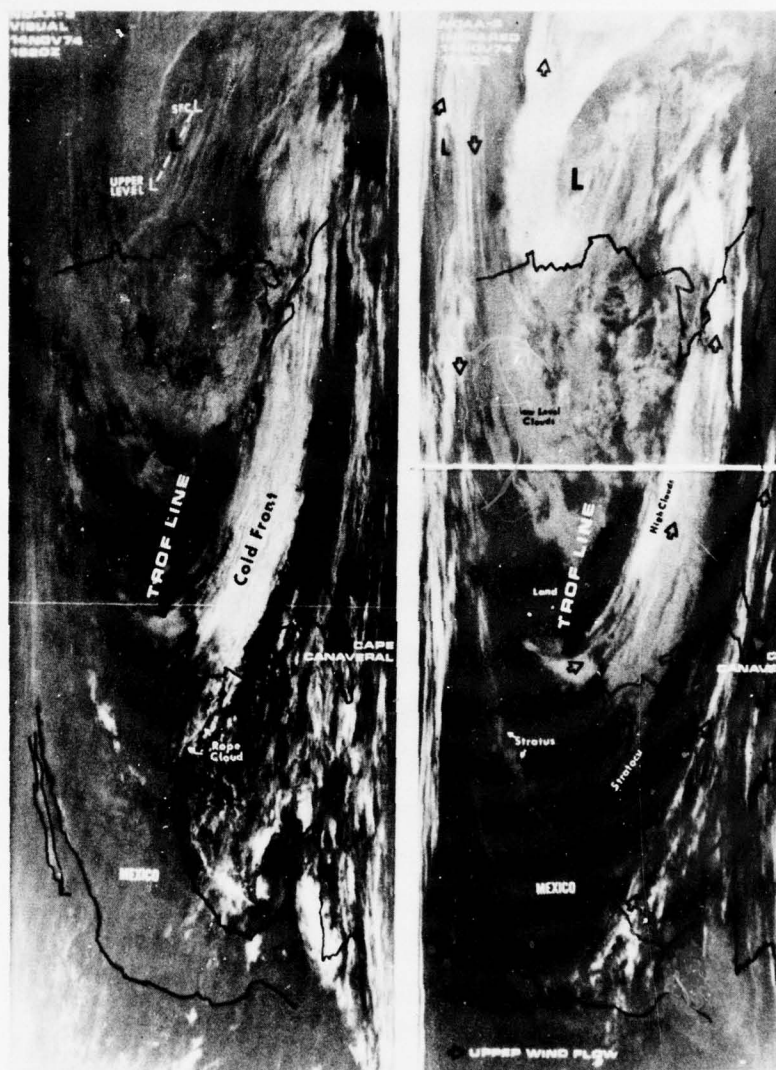


Figure 111. NOAA-3 simultaneous visual and infrared imagery of a trough in conjunction with a cold front (14 Nov 74).

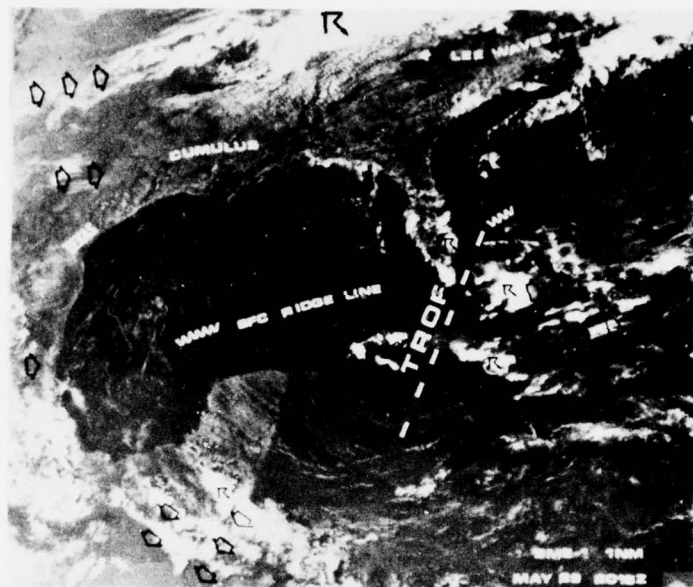


Figure 112. SMS-1 view of a trough off the southern coast of Florida (29 May 74).

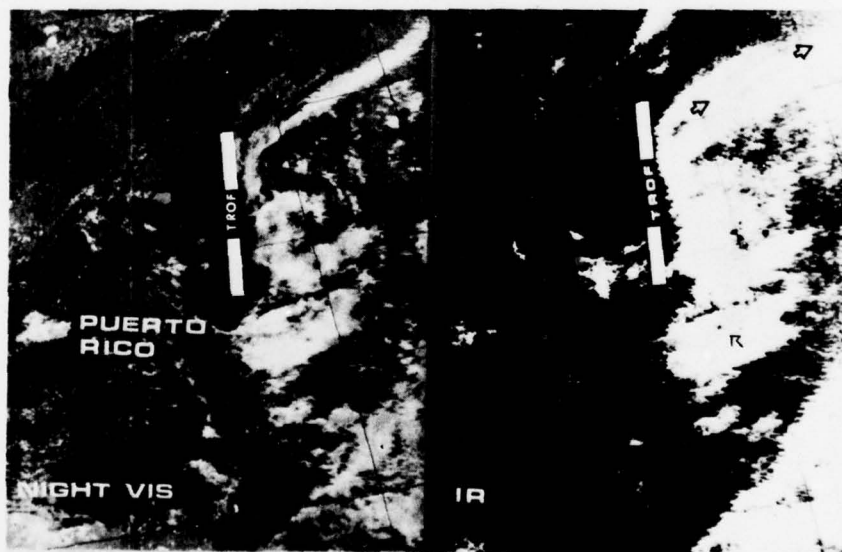


Figure 113. DMSP nighttime visual and infrared data illustrating a sharp trough line (date unknown).

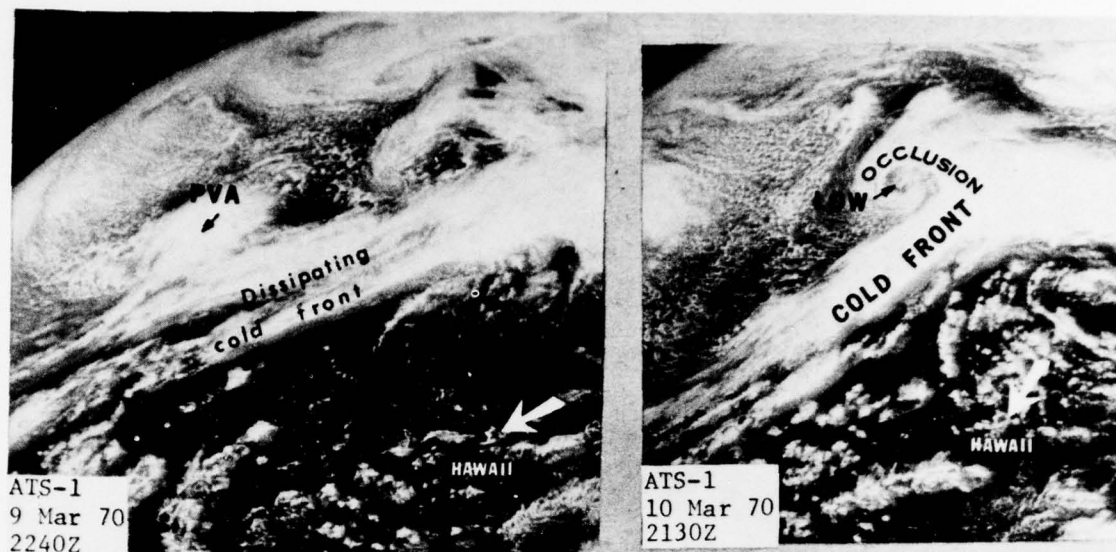


Figure 114. ATS-1 view of a PVA maturing into a frontal system (9-10 Mar 70).

Cut-Off Lows

Just as surface lows and vortices are seen on satellite photographs so are high-level lows and near vortices. These high-level "cut-off lows" are often obscured by multi-layered clouds. Figure 116 is a DMSP visual of a perfect high-level vortex or low. The closed circulation is indicated by the blowoff plumes from the tops of thunderstorms.

Ridge Lines

The point where the wind direction undergoes a maximum change in curvature in a *clockwise* direction in the Northern Hemisphere is known as a ridge line. Ridge lines usually emanate from high-pressure centers and can occur at all levels in the atmosphere. Most low-level ridge lines are orientated in an east-to-west fashion. Figure 117 is a diagram of a low-level ridge line. A diagram of an upper level ridge line is shown in Figure 118. Most upper level ridge lines are orientated in a north-to-south fashion. This flow pattern can occur at various levels or through the entire depth of the atmosphere to 15,000 meters in perfect vertical "stacking" or sloped fashion. Knowing the location of the ridge line is important and can be determined from visual or infrared imagery.

Forecasting this line of wind directional change becomes an easy task with proper positioning. Various clues on the satellite imagery can be used to position the ridge line. Cumulus cloud lines are the easiest and most accurate method of locating the low-level ridge line. An example is shown in Figure 119.

Glints (sun or moon) can also indicate a surface ridge line position (McClain and Strong, [72]). Dark bands through the glint pattern or an area of reduced glint are caused by an absence of reflection to the satellite. Smooth (calm) waters resulting from the light winds in a ridge line cause this phenomenon. Figure 120 is an example of sun glint with a surface ridge line. A ridge line is seen in Figure 121 associated with a moon glint.

High-level ridge line location is best determined from cirrus flow or plume blowoff which indicates clockwise flow. High-level ridge lines can be determined from the cirrus cloud flow. The ATS view shown in Figure 122 illustrates this fact. A high-level ridge line determined from plume blowoff is shown in Figure 123.

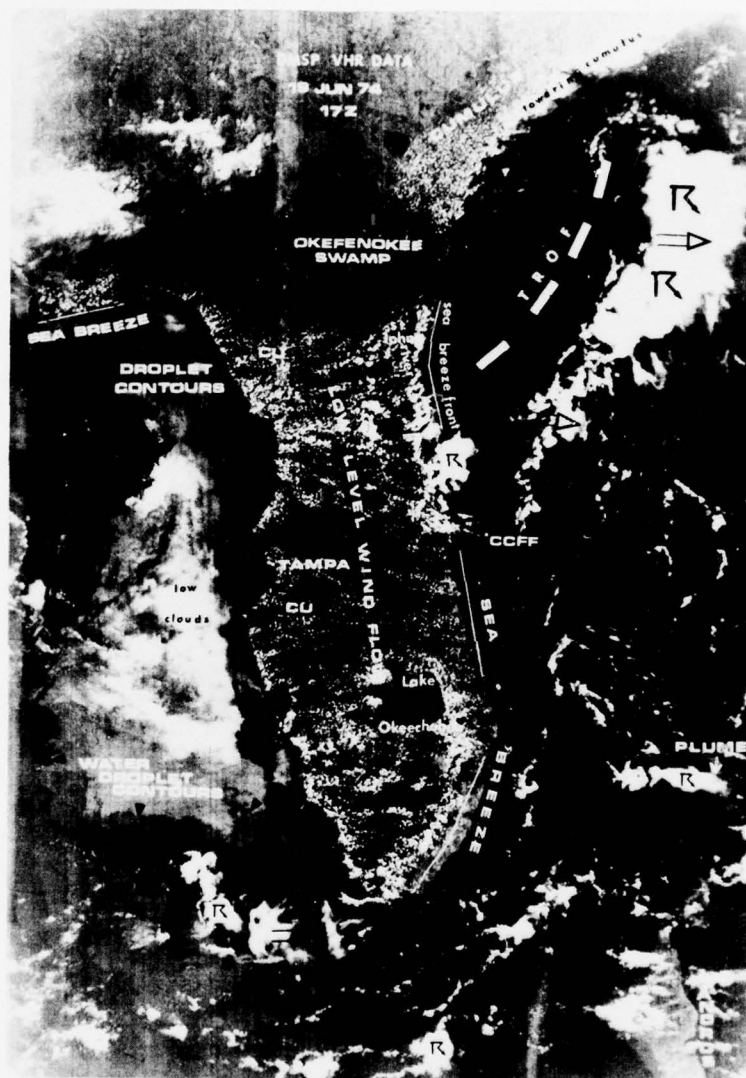


Figure 115. PVA east of trough line near Florida (19 Jun 74).



Figure 116. DMSP visual image of a cut-off low (15 Aug 75).

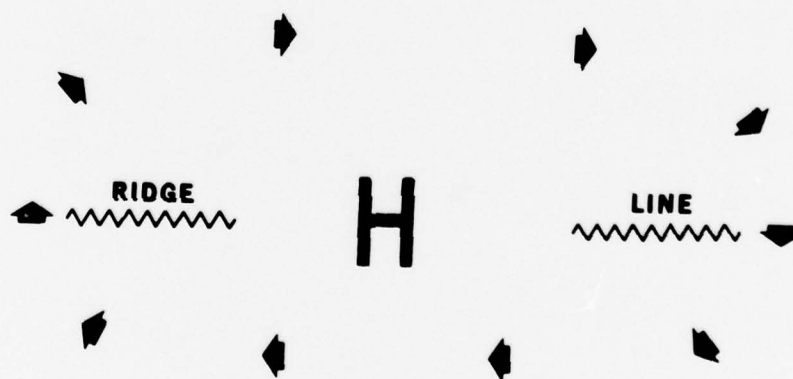


Figure 117. Diagram of low-level ridge lines.

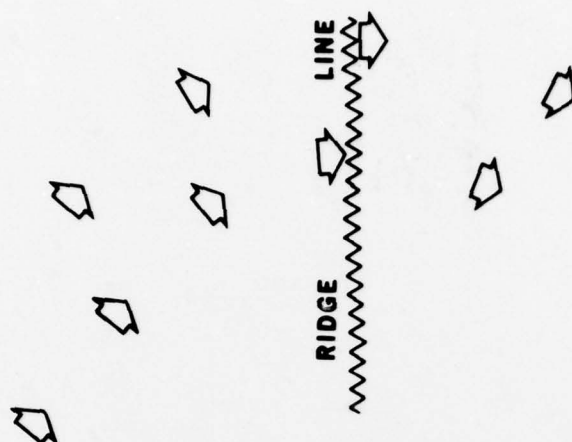


Figure 118. Diagram of an upper-level ridge line.

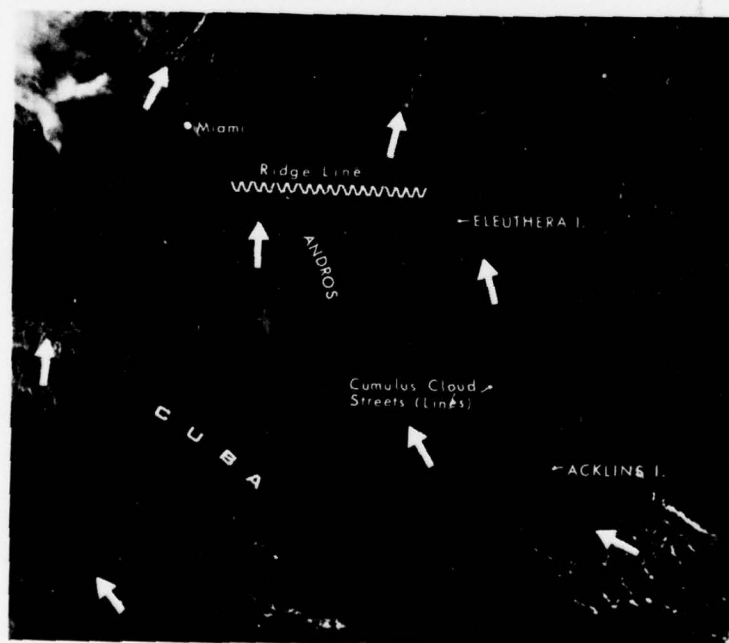


Figure 119. DMSP image of a ridge line determined from cumulus cloud lines (24 Mar 74).



Figure 120. DMSP visual photograph of sun glint and ridge line (15 Aug 75).

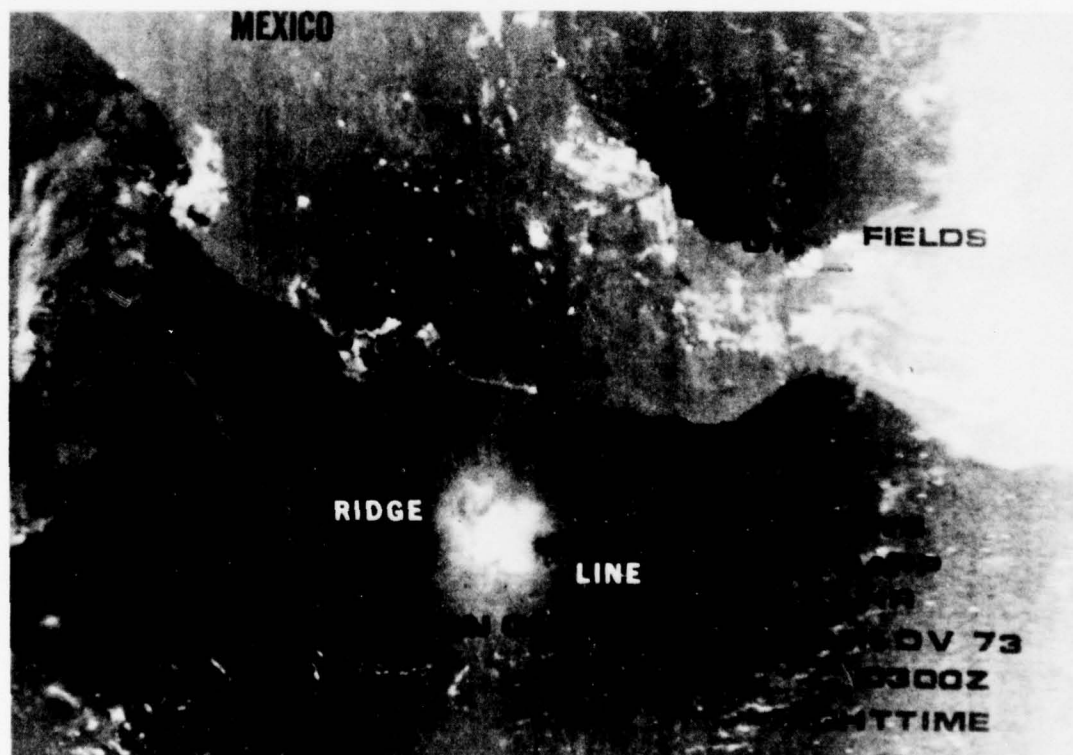


Figure 121. DMSP night visual of moon glint and ridge line (8 Nov 73).



Figure 122. ATS visual photograph of high-level ridge lines (11 Mar 70).

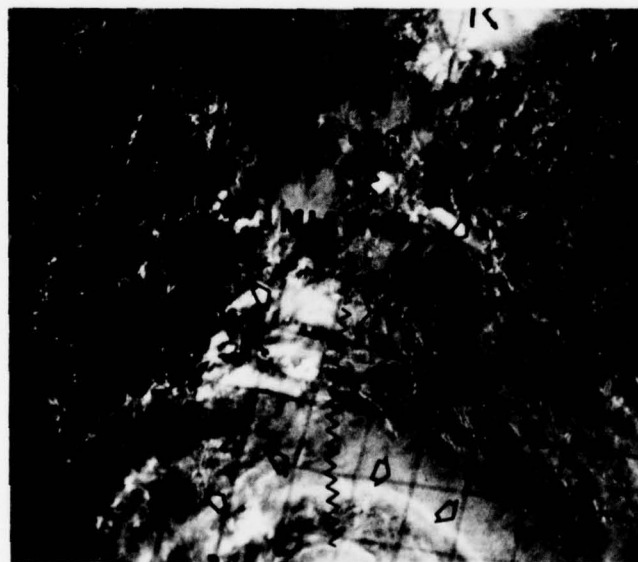


Figure 123. DMSP visual image of a high-level ridge line (date unknown).

"Screaming Eagles"

"Screaming Eagles" are an easily recognized cloud pattern on satellite imagery. This phenomena usually occurs over the ocean areas in the low-latitude region between 25°N and 25°S . The cloud pattern received its name from the resemblance to eagles; however, an individual viewer might desire to call it something different. Figure 124 is an ATS-1 visual image of the "screaming eagles." Figure 125 is an expanded view of the "screaming-eagle" area with the "eagles" dashed in.

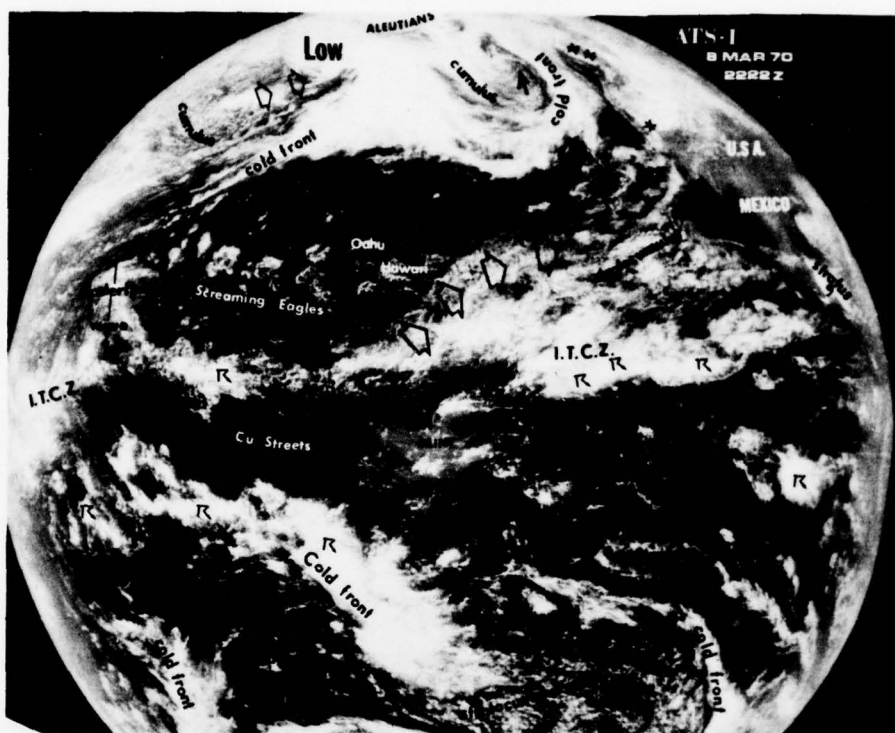


Figure 124. ATS-1 photograph depicting the "screaming eagles" near the Hawaiian Islands (8 Mar 70).

The weather associated with "screaming eagles" consists of rain showers and gusty surface winds to 25 kt. Cloud tops usually extend to 4500 meters. However, the tops can extend to 9000 meters near the equator. The cloud tops of "screaming eagles" are a function of latitude, sloping up toward the equator. Figure 126 is a DMSP visual and infrared view of a "screaming-eagle" cloud pattern.

"Screaming eagles" move across the oceans at an average rate of five degrees per day or about 13 kt (Weldon, [107]). The cloud pattern usually becomes disorganized and dissipates when meeting islands or atolls. The "eagles" will intensify and enlarge when moving into areas east of troughs. In this case, intense thunderstorms can develop.

Easterly Waves

In the previous section, "screaming eagles" were discussed. An easterly wave is very similar to those phenomena, only the easterly waves are larger and have more clouds oriented in a north-to-south direction. In Figure 124 an easterly wave is seen west of the "screaming-eagle" pattern. These waves move westward without the regularity of the "eagles." They tend to stop, start, build, and dissipate at the whims of the



Figure 125. Expanded view of "screaming eagles" (8 Mar 70).

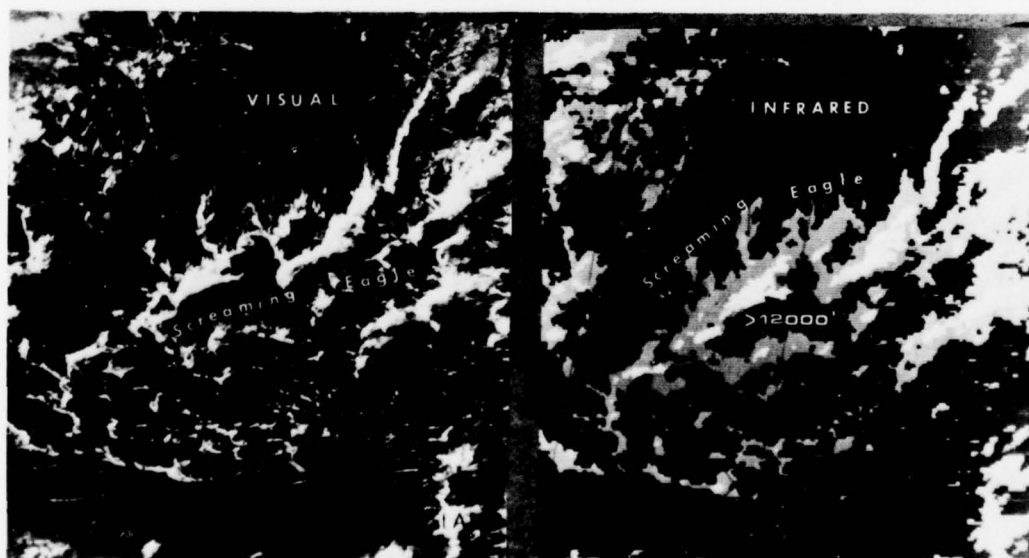


Figure 126. DMSP visual and infrared imagery of "screaming eagles" (9 Mar 70).

upper level wind patterns which control their destiny. A DMSP visual and infrared image of an easterly wave east of Florida is shown in Figure 127.

Intertropical Convergence Zone (ITCZ)

A band of layered clouds and embedded cumulonimbus (thunderstorms) nearly encircling the earth is frequently found near the equator. This cloud system is called the intertropical convergence zone (ITCZ). The monitoring of this perpetual cloud band is best done by the satellite meteorologist since conventional meteorological data is very sparse in this area. The cloud layers and thunderstorms usually extend vertically to 15,000 meters and higher. Most of the clouds in the ITCZ are layered cirrus clouds. The sources of these cirrus clouds are thunderstorms and upward vertical motion. Surprisingly, the thunderstorm coverage is isolated to only a few rather than scattered or numerous as one would imagine by looking at the visual data. Enhancing the visual and examining the infrared photographs carefully can aid in locating the thunderstorm activity.

Figures 128 and 129 are SMS visual and infrared photographs, showing a flight path through the ITCZ. A new picture pair is taken every half-hour and could be used to update the forecast relayed to the pilot. However, the initial weather briefing should have included warnings of possible thunderstorm activity in the flight route. The infrared image shows white cloud tops that would be above 15,000 meters.

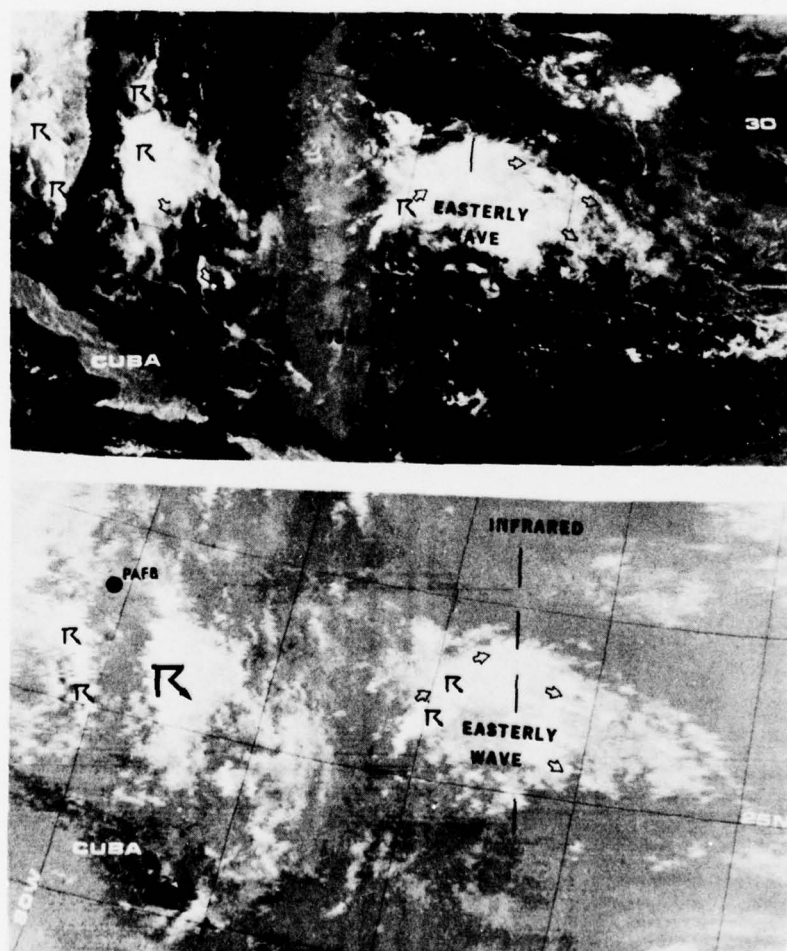


Figure 127. DMSP visual and infrared imagery of an easterly wave (date unknown).

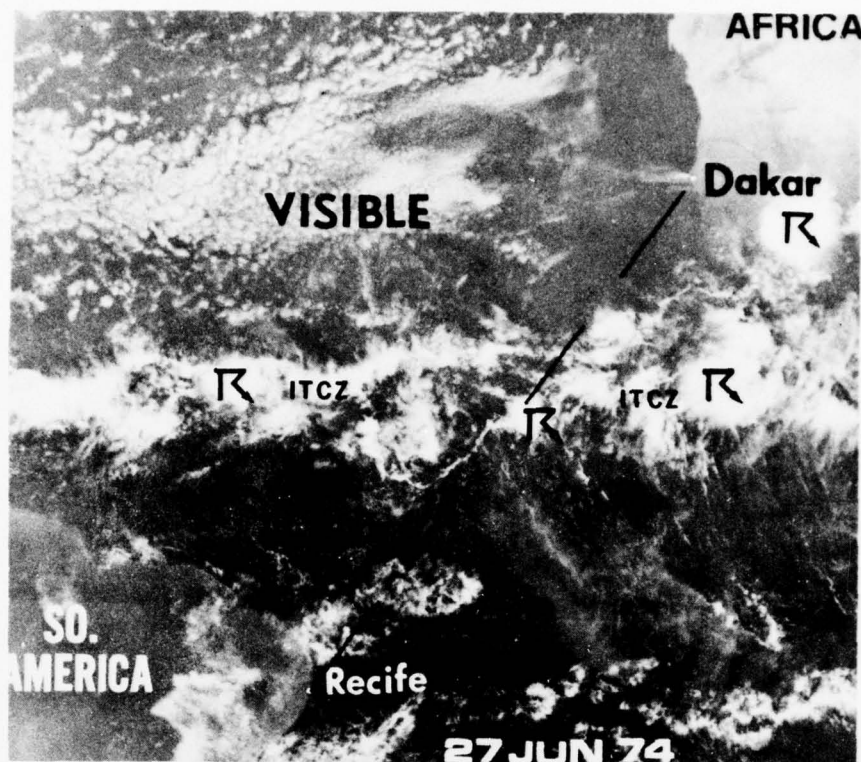


Figure 128. SMS visual image of ITCZ (27 Jun 74).

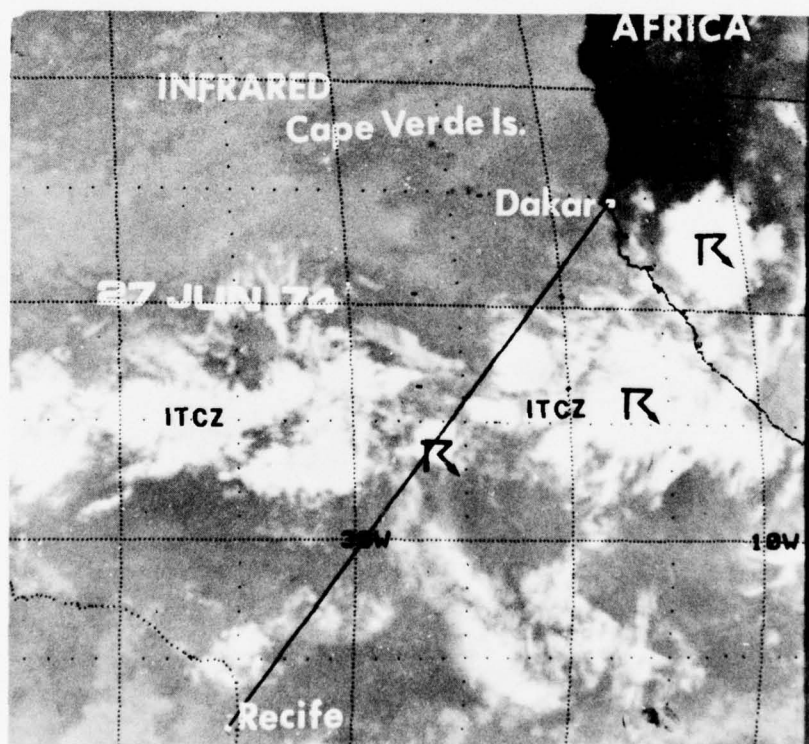


Figure 129. SMS infrared imagery of ITCZ between South America and Africa (27 Jun 74).

Chapter 5

WIND

Since the advent of meteorological satellites in 1960, meteorologists' primary goal has been to incorporate these data into operational weather analyses. In the past, meteorologists were concerned with synoptic-scale cloud formations and disturbances. With the aid of the newer high-resolution satellites, meteorologists can improve their operational analyses by inferring wind direction and speed very accurately. Accurate gridding and infrared height level determination enable wind speed and direction calculations to be made at various levels in the atmosphere. This information can then be used to infer wind speed and direction in cloudless surrounding areas. Most of the empirical-wind computations and estimates mentioned in this chapter have been derived by the author based upon his 15 years experience in operational satellite meteorology. Many of these relations are yet to be published in scientific literature.

Low-Level Flow

The labeling of low- and mid-level flow (up to 6,000 meters) is done with single arrows in this report. Low-level wind flow or low-level mean wind flow can be observed by pattern recognition, as well as cloud movement between successive pictures. Cloud patterns that are useful in correctly inferring low-level wind direction and speed are cumulus/stratocumulus patterns (open cell and closed cell), streets or lines, sea/land breeze, lee waves, eddies, wakes, and anomalous lines.

a. Stratocumulus/Cumulus Cloud Patterns:

(1) **Stratocumulus** cloud areas usually indicate stable air masses with light winds. In the Northern Hemisphere, anticyclonic (clockwise) flow is characteristic of this common cloud pattern (the reverse is true in the Southern Hemisphere). Wind direction can be deduced with the recognition of nearby cloud systems. Wind speeds in stratocumulus clouds not oriented in lines are usually less than 10 kt. Figure 130 shows "closed cell" stratocumulus off the coast of Baja, California.

(2) **Cumulus** cloud patterns indicate cyclonic or counterclockwise motion (Northern Hemisphere) when appearing in the common "open cell" pattern. These "open cell" cloud formations resemble polygons, such as hexagons, as well as stretched-out ellipses. Wind direction usually cannot be inferred from the "open cell" cumulus itself. However, this cloud pattern usually forms in conjunction with other wind-flow indicators such as low-pressure systems. In addition, this cloud pattern forms in stages: polygons, ellipses, stretched-out ellipses, and lines. In the latter three stages wind direction *can* be inferred. The wind direction is parallel to the major axis of the ellipses and also parallel to the lines.

Wind speeds vary with each stage of the "open cell" pattern. Polygon cells usually have speeds ranging from 0 to 10 kt. Speeds increase from 10 to 20 kt in the elliptical pattern, and from 20 to 30 kt in the stretched-out ellipses. When the stretched-out ellipses form into lines, wind speeds can gust to over 30 kt (Anderson, et. al., [5]). Figure 131 is a DMSP visual photograph depicting the polygon stage of the "open cell" pattern.

b. Stratocumulus/Cumulus Streets or Lines:

(1) **Stratocumulus** lines occur behind cold outbreaks of polar air masses, usually over warmer water off the east coast of major continents. As this cold air moves off the continent, low-level stratocumulus clouds form and align themselves to the air-mass movement.

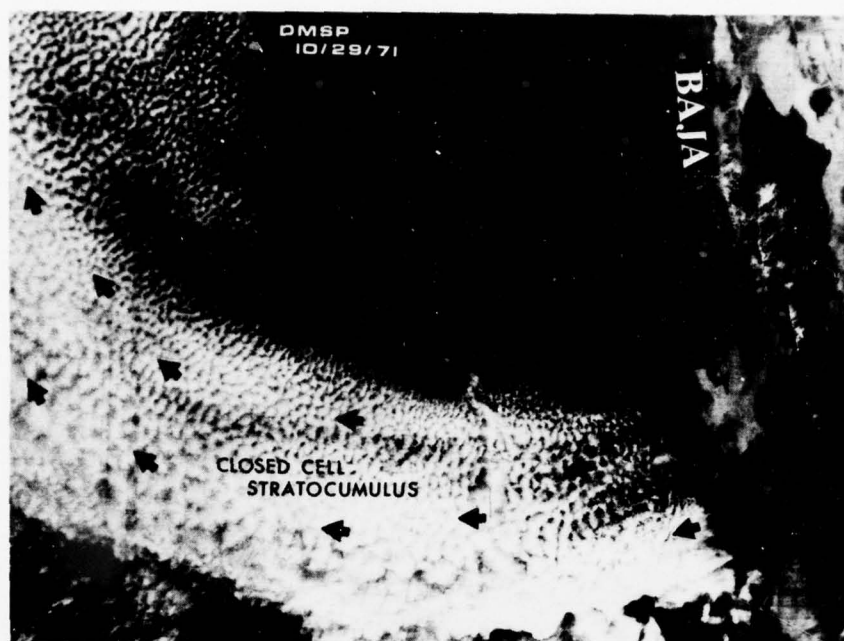


Figure 130. DMSP visual image of low-level wind flow in a "closed cell" pattern (29 Oct 71).

An example of stratocumulus lines is shown in Figure 132. In this photograph, wind speeds are 10 to 20 kt. As the stratocumuli move over warmer water, the clouds become bigger and the wind speed slows down. The wind speeds can vary from 20 to 50 kt depending on the intensity of the pressure systems (Anderson, et. al., [5]). Usually, the stronger winds occur at latitudes above 50°N. Typical stratocumulus lines are seen in Figure 133. Wind speeds at this latitude will vary from 5 to 15 kt.

(2) **Cumulus streets or lines** are small cumulus clouds that align themselves to the trade-wind flow. The wind direction will be parallel to the streets or lines, usually with an easterly component. Wind speeds of 5 to 8 kt will occur in this tropical cloud formation (Brandli, [11]). Figure 134 is an example of cumulus streets in the Atlantic.

c. **Sea/Land Breeze.** The sea-breeze cloud line phenomenon is most often associated with coastal areas in low latitudes. As the air moves off the water onto the shore, the cumulus activity begins inland due to the rising air from the hotter land. Wind speeds are usually 8 to 15 kt with the direction on shore and perpendicular to the shoreline. Cloud lines found off shore in early morning satellite photographs are the result of the land breeze generated by nighttime cooling which causes a reverse circulation.

d. **Lee Waves.** Lee waves form on the downwind side of mountains or hills when the wind has a large component perpendicular to this barrier. This wavelike cloud pattern is often seen associated with the mid-latitude mountain ranges of the world. This phenomena can also be observed downwind of a large island. The wind direction at the wave cloud level is usually perpendicular to the waves and the *mean* speed is calculated using the following equation (Fritz, [53]):

$$v = 6\lambda + 12 \quad (1)$$

where v is the mean wind speed in miles per hour and λ is the wavelength in miles. Turbulence can be expected in the vicinity of these wave clouds. An example of lee-wave clouds is shown in Figure 135.

e. **Other Low-Level Phenomena.** Cloud patterns, such as eddies, can infer wind direction and speed. In these cases, complications arise because of the rotation as well as the translation of the small systems. "Shock wave" clouds, seen in fronts and around dissipating cumulonimbus, can have wind speeds from 20 kt to as high as 80 kt.

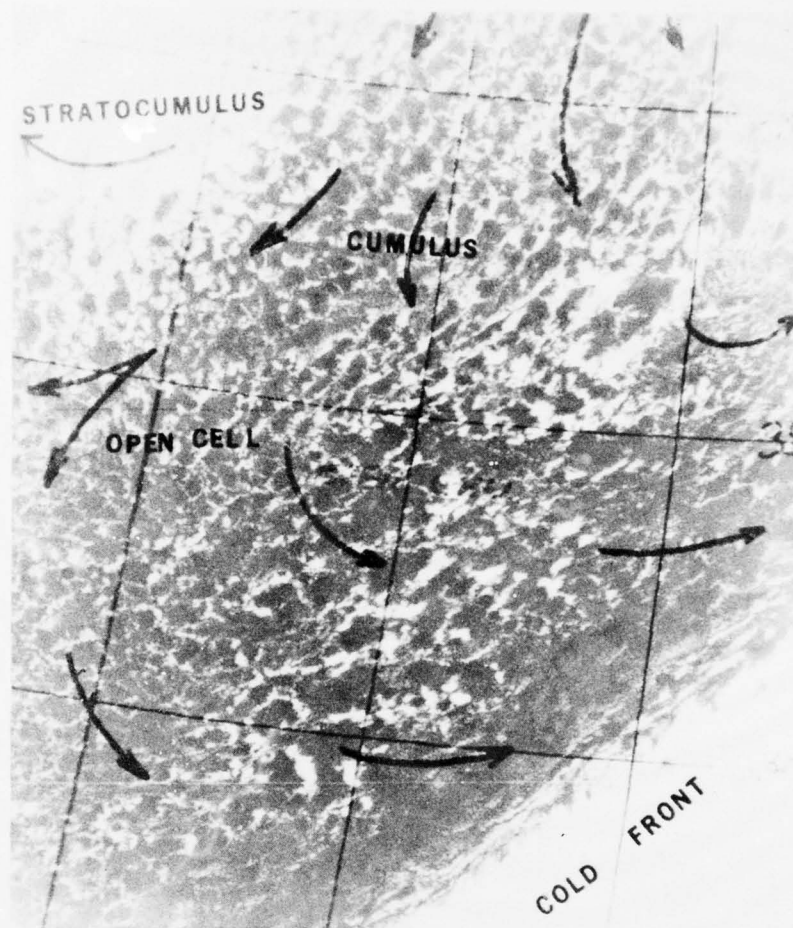


Figure 131. "Open cell" cumulus (19 Feb 73).

f. **High-Pressure Center.** Satellite photographs can be used to locate the high-pressure center, at least at the gradient level. Other levels, such as the surface, can be inferred from this information. Figure 136 is a DMSP visual photograph depicting stratocumulus clouds. North of 30°N latitude and west of 70°W longitude, the stratocumulus clouds are aligned parallel to the gradient-level flow. By constructing perpendicular bisectors of the more pronounced curved cloud lines, one can locate the center of the clouds which should coincide with the gradient level high-pressure center (Brandli and Janes, [21]). The gradient level high-pressure center should be close to the surface high-pressure center if vertical stacking is present. The center of the gradient level high, as depicted on the satellite photograph, is located approximately 30 miles west-northwest of Charleston, South Carolina. Figure 137 is the surface chart for 1200 GMT, 12 December 1975. The analysis indicates a surface high-pressure center just southeast of Charleston. The 500-mb chart for that time period indicated upper level ridging sloping to the west. Therefore, the gradient level high should be just west of the surface high center as shown in Figure 136.

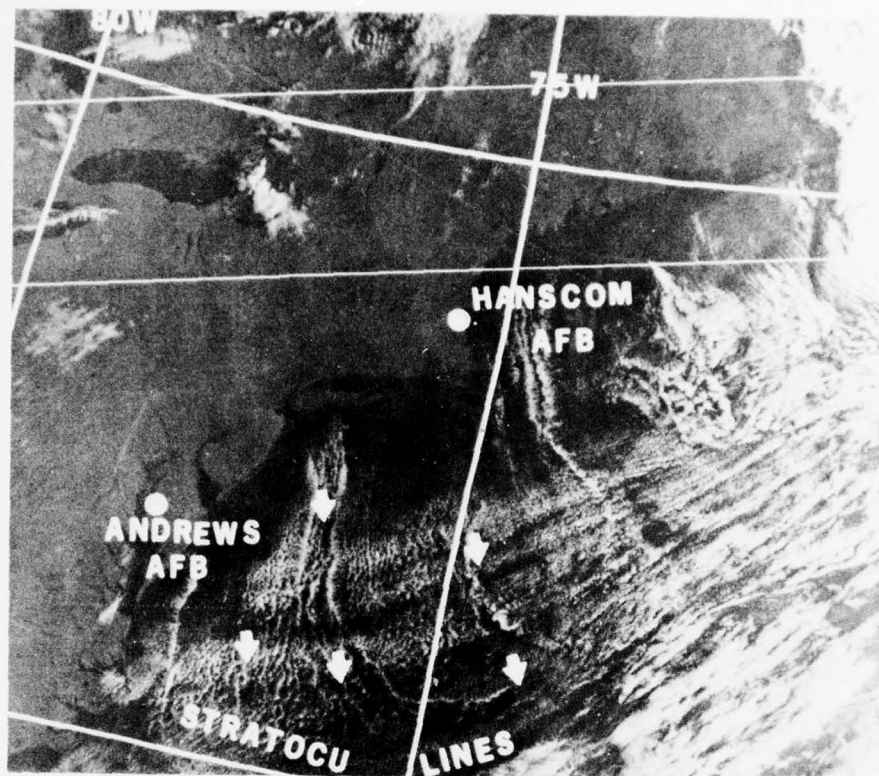


Figure 132. DMSP view of stratocumulus lines off the coast of New England (3 Oct 75).

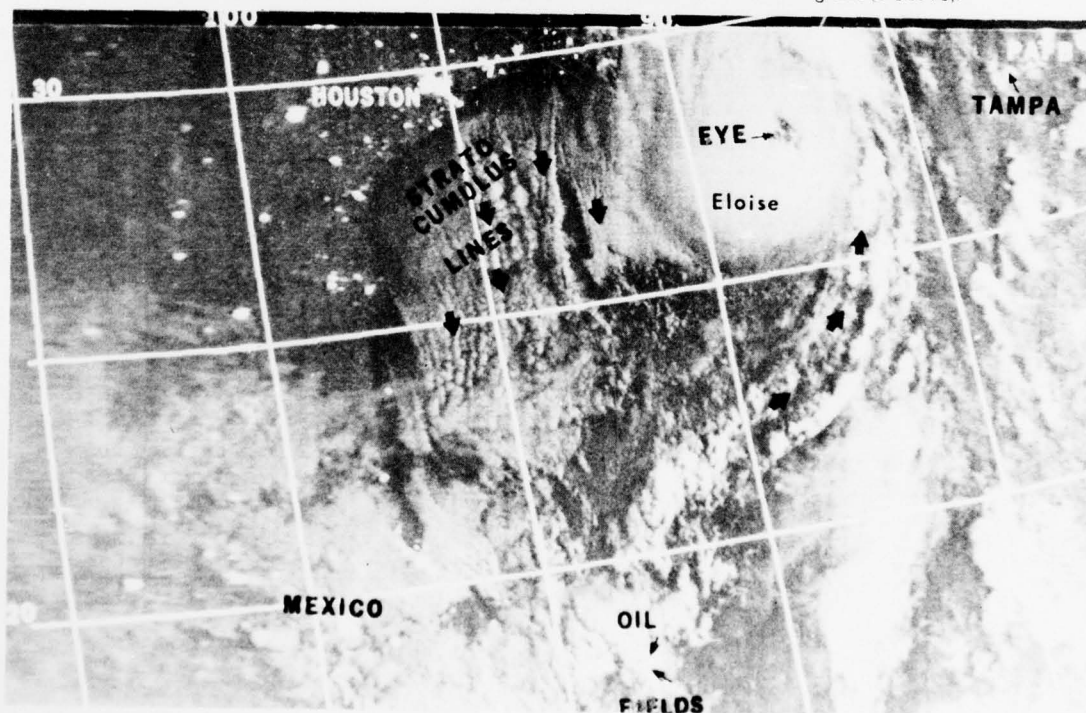


Figure 133. DMSP night visual view of stratocumulus lines off the coast of Texas (23 Sep 75).

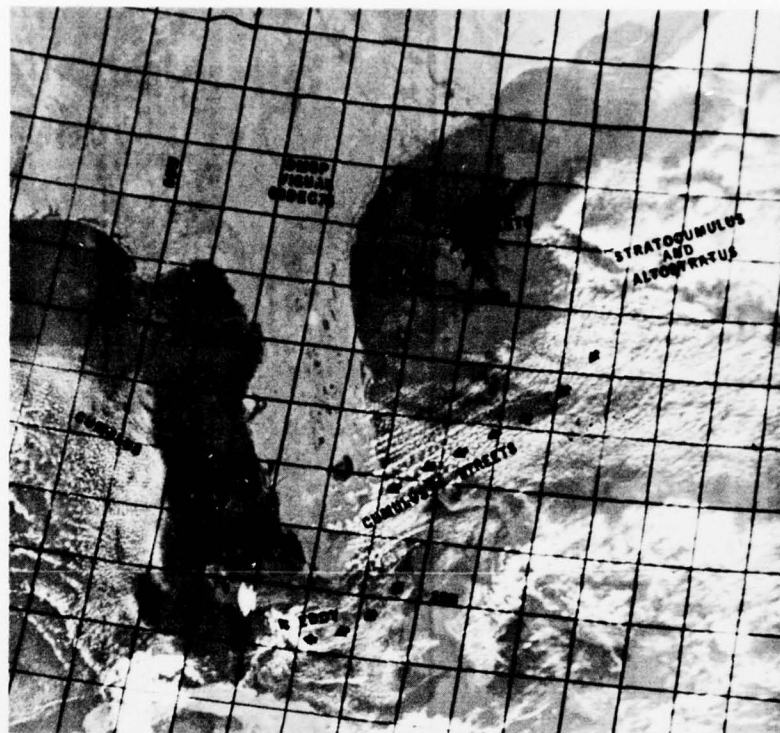


Figure 134. Cumulus streets and lines in the Atlantic (4 Dec 75).

Mid-Level Flow

Mid-level winds are difficult to deduce from satellite imagery. High clouds, when they are present, usually mask the middle clouds. Of course, deducing the mid-level flow can be accomplished by a trained meteorologist using low- and high-level satellite clues.

High-Level Flow

High-level wind flow (above 6000 meters) is labeled by double or open arrows to distinguish it from low- or mid-level flow. The most common signatures of high-level flow are towering cumulus and cumulonimbus cloud plumes, or blowoff, and the various cirrus formations.

a. **Plume Blowoff.** Plumes blowing off the tops of towering cumulus or cumulonimbus clouds are commonly seen on satellite images from the tropics to the poles. The direction of the wind is easily determined by plume examination. Only rarely is the wind difficult to calculate. The use of plume size with respect to cloud or cloud clusters is the key to determining wind speeds. For example, if no plume is seen, the speed at the cloud top is less than 10 kt. If the plume is the same size as the cloud or cloud cluster, the speed is 20 kt; if the plume size is twice the cloud size, the speed is 40 kt, etc. (Figure 138).

The height of the plume is determined from infrared satellite imagery of the cloud source *not* the plume. The plume is sometimes too transparent to infrared radiation and yields erroneous heights. If no infrared imagery is received, radar reports, cloud shadows, conventional weather charts, or rawinsonde reports can and should be used for these cloud-height values. Plume examples are shown in Figures 139, 140 and 141.

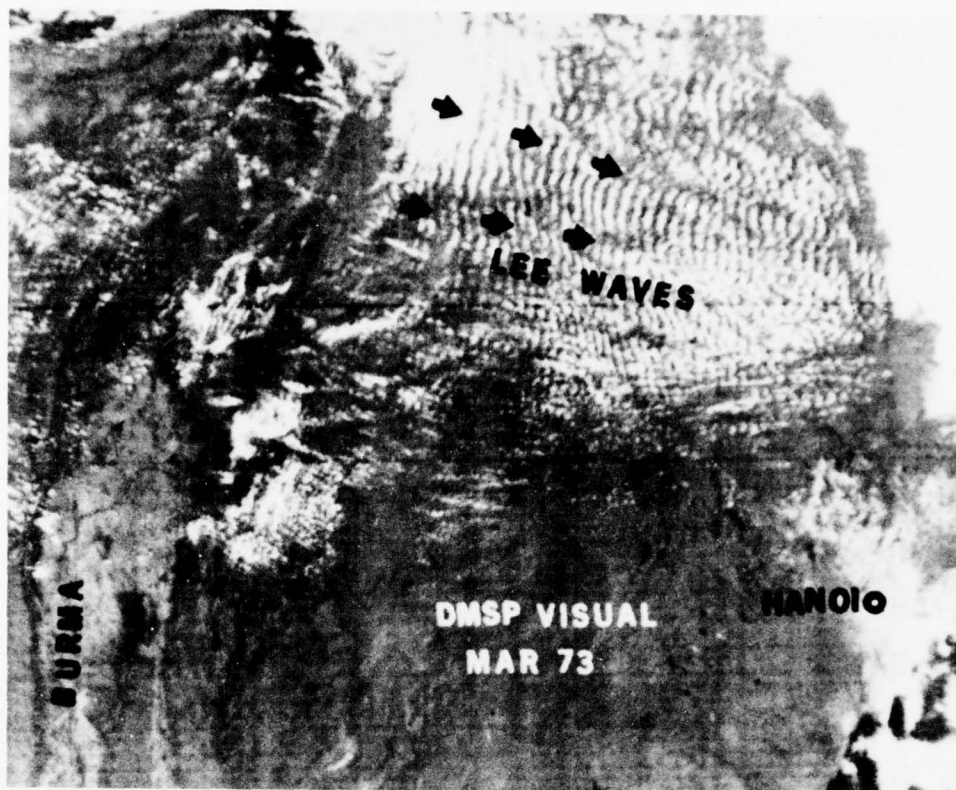


Figure 135. Lee waves over Southeast Asia (Mar 73).

b. **Transverse Cloud Bands.** Transverse banding in cirrus clouds is perpendicular or nearly perpendicular to the upper level wind flow. This banding indicates horizontal divergence away from the wind core; thus, the spreading-out effect. Speeds in the transverse bands are usually 80 to 100 kt (Anderson, et. al., [5]). Near the outflow of upper level anticyclones the curvature involved causes less wind speed and the wind flow is not perpendicular to the bands. Other indicators, such as cirrus plumes, assist in the analysis of transverse banding flow alignment near high-level anticyclones. Figures 142 and 143 are examples of transverse banding.

c. **Wind Shear.** The apparent cirrus plumes will on rare occasions be aligned with the wind shear between the upper level flow and the thunderstorm movement, i.e., mean flow in the thunderstorms (Figure 144). This case usually occurs in conjunction with a rapidly-moving winter cold front. The cold front has a strong upper level flow coupled with intense thunderstorms imbedded in the frontal cloud band. These storms move rapidly with the mean wind flow. The shear between the thunderstorm movement and the upper level flow (12,000 meters or greater) creates plumes oriented with this shear vector (Johnston, [63]). The difference between wind-shear cloud patterns and transverse cloud bands is that the former are oriented with imbedded thunderstorms in a fast-moving front whereas the latter almost always form in a cirrus pattern only.

d. **Jet-Stream Cirrus Shadow.** Conventional meteorological analysis has shown that a cirrus cloud shield will form to the right of and above jet streams (Northern Hemisphere). The upper level jet stream is located (on satellite imagery) approximately 1 degree in the clear away from the edge of the cirrus shield. Depending on sun angle, this cirrus shield can cast a shadow on lower clouds or land. Figure 145 is an expanded DMS visual photograph of a jet-stream cirrus shadow over the southeast United States. Speeds

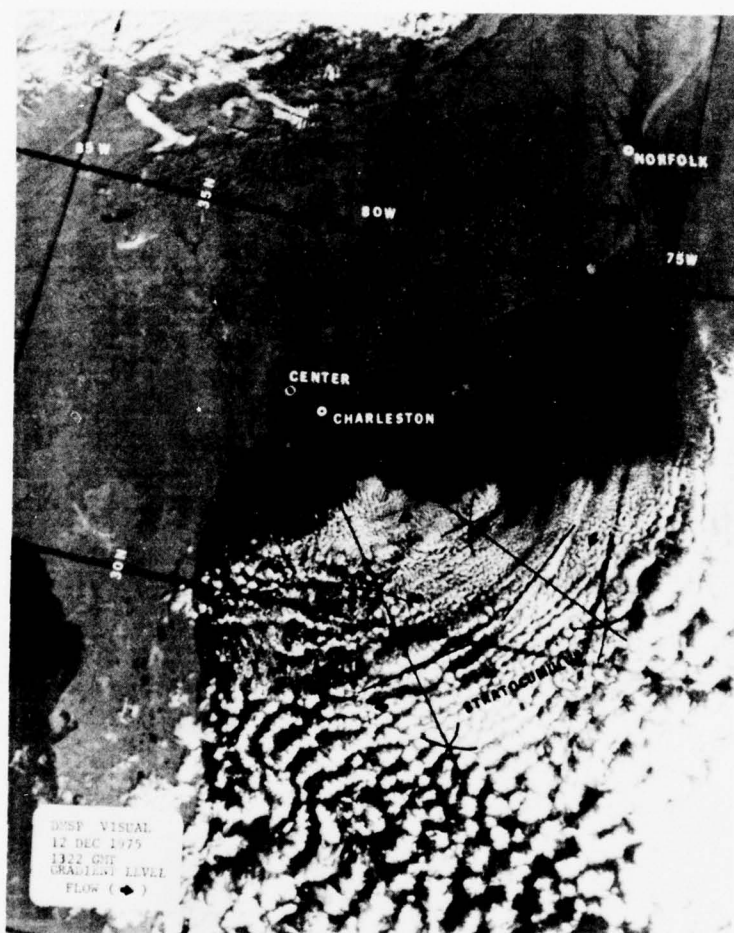


Figure 136. DMSP visual photograph with high-pressure center (12 Dec 75).



Figure 137. Surface chart for 12 December 1975.

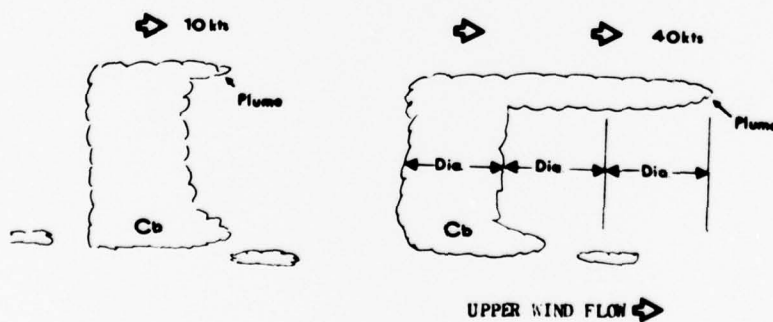


Figure 138. Diagram of plume length versus wind speed.

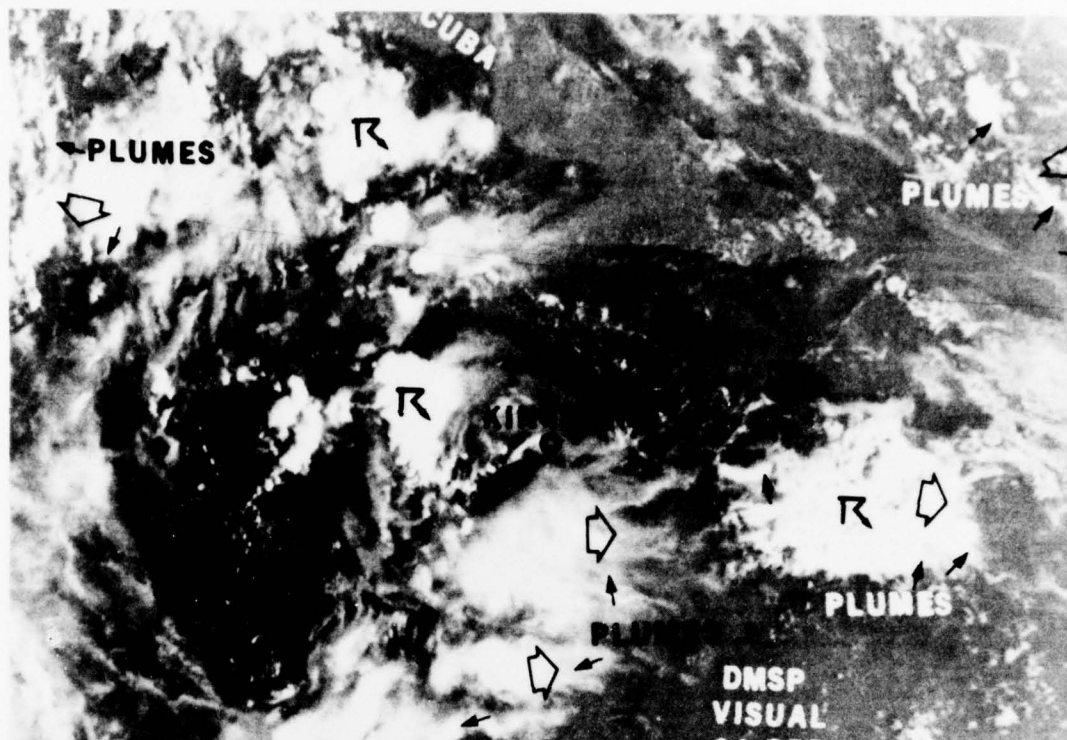


Figure 139. Plume blowoff in Caribbean (24 Sep 75).



Figure 140. Cirrus plumes blowing off CBs in Atlantic and Gulf of Mexico (date unknown).

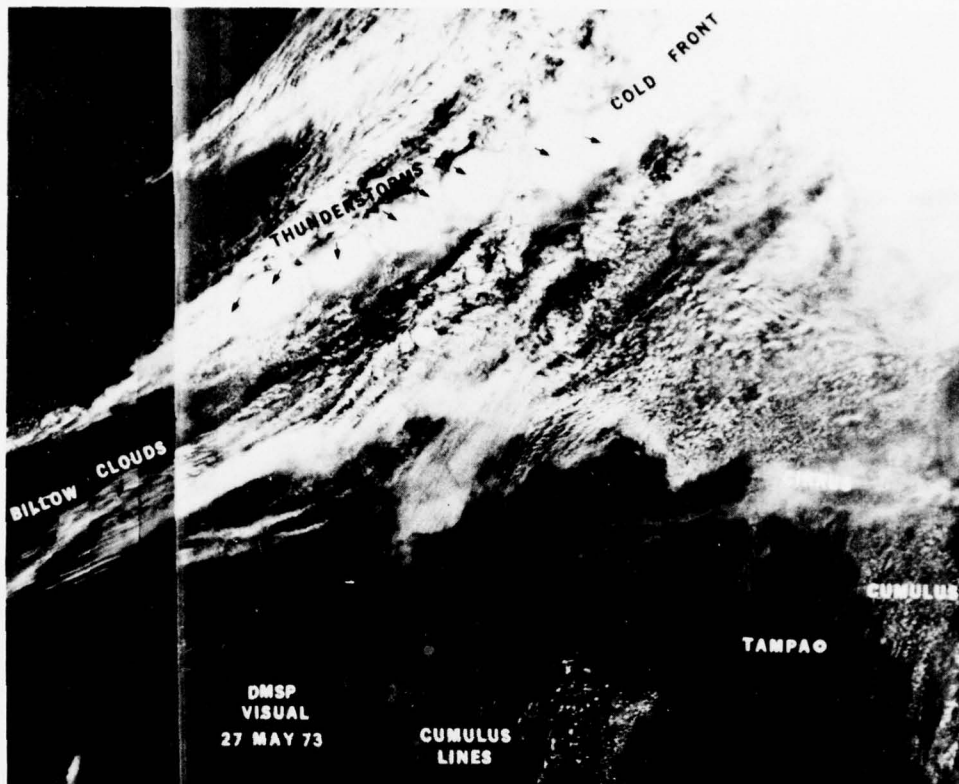


Figure 141. Plumes in an intense cold front (27 May 73).

in the jet can range from 50 to 300 kt, but generally are between 100 and 150 kt. The core of the strongest winds in the jet stream generally is found between 7000 and 12,000 meters, depending on latitude and season. Figure 146 shows a jet stream and cirrus shadow over Europe.

e. **Billow and High-Level Lee-Wave Clouds.** Cloud-height determination of billow clouds using infrared satellite imagery can be difficult because of the cloud size and the clouds' transparency to infrared emission. Experience in a given locale with upper level wind patterns will help the analyst with billow-cloud analysis. The wind flow is perpendicular to the billows and the speed is determined by (Brandli and Lombardo, [23]):

$$v = 18.4\lambda + 16.4 \quad (2)$$

where v is the wind speed in knots and λ is the wavelength of the billow clouds in nautical miles. Turbulence in the billow areas should be considered paramount in any briefing.

High-level lee waves are identical to low-level lee waves with the exception that they form over high mountain ranges. An example of lee waves in the Rocky Mountains is shown in Figure 147.

f. **Cirrus Streaks and Filaments.** Wispy cirrus clouds abound on satellite imagery, especially in the low latitudes. Cirrus streaks are not associated with plumes but do indicate wind flow. In the analysis of speed, one should use other wind-speed indicators; however, speeds are usually 60 kt.

Another wispy cirrus formation is cirrus filaments. On the visual imagery, these cirrus clouds will appear to emanate from a point source (Figure 148). The author has found that, in most cases, the wind flow is usually 60 degrees from the obvious in a counterclockwise direction (i.e., what appears to be a wind vector of 090 will be 030). Wind speeds in the filaments are usually near 50 kt and have a horizontal shear that could be indicative of turbulence. Figure 149 is a DMSP visual image depicting most high-level wind flow indicators.



Figure 142. Transverse banding around Hurricane Gladys (2 Oct 75).

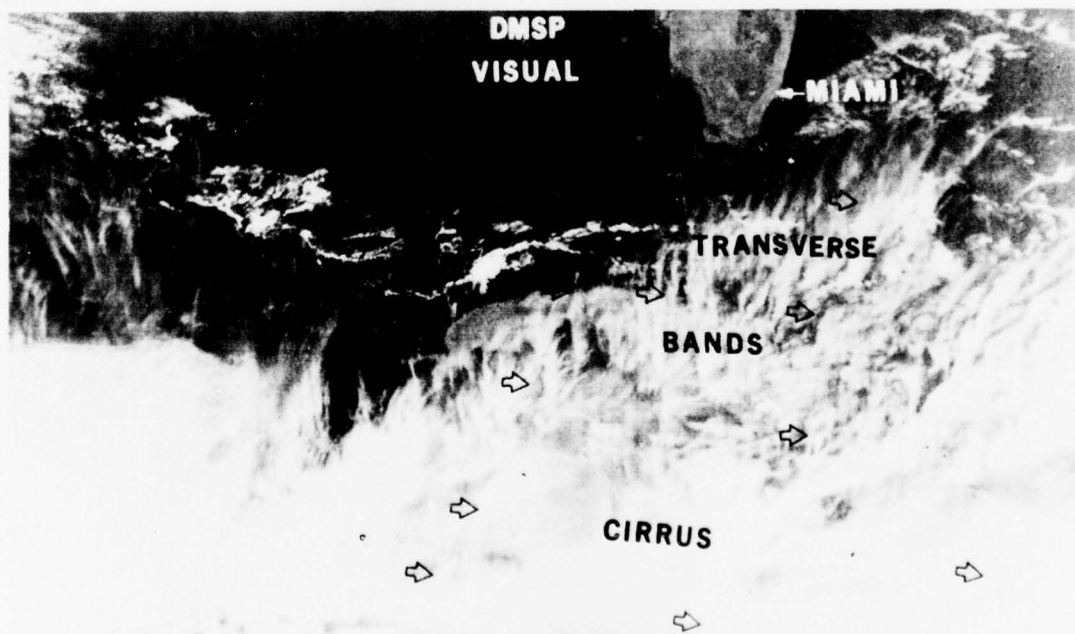


Figure 143. DMSP view of transverse banding south of Florida (date unknown).

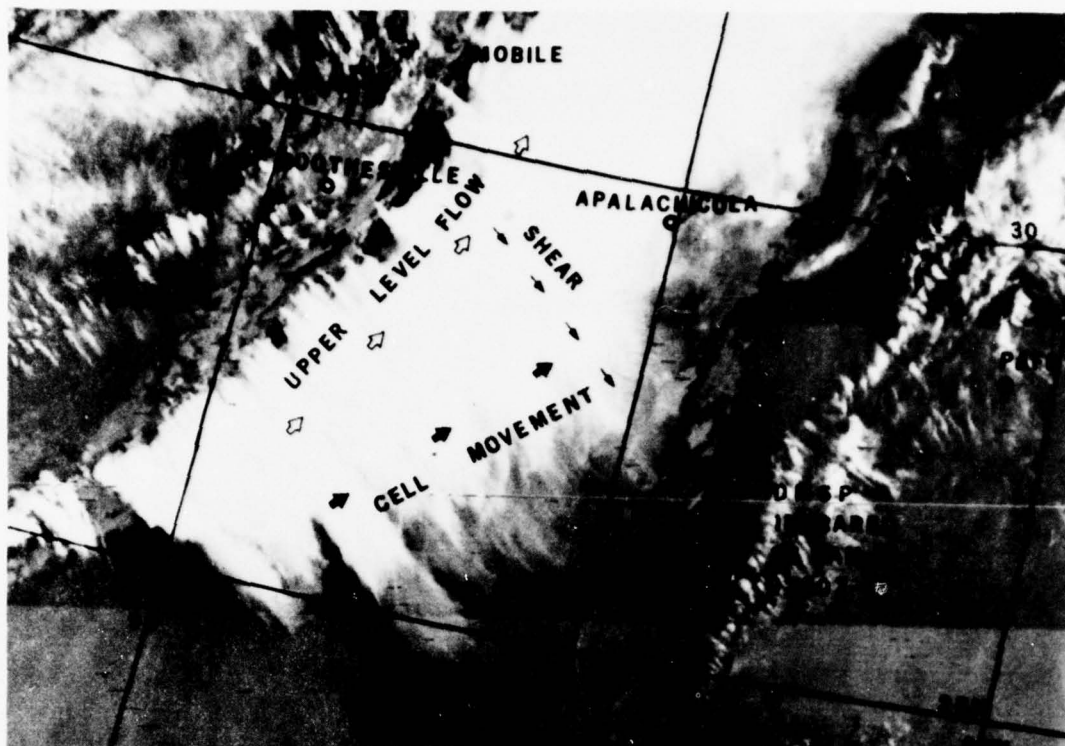


Figure 144. DMSP infrared photograph of a wind-shear pattern (26 Jan 76).

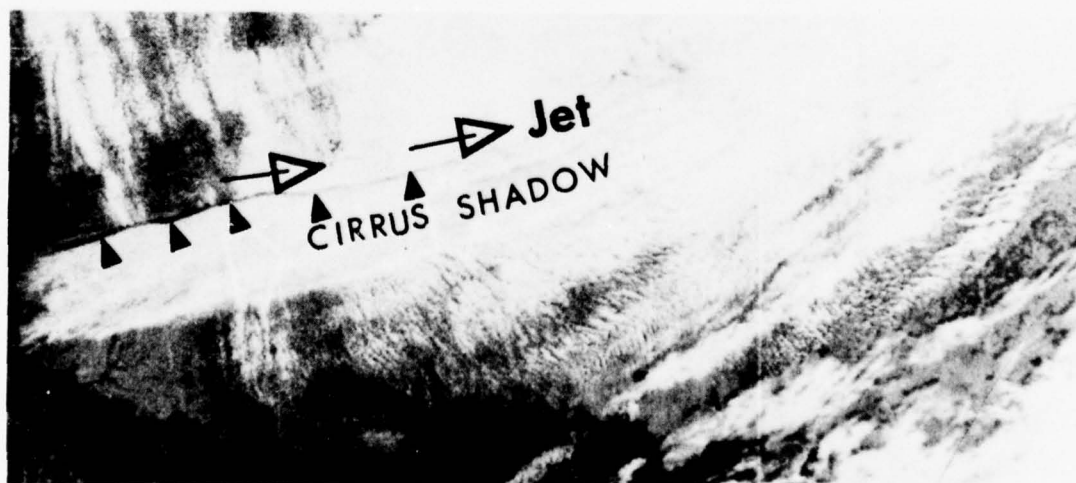


Figure 145. DMSP visual photograph of cirrus shadow (date unknown).

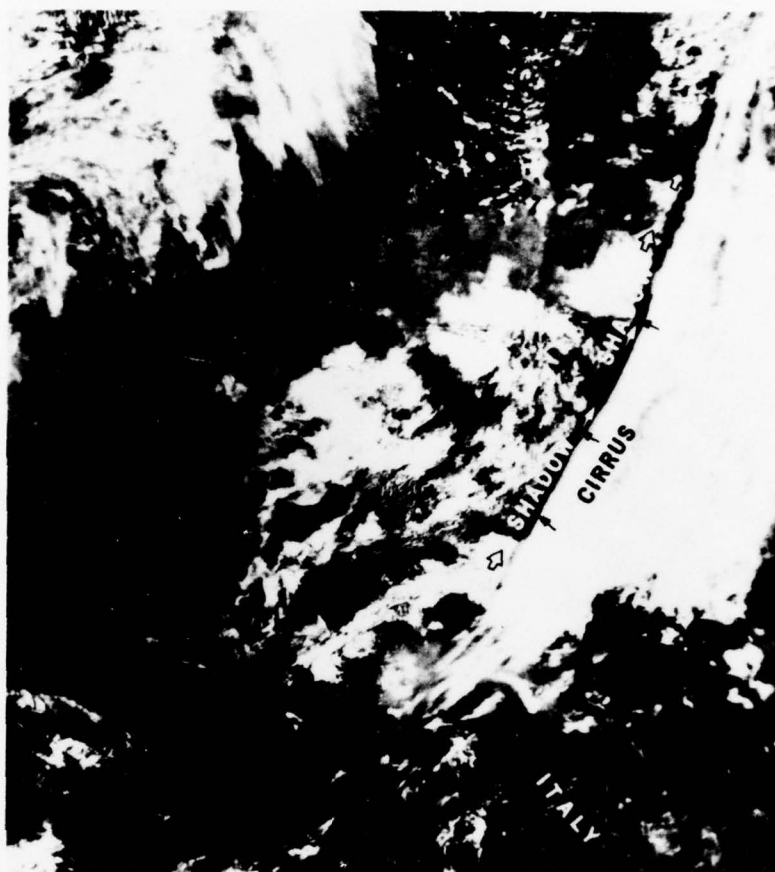


Figure 146. Jet stream and cirrus shadow over Europe (10 Sep 74).

g. **Cloud Movement.** With the advent of high-resolution imagery taken every half hour, cloud movement can be tracked accurately. The cloud movement can indicate mean wind in the cloud layer. Infrared imagery can tell the height of the cloud tops and experience can aid in calculating the base of the cloud. Accurate gridding of the imagery is a must in mean-wind calculation from cloud movement (Brandli and Munson, [24]).

On 28 November 1973, a cold-air mass with a frontal cloud system was moving through north central Florida. This front was oriented north-northeast to south-southwest. In Figure 150, geographically gridded DMSP visual and infrared photograph pairs are presented showing this frontal system in the morning hours. By transferring key positions of the front (leading edge, rope cloud, back edge, etc.) onto a weather plotting chart, a frontal movement forecast can be made (Figure 151). Of course, if development or dissipation occurs or if the system slows, stops, or speeds up, continuity becomes more difficult, *but not impossible*. The accuracy of this November frontal movement forecast is obvious in Figure 152. This DMSP visual and infrared photograph pair shows the frontal position at the same location as the forecast in Figure 151. In this example, extrapolation techniques were successful.

Other systems such as tropical storms, squall lines, and convergent areas can be extrapolated accurately up to 24 hours. In the case of conservative systems such as hurricanes and typhoons, continuity and extrapolation from transferred analyzed imagery are valid even longer. Even individual clouds can be monitored and future positions forecast using geographically gridded meteorological satellite data.



Figure 147. Lee waves in the Rocky Mountains (6 Apr 74).



Figure 148. SMS-1 visual photograph of cirrus filaments (27 Dec 74).

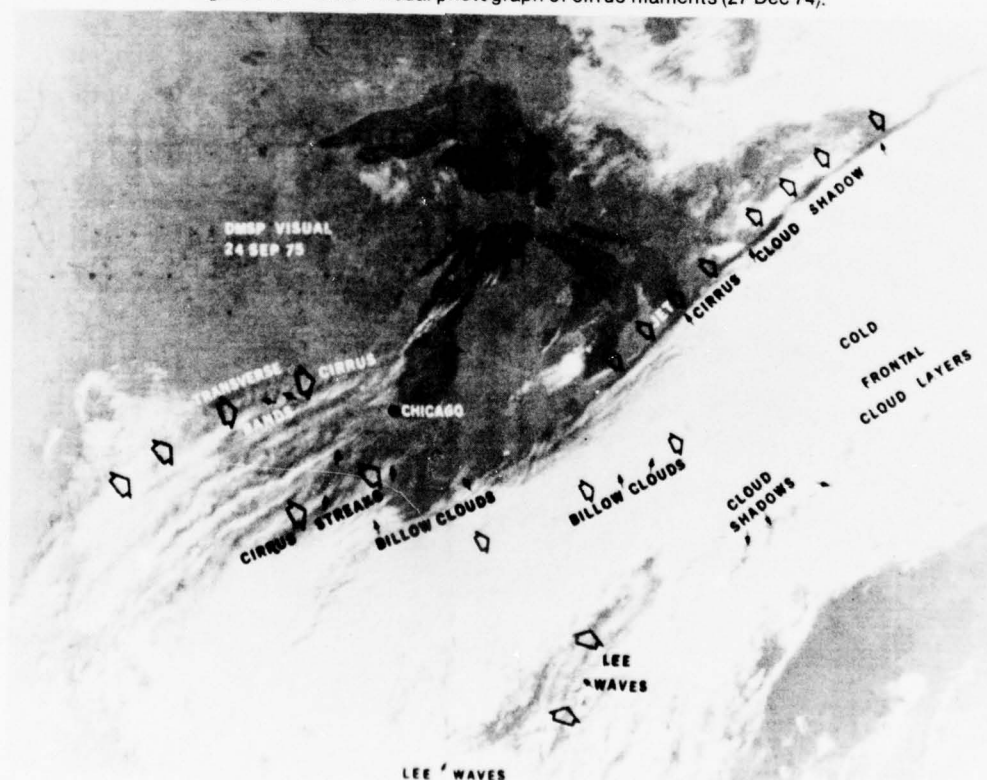


Figure 149. Many upper level wind-flow indicators (24 Sep 75).

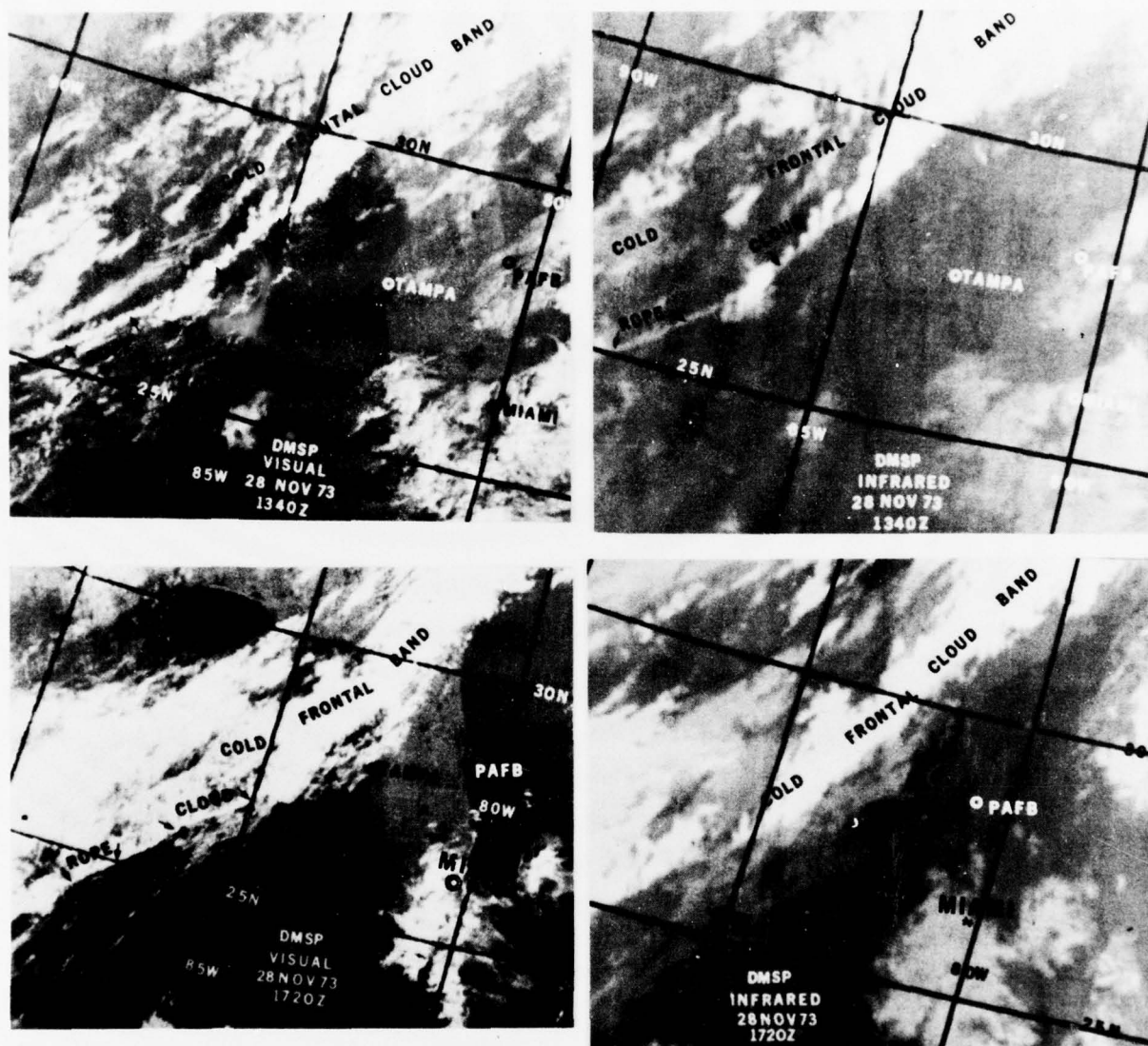


Figure 150. DMSP visual and infrared photographs of a frontal system (28 Nov 73).

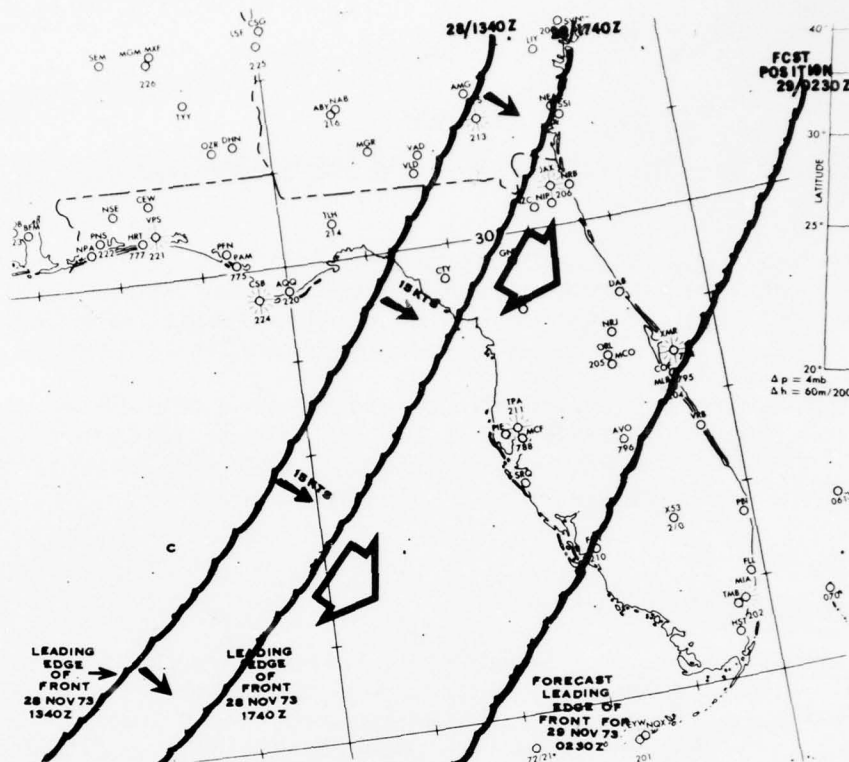


Figure 151. Current and forecast positions of the front.

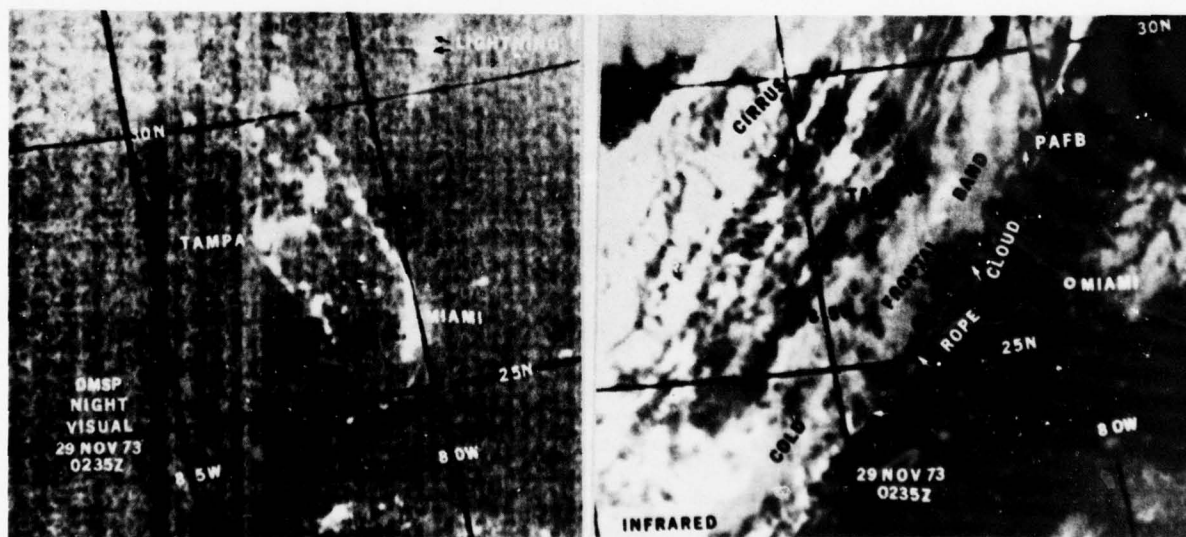


Figure 152. Surface position of front (29 Nov 73).

Chapter 6

EARTH SURFACE AND OTHER MISCELLANEOUS FEATURES

The Earth Resources Technology Satellite (ERTS), launched by NASA, is the primary remote-sensing satellite designed for earth-resource monitoring; however, it sees the same location only once every 18 days. Currently, there is no thermal (infrared) scanner on board to detect land and water temperatures. The high-resolution photographs of existing and future meteorological satellites lend themselves well to some of this remote sensing of the earth.

The DMSP satellite is currently one of the more valuable meteorological satellites capable of viewing our earth resources. With its visual, near-infrared, and infrared sensors, the DMSP satellite provides imagery every 6 hours over any one point on the earth. Current nonmeteorological applications of DMSP data are listed in Table 6, and will be discussed in detail in this chapter.

Geology (Geologic Resources):

a. **Land Features.** Geological study of the earth can be done with photography obtained from the Earth Resources Technology Satellite (ERTS). With the increased spectral interval, the DMSP satellite is capable of providing some coverage of poorly studied areas. Land features (mountains, hills, reservoirs, and vegetation) stand out clearly on early morning photography using the visible spectrum, because shadows cast by irregularities in the earth's surface enhance their definition. Figure 153 is a DMSP image of the Montana and Wyoming areas. The island of Luzon with its rugged terrain is shown in Figure 154. Italy and adjacent islands are shown in Figure 155.

Vegetation and other land features, i.e., fertile valleys and deltas, are observed on meteorological satellite imagery. The expanded spectral interval of the DMSP system allows these anomalies to be resolved more clearly. Figure 156 is a photograph of Cyprus depicting its forested areas.

Soil moisture and related land features seen on satellite imagery are also important in the preservation of our resources. Figure 157 is a DMSP visual photograph of the Nile River which shows moist, vegetated areas.

Sand and sand dunes are features commonly seen on DMSP imagery. Figure 158 is a visual image of Saudi Arabia.

b. **Volcanoes.** Volcanic eruptions, both explosive and effusive, can easily be seen in remote areas with the DMSP sensor. The bright lights of the burning volcano or the smoke pouring from one can be identified unless thick clouds are covering the crater. Figure 159 is a DMSP, no-moonlight visual photograph of the erupting Kilauea crater. The ringed pattern around the volcano is probably a halo formed by ice-crystal clouds, volcanic smoke particles, or an out-of-focus mirror on the sensor. The geometry of the halo (Figure 160) is similar to the geometry of the rings that are occasionally seen around the sun or moon and are caused by ice-crystal cirrus clouds. Ringed patterns are also seen around uncapped oil and gas field fires.

c. **Meteors.** Figure 161 is a DMSP nighttime visual image taken over the Pacific Ocean. In the lower left-hand corner, over Johnston Island, is what appears to be a streak of light. All available evidence indicated that the cause of the light streak was a large meteor falling through the earth's atmosphere (Kim, [64]). A meteor would explain the presence of a clearly visible streak of light on the visual data and the lack of any "sighting on the infrared." US Air Force personnel stationed at Johnston Island confirmed the sighting of a large "falling star" at approximately the same time that the DMSP satellite was orbiting the area.

Table 6. DMSP Nonmeteorological Applications (Dickinson, et. al., [39]).

I. GEOLOGY

- A. Terrain
- B. Vegetation
- C. Soil Moisture and Land Features
- D. Volcanoes
- E. Meteor Trails

II. HYDROLOGY

- A. Rainfall
- B. Flooding
- C. Snow Depth and Coverage
- D. Ice Mapping

III. OCEANOLOGY

- A. Sea Surface Temperatures
 - 1. Effect on Industry (Fishing)
- B. Wave Heights
- C. Iceburg Detection

IV. FIRE DETECTION

- A. Forest Fires

V. MISCELLANEOUS

- A. Oil and Gas Field Fires
- B. Eclipse (Sun and Moon)
- C. Aurora
- D. Earthquakes



Figure 153. Terrain features of Montana and Wyoming (22 Aug 74).



Figure 154. Mountains of Luzon (10 May 73).

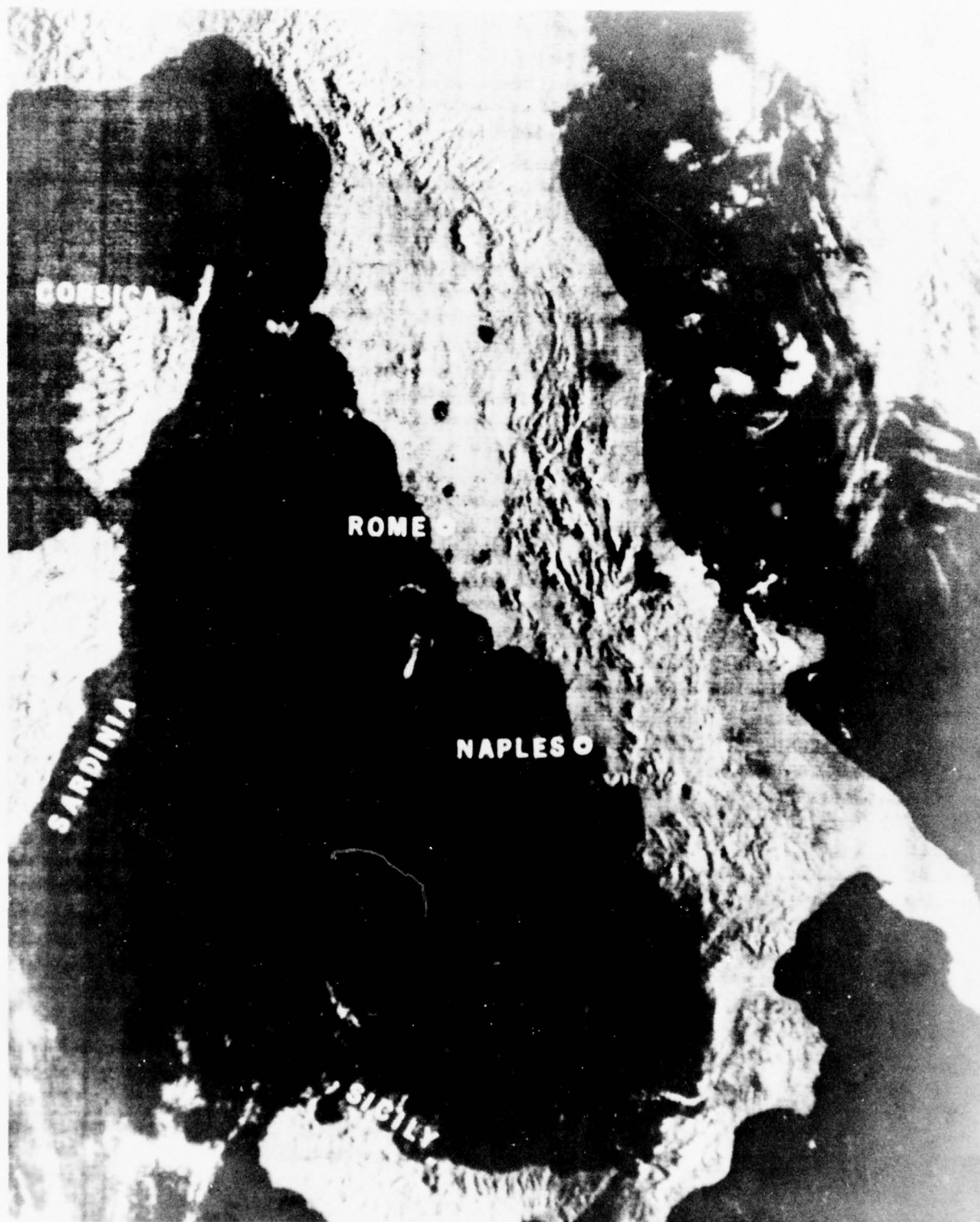


Figure 155. Mountainous areas of Italy and islands (13 Aug 74).

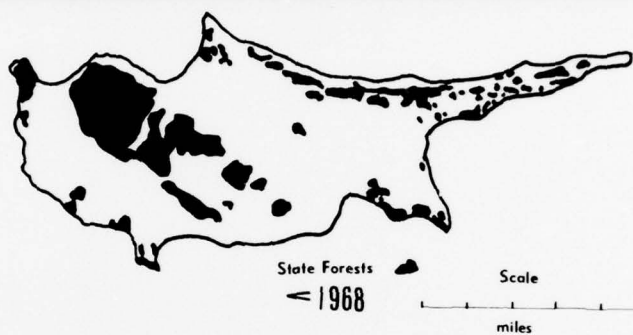
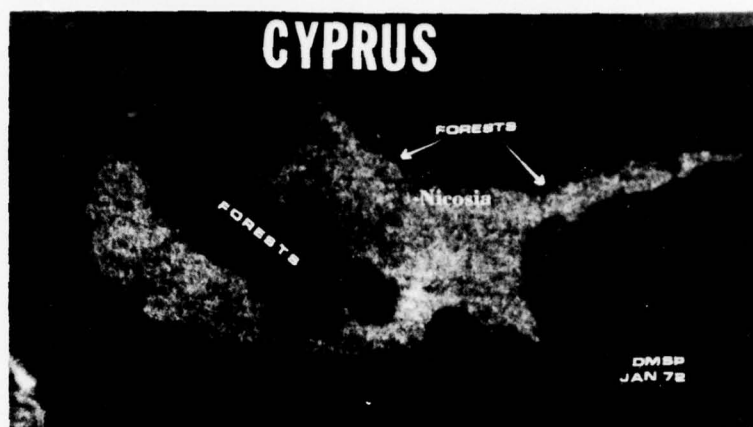


Figure 156. Forests of Cyprus (Jan 72).



Figure 157. Fertile Nile River and Delta (6 Oct 73).

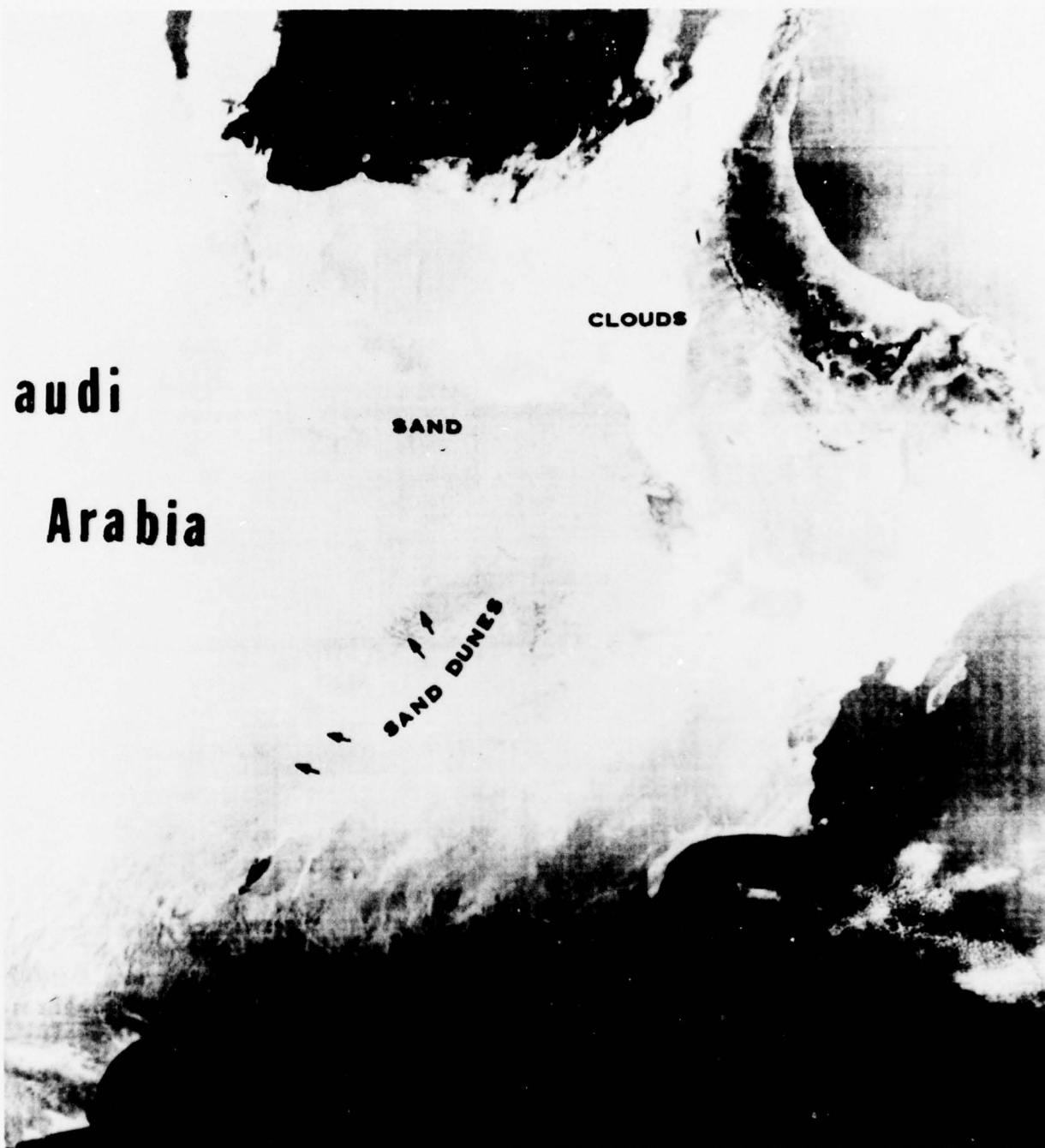


Figure 158. Sand and sand dunes in Saudi Arabia (date unknown).

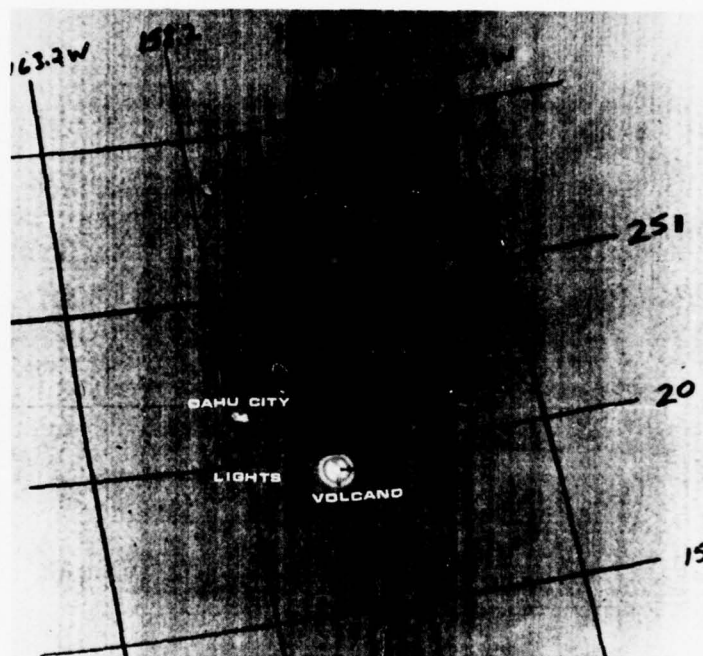


Figure 159. No 1-1 moonlight DMSP view of volcano (28 Dec 70).

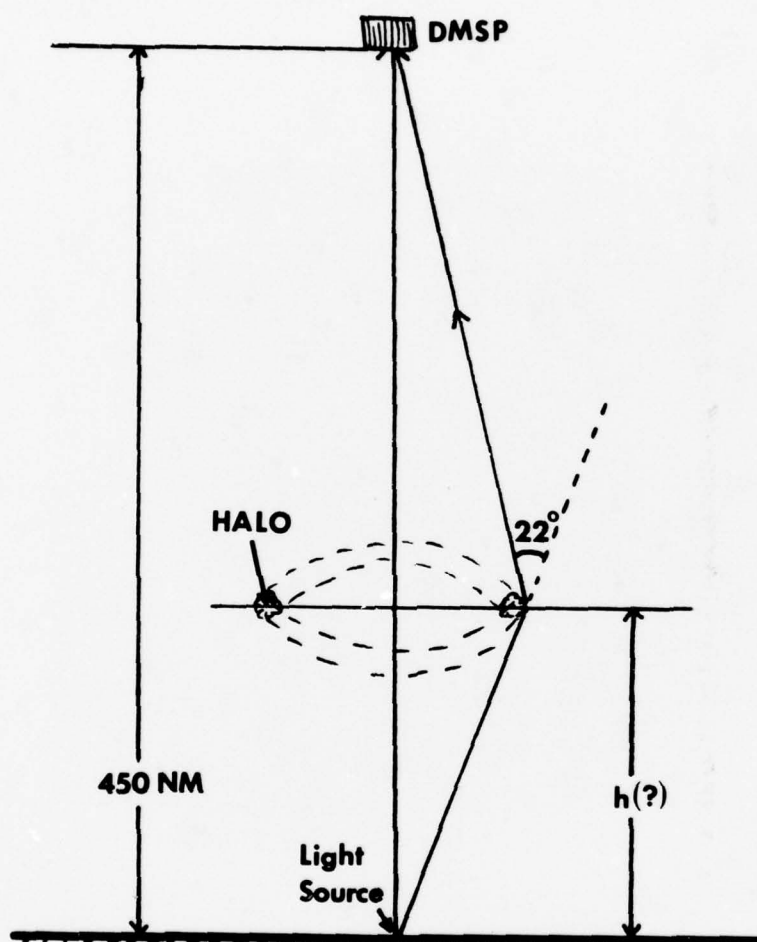


Figure 160. Geometry of volcanic-produced halo (Dickinson, et. al., [39]).

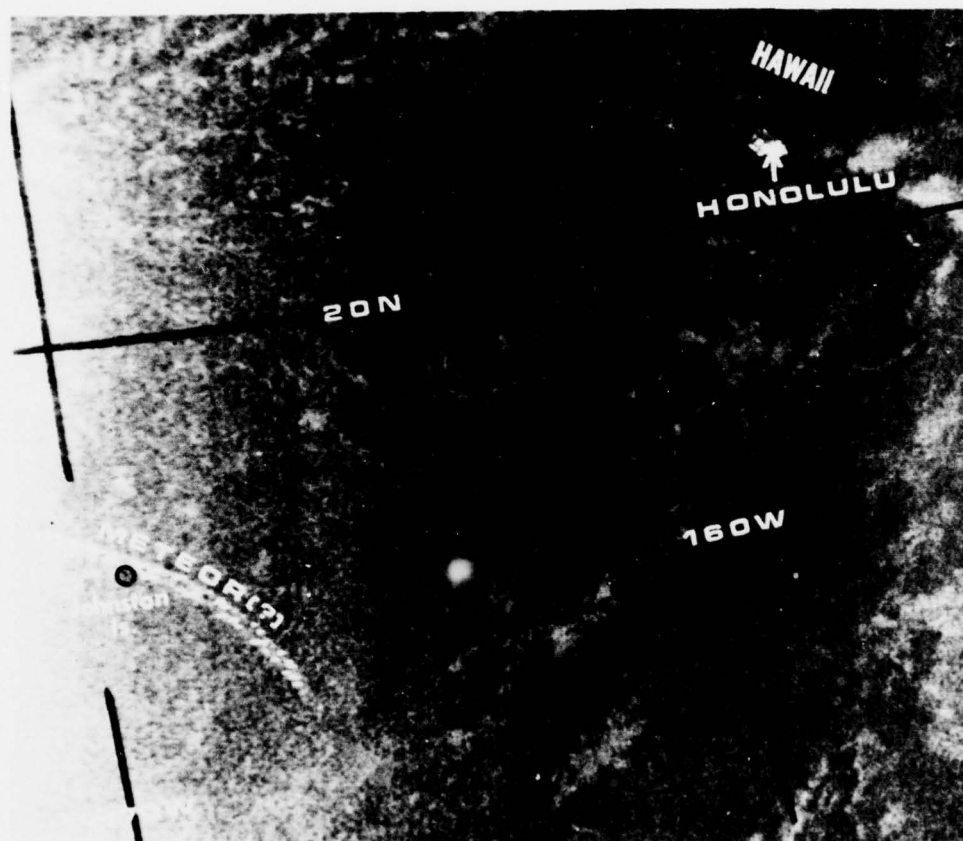


Figure 161. DMSP view of meteor (20 Nov 74).

Hydrology, Oceanology:

a. **Rainfall.** Determining the exact amount of rainfall from satellite photographs is an impossible task. However, observing, forecasting, or determining rain or rain showers from cumulonimbus (\mathcal{R}), towering cumulus, nimbostratus, cumulus congestus, or other clouds, is an easy task if one recognizes the different cloud types on the photographs. The use of visual and infrared imagery should enable many of the rain-producing clouds and systems to be recognized, including the most convective areas. Local effects such as terrain and land/water contrasts will complicate some prognostications.

Follansbee [49] used satellite photographs over Zambia, Africa to get very good rainfall amounts when compared with conventional rainfall measurements. His procedure was to determine the percentage of the subject area covered by each of three rain-producing cloud types (cumulonimbus, nimbostratus, and cumulus congestus) and apply an empirically-determined coefficient to each cloud type to arrive at a total rainfall prediction.

Another relationship for cumulonimbus clouds was to consider the average cumulonimbus cloud lasting 3 hours with a rainfall rate of 1/3 inch per hour over the entire area. Of course, a maximum of 1 inch per hour would occur at the center and a trace of rain would occur at the outer edges of the cell(s).

Another technique (Gruber, [55]) requires the use of brightness values with a density step wedge and the simultaneous infrared imagery to determine convective areas. This method suggests that meaningful rainfall estimates can be made using satellite observations.

b. **Flooding.** Hydrological problems of drought and flooding, which are closely associated with meteorology, merit the attention of the satellite meteorologist. Hydrologists and meteorologists alike can study fluctuations in the amounts of water being carried by rivers and make forecasts for periods of flooding. Reservoirs can also be monitored for depletion of water supply by inverting the DMSP visual imagery so that land contrasts stand out. By this method, the monitoring of rivers becomes an easy task. Figure 162 is a DMSP inverted visual photograph showing swollen rivers in the southeast United States.

c. **Snow.** Visual mapping of snow is an important hydrological project. This mapping can be routinely accomplished by using meteorological satellites, provided cloud cover can be distinguished from the white snow.

A common snow pattern seen on satellite imagery is a dendritic pattern. This term was taken from geologists due to its similarity to geological formations. The pattern is caused by mountain valleys, rivers, and tree lines which contrast sharply to the snow-covered areas. Figure 163 is a DMSP image of dendritic snow patterns in Turkey.

Cloud cover can seriously degrade snow pattern recognition. Accurate gridding and knowledge of the synoptic situation will aid in distinguishing between the patterns. Figure 164 shows snow along the west coast of North America in conjunction with extensive cloud cover.

In areas where snowfall is rare, examination of successive photographs can rule out cloud cover. Snow cover on the peaks of Mauna Kea, Mauna Loa, and Mt. Haleakala in the Hawaiian Islands is shown in Figure 165.

One can estimate snow depth, coverage, and location from meteorological satellite imagery. Studies have been done on determining snow depth and extent using VHR data from the NOAA-2 satellite. Densitometer examinations of the visible band images have indicated that, generally, there is a direct correlation between increasing brightness and increasing snow depth (McGinnis, et. al., [73]). Snow depth as well as coverage is apparent in Figure 166. Heavy snow can be seen around Nashville, Tennessee, and Springfield, Missouri. Rivers, highways, and cities can be detected in Figure 167.

Figure 168 is another DMSP visual image of snow cover in the midwest. Snow depths observed in the snow-band area at 1200 GMT on 22 November 1975 are plotted on the photograph. A good correlation exists between the relative brightness and texture of the snow and observed depth. This image was initially gridded by one-degree squares. Assuming a water-to-snow equivalence of 1:8 and an average snow depth of 6 inches over the area covered, the total amount of liquid water on the ground at the time of the observation was estimated at 1.5×10^9 gallons (Maier, et. al., [69]).

Knowledge of snow melt is vital for runoff predictions and for the regulation of water reservoirs to

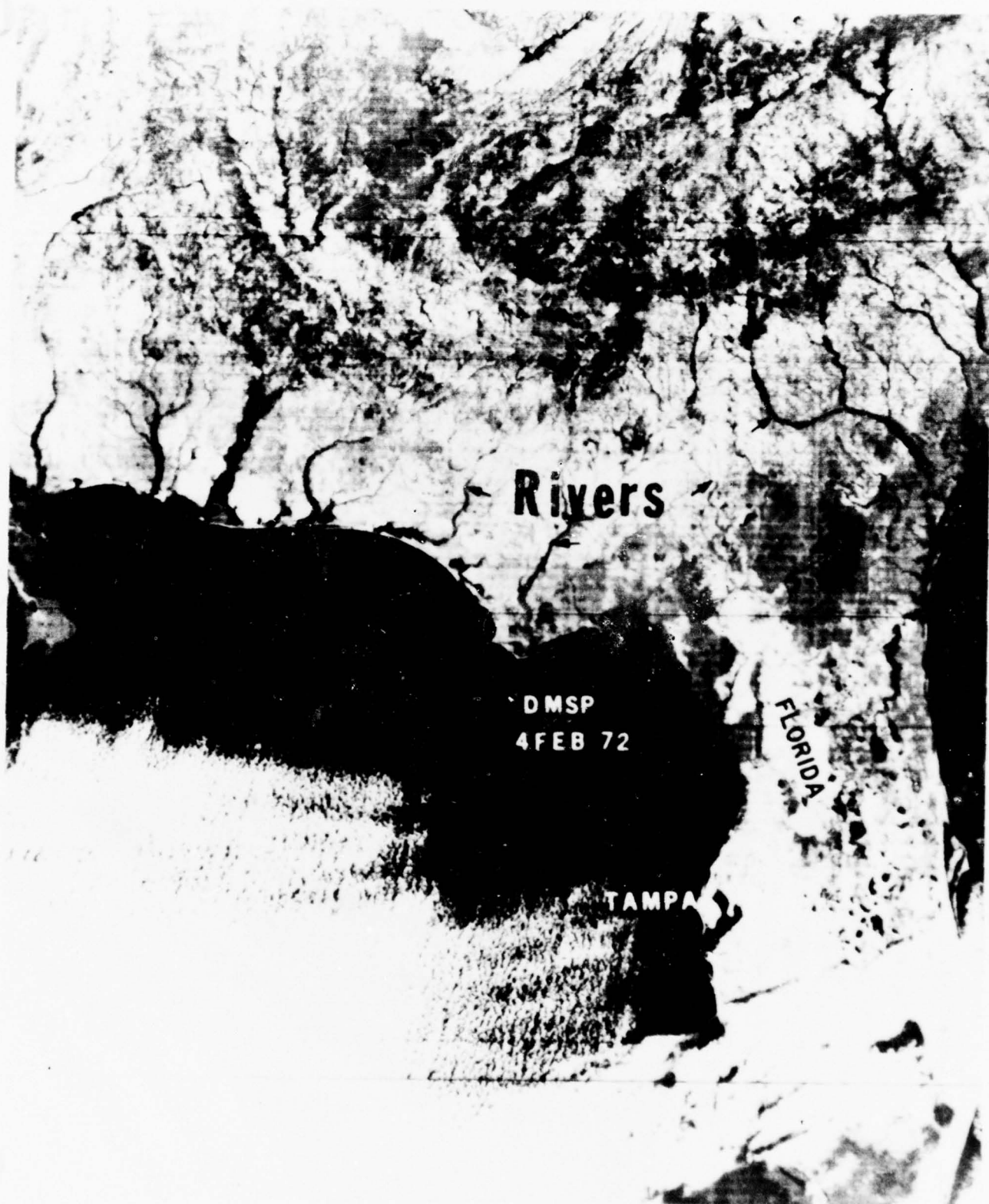


Figure 162. DMSP inverted visual photograph of swollen rivers (4 Feb 72).



Figure 163. Dendritic snow in Turkey (date unknown).

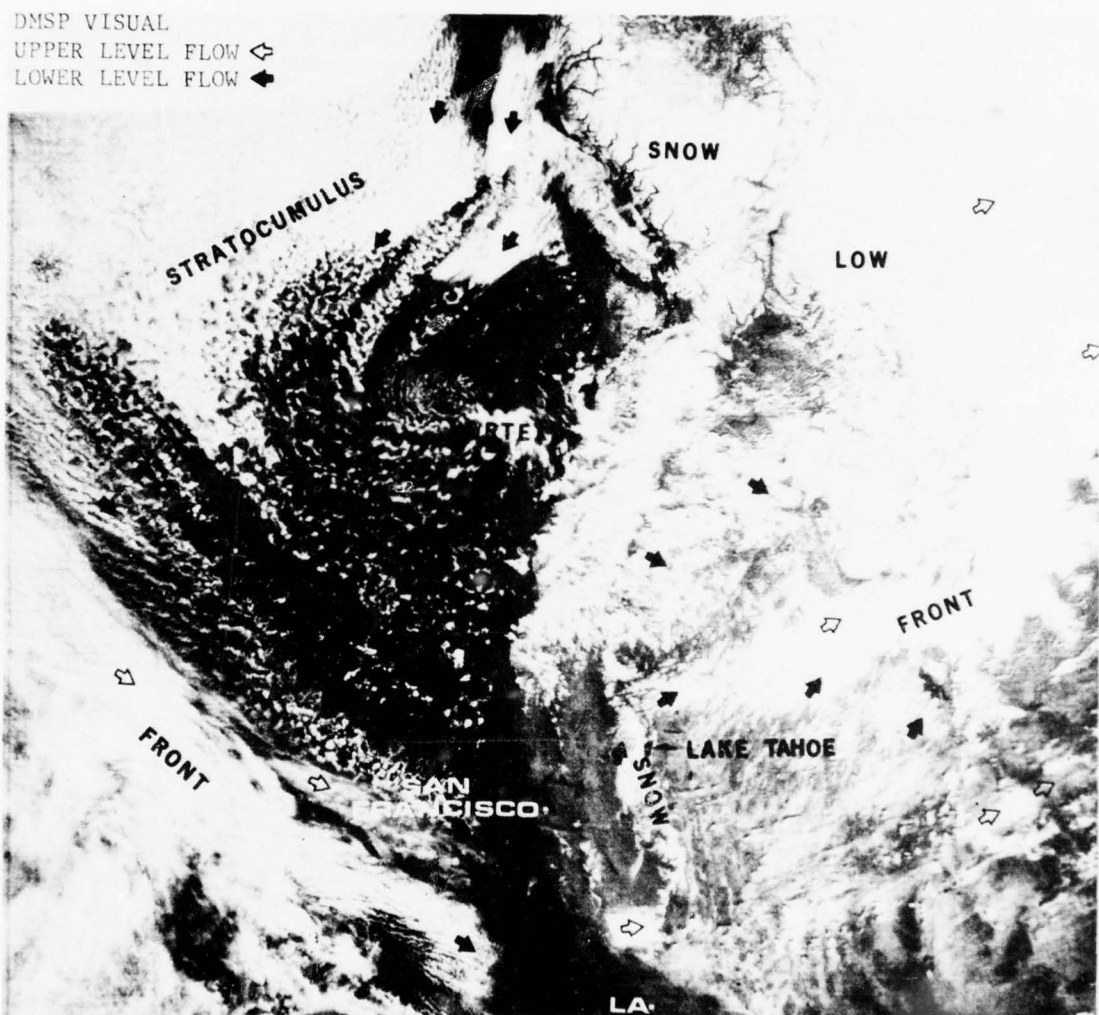


Figure 164. Snow and cloud cover along west coast of North America (date unknown).

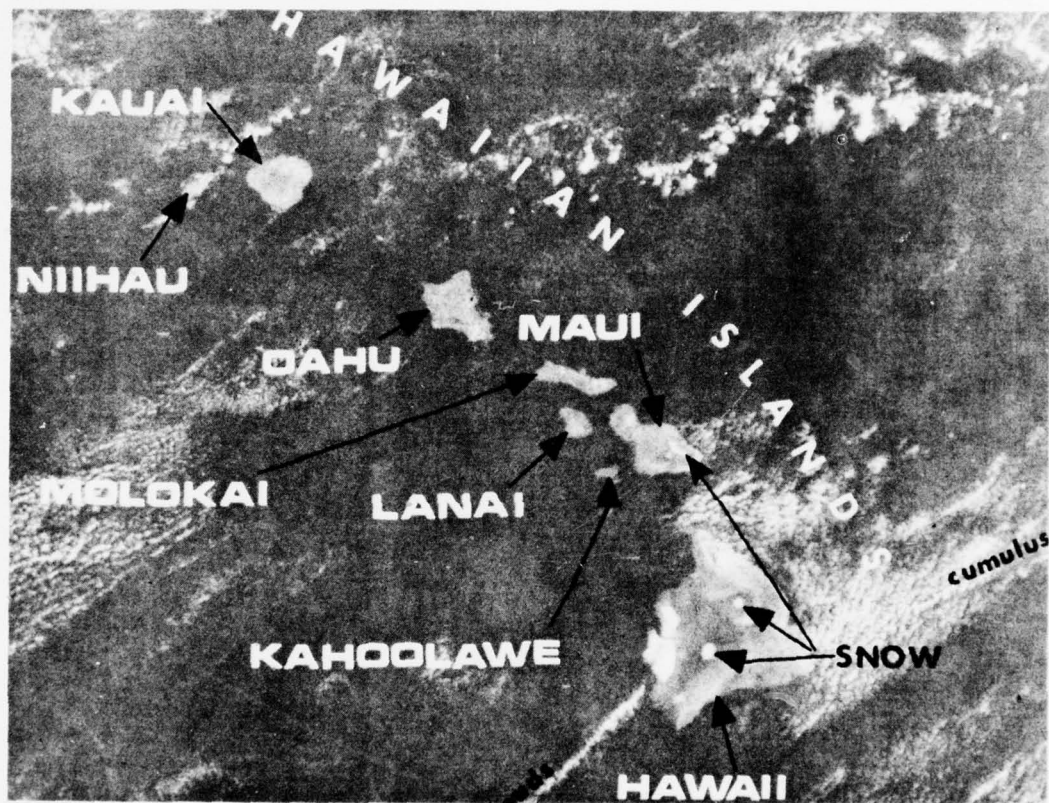


Figure 165. Snow in Hawaiian Islands (date unknown).

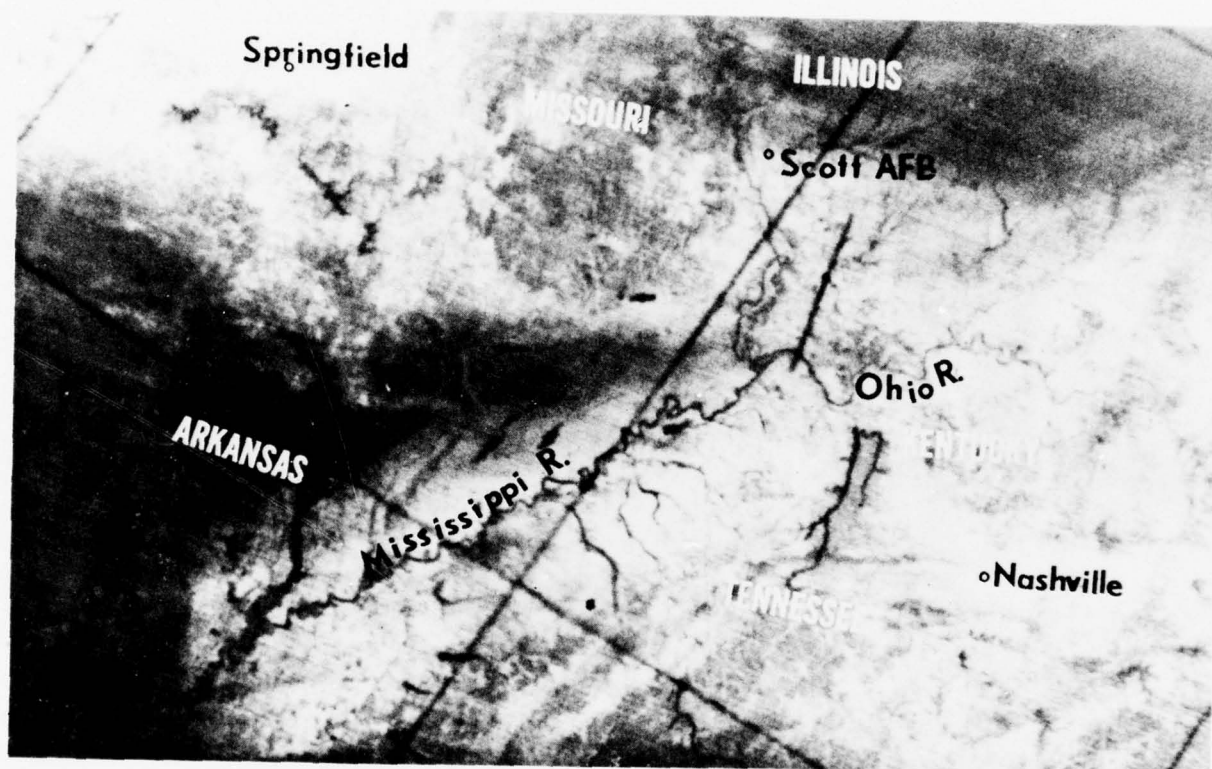


Figure 166 Snow depth and coverage over midwest (9 Feb 71).



Figure 167. Snow cover extent and depiction of rivers, highways, and cities (15 Jan 74).

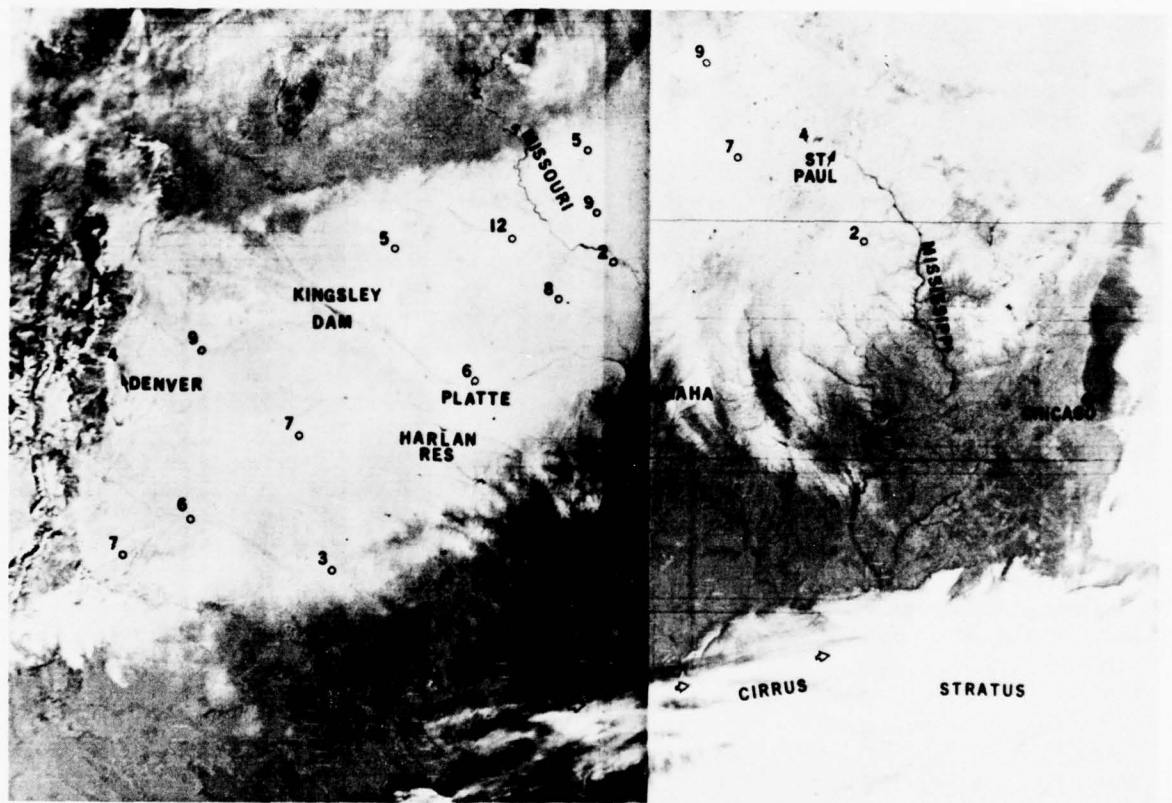


Figure 168. Snow cover and observed snow depth (22 Nov 75).

control flooding in addition to providing storage to meet water demands during dry periods. Interpretation of DMSP satellite imagery can be a valuable source of information for this function.

d. **Ice.** The observing, mapping and forecasting of ice is another important feature for hydrologists as well as navigators and fishermen. Simultaneous visual and infrared imagery is best suited for a study such as this. Figure 169 is a NOAA-3 visual and infrared photograph showing ice on Hudson Bay and Lake Superior. On the visual image, melted ice in James Bay and residual ice on Lake Superior can be seen quite clearly. Infrared imagery obtained on cloudless days provides the means for studying the temperature field of the underlying surface. Although clouds make the use of infrared imagery difficult, the very repetitiveness of the observations is sufficient to obtain extremely useful data. Figure 170 shows DMSP visual and infrared imagery taken over a 2-day period. The difficulty in determining ice, snow, and clouds is obvious from the imagery. Infrared detection of cold clouds, ice, and snow by itself would be almost impossible without simultaneous visual data. An iceberg is located east of Cape Darnley. The location and tracking of large icebergs using high-resolution meteorological satellite imagery can be accomplished accurately with geographically gridded photos. These hazards to northern or southern shipping lanes are presently being mapped in a routine fashion by NOAA, Department of Defense, and other agencies. Figure 171 shows an iceberg quite clearly in the Weddell Sea off the coast of Antarctica.

e. **Ocean Surface Temperatures and Features.** The use of infrared imagery of the surfaces of the seas and oceans plays an important part in the study of ocean currents. Warm currents, eddies, and other temperature anomalies are easily mapped from the infrared sensors of meteorological satellites. The resolution of the DMSP and NOAA satellites is more than adequate to provide thermal sea-surface temperatures. However, surface temperatures derived from satellite sensors are radiation temperatures and not the sensible surface temperatures normally taken by oceanographers using bucket thermometers. Experienced meteorologists have learned to realize the limitation of actual values of radiation temperature. Their particular interest is where and when these temperature values change (LaViolette, et. al., [67]). Many weather phenomena are related to sea-surface temperatures including the formation of hurricanes and typhoons and their movements.

Figure 172 illustrates the flexibility of the DMSP satellite in locating and analyzing warm ocean eddies. The upper left photograph is a night visual with a simultaneous infrared photograph in the upper right. The temperature range of the infrared photograph is 289°K to 259°K (black to white) with 16 gray shades possible. In the lower left photograph, four gray shades are depicted with a range from 283°K to 279°K. These four gray shades represent temperatures of greater than 283°K (black), 283°K to 281°K (dark gray), 281°K to 279°K (light gray), and less than 279°K (white). The temperature of the warm eddies is 283°K or warmer. To confirm this approximate temperature, four more gray shades were requested from 286°K to 282°K (lower right photograph). These four gray shades represent temperatures of greater than 286°K (black), 286°K to 284°K (dark gray), 284°K to 282°K (light gray), and less than 282°K (white). This additional information determined the radiating temperature of the eddies to be 283°K.

Acquisition of oceanic thermal emission data by meteorological satellites with various instrument calibration errors (signatures) can provide global sea-surface temperature measurements, provided cloud cover is scrutinized very closely. It would be impossible to cover the earth's water surfaces with buoys; therefore, satellite infrared imagery is the only practical means of mapping these important sea-surface temperatures. The U.S. Navy, its submarine fleet, and the fishing industries of the world will depend on accurate satellite infrared imagery. However, the calibration problems of satellite infrared radiometers discourage oceanographers and meteorologists from using these data. This author believes that the only solution to this dilemma is to standardize radiometric calibration curves and develop infrared signatures for ocean areas.

Figures 173 and 174 are geographically gridded DMSP infrared images showing the development of a shelf water vortex south of Cape Hatteras. Due to persistent cloud cover off the east coast, these eddies are seldom captured on satellite imagery. Also, note the intrusions of cooler water which appear to be from the Charleston, Delaware, and Hudson Rivers. Location and tracking of such eddies and intrusions are extremely useful to Naval and Coast Guard operations. Through the use of thresholding, the eddies may be isolated and evaluated for temperature, configuration, movement, and position. Figure 175 is a DMSP

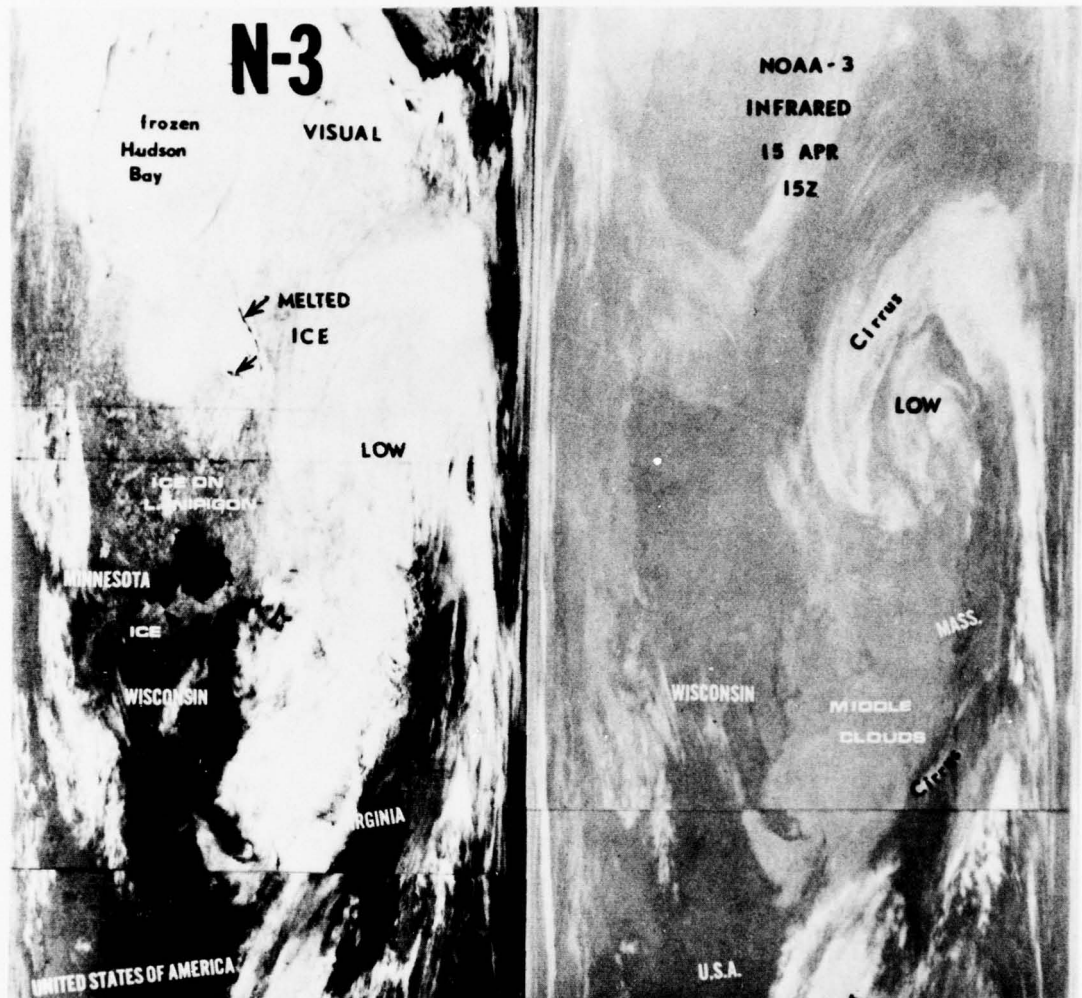


Figure 169. NOAA-3 visual and infrared imagery of ice (15 Apr 75).

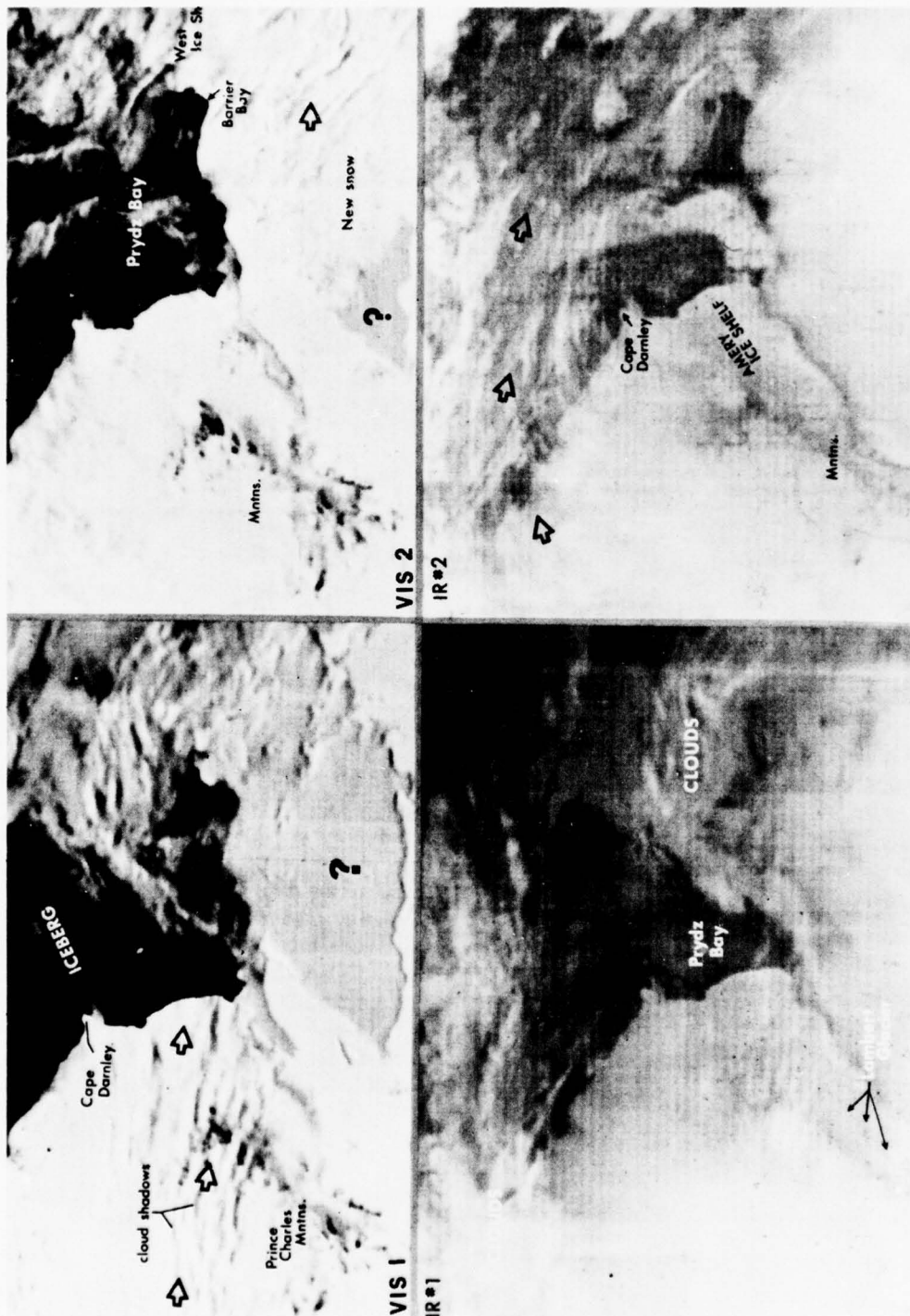


Figure 170. DMSP infrared and visual imagery of ice in Antarctica (date unknown).



Figure 171. DMSP visual image of ice and icebergs in Weddell Sea (24 Jan 74).

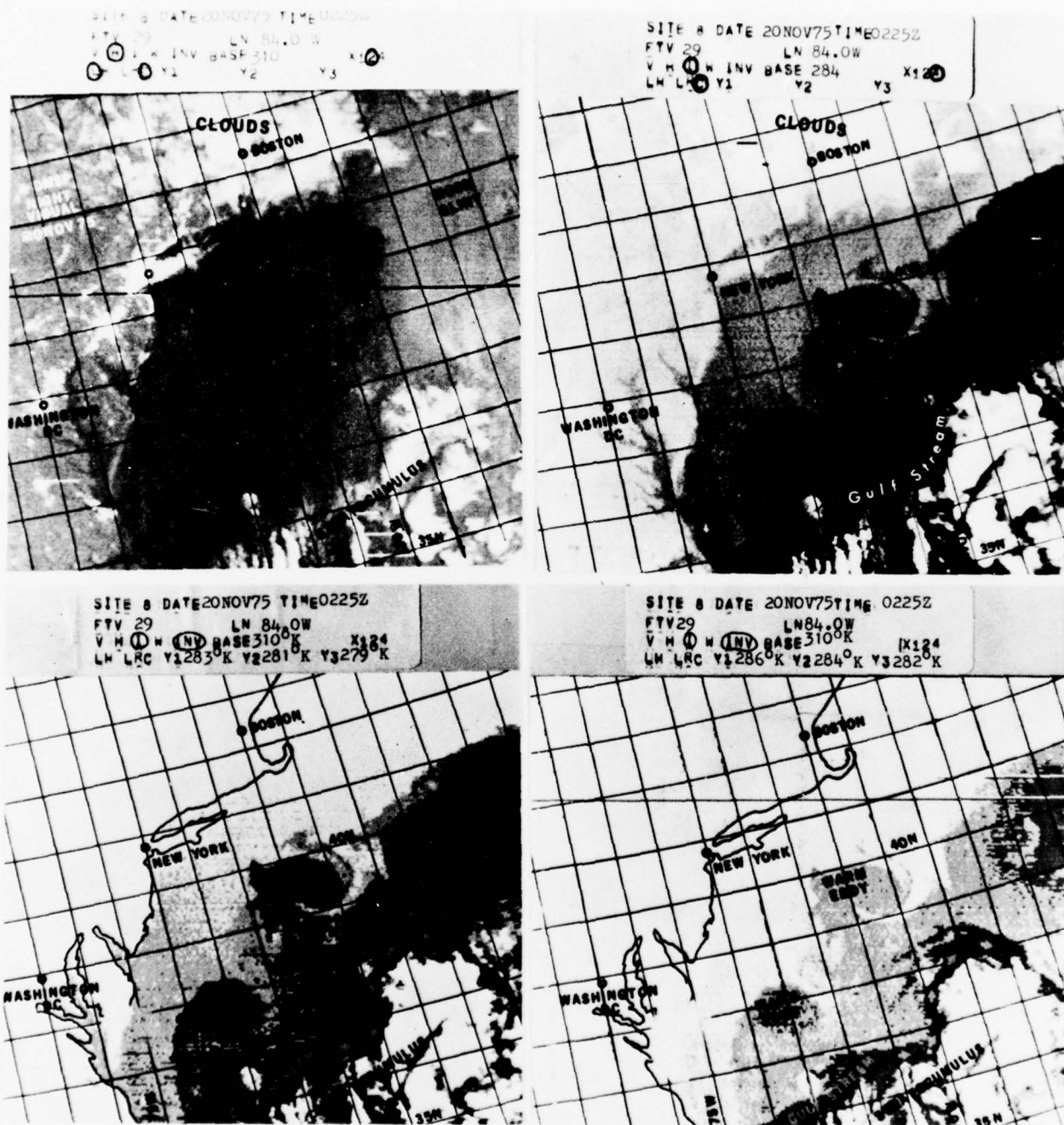


Figure 172. DMSP visual and infrared composite of warm eddies (20 Nov 75).

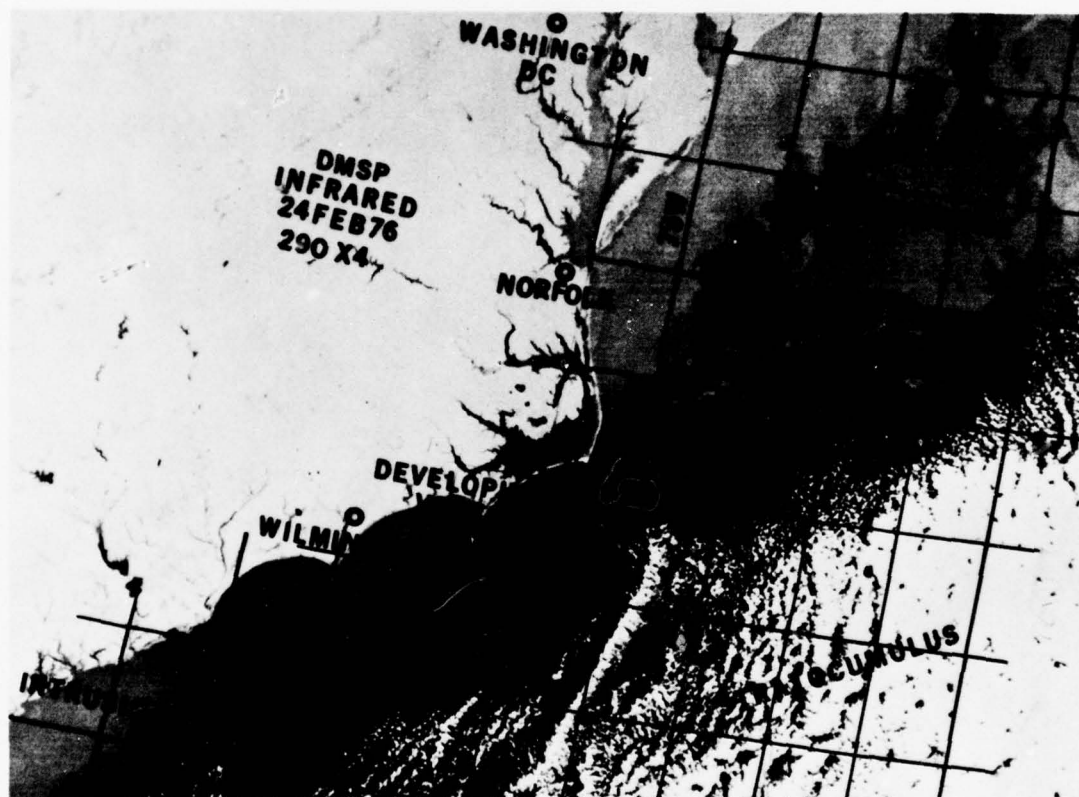


Figure 173. DMSP infrared image of a developing shelf water vortex (24 Feb 76).

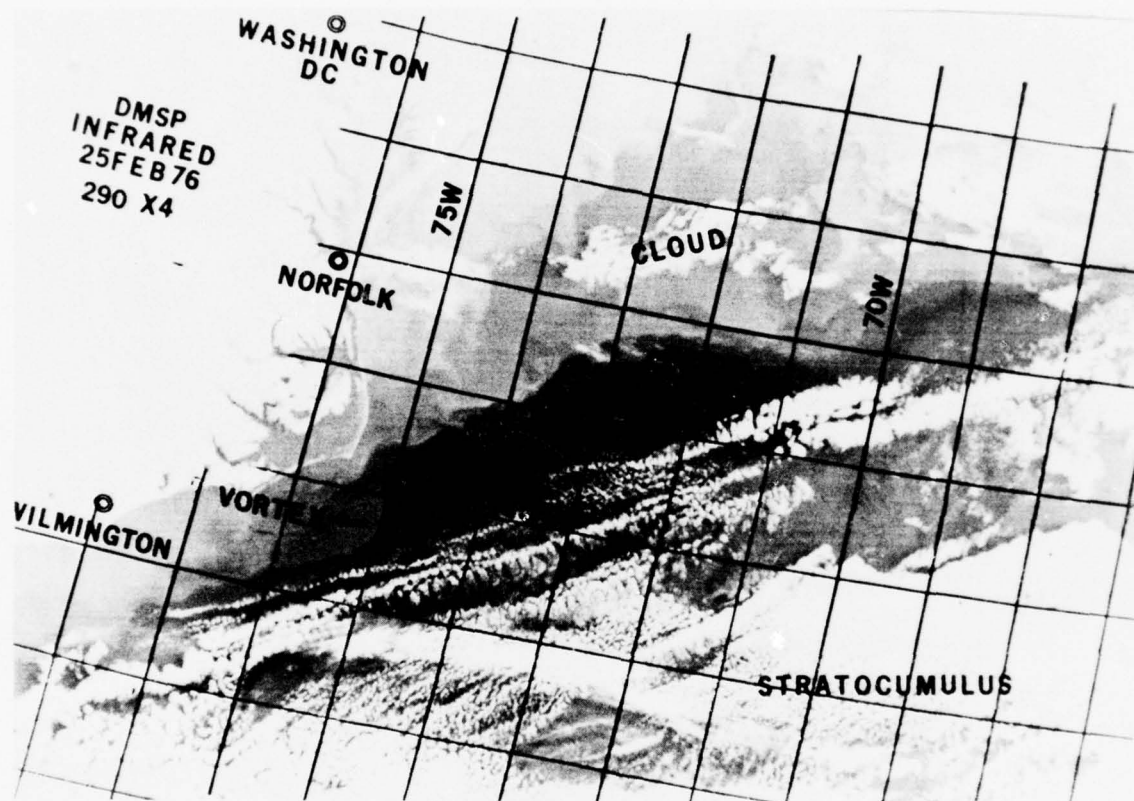


Figure 174. DMSP infrared image of the vortex (25 Feb 76).

infrared image of an eddy off the coast of Florida. This eddy is a warm eddy with an area of shallow cooler water in the center.

A cold eddy is seen in Figure 176. In this photograph the movement of the Labrador current is seen as it winds into the eddy.

The effect of ocean thermal boundaries on the distribution of fish is well-known in the fishing industry. Meteorological satellites can be of great value in assisting the fishing industry by monitoring the location and changes of important oceanic convergence zones throughout the world (Fett, [47]). Figure 177 is a composite chart of the Sea of Japan, and an example of a Japanese fishing vessel. The oceanographic chart shows major oceanic features surrounding Japan and Korea. The notable convergence zone is the zone of mixing between the cold Liman current and the warm Tsushima current in the Sea of Japan. The infrared imagery depicts this zone of mixing where the warm areas (black) progress to cooler areas (lighter shades of gray). Fishing fleets are seen in this same area on the nighttime visual imagery. The unusually strong density of the light from the fishing vessels suggests that the vessels are using exterior lights to lure certain species of fish.

f. Wave Heights. Meteorological satellite data can be useful to oceanographers in the determination of ocean wave heights. Wind direction and speed as well as the fetch (distance over water the wind is blowing) are precursors of certain wave heights.

An example of a classic wave anomaly to hit the Hawaiian Islands is shown in Figure 178. A cold front is seen northwest of the Hawaiian Islands moving southeast. Behind the cold front is an area of cumulus cloud patterns ("open cell") that is indicative of strong surface winds (15 to 20 kt and greater). The length of the fetch and the wind speed are good indicators of wave heights. On 1 December, 50-ft waves were measured on the northern shore of Oahu. Islands such as French Frigate Shoals, northwest of Oahu, were completely under water.

Wave-height determinations can also be made from glints on the ocean surface. When a light source of strong intensity and the meteorological satellite are in the correct geometric relationship, the light will reflect off a smooth surface such as water, snow, ice, or clouds. The glint will appear only on the visual imagery, thus the infrared will confirm the presence or absence of a glint.

Another example of a smooth ocean area where the sun is reflected away from the satellite sensor is in Figure 179. The area off the east coast of the United States shows black areas on the visual that look like suspicious land masses. The simultaneous infrared photograph shows no corresponding phenomena, thus confirming the reflection of calm seas.

Fire Detection

The United States and other countries spend millions of dollars annually for forest-fire detection. The low moonlight DMSP sensor, as well as other sensors of this system, could be of great assistance in locating forest fires. In addition, the extent of the fire and burned area and possible relief by rain can be quickly determined by satellite meteorologists using the visual and infrared imagery. One extremely valuable use would be in sparsely populated regions where a fire could go undetected for several days.

Figure 180 is a DMSP nighttime visual photograph depicting a fire in the Florida Everglades. Figure 181 is a DMSP simultaneous visual and infrared photograph of the same area. The fire, smoke, and a burnt area can be seen on the visual imagery. A hot area on the infrared corresponds to the actual fire and burnt area.

Other Phenomena

City lights and oil and gas field fires can also be identified on DMSP imagery. Figure 182 is a DMSP image of North America. In the examination of this figure, the brightness (i.e., intensity) of illumination from all major and minor cities can be seen. The identification of uncapped oil and gas fields, as well as refineries, are easily observed on the DMSP imagery as shown in Figures 183 through 186. A ringed pattern with a black line emanating from the source characterizes these oil and gas fires (Brandli, [18]).

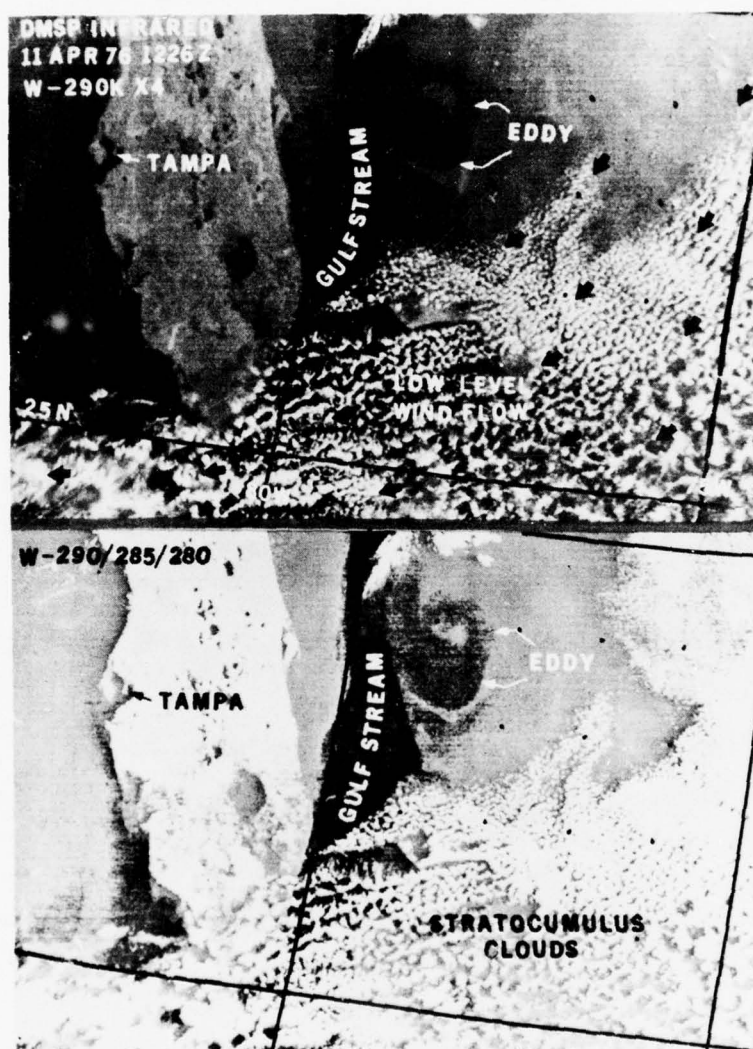


Figure 175. DMSP infrared images of a warm eddy (11 Apr 76).

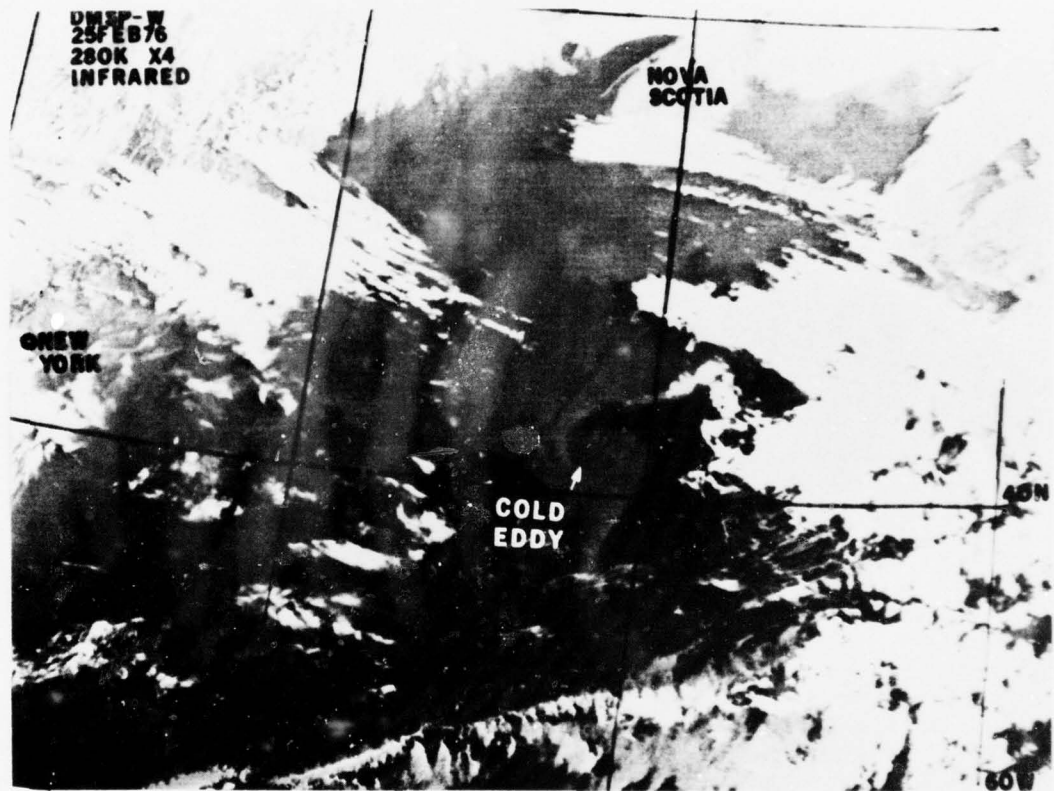


Figure 176. DMSP infrared image of a cold eddy (25 Feb 76).

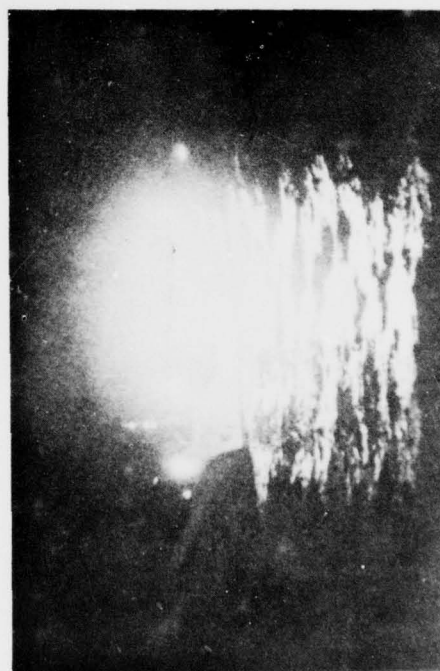
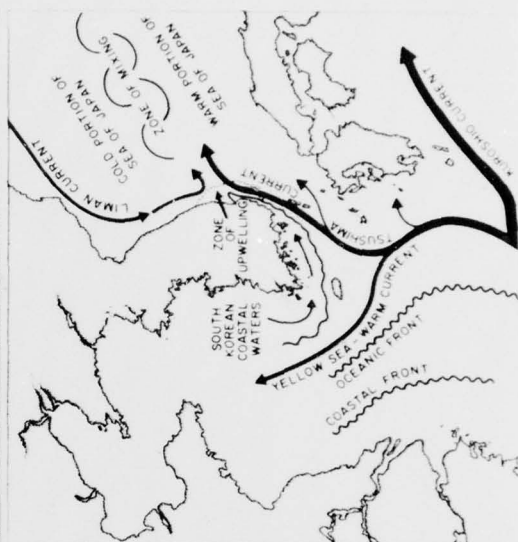


Figure 177. Composite photograph of Japan and fishing fleet (Fett, [45]).

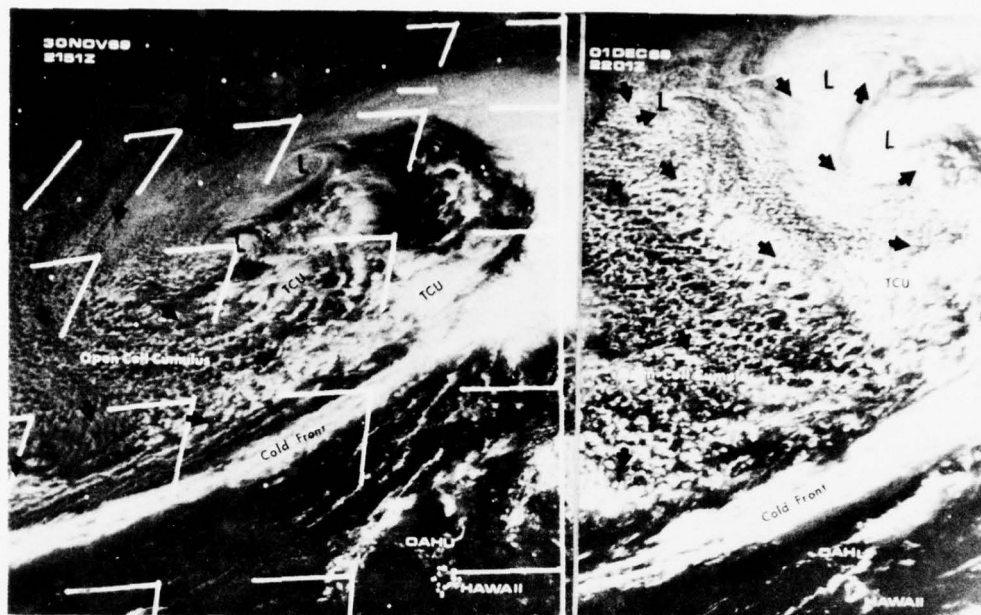


Figure 178. ATS view of record wave heights in Hawaii (30 Nov-1 Dec 69).

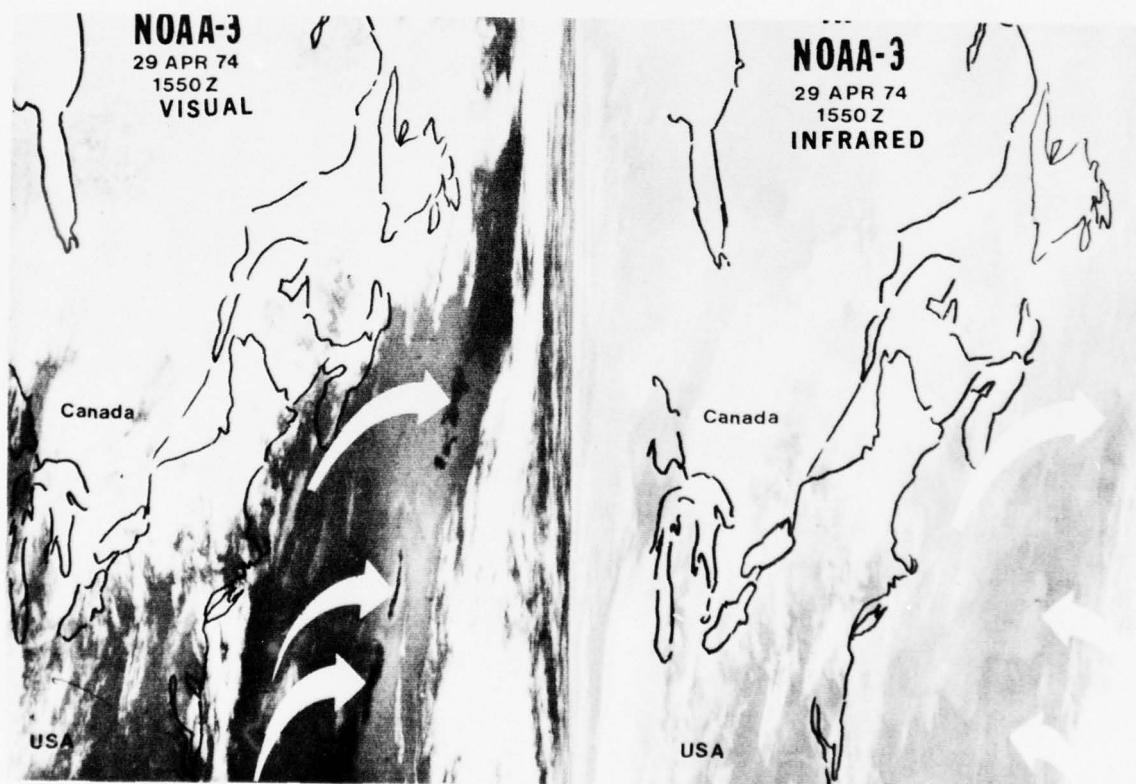


Figure 179. Sun glint off the coast of New England (29 Apr 74).



Figure 180. DMSP nighttime visual photograph of forest fire (30 Apr 74).



Figure 181. Simultaneous visual and infrared photograph of fire (30 Apr 74).

The occurrence of a solar eclipse on the earth is a rare event. The DMSP was able to capture a picture of how the shadow of a total eclipse on the earth appeared from 800 km in space. Figure 187 is a DMSP visual image over Africa as the moon passed in front of the sun. The simultaneous infrared data (not shown) recorded no thermal ground changes.

On 3 February 1976 a devastating tremor hit the country of Guatamala near the east central border. Since DMSP imagery was available over the area, several transparencies were processed before and after the earthquake (Figures 188 and 189). Several interesting features were noted in the water temperatures south of Guatamala; in particular, notice the area of warm water which may be associated with an underwater fissure (this area is in a cool current region). Further investigation of these data and other earthquakes may show a significant correlation between the water temperatures and tremors.



Figure 182. DMSP nighttime visual photograph of North American lights (date unknown).

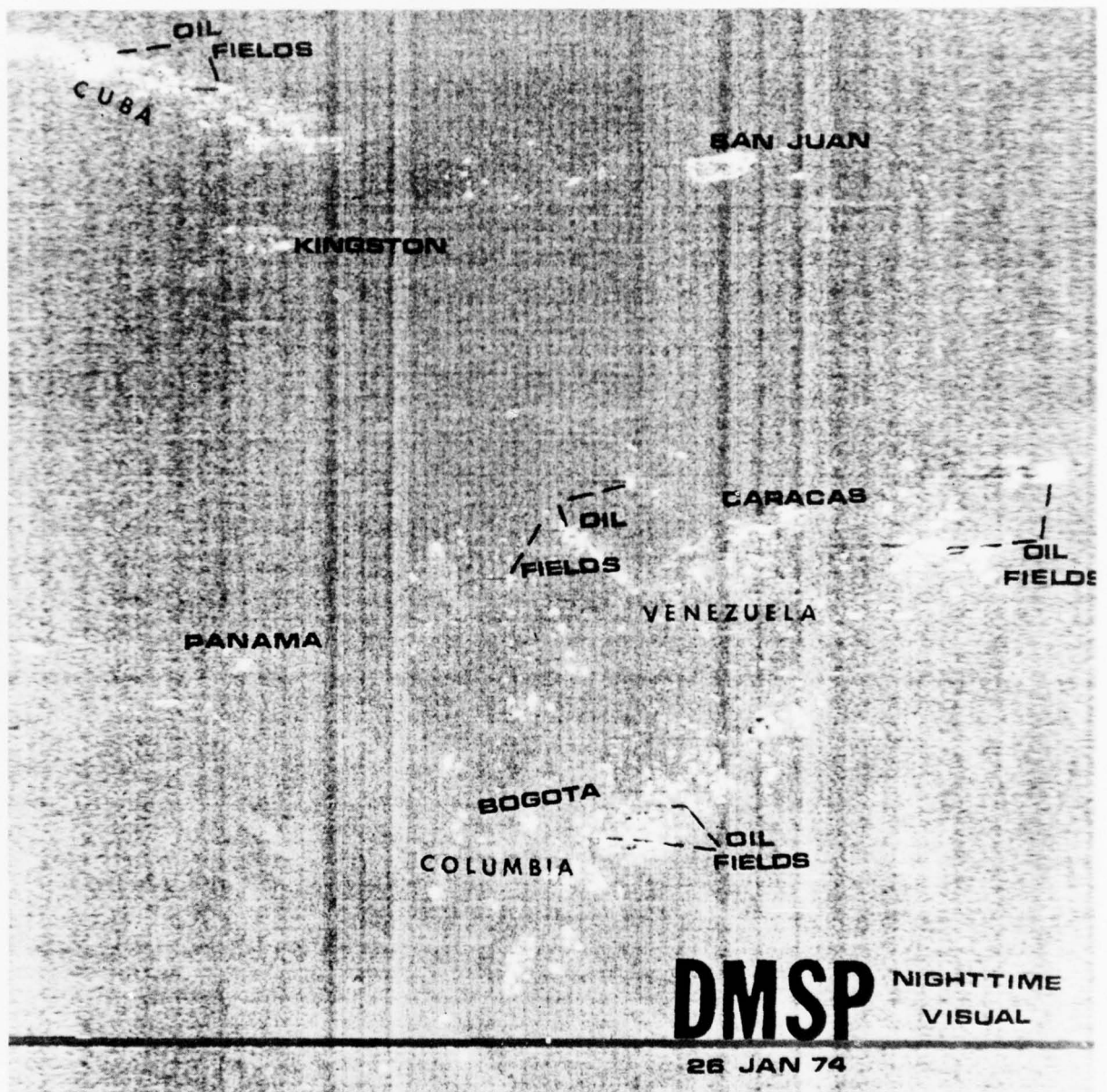


Figure 183. Oil fields of South America (26 Jan 74).

August 1976

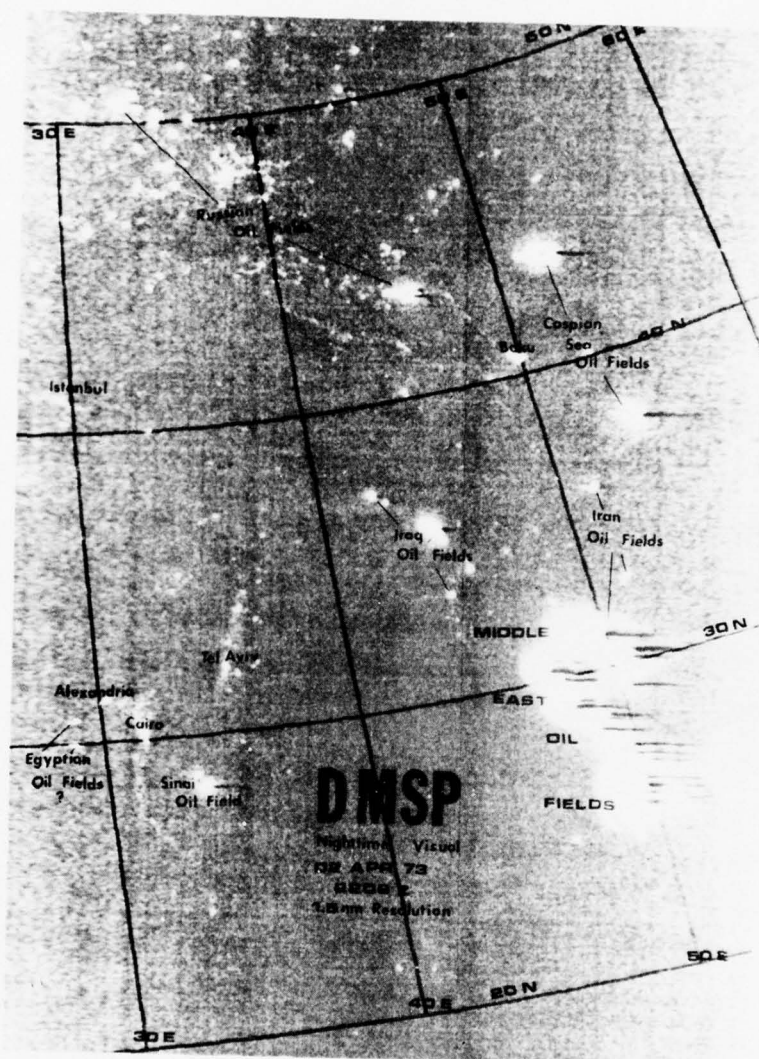


Figure 184. Oil fields of the Middle East (2 Apr 73).

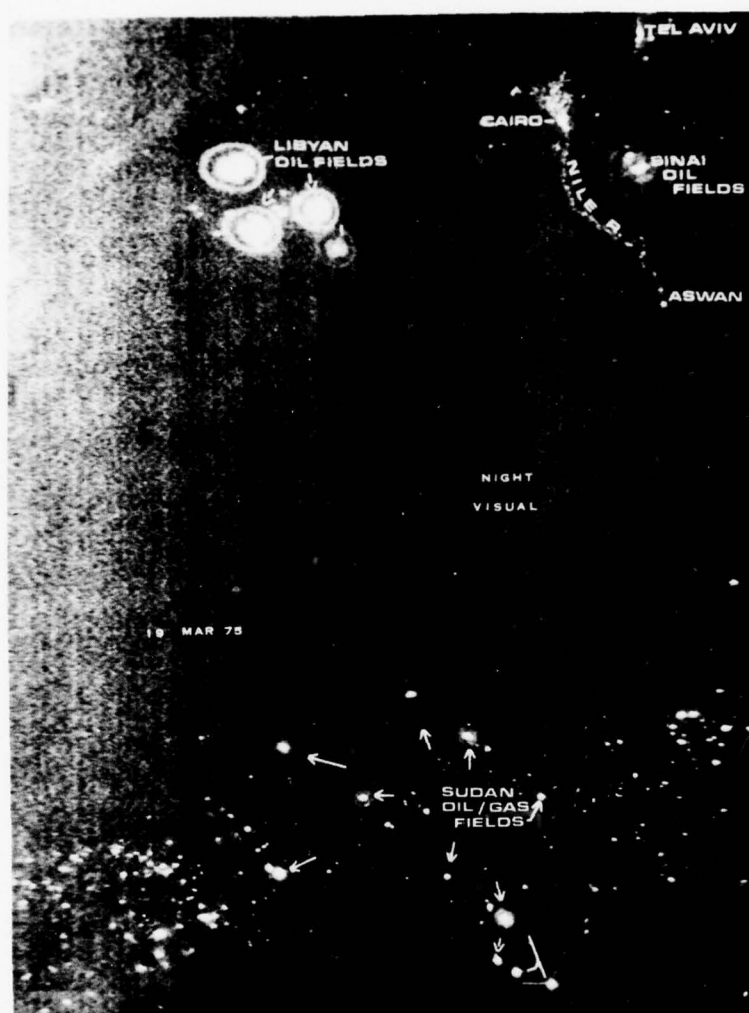


Figure 185. Oil fields of Africa (19 Mar 75).

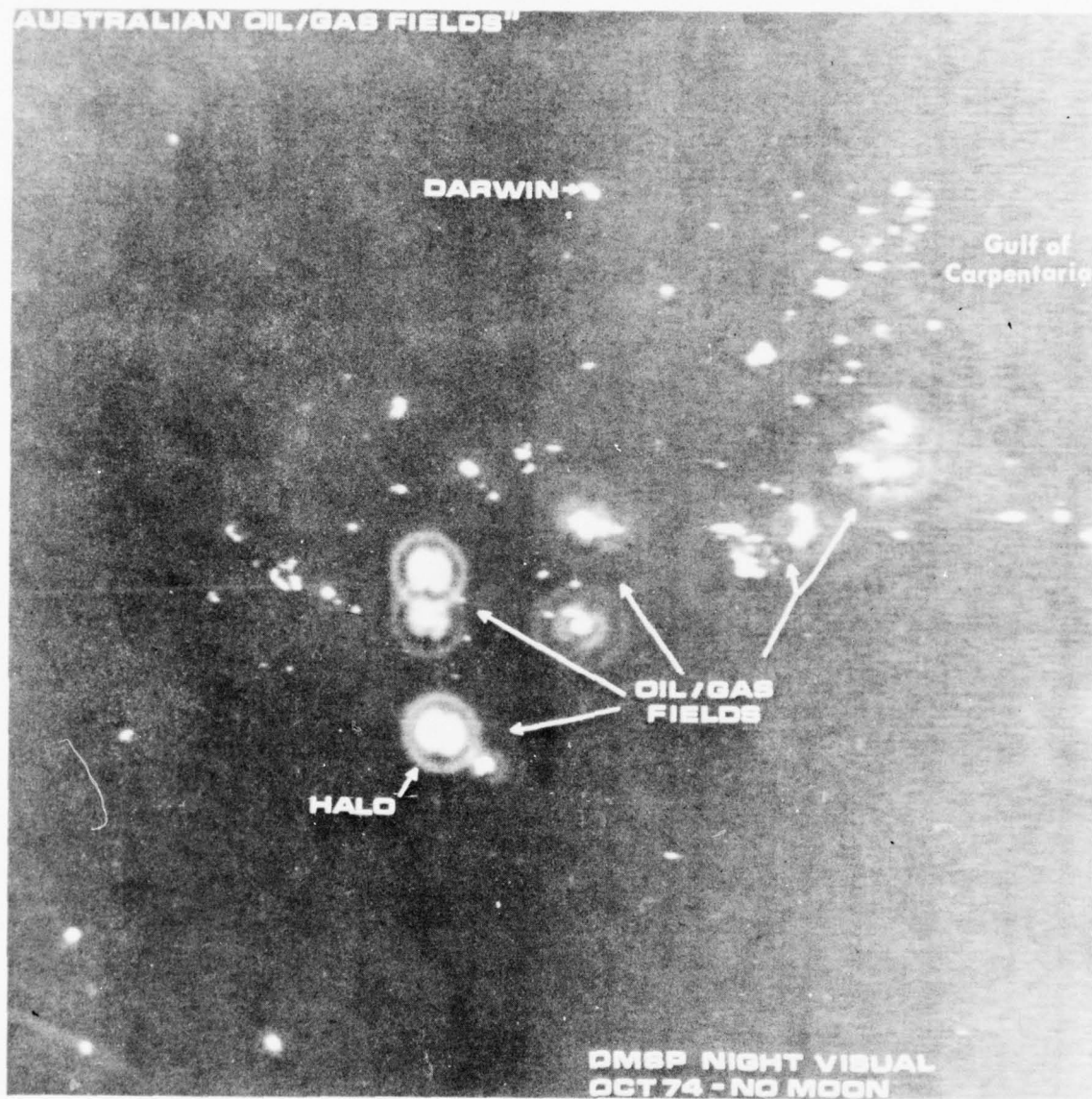


Figure 186. Oil fields of Australia (Oct 74).

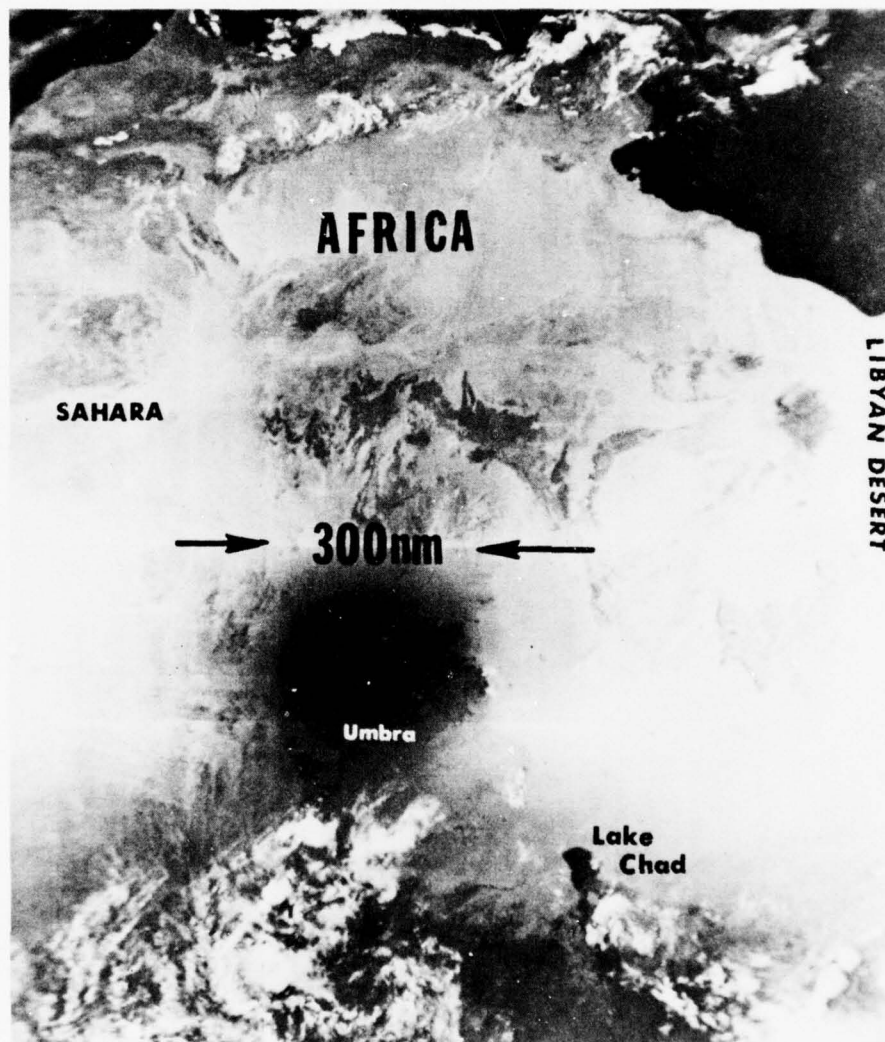


Figure 187. DMSP view of the eclipse of the sun (30 Jun 73).

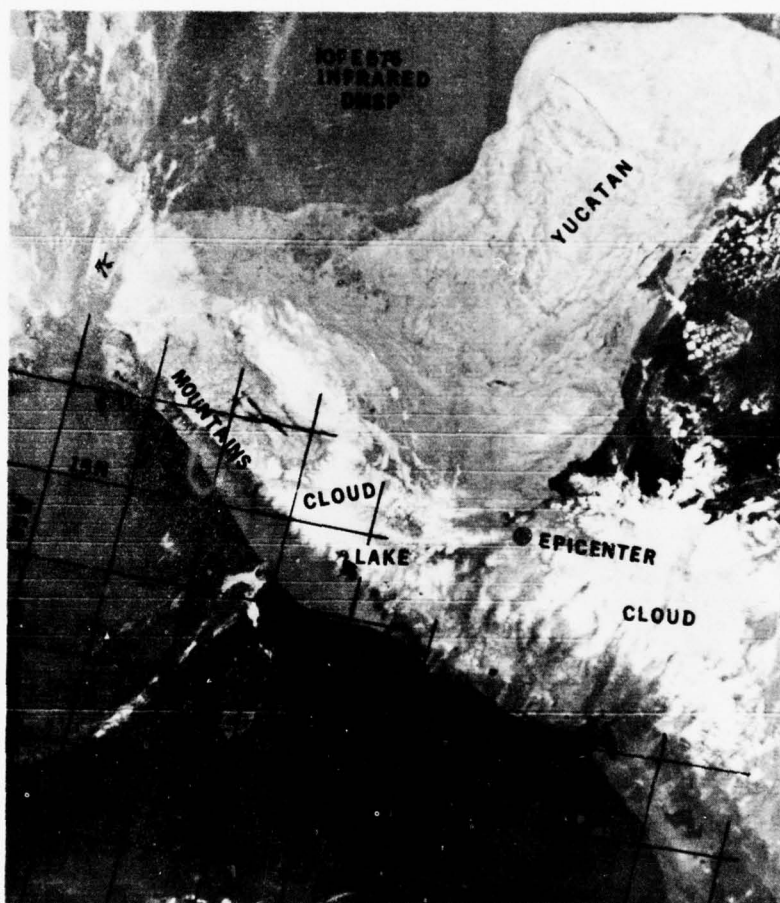


Figure 188. DMSP infrared before earthquake (23 Jan 76).

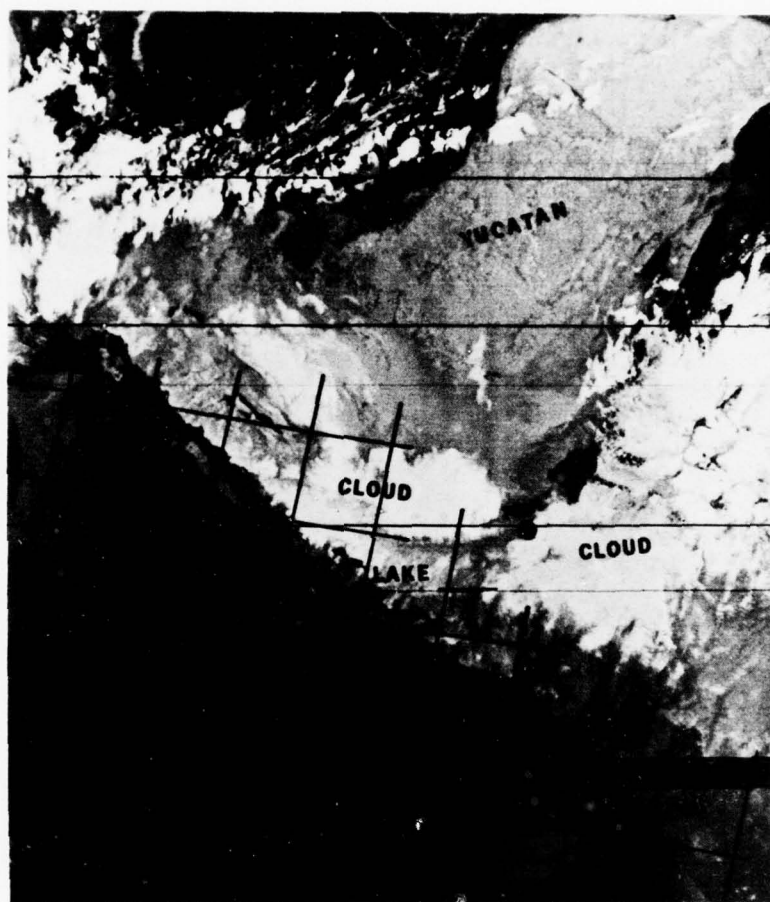


Figure 189. DMSP infrared after earthquake (10 Feb 76).

Chapter 7

DATA PREPARATION AND PRESENTATION

Preparation

Before a satellite picture is received, at least a half-hour should be spent on the various facets of acquiring the imagery. The preparation for receiving satellite data involves the following recommended steps.

a. Mission and Data Type. The satellite meteorologist should become totally familiar with the optimum mission requirements. All important geographical points in the area of interest should be known. What type of weather patterns are the mission planners concerned with? Where are the alternate areas? When will these data be needed and will there be a continued need? After these questions have been answered, the next step is to determine what type of imagery is going to be received and which best satisfies mission requirements.

Satellite imagery is available in a near real-time mode or in delayed-transmission products such as facsimile maps, coded products, taped data, and televised products. Usually, real time satellite acquisition is the best kind. At least one tape recorder should be used to tape the transmission. These tapes can then be played back later for extra copies of the data.

b. Ephemeris. Another facet in the preparation phase is the satellite ephemeris and continuity. The ephemeris is the satellite position at given times (Figure 190). The satellite meteorologist should check the ephemeris every morning. In fact, for an important mission, the ephemeris should be converted to ground tracks (Figure 190, bottom) and plotted on geographical maps. These maps can show orbit numbers, dates, and vehicle numbers. By converting the ephemeris to ground tracks, weak points in the area of interest will be identified. If there is going to be poor satellite coverage, contingency plans can then be made, such as receiving delayed or facsimile satellite imagery. An example of poor satellite coverage is what is called split satellite paths where the important area to be viewed occurs between two successive satellite revolutions. It is at this point (edge of the imagery) where the poorest resolution and viewing is realized. In this case, it might be better to use poorer resolution data that passed over the area of interest in place of the better satellite imagery that viewed the key location on the edge of the photograph.

c. Synoptic Situation. Another part of the preparation is the complete understanding of the synoptic situation. This synoptic situation should be checked every 6, 12, 24, and 48 hours into the past, using conventional weather charts and satellite imagery. The last satellite photograph available should always be checked by the satellite meteorologist. It is important to emphasize the synoptic pattern on satellite imagery with regard to key geographic locations, such as major bases, land masses, oceans, or rivers. The geography that will affect the mission plan should be delineated on the imagery and referenced in the synoptic discussion.

d. Contingency. Suppose the equipment breaks down, the antenna does not function properly, or the ephemeris is wrong. These problems will have to be dealt with at one time or another. Because of the time taken to study the synoptic situation, the satellite meteorologist will know what should have been on the imagery. By taking the latest piece of satellite imagery and adding cloud movement and known synoptic changes, the old imagery can be reconstructed to nearly fit the present weather situation.

e. Gridding Devices. Depending on the mission and time of receipt of the satellite data, all gridding devices should be on hand. Using the ephemeris, the satellite meteorologist will know, geographically,

August 1976

THIS PAGE IS BEST QUALITY PRACTICABLE
FROM COPY FURNISHED TO DDC

AWS-TR-76-264

APT LOOK ANGLES
NOAA 3 137.50 MHZ

MERRITT ISLAND, FLORIDA

18 DEC 1974

ORBIT LONGITUDE TIME (Z)
NRH DEGREES HRS MIN SEC

TIME (Z) HRS MIN SEC	ELEVATION DEGREES	AZIMUTH DEGREES	ALTITUDE KILOMETERS	LATITUDE DEGREES	LONGITUDE DEGREES
14 23 29	2.78	20.64	1510	59.90N	64.16W
14 24 29	6.35	19.21	1510	57.10N	67.08W
14 25 29	10.35	17.19	1510	54.30N	70.02W
14 26 29	14.79	16.35	1510	51.35N	71.92W
14 27 29	19.41	15.07	1510	48.40N	73.82W
14 28 29	25.81	14.00	1510	45.45N	75.37W
14 29 29	32.90	12.28	1510	42.50N	76.92W
14 30 29	41.00	10.23	1510	39.50N	78.27W
14 31 29	52.20	6.29	1510	36.50N	79.62W
14 32 29	64.20	359.02	1505	33.50N	80.77W
14 33 29	78.14	331.81	1500	30.50N	81.92W
14 34 29	78.11	244.95	1500	27.50N	83.02W
14 35 29	64.5	217.48	1500	24.50N	84.12W
14 36 29	52.4	209.29	1500	21.45N	85.12W
14 37 29	41.33	206.41	1500	18.40N	86.12W
14 38 29	32.04	204.35	1500	15.35N	87.07W
14 39 29	25.50	203.08	1500	12.30N	88.02W
14 40 29	15.58	202.11	1500	9.25N	88.92W
14 41 29	14.51	201.42	1500	6.20N	89.82W
14 42 29	10.10	200.30	1500	3.15N	90.72W
14 43 29	6.17	200.41	1500	.10N	91.62W
14 44 29	2.67	200.22	1500	2.90S	92.52W

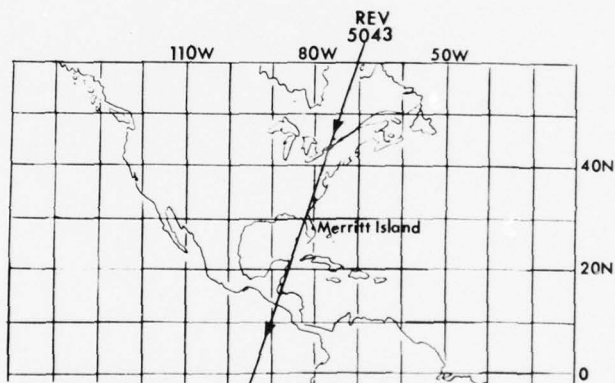


Figure 190. NOAA-3 ephemeris and plotted satellite ground track.

where the satellite pass is going to be. With this information, the correct grids can be set up, ready for tracing. Known landmarks should be chosen with regard to latitude and longitude. There should be no need to thumb through atlases looking for these points after data has been received. Figure 191 shows recommended gridding tools.

Gridding

Gridding (placing latitude and longitude lines correctly on the photo) is, by far, the most important step in displaying satellite imagery. The most accurate method of gridding satellite images is done by hand using a flexible curve. Point-to-point transfer or tracing from a grid master are suggested ways of gridding. While gridding the imagery, the satellite meteorologist can recognize any satellite attitude problem and correct it immediately. More importantly, he can be interpreting the photograph as he is gridding. Figure 192 is an accurately gridded DMSP visual photograph illustrating daily operational use of satellite imagery.

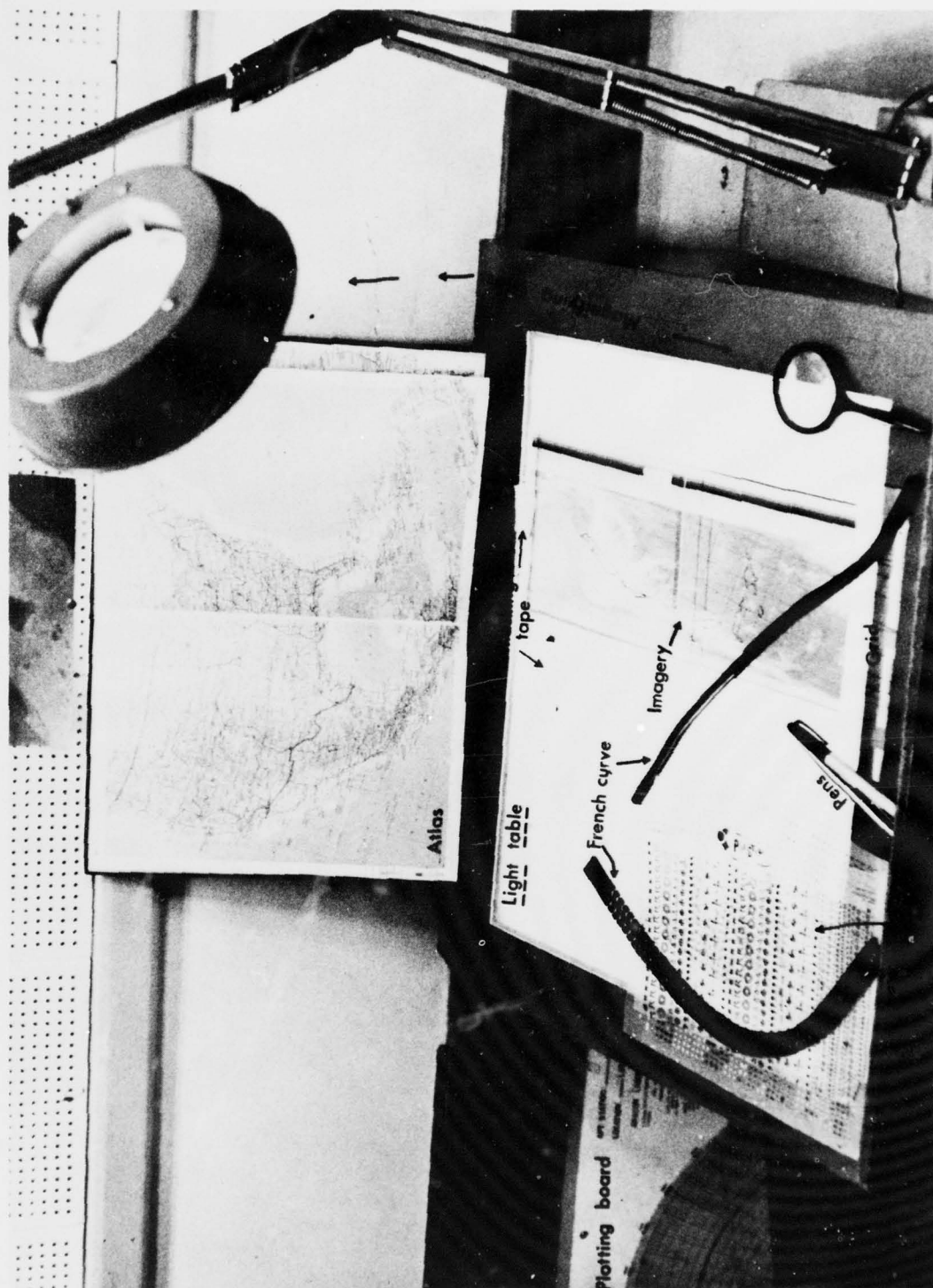


Figure 191. Recommended gridding tools.

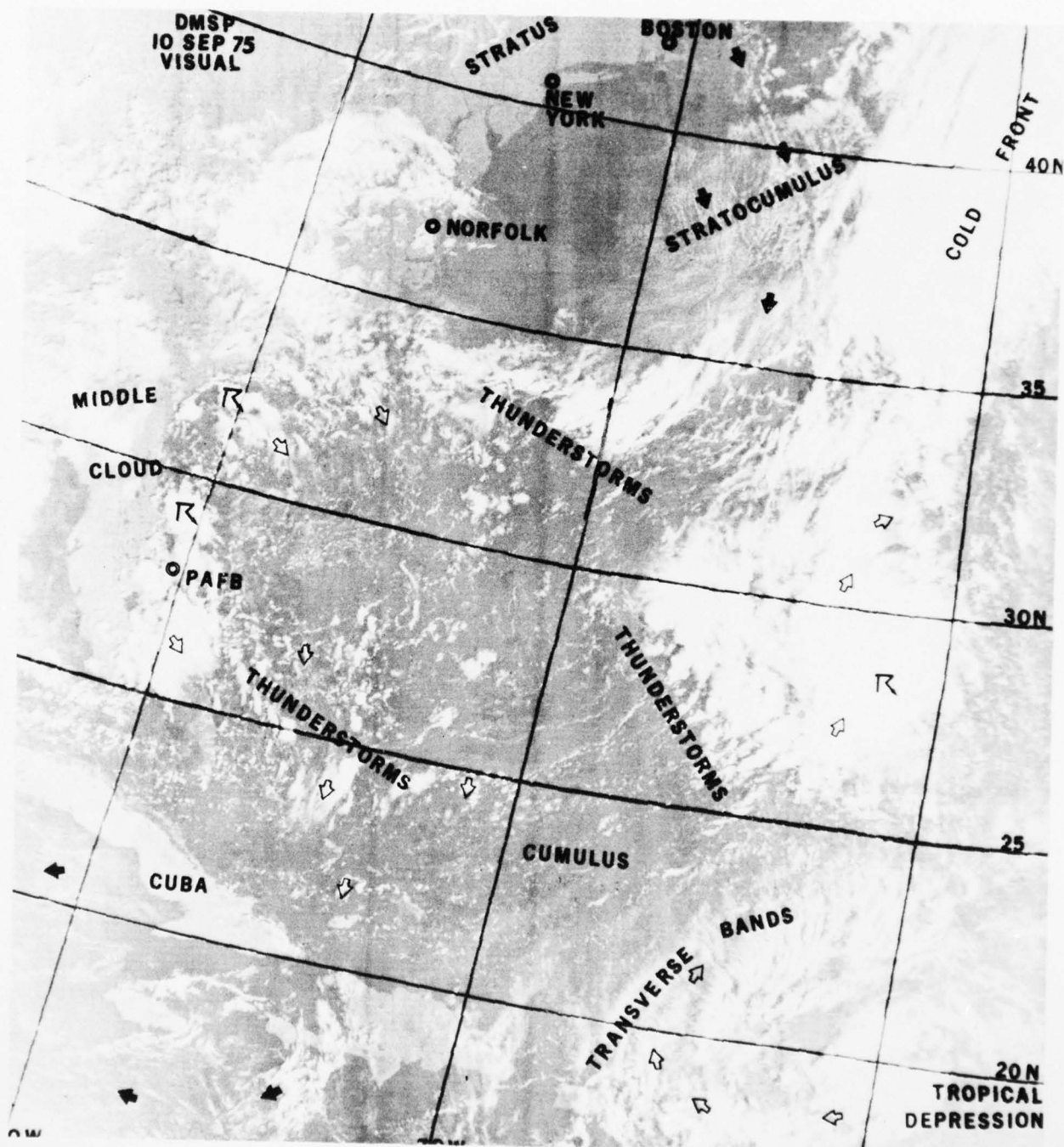


Figure 192. DMSP visual illustrating daily operational use of satellite imagery (10 Sep 75).

Nighttime infrared imagery can be extremely difficult to grid. Geographical features may be hard to pinpoint because of similar land and water temperatures. Figure 193 is a nighttime infrared photograph showing the similarities of land and water temperatures. With DMSP data, night visual imagery depicting city lights can be used in conjunction with the simultaneous infrared products for accurate gridding.

Grids for every satellite are available or can be constructed from the data. Most civilian and/or military agencies have slides or actual overlays/underlays for use on the various satellite imagery. Every 5 or 10 degrees should be placed on the imagery, depending on the mission. In some cases, every degree might need to be drawn. In the next figure (Figure 194), five ESSA-8 photographs were geographically gridded placing every degree of latitude and longitude. These photographs were used to accurately position Hurricane Ginger in its track (path) toward the Carolina coast.

Most of the latest satellite data is computer gridded. Careful geographical checks should be made to insure that the latitude/longitude lines are correct. Figures 195 and 196 show computer gridded satellite imagery. Figure 197 is an ESSA-8 image showing an error of 600 nautical miles (NM).

For some polar-orbiting vehicles, geographic overlays have been constructed, although some users of these data prefer seeing geographical outlines. The overlays do not always line up correctly. The next figure (Figure 198) shows an overlay error along the Gulf of Siam coast. Gridding photographs in Southeast Asia had many advantages. The coast line along North and South Vietnam had check points at almost every degree of latitude and numerous distinctive geographical features (Figure 199). This convenience in nature made easier memorization of known latitude/longitude intersections for quick gridding of the imagery.

Presentation

All satellite imagery should be gridded correctly and lettered commensurate with the quality of the received photographs. A plain satellite picture can sometimes be more impressive than a poorly marked one. Enhancement of the imagery by use of a few techniques discussed in this chapter can add to any presentation and/or briefing. After operational use, the imagery can then be used for technical papers, seminars, or post-analysis discussions.

a. **Press-type.** Professional lettering is important in presenting data. In addition to meteorological symbols that can be pressed on the pictures, Detachment 11, 2d Weather Squadron, has designed its own letter sheet with common meteorological geographic and mission words that are frequently used at the Air Force Eastern Test Range (AFETR) (Figure 200).

b. **Data Display.** Depending on the mission, there are several methods available to display satellite imagery. For transparent data, a vertical light table is recommended for briefings given in person or via a television system. Figure 201 displays DMSP visual imagery on a light table.

Mounting satellite imagery on poster board is another way to display data. Figures 202 and 203 are examples of satellite imagery used at the AFETR for the SKYLAB and Apollo-Soyuz missions.

Figure 204 is a DMSP nighttime visual photograph, with moonlight, before lettering was accomplished. In this phase, the photograph means nothing to a viewer. After lettering (Figure 205), one viewing the picture can understand the synoptic situation, location, and type of imagery.

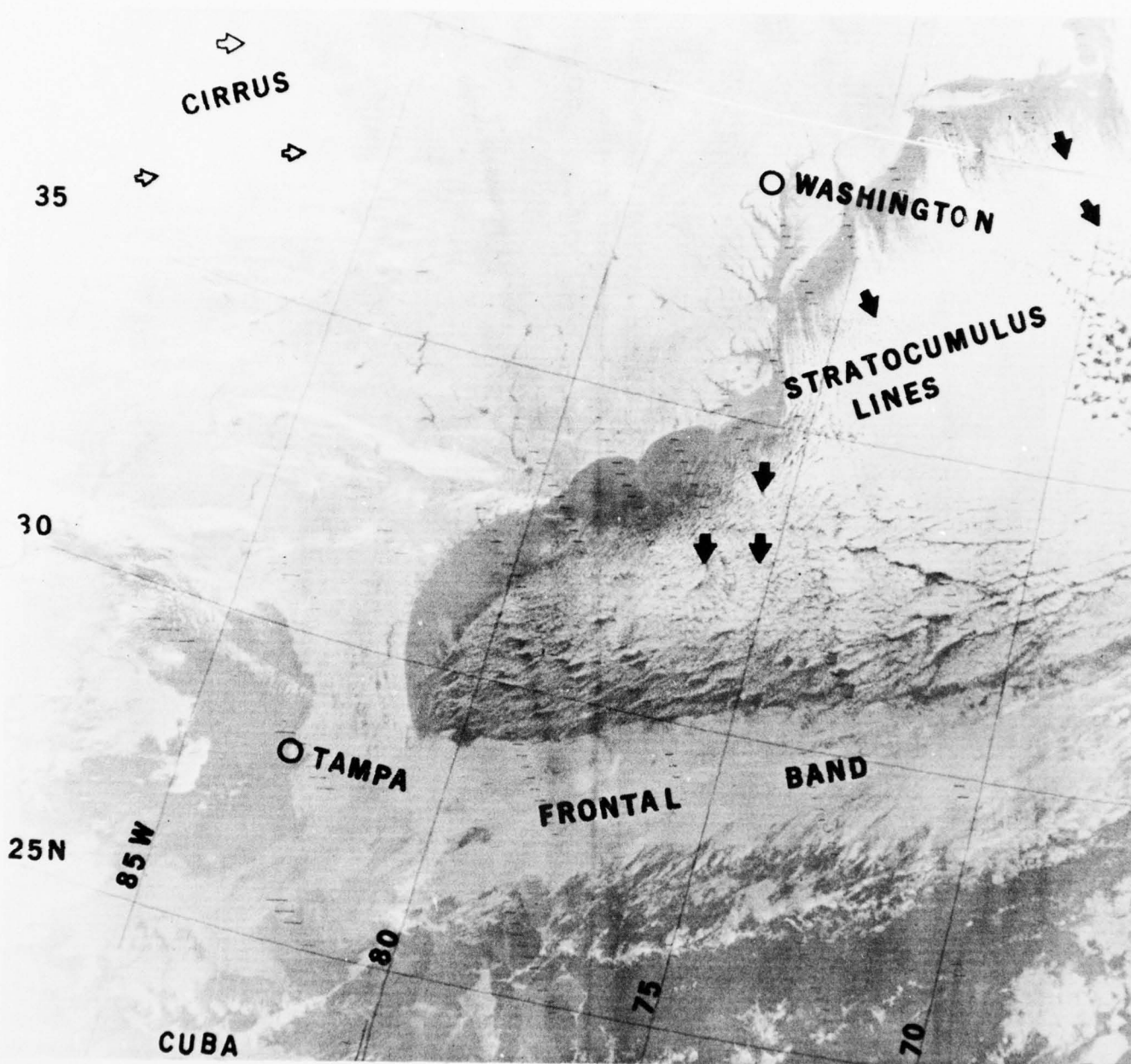


Figure 193. DMSP nighttime infrared photograph showing similar land and water temperatures (5 Jan 76).

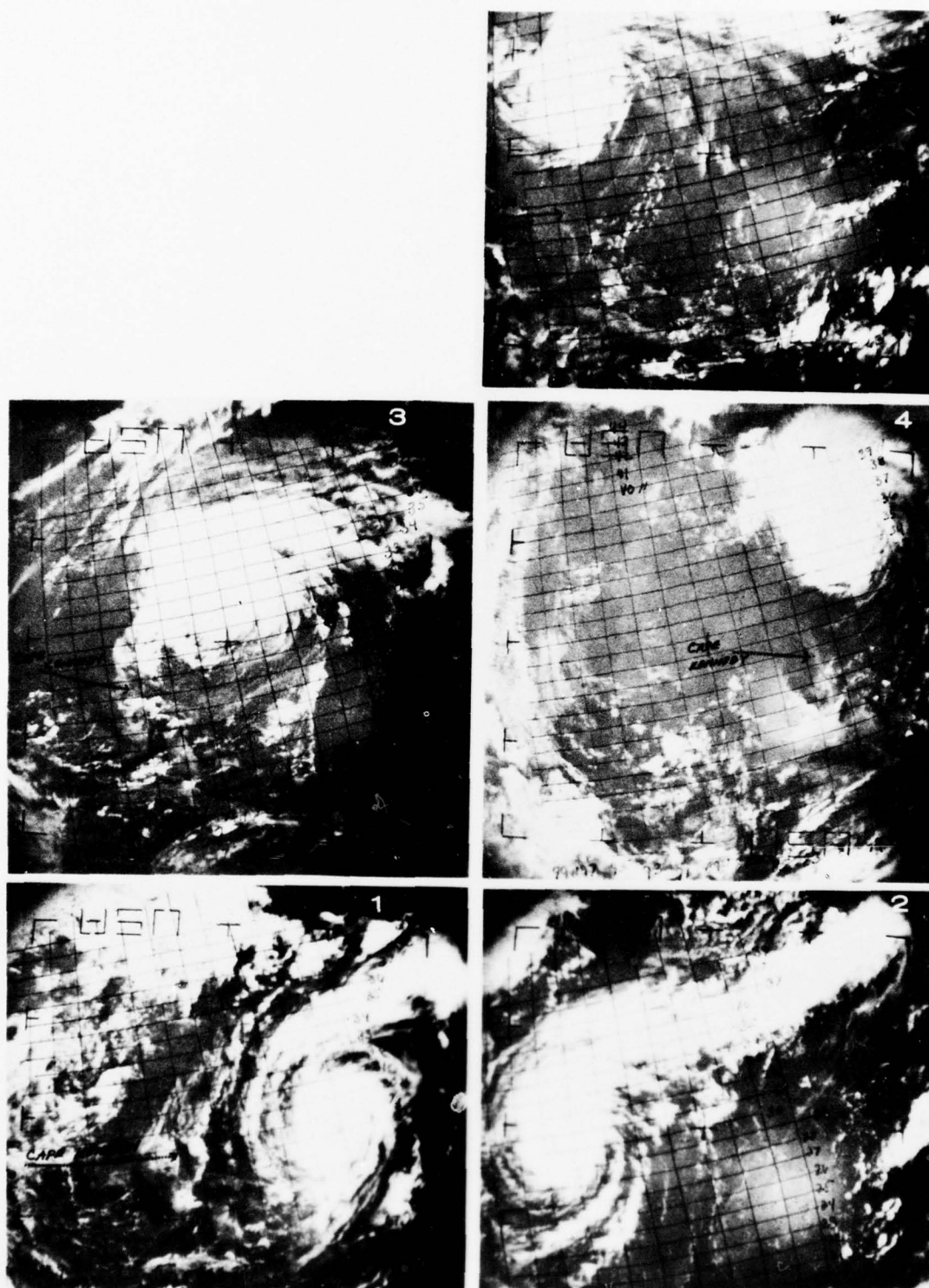


Figure 194. ESSA-8 photographs illustrating every degree of gridding (27 Sep - 1 Oct 71).

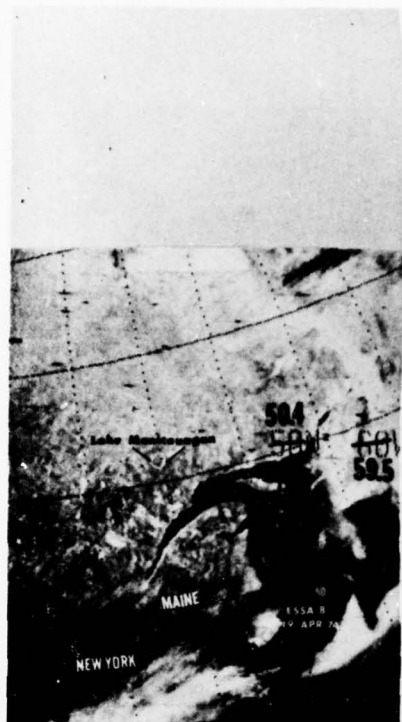


Figure 195. ESSA-8 computer gridding error (9 Apr 74).

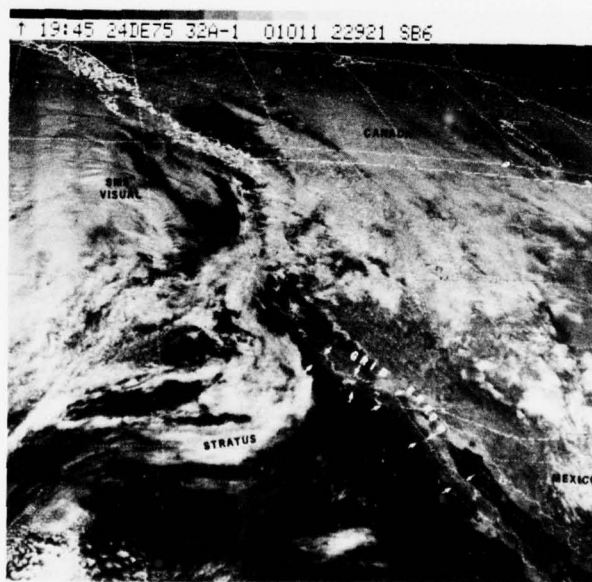


Figure 196. SMS computer gridding error (24 Dec 75).



Figure 197. Gridding error of 600 NM (date unknown).

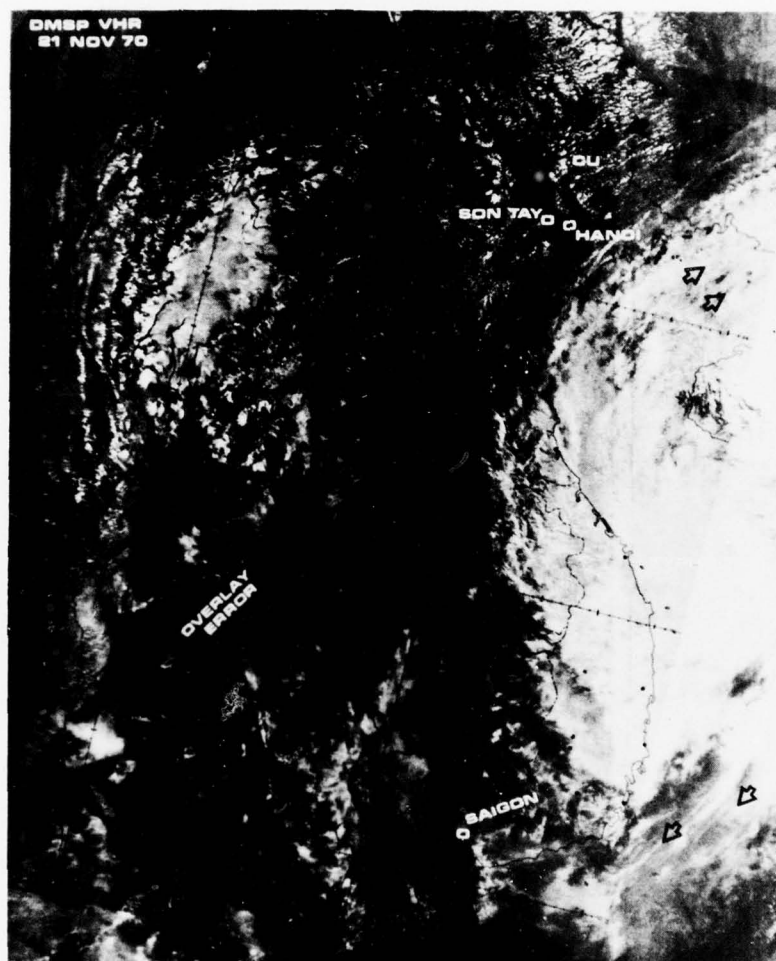


Figure 198. Overlay error of Southeast Asia visual imagery (21 Nov 70).

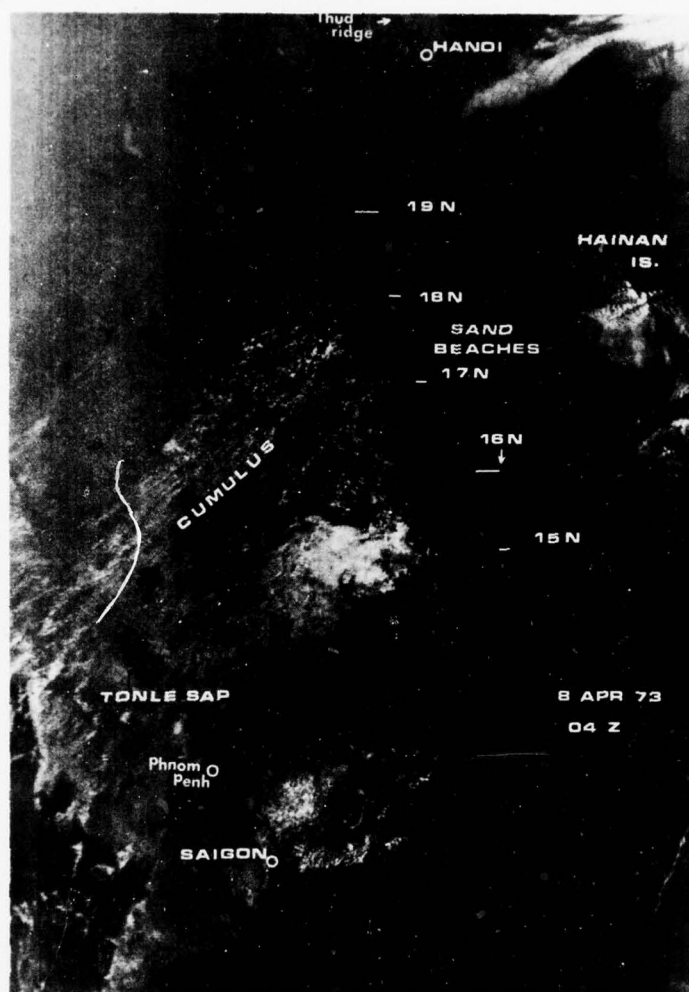


Figure 199. Gridding check points along Vietnam coast (8 Apr 73).

P4625

[illegible]

The image displays a series of 15 rows of geometric patterns, arranged in a grid-like structure. The patterns are as follows:

- Row 1: A horizontal row of 15 five-pointed stars.
- Row 2: A horizontal row of 15 capital letters 'R'.
- Row 3: A horizontal row of 15 concentric circles.
- Row 4: A horizontal row of 15 triangles.
- Row 5: A horizontal row of 15 squares.
- Row 6: A horizontal row of 15 squares.
- Row 7: A horizontal row of 15 squares.
- Row 8: A horizontal row of 15 squares.
- Row 9: A horizontal row of 15 squares.
- Row 10: A horizontal row of 15 squares.
- Row 11: A horizontal row of 15 squares.
- Row 12: A horizontal row of 15 squares.
- Row 13: A horizontal row of 15 squares.
- Row 14: A horizontal row of 15 squares.
- Row 15: A horizontal row of 15 squares.

Figure 200. Example of customized lettersheet.

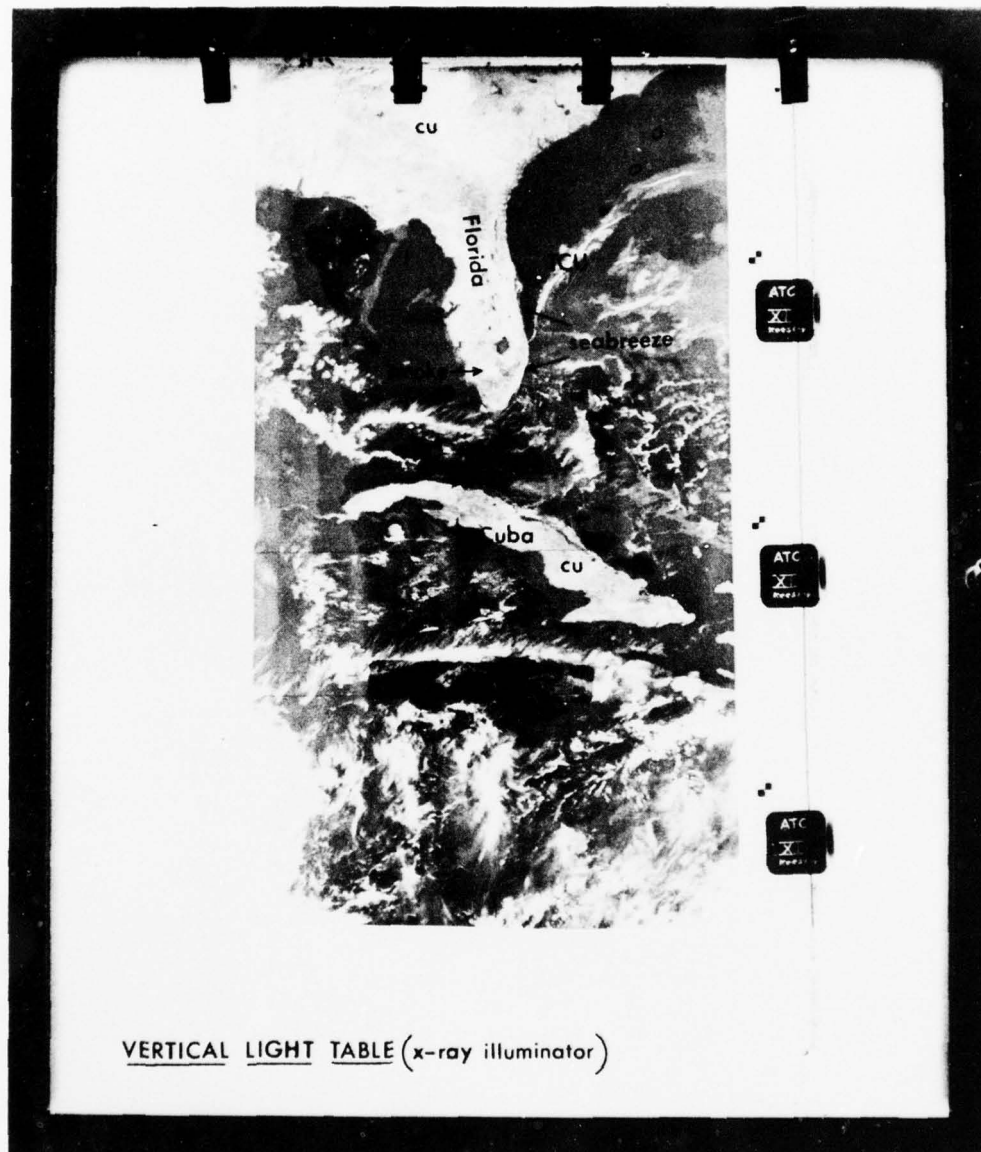


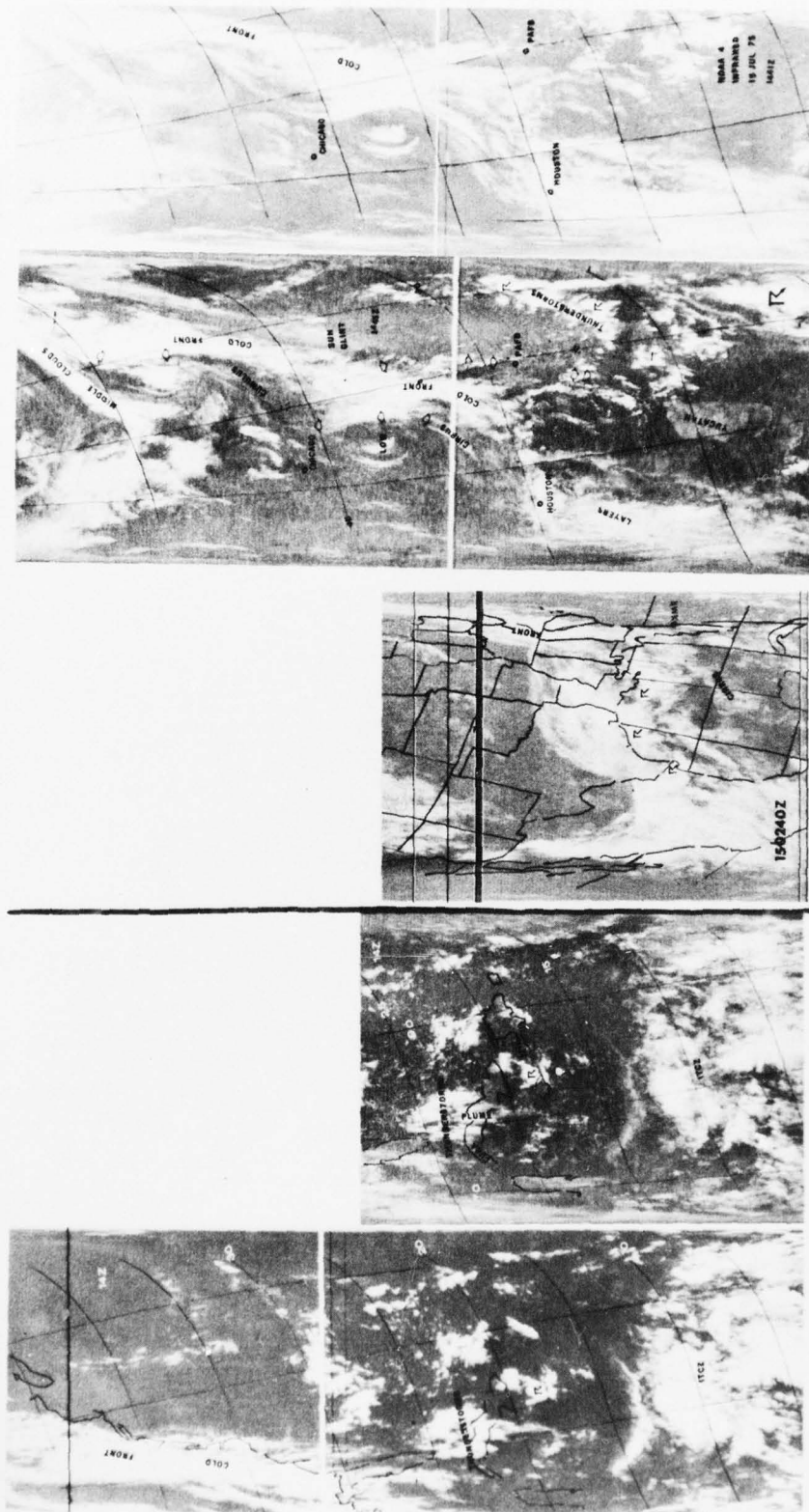
Figure 201. Transparent data display using a vertical light table.



Figure 202. ESSA-8 imagery display for a SKYLAB mission

CAPE CANAVERAL FLA

APOLLO SOYUZ



INFRARED

VISUAL

INFRARED

INFRARED

15 JULY 75

14 JULY 75

DET 11 6TH WEATHER WING

Figure 203. Data display for the Apollo-Soyuz Test Project (14-15 Jul 75).

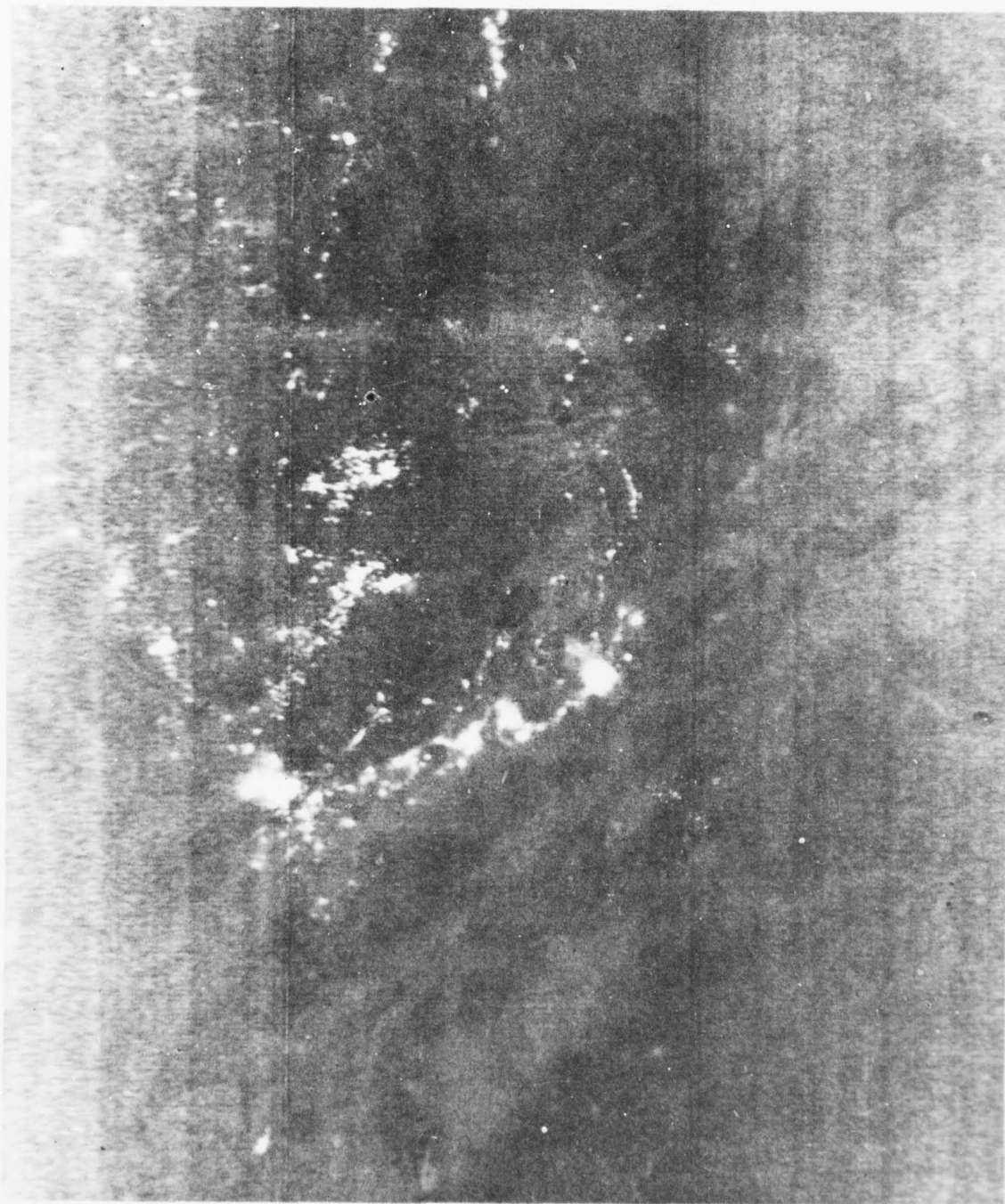


Figure 204. Unlettered DMSP image (Nov 73).

AD-A067 090

AIR WEATHER SERVICE SCOTT AFB ILL
SATELLITE METEOROLOGY.(U)
AUG 76 H W BRANDLI
AWS-TR-76-264

F/G 4/2

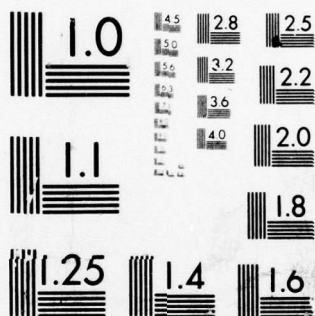
UNCLASSIFIED

3 of 3
AD
A067090



NL

END
DATE
FILMED
6--79
DDC



MICROCOPY RESOLUTION TEST CHART
NATIONAL BUREAU OF STANDARDS-1963-A

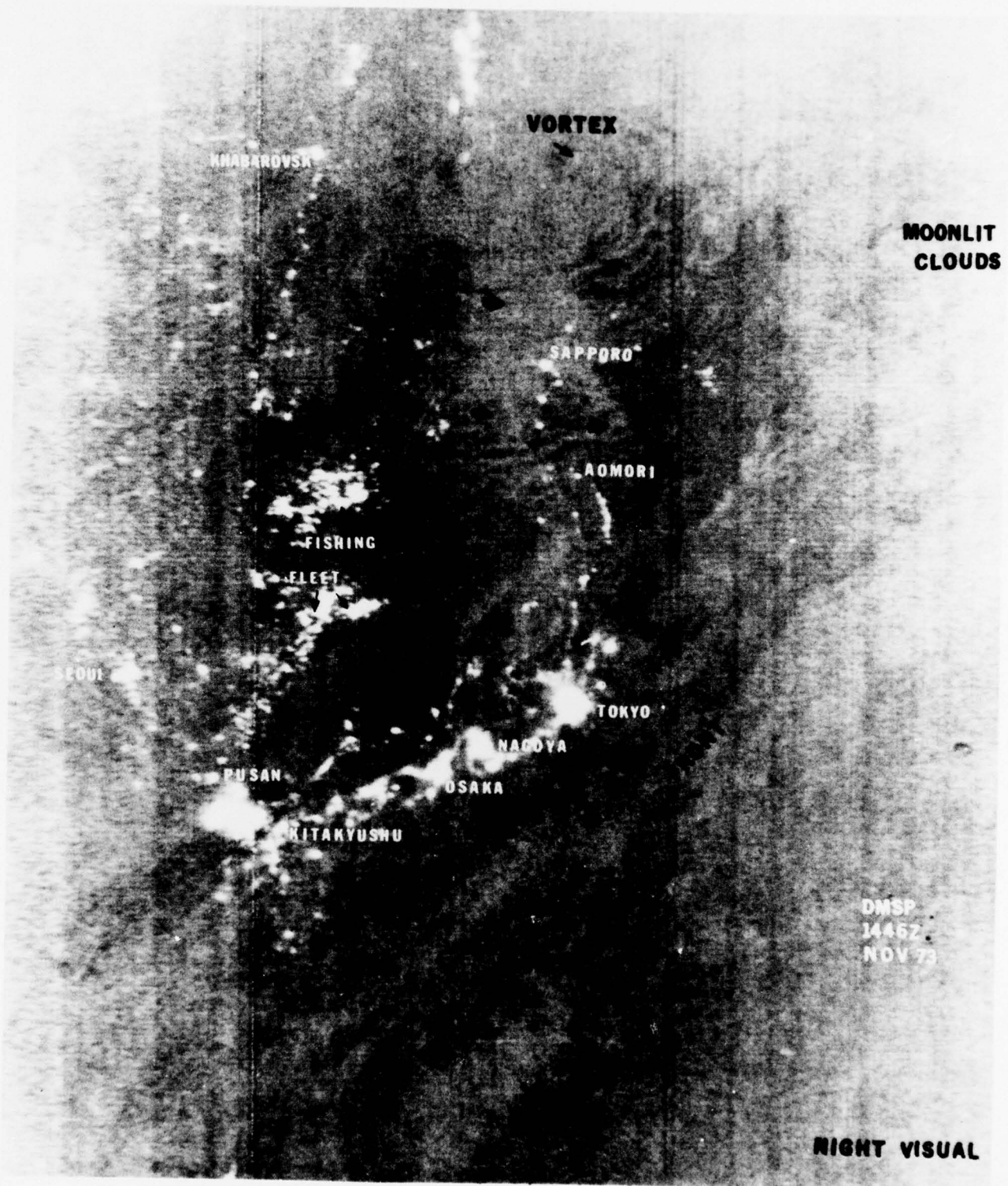


Figure 205. Lettered DMSP nighttime visual image of Japan (Nov 73).

REFERENCES AND BIBLIOGRAPHY

- [1] AFCRL Newsletter, No. 444, 6 April 1973.
- [2] AFSC: *Block 5D-A Compendium*, Hq. Space & Missile Systems Org., AFSC, USAF, 1975.
- [3] Alexander, T.: "Ominous Changes in the World's Weather," *Fortune*, February 1974, p. 95.
- [4] Allison, L.J., et al.: "Meteorological Satellite Accomplishments," *Rev. Geophys. Space Phys.*, Vol. 13, No. 3, July 1975, pp. 737-745.
- [5] Anderson, R.K., et al.: "Application of Meteorological Satellite Data in Analysis and Forecasting," *AWS TR 212*, Hq Air Weather Service, Scott AFB, IL., June 1969.
- [6] Ashman, J.P., Brandli, H.W., and Oliver, J.W.: "Expansion of Meteorological Satellite Potential," *11th Space Cong. Proc.*, 1974.
- [7] Baig, S.R.: "Ocean Thermal Features as Seen from GOES-1," *Satellite Appl. Info. Note 76/7*, NOAA/NESS, Washington, D.C., 1976.
- [8] Barnes, J.C., Bowley, C.J., and Cogan, J.L.: "Snow Mapping Application of Thermal Infrared Data from the NOAA Satellite Very High Resolution Radiometer (VHRR)," *ERT Doc. No. 0438-F*, Environ. Rsch. & Tech., Inc., Concord, MA., November 1974, 72 p.
- [9] Bitner, R.E.: "Guide for Interpretation of Satellite Photography and Nephanalyses," *Proj. FAMOS Rsch. Rpt. No. 4-67*, NAVAIRSYSCOM, 1967.
- [10] Brandli, H.W.: "Aurora Borealis and City Lights," *Monthly Weather Rev.*, Vol. 102, No. 7, July 1974, pp. 533-534.
- [11] Brandli, H.W.: "Cumulus Cloud Lines or Streets Near the Equator," *Bull. Am. Meteorol. Soc.*, Vol. 55, No. 4, April 1974, pp. 315-317.
- [12] Brandli, H.W.: "Display and Presentation of Satellite Imagery," *Aerospace Sci. Rev.*, No. 74-1, Hq Air Weather Service, Scott AFB, IL., March 1974, pp. 2-3.
- [13] Brandli, H.W.: "Earth Resources Capability of DMSP," *Forest Sci.*, 1974.
- [14] Brandli, H.W.: "Moon Glint," *Monthly Weather Rev.*, Vol. 103, No. 7, July 1975, pp. 655-656.
- [15] Brandli, H.W.: "Real Time ESSA 8 APT Tracked Over Australia Received at Florida Over 11,000 Miles Away," *Monthly Weather Rev.*, Vol. 100, No. 10, October 1972, p. 749.
- [16] Brandli, H.W.: "Solar Eclipse from DAPP Satellite," *Bull. Am. Meteorol. Soc.*, Vol. 55, No. 5, May 1974, pp. 414-415.
- [17] Brandli, H.W.: "Study of Small-Scale Occlusion in Pacific," *Aerospace Sci. Rev.*, No. 75-3, Hq Air Weather Service, Scott AFB, IL., May 1975, pp. 2-8.
- [18] Brandli, H.W.: "U.S. Air Force/Air Weather Service Nighttime Spectacular," *Air Univ. Rev.*, Vol. XXV, No. 5, July-August 1974, pp. 44-50.
- [19] Brandli, H.W., Ashman, J.P., and Olivier, M.G.: "Newest Synchronous Meteorological Satellite Positions Synoptic Features and Other Meteorological Intelligence Every Half-Hour," *Aerospace Sci. Rev.*, No. 75-1, Hq Air Weather Service, Scott AFB, IL., January 1975, pp. 2-7.
- [20] Brandli, H.W., and Janes, S.A.: "ESSA 8—The Workhorse of Weather Satellites," *Bull. Am. Meteorol. Soc.*, Vol. 57, No. 11, November 1976, pp. 1357-1359.
- [21] Brandli, H.W., and Janes, S.A.: "Locating the Center of the High from a Satellite Photo," unpublished.
- [22] Brandli, H.W., and Kadlec, P.W.: "Satellite View of Aircraft Induced Trails," unpublished.
- [23] Brandli, H.W., and Lombardo, F.A.: "High Level Wave Clouds not Associated with Terrain (Billows)," *Bull. Am. Meteorol. Soc.*, Vol. 55, No. 12, December 1974, pp. 1472-1474.
- [24] Brandli, H.W., and Munson, R.D.: "Frontal Cloud Movement from Gridded Imagery," *Monthly Weather Rev.*, Vol. 104, No. 7, July 1976, pp. 972-974.
- [25] Brandli, H.W., Oliver, J.W., and Estu, R.J.: "NOAA 2 Scanning Radiometer Visual and Infrared Imagery Received Real-Time Over a 50,000-Mile Transmission Link," *Monthly Weather Rev.*

- Vol. 101, No. 6, June 1973, pp. 538-539.
- [26] Brandli, H.W., Olivier, M.G., and Little, Mo. O.: "Small Vortex Develops Into a Tropical Depression," unpublished.
 - [27] Brandli, H.W., and Orndorff, J.W.: "The Round Lake," *Atmosphere*, Vol. 14, No. 1, 1976, pp. 55-56.
 - [28] Brandli, H.W., and Orndorff, J.W.: "Satellite-Viewed Cloud Lines, Anomalous or Others," *Monthly Weather Rev.*, Vol. 104, No. 2, February 1976, pp. 210-213.
 - [29] Brandli, H.W., and Persin, K.: "Aurora Borealis, Auroral Glint, Volcano, and City Lights," *Bull. Am. Meteorol. Soc.*, Vol. 55, No. 10, October 1974, pp. 1241-1242.
 - [30] Brandli, H.W., and Taylor, L.O.: "Invisible Billow Clouds," *Monthly Weather Rev.*, Vol. 103, No. 12, December 1975, pp. 1140-1142.
 - [31] Brandli, H.W., and Webb, J.A.: "ESSA 8 APT Shows Lee Waves Near Aleutian Islands," *Monthly Weather Rev.*, Vol. 98, No. 5, May 1970, pp. 406-407.
 - [32] Bristor, C.L., and Pichel, W.: "3-D Cloud Viewing Using Overlapped Pictures from Two Geostationary Satellites," *Bull. Am. Meteorol. Soc.*, Vol. 55, No. 11, November 1974, pp. 1353-1355.
 - [33] Cochran, D.R.: "From Pictures to Winds," *Monthly Weather Rev.*, Vol. 102, No. 2, February 1974, pp. 191-193.
 - [34] Colwell, R.N.: *Monitoring Earth Resources from Aircraft and Spacecraft*, SP-275, Scientific and Technical Information Office, NASA, Washington, D.C., 1971, 170 p.
 - [35] Conover, J.H.: "Cloud Interpretation from Satellite Altitudes," *AFCRL TR-62-680*, Air Force Cambridge Research Laboratory, Hanscom AFB, MA., July 1962.
 - [36] Corliss, W.R.: *Satellites at Work*, NASA, Washington, D.C., June 1971.
 - [37] Dandekar, B.S.: "Factors Involved in Optical Programs for the Polar Cap," *AFCRL Technical Report 72-0746 (or ERP No. 428)*, Air Force Cambridge Research Laboratories, Cambridge, MA., December 1972, 31 p.
 - [38] DeRycke, R.J.: "Sea Ice Motions off Antarctica in the Vicinity of the Eastern Ross Sea as Observed by Satellite," *J. Geophys. Res.*, Vol. 78, No. 36, December 1973, pp. 8873-8879.
 - [39] Dickinson, L.G., Boselly, S.E., and Burgmann, W.S.: "Defense Meteorological Satellite Program (DMSP) User's Guide," *AWS TR-74-250*, Hq Air Weather Service, Scott AFB, IL., December 1974, 109 p.
 - [40] Dickson, L.G., Brandli, H.W., and Lombardo, F.: "Determination of Wind Velocity from Satellite Observed Billow Clouds," paper presented at 54th Annual Meeting of the American Geophysical Union, Washington, D.C., 16-20 April 1973 (Abstract appears in *EOS*, Vol. 55, No. 4, April 1973, p. 289).
 - [41] Dvorak, V.F.: "A Technique for the Analysis and Forecasting of Tropical Cyclone Intensities from Satellite Pictures," *NOAA-TM-NESS 45*, Washington, D.C. February 1973, 19 p.
 - [42] Erickson, C.O.: "A Jet Stream Cirrus Shield," *Monthly Weather Rev.*, Vol. 102, No. 3, March 1974, pp. 260-261.
 - [43] Erickson, C.O.: "An Evaluation of the Accuracy of Tropical Cyclone Intensities and Locations Determined from Satellite Pictures," *NOAA TMERL WMPO-20*, Weather Modification Program Office, Boulder, CO., February 1975.
 - [44] Erickson, C.O.: "Use of Geostationary-Satellite Cloud Vectors to Estimate Tropical Cyclone Intensity," *NOAA TM NESS 59*, Meteorological Satellite Laboratory, Washington, D.C., September 1974, 37 p.
 - [45] Erickson, C.O., and Whitney, L.F. Jr.: "Gravity Waves Following Severe Thunderstorms," *Monthly Weather Rev.*, Vol. 101, No. 9, September 1973, pp. 708-711.
 - [46] Fett, R.W.: "Fishing Fleet Activities Revealed by Nighttime Data from the Defense Meteorological Satellite Program (DMSP)," *Marine Fisheries Rev.*, Vol. 37, No. 4, April 1975.
 - [47] Fett, R.W., and Brand, S.: "Tropical Cyclone Movement Forecasts Based on Observations from Satellites," *Tech. Paper No. 1-74*, Environmental Prediction Research Facility, Monterey, CA., January 1974, 70 p.
 - [48] Fett, R.W., and Rabe, K.: "Island Barrier Effects on Sea State and Atmospheric Moisture as Detected by a Numerical Wave Model and Sensors of the Defense Meteorological Satellite Program (DMSP)," Naval Air System Command, Department of the Navy, Washington, D.C.,

October 1975.

- [49] Fishlock, David: *A Guide to Earth Satellites*, American Elsevier, Inc., New York, 1971.
- [50] Follansbee, W.A.: "Estimation of Average Daily Rainfall from Satellite Cloud Photographs," *NOAA TM NESS 44*, Washington, D.C., January 1973, 39 p.
- [51] Fortuna, J.J., and Hambrick, L.N.: "The Operation of the NOAA Polar Satellite System," *NOAA TM NESS 60*, Office of Systems Integration, Washington, D.C., November 1974, 127 p.
- [52] Frank, N.L.: "The 'Inverted V' Cloud Pattern—An Easterly Wave?" *Monthly Weather Rev.*, Vol. 97, No. 2, February 1969, pp. 130-141.
- [53] Fritz, S.: "The Significance of Mountain Lee Waves as Seen from Satellite Pictures," *J. Appl. Meteorol.*, Vol. 4, No. 1, February 1965, pp. 31-37.
- [54] Gaby, D.C., et al.: "Atlantic Tropical and Subtropical Cyclone Classifications for 1975," *NOAA TM NESS 75*, Washington, D.C., March 1976, 14 p.
- [55] Gruber, A.: "Estimating Rainfall in Regions of Active Convection," *J. Appl. Meteorol.*, Vol. 12, No. 1, February 1973, pp. 110-118.
- [55] Haurwitz, B.: *Dynamic Meteorology*, McGraw-Hill Book Company, Inc., New York, 1941, 365 p.
- [57] Hebert, P.J., and Poteat, K.O.: "A Satellite Classification Technique for Subtropical Cyclones," *NOAA TM NWS SR-83*, Fort Worth, TX., July 1975, 25 p.
- [58] Hiser, H.W., et al.: "Application of Remote Sensing for Prediction and Detection of Thermal Pollution," Presented at *4th Annual Remote Sensing of Earth Resources Conf.*, Tullahoma, TN., March 1975.
- [59] Jager, G., Follansbee, W.A., and Oliver, V.J.: "Operational Utilization of Upper Tropospheric Wind Estimates Based on Meteorological Satellite Photographs," *ESSA NESC TM-8*, National Environmental Satellite Center, Washington, D.C., October 1968, 23 p.
- [60] Janes, S.A., Brandli, H.W., and Orndorff, J.W.: "'The Blue Line' Depicted on Satellite Imagery," *Monthly Weather Rev.*, Vol. 104, No. 9, September 1976, pp. 1178-1181.
- [61] Johnson, J.D., Parmenter, F.C., and Anderson, R.: "Environmental Satellites: Systems, Data Interpretation and Applications," NOAA, NESS, Washington, D.C., May 1975.
- [62] Johnston, E.C.: "Rapid Frontal Wave Development," *Monthly Weather Rev.*, Vol. 102, No. 11, November 1974, pp. 804-806.
- [63] Johnston, E.D.: "Vertical Wind Shear vs Upper Flow as Revealed by Cirrus Plumes," *Satellite Applications Information Note 276-2*, NOAA/NESS, Washington, D.C., 1976.
- [64] Kim, J.S.S.: "Satellite Picture of a Meteor Over the Central Pacific Ocean," *Weatherwise*, Vol. 28, No. 6, December 1975, pp. 258-259.
- [65] Kondrat'yev, K. Ya.: "Satellites and the Problems of the Earth's Natural Resources," NASA, Kennedy Space Center, FL., 1973.
- [66] Kuettner, J.P.: "Cloud Bands in the Earth's Atmosphere: Observations and Theory," *Tellus*, Vol. XXIII, Nos. 4-5, 1971, pp. 404-426.
- [67] LaViolette, P.E., Stuart, L. Jr., and Vermillion, C.: "Use of APT Satellite Infrared Data in Oceanographic Survey Operations," *Trans. AGU*, Vol. 56, No. 5, May 1975, pp. 276-282.
- [68] Maier, M.W., and Brandli, H.W.: "Real-Time Satellite Photographs for Skylab Support," *Weather*, Vol. 29, No. 3, March 1974, pp. 95-101.
- [69] Maier, M.W., Janes, S.A., and Brandli, H.W.: "A Satellite View of 1975 Pre-Thanksgiving Snow Storm in the Great Plains," unpublished.
- [70] McClain, E.P.: "Earth Satellite Measurements as Applied to Sea Ice Problems," *Approaches to Earth Survey Problems through Use of Space Techniques*, COSPAR Symposium, Constance, F.R.G., 23-25 May 1973.
- [71] McClain, E.P.: "Potential Value of Earth Satellite Measurements to Oceanographic Research in the Southern Ocean," *NOAA TM NESS-61*, Washington, D.C., February 1975, 18 p.
- [72] McClain, E.P., and Strong, A.E.: "On Anomalous Dark Patches in Satellite-Viewed Sunlight Areas," *Monthly Weather Rev.*, Vol. 97, No. 12, December 1969, pp. 875-884.
- [73] McGinnis, D.F. Jr., Pritchard, J.A., and Wiesnet, D.R.: "Snow Depth and Snow Extent Using VHRR Data from the NOAA-2 Satellite," *NOAA TM NESS-63*, Washington, D.C., February 1975, 10 p.

- [74] McGinnis, D.F. Jr., and Rango, A.: "Earth Resources Satellite Systems for Flood Monitoring," *Geophysical Research Letters*, Vol. 2, No. 4, April 1975, pp. 132-135.
- [75] Meyer, W.D.: "Data Acquisition and Processing Program: A meteorological data source," *Bull. Am. Meteorol. Soc.*, Vol. 54, No. 12, December 1973, pp. 1251-1254.
- [76] Mills, J.R.: "Low-Level Perturbations in the Eastern North Pacific Ocean Trades," *Aerospace Sci. Rev.*, No. 74-1, Hq Air Weather Service, Scott AFB, IL., March 1974, pp. 5-9.
- [77] NASA: "NIMBUS III User's Guide," Goddard Space Flight Center, National Aeronautics and Space Administration, Greenbelt, MD., 1969, 238 p.
- [78] NASA: "NIMBUS IV User's Guide," Goddard Space Flight Center, National Aeronautics and Space Administration, Greenbelt, MD., March 1970, 214 p.
- [79] NASA: "NIMBUS 5 User's Guide," Goddard Space Flight Center, National Aeronautics and Space Administration, Greenbelt, MD., November 1972, 162 p.
- [80] NASA: "NIMBUS 6 User's Guide," Goddard Space Flight Center, National Aeronautics and Space Administration, Greenbelt, MD., February 1975, 227 p.
- [81] NASA: "NIMBUS 4 Data Catalog," Goddard Space Flight Center, National Aeronautics and Space Administration, Greenbelt, MD., 1972.
- [82] NASA: "NIMBUS 5 Data Catalog," Goddard Space Flight Center, National Aeronautics and Space Administration, Greenbelt, MD., 1975.
- [83] Novak, C.S.: "Deriving Upper Tropospheric Winds by Computer from Single Image, Digital Satellite Data," *ESSA NESCTM 13*, National Environmental Satellite Center, Washington, D.C., June 1969, 32 p.
- [84] NSSDC: "Compendium of Meteorological Satellites and Instrumentation," *NSSDC 73-02*, National Space Science Data Center, NASA, Greenbelt, MD., July 1973, 455 p.
- [85] NSSDC: "Report on Active and Planned Spacecraft and Experiments," *NSSDC 74-01*, National Space Science Data Center, NASA, Greenbelt, MD., January 1974, 621 p.
- [86] Oliver, J.W., and Brandli, H.W.: "Meteorological Satellite Capabilities at the Air Force Eastern Test Range and their Application for Space Vehicles," Presented at *6th Conf. on Aero. and Aeron. Meteor.*, El Paso, TX., November 12-15, 1974, pp. 62-65.
- [87] Olivier, M.G., and Brandli, H.W.: "Cloud Dissipation Off the West Coast of Florida," *Bull. Am. Meteorol. Soc.*, Vol. 56, No. 1, January 1975, pp. 60-62.
- [88] Pike, C.P. (ed): "Defense Meteorological Satellite Program Auroral-Ionospheric Interpretation Guide," *AFCRL TR-75-0191* (or *SIG No. 306*), Air Force Cambridge Laboratory, Hanscom AFB, MA., April 1975, 86 p.
- [89] Purcell, H.D.: *Cyprus*, Frederick A. Praeger, Inc., New York, 1968.
- [90] Reinke, D.L., and Brandli, H.W.: "Warm Cloud Over North Central Florida," *Monthly Weather Rev.*, Vol. 104, No. 10, October 1976, pp. 1328-1329.
- [91] Rogers, C.W.C.: "A Technique for Estimating Low-Level Wind Velocity from Satellite Photographs of Cellular Convection," *J. Appl. Meteorol.*, Vol. 4, No. 3, June 1965, pp. 387-393.
- [92] Russell, C.G.: "Some Techniques for Short-Range Terminal Forecasting," *AWS TR 233*, Hq Air Weather Service, Scott AFB, IL., September 1970, 48 p.
- [93] Scully-Power, P.D., et al.: "A Multisystem Technique for the Detection and Measurement of Warm Core Ocean Eddies," *IEEE Ocean*, 1975, pp. 761-768.
- [94] Shenk, W.E., and Salomonson, V.V.: "Visible and Infrared Imagery from Meteorological Satellites," *Applied Optics*, Vol. 9, No. 8, August 1970, pp. 1747-1760.
- [95] Siebers, J.O., et al.: "Guide for Using GOES/SMS Imagery in Severe Weather Forecasting," *USAFETAC*, 1 April 1975, 56 p.
- [96] Silverman, S.M., et al.: "Airglow and Aurorae," Chap. 13 in: *Handbook of Geophysics and Space Environment*, Air Force Cambridge Research Laboratories, MA., 1965, 29 p.
- [97] Snyder, J.F., Ashman, J.P., and Brandli, H.W.: "Meteorological Satellite Coverage of Florida Everglades Fires," *Monthly Weather Rev.*, Vol. 104, No. 10, October 1976, pp. 1330-1332.
- [98] Spangler, M.J.: "What's the Weather Down There?" Preprint 186 from: *Westinghouse Engineer*, October 1974, 10 p.
- [99] Strong, A.E.: "New Sensor on NOAA-2 Satellite Monitors the 1972-73 Great Lakes Ice Season,"

- Remote Sensing and Water Resources Management*, Proc. No. 17, June 1973, pp. 171-178.
- [100] Strong, A.E.: "Remote Sensing of Algal Blooms by Aircraft and Satellite in Lake Erie and Utah Lake," *Remote Sensing of Environment*, Vol. 3, 1974, pp. 99-107.
- [101] Strong, A.E., and Ruff, I.S.: "Utilizing Satellite-Observed Solar Reflections from the Sea Surface as an Indicator of Surface Wind Speeds," *Remote Sensing of Environment*, Vol. 1, 1970, pp. 181-185.
- [102] Thomas, J.E., et al.: "Visual Observation of Propagating Gravity Waves on ATS III Satellite Film Loops," *ECOM-5553*, Atmospheric Sciences Laboratory, US Army Electronics Command, White Sands Missile Range, NM., January 1975, 22 p.
- [103] USAF: "DMSP Capability at Cape Kennedy AFS, Florida," Staffmet Section, Det. 11, 6th Weather Wing, 1974.
- [104] USAF: "Tropical Cyclone Position and Intensity Analysis Using Satellite Data," *IWWP 105-10*, 1st Weather Wing, August 1974, 97 p.
- [105] Vesely, C.J., and Botzong, W.B.: "Defense Meteorological Satellite Program," Presented at *6th Conf. on Aero. and Aeron. Meteor.*, El Paso, TX., 12-15 November 1974, pp. 146-149.
- [106] Webb, W.L.: "Meteorological Satellite Applications," Atmospheric Science Laboratory, White Sands Missile Range, NM., 1975.
- [107] Weldon, R.: "Low Level Circulation Systems in the Easterlies," *Satellite Applications Information Note 11/75-1*, NOAA/NESS, Washington, D.C., 1975.
- [108] Widger, W.K., Sherr, P.E., and Rogers, C.W.C.: "Practical Interpretation of Meteorological Satellite Data," *AWS TR 185*, Hq Air Weather Service, Scott AFB, IL., March 1965, 380 p.
- [109] Wiesnet, D.R.: "The Role of Satellites in Snow and Ice Measurements," *NOAA TM-NESS 58*, Environmental Sciences Group, Washington, D.C., August 1974, 12 p.
- [110] Wiesnet, D.R., McGinnis, D.F. Jr., and Forsyth, D.G.: "Selected Satellite Data on Snow and Ice in the Great Lakes Basin 1972-1973 (IFYGL)," *Proc. 17th Conf. Great Lakes Res.*, 1974, pp. 334-347.
- [111] Wiesnet, D.R., McGinnis, D.F. Jr., and Pritchard, J.A.: "Mapping of the 1973 Mississippi River Floods by the NOAA-2 Satellite," *Water Resources Bulletin*, Vol. 10, No. 5, October 1974, pp. 1040-1049.
- [112] Wilkins, E.M., Eden, D.D., and Chivian, J.S.: "Spectral Variations of Cloud Reflectance Deduced from Apollo 9, SO-65 Photography," *Remote Sensing of Environment*, 1970, pp. 221-230.
- [113] Woodley, W.E., Sancho, B., and Miller, A.H.: "Rainfall Estimation from Satellite Cloud Photographs," *NOAA TM ERL OD-11*, NOAA Environmental Research Laboratories, Boulder, CO., February 1972, 43 p.
- [114] Yates, H.W., and Bandeen, W.R.: "Meteorological Applications of Remote Sensing from Satellites," *Inst. Electrical and Electronics Engineers, Inc.*, Vol. 63, No. 1, January 1975.

LIST OF ABBREVIATIONS, ACRONYMS AND SYMBOLS

AFGWC	Air Force Global Weather Central
APT	Automatic Picture Transmission
ARIA	Advanced Range Instrumented Aircraft
AS	Altostratus
ATS	Application Technology Satellite
AWS	Air Weather Service
C	Centigrade
CB	Cumulonimbus Clouds (Thunderstorms)
CI	Cirrus
CS	Cirrostratus Clouds
CU	Cumulus Clouds
DAPP	Data Acquisition and Processing Program (now DMSP)
Det	Detachment
DMSP	Defense Meteorological Satellite Program
DMZ	De-Militarized Zone
ESSA	Environmental Sciences Service Administration (now NOAA)
ERTS	Environmental Resource Technology Satellite
ft	Feet
GSTS	Gusts
HR	High Resolution
hts	Heights
IR	Infrared
ITCZ	Intertropical Convergence Zone
K	Kelvin
kt	Knots
Lyrs	Layers
NM	Nautical Mile
NOAA	National Oceanic and Atmospheric Administration
R	River
Res	Resolution
Rev	Revolution
ST	Stratus
SC	Stratocumulus Clouds
SMS	Synchronous Meteorological Satellite
TCU	Towering Cumulus Clouds
TSP	Test Support Point
USAF	United States Air Force
VHR	Very High Resolution
VIS	Visual
WHR	Very High-Resolution Infrared
WWG	Weather Wing
*	Snow
9	Drizzle
∇	Rainshowers
⇨	Upper-Level Wind Flow
⇩	Low-Level Wind Flow
μ	Micron
⚡	Thunderstorms

INDEX

- Actiniform Clouds, 38, 40, 41
- African Oil Fields, 153
- Africa, 129, 138, 155
- Altostratus, 43, 47, 48
- Anomalous Lines, 41, 45, 47, 51, 57
- Anomalous Gray Areas, 59, 63, 64
- Appalachians, 41, 43
- Applications Technical Satellite (ATS), 4, 95, 100, 148
 - ATS-1, 4, 19, 95, 101
 - ATS-3, 4, 7, 19, 60, 56
- Aurora Australis, 59, 62, 64
- Aurora Borealis, 12, 14, 16, 59, 62, 65, 67, 150
- Australian Oil Fields, 154
- Automatic Picture Transmission (APT), 3, 19

- Bands, Transverse, 50, 55, 110, 115
- Billow Clouds, 41, 44, 50, 56, 114, 119
- Bow Shock, 42, 46

- Calibration, 17, 18, 21
- Cirrus, 48-55
- Cirrus Filaments, 50, 54, 114, 119
- Cirrus Shadow, 50, 54, 110-114, 116, 117, 119
- Cirrus Streaks, 50, 54, 114, 119
- City Lights, 12, 14, 16, 17, 49, 53, 65, 67, 84, 91, 137, 150
- Clouds, 32, 57
- Cloud Movement, 12, 19, 117, 120, 121
- Cold Front, 68, 74, 75, 110
- Cone Shock, 41, 45, 106
- Cumulonimbus, 43, 44, 49, 50, 129
- Cumulus, 12, 33, 36, 37, 42, 46, 105, 107
- Cumulus Lines, 33, 106, 109
- Cumulus Streets, 33, 37, 106, 109, 113, 114
- Cut-off Low, 95, 97
- Cyclone, 80, 82-84, 86, 92

- Data Display, 162, 170-174
- Data Preparation and Presentation, 158-174
- Day Visual, 12-15
- Defense Meteorological Satellite Program (DMSP), 1, 3, 4, 5, 6, 12, 14-17, 19, 20, 22, 34-37, 39-49, 51-58, 59, 61-65, 67, 69-71, 77, 78-85, 88-92, 94, 97-103, 106, 108, 110, 111, 113-116, 120, 122, 123, 124 126-135, 137, 138, 140-146, 149, 150-157, 159, 161-163, 170, 173, 174
- Dust, 56, 60, 61

- Earth Resources Technology Satellite, (ERTS), 51, 122
- Earth Surface, 122-157
- Earthquakes, 138, 156, 157

Easterly Wave, 101, 103
 Eclipse, 138, 155
 Eddies, 41, 42, 45, 46, 106, 135, 142, 145, 146
 Ephemeris, 158, 159
 ESSA, 1-3, 38, 87, 148, 162, 164-166, 171
 Europe, 48, 65
 Everglades, 57, 62, 137, 149
 Expanded Viewing Interval, 12, 15, 41

 Fields, Gas, 151-154
 Fields, Oil, 16, 17, 151-154
 Fingerprints, 42, 46
 Fires, 12, 14, 16, 17, 57, 61, 84, 122, 137, 138, 149, 150
 Fire Detection, 137
 Floods, 129, 132
 Fog, 38-40, 79, 83
 Frontal Rope Cloud, 68-72
 Frontal Wave, 68, 73-75
 Fronts, 68-77, 78, 79

 Geology, 122-129, 130
 Geostationary Operational Environmental Satellite (GOES), 5, 8-11, 12-14, 16, 22
 Geostationary Satellite, 4-11
 Glint, 56, 58, 59, 95, 99, 136, 148
 Great Lakes, 43, 47, 79, 82
 Gridding, 159, 161-168
 Gulf Stream, 133, 135, 142-146

 Haze, 51, 56, 58, 59
 High-Level Clouds, 43, 44, 48-57
 High-Level Wind Flow, 109, 110, 112-121
 Hurricane, 49, 51, 80, 82-84, 86-92
 Hurricane Alice, 82, 87
 Hurricane Carmen, 49, 51
 Hurricane Eloise, 83, 88
 Hurricane Ginger, 162, 164
 Hurricane Gladys, 115
 Hydrology, 129-148

 Ice, 131, 133, 139, 140, 141
 Improved Television Operational Satellites (ITOS), 1, 3
 Infrared (IR), 9, 12, 14-21, 44, 49-55
 Intertropical Convergence Zone (ITCZ), 32, 48, 103, 104
 Invisible Clouds, 41, 44, 56
 Italy, 79, 84, 122, 126

 Jet Stream, 110, 114, 116, 117

 Koolau Mountains, 41, 42
 Korea, 136, 147

 Land Features, 122-130
 Lee Waves, 41, 43, 48, 106, 110, 114, 118

Lightning, 77, 80, 81
Low-Level Clouds, 32-47
Luzon, 122, 125

Meteor, 122, 131
Meteorological Satellites, 1-11
Mexican Oil Fields, 17
Mexico, 17
Middle East Oil Fields, 152
Mid-Level Clouds, 43, 47, 48
Miscellaneous Cloud Lines, 41, 42, 45-47
Mississippi River, 12, 14, 15
Montana, 122, 124
Moon Glint, 95, 99
Movie Loops, 19, 22

(NASA) National Aeronautical & Space Administration, 1, 22-31, 122
(NESS) National Environmental Satellite Service, 22, 23
(NOAA) National Oceanic & Atmospheric Administration, 1, 3, 4, 12-14, 17-19, 21-23, 50, 62, 68, 73, 75, 77, 79, 93, 131, 133, 139, 148
Night Visual, 12, 14, 16, 17, 84, 91, 137, 138, 149-154, 162, 163, 173, 174
Nile Delta, 122, 127
Nile River, 122, 127
Nimbus, 1, 3, 22-31
Normalization, 19

Occluded Front, 68, 73-75
Oceanology, 133, 135-137, 142-148
Ocean Surface Temperatures, 133-137, 142-148
Oil Fields, 137-138, 151, 152, 153, 154

Plumes, 43, 49, 95, 109-114
Polar Orbiting, 1, 162
Pollution, 51, 56, 58, 59
Positive Vorticity Advection Area, 73, 91, 95, 96
Press-type, 162, 169

Radiometer, Scanning, 3
Rectification, 19
Reefs, 59, 63
Resolution, 12-20
Ridge Line, 95, 97-100

Sand, 122, 128
Scanning Radiometer, 3
Screaming Eagles, 101, 102
Sea-Breeze Front, 74, 76, 106
Sea Fog, 38, 40
Severe Weather, 75, 77-81
Shock Waves, 41, 42, 45, 46, 106
Smog, 51, 56, 58, 59
Smoke, 57, 61, 62
Snow, 130, 131, 133-138

Solar Disk, 62, 67
South American Oil Fields, 151
Southeast Asia, 162, 167, 168
Soviet Union, 16
Squall Line, 75, 77
Stereographic Viewing, 19, 22
Stratocumulus, 32-35, 105, 106
Stratocumulus Lines, 33-35, 105, 106, 108
Stratus, 38, 39
Sun-Synchronous Satellites, 1-6
(SMS) Synchronous Meteorological Satellite, 5, 8-10, 12-14, 16, 22, 32, 33, 40, 50, 54-56, 58, 59, 61, 68, 73, 74, 76, 94, 103, 104, 119, 165

Thunderstorms, 43, 44, 49, 50, 74, 75, 110
Tornado Activity, 75, 77, 78
Towering Cumulus, 33
Transverse Bands, 50, 55, 110, 115
Tropical Storm Alice, 82, 87
Troughs, 89, 91-94, 96
Turbulence, 105-119
Typhoon, 80, 82-84, 89-91
Typhoon Betty, 83, 89
Typhoon Pamela, 84, 90
Typhoon Patsy, 84, 90
Typhoon Rita, 49, 52

Vertical Temperature Profile, 22, 23
Visual, 12-17
Volcano, 122, 129, 130
Vortex, 73, 75, 79, 80, 82-85, 95, 135, 143, 144

Warm Front, 68, 73-75
Wave Heights, 136, 137, 148
Weather Systems, 68-104
Wind, 105-121
Wind, High-Level, 109-119
Wind, Low-Level, 105-112
Wind, Mid-Level, 109
Wind Shear, 110, 116